Chemistry and Transport of Silver Nanoparticles in Environmentally Relevant Conditions

By

LAURA-JAYNE ELLIS

A thesis submitted to the University of Birmingham for the degree

of

DOCTOR OF PHILOSOPHY

School of Geography, Earth and Environmental Sciences

College of Life and Environmental Sciences

The University of Birmingham, UK

September 2014

Abstract

Silver nanoparticles (AgNPs) are added to many consumer products such as food packaging, textiles, and plasters due to the anti bacterial properties (Benn and Westerhoff, 2008, Nowack *et al,* 2011). Little information is known about the behaviour, transformations and fate of AgNPs once released into the environment. Studies have attempted to assess possible transformations using small scale laboratory experiments in simple media, but no large scale studies comparing two similar sized different coated AgNPs in seasonal variations of natural water has yet been accomplished.

Using controlled synthesis methods we were successfully able to characterise two sizes of citrate AgNPs of 35 ± 2 nm (DLS) and 23 ± 2 nm (DLS) both with a PDI of 0.1. Citrate stabilised AgNPs using methods originally produced by Cumberland and Lead (2009) and PVP AgNPs (Tejamaya *et al*, 2012) were also successfully synthesised with an average size of 11.5 ± 2.5 nm and characterised using a multi-method approach (UV-Vis, DLS, AFM and TEM).

The fate and transport of citrate (Cumberland and Lead, 2009) and PVP AgNPs (Tejamaya *et al*, 2012) was determined using large scale mesocosm studies with simple synthetic water and seasonal variations of natural lake water. Measurements of total Ag concentrations and UV-vis were determined daily for 14 days and on days 21 and 28, to assess the fate, transport and surface coating specific trends. We were able to produce a simple diffusion-sedimentation mathematical model (Socolofsky and Jirka 2004, and Hinderliter *et al,* 2010) to help validate the concentration and thus incure the behavioural mechanisms of the AgNPs in the mesocosms in the surface, middle and bottom depths of

the mesocosm. The model modifies sedimentation and diffusion equations created by Hinderliter *et al,* 2010, solved by the boundary conditions created by Socolofsky and Jirka 2004 for particles moving vertically through a 1 meter tall column.

Studies using simple synthetic waters identified that the ionic strength had a direct impact upon the behaviour and transformations observed by the different surface coated AgNPs. When citrate and PVP AgNPs were released into ultrapure water there were no observable effects to particle instability in each depth of the mesoscosms. The SPR data for the citrate AgNPs gave a single sharp peak between 390-396nm and the PVP AgNPs gave a peak at 400nm, agreeing with the reported literature for stable suspended AgNPs (Cumberland and Lead, 2009, Tejamaya *et al,* 2012).

When released in simple ionic media, citrate AgNPs aggregated and had increased dissolved Ag concentrations. The SPR data revealed extensive band stretching in the regions of 500-800nm indicating the presence of larger AgNPs. The modelled concentration parameters were fitted in the lower depths using a 230 nm citrate AgNP, to validate aggregation and sedimentation behaviour. In comparison, the PVP AgNPs were more stable at 13 ± 8 nm (TEM) in the surface water and 16 ± 6 nm after 24 hours post release, with no increased effects to dissolution. The model parameters were also fitted using the primary particle sizes. The addition of Suwannee river fulvic acid (SRFA) in the presence of a simple ionic media demonstrated stabilising effects to the citrate AgNPs by reducing dissolution and increasing the AgNP presence using UV-vis observations.

When citrate AgNPs were released in to natural lake water we observed different behaviours between the seasonal variations. The spring natural water had a TOC concentration of 12.59 mg L^{-1}, to which citrate AgNPs were persistent for 11 days in the

surface water. The citrate AgNPs also demonstrated aggregation on immediate introduction, as shown by the SPR data. The PVP AgNPs were detectable by the UV-vis for the duration of the study (28 days) and maintained their stability as shown in the model, SPR and TEM data. The summer water contained the highest TOC concentrations of 31.70 mg L^{-1} and low ionic strength using ICP-MS elemental concentration analysis. For the citrate AgNPs, we observed reduced aggregation shown by the decrease in SPR band stretching in the 500-800nm region (Li *et al,* 2010). To compare, the PVP AgNPs were detectable for 28 days in the surface water (UV-vis) maintaining their stability and low size frequency (TEM).

The autumn season water contained high ionic strength with a TOC concentration of 28.31 mg L^{-1}, resulting in destabilising effects to the citrate AgNPs. Their presence was reduced to 8 days in the surface water with increased aggregation, as seen in the model, SPR and TEM data. The PVP AgNPs remained stable throughout the study, as confirmed by the model, SPR and TEM data. The winter water had the lowest TOC concentrations at 4.3 mg L^{-1} and the highest ionic strength. The citrate AgNPs demonstrated increased aggregation by UV-Vis and increased dissolution. No significant changes were observed with the PVP AgNPs.

Overall PVP AgNPs remained stable in all the seasonally variable natural water when compared to the citrate AgNPs. SPR analysis revealed there was little evidence to support NP instability in all experiments and the transport mechanism followed mainly diffusion. TEM imaging revealed smaller size distributions compared to the citrate AgNPs. Evidence suggests that NOM has no major impact on the fate or behaviour of the PVP AgNPs, as they remained stable despite the TOC concentration.

At different times of the year the transformations of the NPs will change, during the warmer months AgNPs will persist in particulate forms for longer periods of time in the surface waters, particularly those with polymer coatings. Therefore based on the information presented in this study we can make predictions that once Ag-NPs are released into natural waters, irrespective of their surface coating they will persist, particularly in waters which have higher concentrations of NOM. Releases of AgNPs from consumer goods used specifically for antibacterial produces will inevitably create elevated environmental concentrations of Ag. Higher concentrations of Ag will inevitably be bioavailable to small aquatic organisms where it can potentially exploit toxic consequences.

Acknowledgements

Firstly I would like to thank my supervisor Professor Jamie Lead. It has been a massive honour to work and be a part of you research group. Thank you to Mohammed Baalousha, for his co-supervision and training throughout the project especially with the final stages of my writing up. I would also like to thank Eva Valsami-Jones for all her help and support. To the partners of NanoBEE for developing the project, and giving me this opportunity to work with you. To the University of Birmingham, School of Geography, Earth and Environmental Sciences and NERC who provided the financing and facilities for this project to be able to take place.

Many staff had their involvement in making this project possible, Paul Stanley and Theresa Morris located at the electron microscopy for their help and support with TEM imaging and analysis. Dr. Steve Backer for his ICP-MS analysis on my water samples. I would like to thank Ruth Merrifeld for all your help and Professor Jon Sadler for your advice on statistics.

Thank you to everyone in the group, I have made some amazing lifelong friends. To Marie who started with me on the same NanoBEE project, and was always there to pick one another up when times got hard. We made it to the end together. Not forgetting our amazing conference experiences in London and California, especially when we gave up hope after losing our luggage in Paris! Isabella, for all the food and gig dates. Mila for always smiling and being a great friend and help with the PVP particle synthesis. To Adam, Christine and Fatima, thanks you for all your support and help, especially the laughs and jokes in the lab. To Paula and Kayla for all the smiles and giggles in the lab. To

everyone in room 325, Grace especially, thank you for inventing office chair Olympics and all the lunch dates.

Finally and most importantly, to my family, especially to my Mum, Spencer, Andrew, and Vikki I Love you all dearly. Thank you for all of the support and understanding. My best friend and boyfriend, Daniel, not only did you hang over a lake, get terrorised by a swan and countless ducks helping me collect water for my experiments, you were always there through the tears and tantrums. Thank you.

Thank you to my beautiful Nan. You made me the person I am today. Thank you for showing me that dreams can be a reality when your determined enough to reach them. I hope I have done you proud.

Table of Contents

List of Figures

List of Tables

Abbreviations

A	Cross section area of the column
AFM	Atomic Force Microscopy
Ag	Sliver
Ag^+	Ionic Silver/Silver Ions
AgCl	Silver Chloride
$AgNO_3$	Silver Nitrate
AgNPs	Silver Nanoparticles
Ag_2S	Silver Sulfide
Al	Aluminium
As	Arsenic
Au	Gold
B	Boron
Ba	Barium
Br	Bromine
C_{AgNP}	AgNP Concentration
Ca	Calcium
Ce	Cerium
CNT(s)	Carbon Nanotube(s)
CNW	Carbon Nanowire(s)
Co	Cobalt
C_O	Dosing Concentration
CO_2	Carbon Dioxide
Cr	Chromium
Cu	Copper
d	Diameter
D	Diffusion Coefficient
D_{Ag}	Ag^+ Concentration
DEFRA	Department for Environmental, Food and Rural Affairs

DLS	Dynamic Light Scattering
DO	Dissolved Oxygen
DLVO	Derjaguni-Landau-Verwey-Overbeek theory
DNA	Deoxyribonucleic Acid
EDX	Energy Dispersive X-rays
EELS	Electron Energy Loss Spectroscopy
EPA	Environmental Protection Agency
FA	Fulvic Acid
FAAS	Flame Atomic Absorption spectroscopy
Fe	Iron
Fl-FFF	Flow-Field Flow Fractionation
G	Gravitational Force
g mL^{-1}	Grams per Millilitre
Ga	Gallium
Ge	Germanium
HA	Humic Acid
HNO_3	Nitric Acid
HS	Humic Substances
ICP-MS	Inductively coupled plasma mass spectrometry
K	Potassium
K	Kelvin
KeV	kiloelectron volt
L	Length
L	Litres
Li	Lithium
LoD	Limit of Detection
M	Mass of Ag
m	Meter
m^2	Meters Squared
m^2 s	Meters Squared per Second
Mg	Magnesium

mg	Milligrams
mg L^{-1}	Milligrams per Litres
mm	Millimetre (10^{-3})
mM	Millimolar
Mn	Manganese
Mo	Molybdenum
N_2	Nitrogen Gas
N_A	Avogadro's number
Na	Sodium
$NaBH_4$	Sodium Borohydride
Ni	Nickel
nm	Nanometre (10^{-9})
NM(s)	Nanomaterial(s)
NOM	Natural Organic Matter
NP/NPs	Nanoparticle(s)
O	Oxygen
P	Phosphorous
Pb	Lead
PdI	Polydispersity Index Size
PEG	Polyethylene glycols
Po	Polonium
Rpm	Revolutions per minute
PVA	Poly(vinylalcohol)
PVP	Poly(vinylpyrrolidone)
R	Gas Constant
R^2	Pearsons Correlation Coefficient
Rb	Rubidium
Sb	Antimony
SDS	Sodium dodecyl sulfate
Se	Selenium
SEM	Scanning Electron Microscope/Microscopy

Si	Silicon
Sn	Tin
SPEM	Scanning Photoelectron Microscopy
SPM	Scanning Probe Microscopy
SPR	Surface Plasmon Resonance
SRFA	Suwannee River Fulvic Avid
Sr	Strontium
STM	Scanning Tunnel Microscopy
T	Temperature
t	Time
T_{Ag}	Total Ag Concentration
TEM	Transmission Electron Microscopy
Ti	Titanium
TOC	Total Organic Carbon
μ	Viscosity of Solution
U	Sedimentation velocity
UPW	Ultrapure water
UV-vis	Ultraviolet-visible spectroscopy
μm	Micrometer (10^{-6})
V	Vanadium
V	Dosing Volume
W	Tungsten
XRD	X-ray Diffraction
XPS	X-ray Photoelectron Spectroscopy
Zn	Zinc
Zr	Zirconium

Chapter 1 Introduction

1. Introduction

1.1. Nanoscience and Nanotechnology

There are several definitions of the term “nanomaterial” (NM) and thus what qualifies a material to be “nano”. The word ‘nano’ describes dimensions in the order of 10^{-9}, which is one billionth of a meter in size (Rai *et al,* 2009). The International Organization for Standardization (ISO) defined that NMs must have one external dimension in the region of 1-100 nm in size, whereas nanoparticles (NPs) must have all unique physicochemical characteristics within the range of 1-100 nm (ISO, 2008, Baalousha, 2009, Fabrega *et al,* 2009a and Fiorino, 2010). Similarly, the European Commission Recommendation defined NMs as:

‘‘Natural, incidental or manufactured material containing particles, in an unbound state or as an aggregate or agglomerate where, 50 % or more of the particles in the number size distribution, one or more external dimensions is in the size range 1-100 nm’’ (EU, 2011).

The difference between these definitions show they are not consistent with each other. The ISO defines NMs as having one dimension in the ‘nano’ scale (1-100 nm), whereas the European Commission Recommendation refers to the material having <50% of the dimensions in the ‘nano’ range. These can be classified as agglomerates or aggregates containing only part dimensions in the ‘nano’ region.

The European Commission Recommendation defined three categories of NPs: natural, incidental and manufactured (EU, 2011). Natural NPs have been present in the environment for millions of years and are present in all compartments of the Earth including the hydrosphere, geosphere and atmosphere (Wigginton *et al,* 2007). Natural NPs are produced from processes such as volcanic eruptions, pollination, natural weathering and erosion. All of which are ubiquitous in the environment (Navarro *et al,* 2008). The largest producers of natural NPs are attributed via biological degradation and precipitation processes. Natural NPs normally contain a hydroxyl group as they are produced in an aqueous environment and are not coated with a capping agent (Waychunas *et al,* 2009).

Incidental NPs are a by-product of industrial processes and are accidently released into the environment during manufacturing, mining processes and other anthropogenic activities. Particular examples are soot, exhaust fumes, wear of tyres, catalytic converters and fine particulates produced from combustion products. Note, incidental NPs are not specifically synthesised particulates but are formed as a waste product (Nowack and Bucheli, 2007). Incidental NPs tend to be very polydispersed with irregular morphology. Often, they contain organic carbon, metals and elements of sulphate and sulphide (Navarro *et al,* 2008).

Manufactured NPs are purposefully produced and are specifically designed to carry a precise function. Ideally, NP containing products should be made under tight constraints to ensure that the NMs have the same crystalline structure, uniform size and morphology, with no aggregation (Kannan *et al,* 2011). Unfortunately the majority of

manufactured nano-enabled products contain polydispersed particles and often contain lots of impurities (Ju-Nam and Lead, 2008).

1.1.1 History of Nanotechnology

As far back as the 4th century, silver NPs (AgNPs) were unknowingly used in crafted products. The most famous was the Lycurgus Cup which is composed of dichroic glass to exploit the optical properties of silver (Ag) and gold (Au) colloids, as seen in figure 1.1 (Freestone *et al,* 2007).

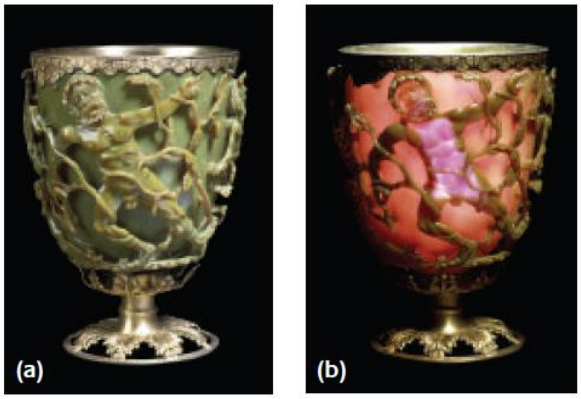

Figure 1.1: The Lycurgus Cup, extracted from Freestone et al (2007), a) shows normal reflected light and b) shows the colour change due to Ag and Au NPs while transmitted light passes through the glass.

In 1959 the founding concepts of nanotechnology was first laid by Professor Richard Feynman (Feynman, 1959) in his speech "there is plenty of room at the bottom". Later, Professor Norio Taniguchi used materials in the nanoscale and saw a potential market for exploiting materials for their size range and quantum effects (Taniguchi, 1974). Nanomaterial development was also aided by the advancement of the electron microscope, which later led to the discoveries of fullerenes and carbon nanotubes (CNTs). The electron microscope was developed in the 1930s which enabled scientists to use

much higher resolutions than those previously achieved by light microscopy. The development of the electron microscope enabled the visualisations of DNA (2 nm) and viruses (1 nm - 100 µm) in the size region of micrometers (µm) and nanometres (nm) (Bozzola and Russell, 1999). The turning point for nanoscience was the development of the scanning tunnel microscope (STM) in 1981 (Basu-Dutt *et al,* 2012), of which derived the scanning probe microscope (SPM) that enabled surface visualisations of materials at the atomic scale (figure 1.2) (Kalinin and Gruverman, 2010). This led further to the invention of the atomic force microscope (AFM) in 1986. Like the SPM, AFM uses a probe to scan the surface of desired materials exploiting oscillatory modes to enable the visualisation of materials in different environments including solids, liquids and gasses (Binnig *et al,* 1986).

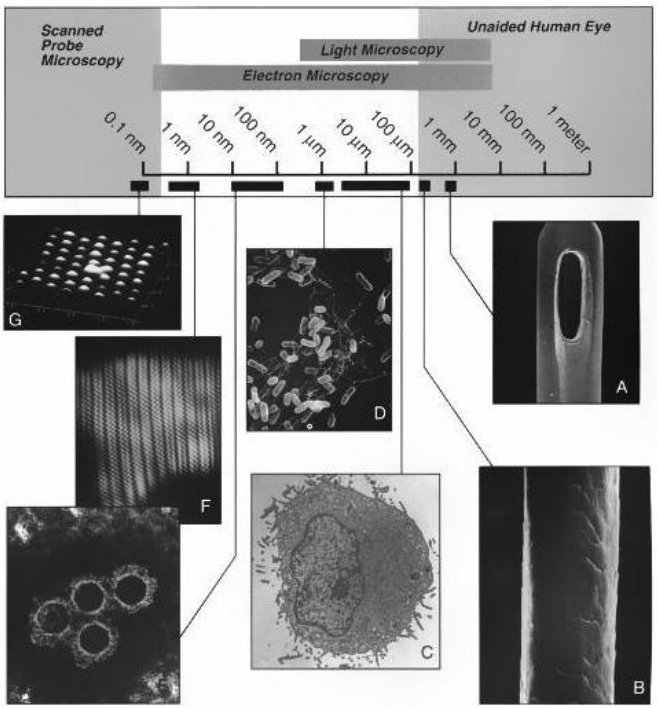

Figure 1.2: Size resolution of various microscope techniques, a) identifies a sewing needle head, by SEM, b) a human hair by SEM, c) a section of a cell by TEM, d) bacteria cell by SEM, e) a clump of viruses by TEM, f) macromolecules by TEM, and g) is a single atom by SPEM. Figure extracted from Bozzola and Russell (1999).

The 1980s saw the first discovery of the carbon fullerene molecule C_{60} discovered by Kroto *et al* (1985). Fullerenes are produced via carbon clusters and composed of a hollow spherical shape as seen in figure 1.3. Today Fullerenes are used in many commercial products including electronics (Bogdanov *et al,* 2000).

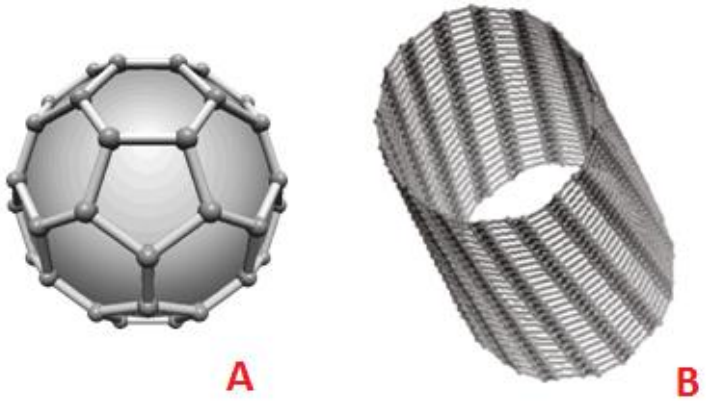

Figure 1.3: A) A hollow spherical formation of the C_{60} Buckminsterfullerene, first discovered in 1986. Extracted from: http://www.nano-enhanced-wholesale-technologies.com/faq/carbon-forms.htm. B) Identifies the structure of a single walled CNT, extracted from Basu-Dutt et al (2012).

Following the discovery of fullerenes, further research saw the development of carbon nanotubes (CNT) and carbon nanowires (CNW) in the 1990s. CNTs are hollow cylinders made from carbon sheets, and enhanced to exploit their unique thermal, structural and electronic properties (figure 1.3) (Basu-Dutt *et al,* 2012). The later advancement of graphene sheets composed of layers of carbon atoms have essentially revolutionised the functionality of nano-sized products (Dreyer *et al,* 2010).

1.1.2 Current Uses of Nanotechnology

At present, nanotechnology is one of the fastest growing industries in the world (Piccinno *et al,* 2012). Engineered NMs have seen a dramatic increase in use in the electronics, cosmetic, textile and food industries over the last decade (Magnuson *et al,* 2011). It is suggested that the amount of engineered NMs is expected to increase from 2000 tonnes in 2004 to an estimated 58,000 tonnes between 2011 and 2020 (Nowack and Bucheli, 2007). According to The Project on Emerging Nanotechnologies Consumer Products Inventory (2014), there are 1628 products on the market which have been identified by industry to contain NM products (figure 1.4) and many more unlabeled nano-enabled products. Table 1.1 presents the number of the most commonly used NM containing products and figure 1.4 shows the increase of nano-enabled products from 2005-2013, showing the rapid increase over the years.

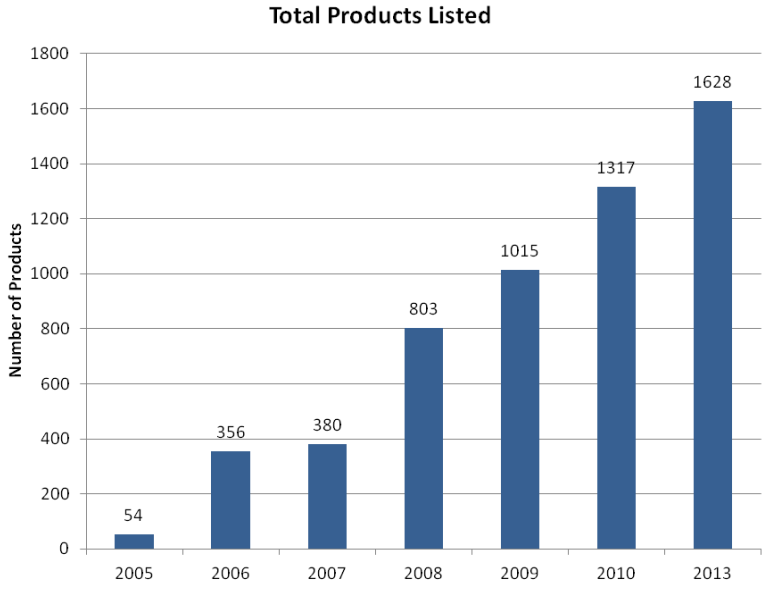

Figure 1.4: Evolution of the total number of nano-enabled products in the past decade according to the Woodrow Wilson database. Taken from: Project on Emerging Nanotechnologies Consumer Products Inventory (2014): www.nanotechproject.org/cpi/

Table 1.1: Examples of manufactured NMs used in industry and their purposes of function.

Nanomaterial	Property and Applications of Use	Commercial ?	Reference
Metals			
Silver	Antibacterial properties , added to medical products, toys and textiles particularly that of clothing to reduce odor-containing bacteria	Yes	Fabrega *et al,* 2009a, Benn and Westerhoff 2008
Gold	Developed for its catalytic activity, drug delivery systems, where synthesised NPs with controlled charge, shape and size allows them to be engineered specifically to be taken up by cells	Yes	Gu, *et al,* 2003, Fabrega *et al,* 2009a
Copper	Antibacterial properties	Yes	Rispoli *et al,* 2010
Iron	Used in groundwater remediation to immobilise heavy metals.	Yes	Phenrat *et al*,2007) Gaiser *et al,* (2009)
Oxides			
Iron Oxide	Waste water remediation treatments	No	Xu *et al,* 2012
Cerium oxide	fuel catalyst	Yes	Van Hoecke *et al,* 2012, Piccinno *et al,* 2012
Titanium dioxides	Photocatalytic processes such as solar cells, used in paint coatings, cosmetics	Yes	Piccinno *et al*, 2012, Nowack and Bucheli, 2007
Zinc Oxides	Antimicrobial and high UV absorption efficiency, used in paints and coatings	Yes	Raghupathi *et al,* (2011)Li *et al,* (2008)
Carbonaceous			
Carbon nanotubes	Crystal lattices used in nanosensors, mechanics and electrical engineering	Yes	Llobet, 2013
Fullerenes	Electro-conductivity, Thermal and optical properties	Yes	Li *et al,* (2008)
Grapheme	Electrical and conductive properties	Yes	Dreyer *et al,* 2010
Quantum dots			
Quantum dots	Imaging purposes	Yes	Piccinno *et al,* 2012

Increased production of NMs poses new concerns to environmental and health issues due to their novel properties, size and inevitability their release into the environment (Ninham, 1999). The physicochemical properties of NPs differ from their bulk counterparts, including reduced size, increased surface area and elevated surface energy, and quantum confinement, which changes the NP optical properties including surface plasmon resonance (SPR) (Ju-Nam and Lead, 2008). The risks associated with NMs are difficult to assess as their effects are poorly understood. The ways in which NM products are developed are constantly being manipulated and advancing due to changing future of nano requirements. There is also the concern that NMs do not fit under any legal framework that separate their properties from the bulk material, and because NMs are constantly revolutionising, so fourth are the risks that are associated with the NMs (Fiorino, 2010). The desired novel properties of NMs used in consumer products maybe the cause of their toxicity, although further ongoing research is yet to determine this statement.

1.2 Silver and Nanosilver

Silver (Ag) occurs naturally in the Earth's crust in many forms (such as ionic and metallic) and has high electrical conductivity and optical properties (Hammond 2010). Ag has been widely used throughout history for its antibacterial and antifungal properties (Castellano *et al,* 2007, Rai *et al,* 2009, Fabrega *et al,* 2011), and there is historical evidence to support that Ag was used as early as 3000BC (US EPA, 2010). In the 1500's silver nitrate ($AgNO_3$) was used in the treatment of abscesses and in the 1700's, Ag salts were used to treat viral diseases following up to the 1900s where it was used to promote wound

healing (Klasen, 2000, Castellano *et al,* 2007). Simultaneously, Ag salts were also used to treat burn victims (Silver, 2003) and treat patients in World War I using Ag as antiseptics (Quadros and Marr, 2010). It was only after the use of antibiotics and penicillin became more popular in the 1940s that the use of Ag in medical cases ceased (Chopra, 2007).

Before digital cameras, $AgNO_3$ was heavily used in the photographic industry for film processing which elevated environmental Ag concentrations during the 1970s (Ma *et al,* 2012, Reidy *et al,* 2013). With this in mind, on 4th May 1976 the European Commission devised a document that listed all substances that caused "Water Pollution by Discharges of Certain Dangerous Substances". Ag was then determined a pollutant and had to be regulated due to its potential toxicity (Council Directive 76/464/EEC). The Environmental Protection Agency (EPA) also listed Ag as a water pollutant in 1977 (US EPA, 2010), which resulted in a decrease in Ag concentrations in the environment. Although, increased releases of AgNPs (and their ionic counterparts as they break down), now threaten increased environmental Ag concentrations once more.

Since the advances of medicine many pathogenic bacteria have gained resistance to antibiotics and medicinal treatments (Austin *et al,* 2011). The use of Ag has recently become more popular as pharmaceutical companies develop NMs to exploit their antibacterial properties (Chopra, 2007, Cumberland and Lead, 2009, Fabrega *et al,* 2011), due to their high surface area to volume ratio and novel size (Kannan *et al,* 2011). Recent advances have seen the development of antibacterial glass which has Ag incorporated for clinical uses (US EPA, 2010). Studies have also shown AgNPs have been reported to inhibit HIV1 cell transmission and infection (Lara *et al,* 2011). Similarly, the use of AgNPs has been researched in the treatment of cancer (Austin *et al,* 2011). These medical advances

are because researchers can now specifically engineer AgNPs to have a controlled size, shape and surface coating that makes them specific for purpose (MacCuspie *et al,* 2011).

Nanosilver has now been added to many consumer products such as food packaging, textiles, plasters, bandages, and in biocidal treatments (Benn and Westerhoff, 2008, Nowack *et al,* 2011, Lem *et al,* 2012). The problem occurs when nanosilver is released as a product of waste from these goods (Fabrega *et al,* 2009a). The desired antibacterial action of Ag becomes a problem once released in the environment as nanosilver dissolves and produces ionic species that are potentially toxic to aquatic microorganisms (Lovern *et al,* 2007). Therefore, risk assessments need to be conducted in order to control the amount of NM releases into the environment (Sotiriou and Pratsinis, 2010). At current, global production of nanosilver is estimated to be approximately 320 tonnes per year (Nowack *et al,* 2011). Overall, increasing uses of AgNP products will see elevated levels of AgNPs as a waste product subsequently discharged into the environment, concentrations of Ag will need to be monitored to prevent adverse reactions to aquatic organisms (Park *et al,* 2011).

1.3 Releases of Nanomaterials into the Environment

Releases of all NMs into the environment can be from accidental release, surface run off, during production or transportation and general wear/uses of the NP containing material. One of the most likely sources for accidental run off is said to be that of NP based paints (Kaegi *et al,* 2008, Muller and Nowack, 2008). NMs are released due to the effects weather related conditions and the leaching of the NPs from exterior coatings, which are then transported to surface waters via storm water (Kaegi *et al,* 2010) and cannot be

regulated as a point source of control, as the concentrations are difficult to quantify. For nanosilver due to its specific application, the release potential will occur via waste water systems travelling downstream to lakes, rivers, ground water and even drinking water (Elzey and Grassian 2010). The potential implications for exposure will be to a number of aquatic and terrestrial organisms, including bacteria (Wigginton *et al,* 2010). Ag can be released either as a nanoparticle, colloidal aggregate or as silver ions (Ag^{+}) (Liu and Hurt, 2010).

Measurements of environmental concentrations of NPs, and releases of NPs from consumer products are mostly absent in the available literature (Gottschalk *et al,* 2009). The lack of information is mainly because funded research has concentrated its efforts on human health implications that NPs directly may impose, rather than environmental (Nowack and Bucheli, 2007). Therefore, little information is available on the transport and transformations to NPs once they are released into natural waters (US EPA, 2010). There are no methods yet developed to measure the current releases of nanomaterials into the waste water systems (Gottschalk *et al,* 2010) although, research has been conducted to attempt to predict such exposures. Benn and Westerhoff (2008) have attempted to identify the release of engineered AgNPs from socks during washing, and their fate in wastewater treatment plants. Each of the socks studies contained up to 1360 µg-Ag/g-sock and the results identified up to 650 µg of Ag in 500 mL of distilled water. Upon analysis the recovered NP diameter sizes were between 10-500 nm. The researchers used a model to predict the environmental fate into waste water treatment plants (WWTPs). Results identified that WWTPs are able to remove large quantities of silver. Benn and Westerhoff (2008) also predicted with increasing consumer usage lager

concentrations of Ag will be dispersed into the environment via agricultural fertilizing processes. It was therefore concluded that the washing of textiles containing NP products such as Ag can be released directly into sewer systems and the majority of NPs from consumer products will reach a waste water treatment plant (Benn and Westerhoff, 2008).

Further research conducted by Lowry *et al* (2012), assessed Ag transportation between soils, water and sediment using mesocosm experiments in a natural water environment. They concluded that 70% of the dosed Ag was found in the soil and sediment compartments. The movement between soils to sediments determined that 'runoff' from these embankments was a potential pathway for AgNP exposure into surface waters (Lowry *et al,* 2012).

Water quality standards are usually based on total or dissolved metal release concentrations, although this does not give adequate information on the bioavailability or the potential toxicity that could occur from exposure (De Schamphel and Jansen, 2002). Therefore with the increased use of NMs in industry, it is inevitable that the environmental and human exposure is expected to increase (Nowack and Bucheli, 2007). The way in which NMs enter the environment depends greatly upon how they are engineered, used, and disposed of. The potential pathways are explored in figure 1.5.

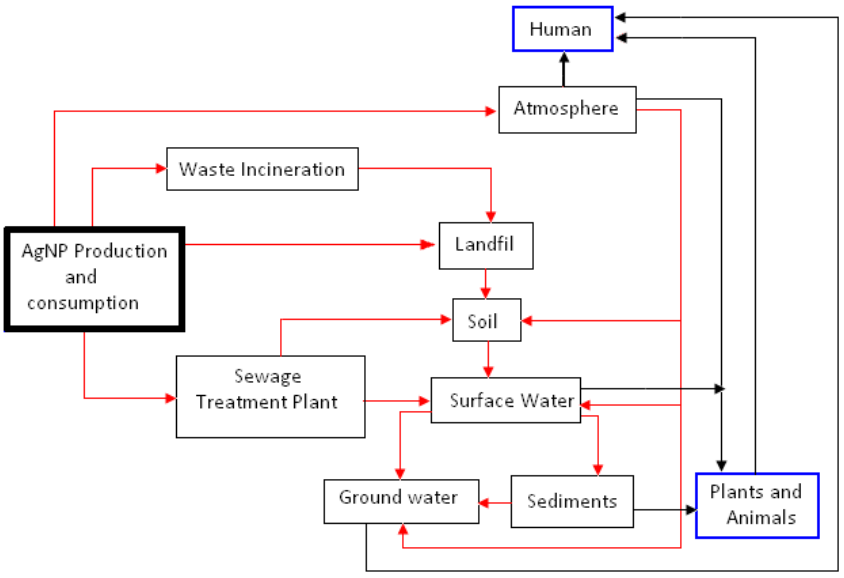

Figure 1.5: Potential sources of AgNP exposures. Red lines follow the possible pathways in which AgNPs follow before they end up in the environmental compartments. Black lines follow the human, plants and animal risk of exposure from these environmental compartments. Diagram modified from Gottschalk et al (2009) and Nowack and Bucheli (2007).

The fate of NMs in waste water treatment plants remains very important (Farre *et al,* 2008). Once discharged into waste waters can either be treated by sewage treatment plants, where small amounts can be released untreated via effluents or be released into natural surface waters (See Figure 1.5) (Kaegi *et al,* 2008). Sewage sludge is normally applied to agricultural land. The department for environmental, food and rural affairs states that 75% of sludge is used as a fertilizer and small quantities of sludge are disposed of in landfills. Therefore, release into the environment from applications in agriculture also needs to be considered (Koelmans *et al,* 2009, Gottschalk *et al,* 2010b), due to risks of NM exposure to vegetation for human consumption (Fabrega *et al,* 2009a). However, if the NMs still remain in the sewage sludge after treatment and is sent to landfill, there is potential exposure into local soils and groundwater creating further environmental

contamination (Blaser *et al,* 2008). Overall, NPs and imperfections to the manufactured particles need to be considered for their transformations and transport into environmental compartments, potential hazards, and exposure risk to humans (Nowack and Bucheli, 2007).

1.4 Synthesis and Modifications to AgNPs

Being able to synthesize stable NPs of known size, stability, morphology, and chemical functionality, can provide the basic understanding NM transport and behaviour that can be used to model environmentally relevant conditions (Fabrega *et al,* 2011).

1.4.1 Synthesis

Manufactured NPs are attempting to control the synthesis and physicochemical aspects of the NPs for their use in industrial products, via appropriate synthesis techniques that concentrate on the size distribution to fit the function of purpose. The physicochemical properties of NPs such as the size, shape and surface coatings will determine the fate and toxicological impact of the NPs once released into the environment (Reschiglian *et al,* 2010). Three different strategies are currently being used to synthesis NMs: (1) top-down physical methods, (2) bottom up chemical approaches (figure 1.6) and (3) biosynthesis using organisms to produce NPs.

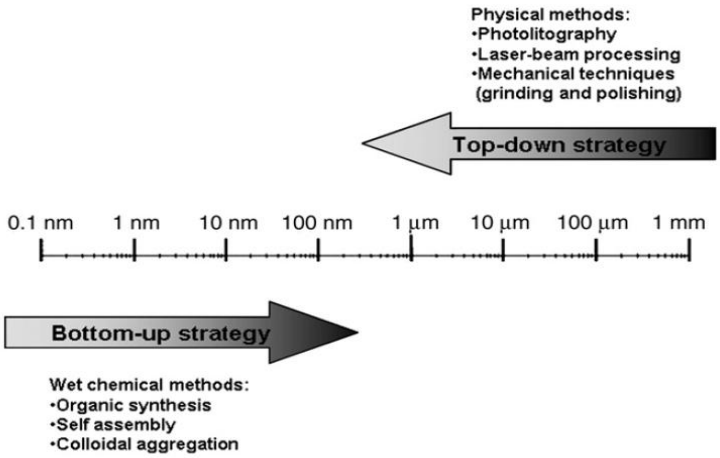

Figure 1.6: ***Top-down bottom-up strategies of synthesis. Picture: Ju-Nam and Lead (2008).***

Top-down methods produce particles and colloids via physical methods such as grinding, quenching or milling from the bulk material (Ju-Nam and Lead, 2008). Bottom up methods are the most preferred methods to synthesise NP suspensions and use wet chemical approaches in the presence of metal salts, reducing agent and a suitable surface stabilizer (Tolaymat *et al,* 2010, Stamplecoskie and Scaiano, 2012). The experimental design of NP synthesis largely controls parameters such as the size, shape, stability and reactivity of the particles (Kannan *et al,* 2011). Size, shape and structure are controlled by the order in which the chemicals are added, concentrations of reagents, capping agents, reaction temperature and continuous stirring which can be adjusted accordingly. The first description of silver colloids was in 1889 by Carey Lea, who used the reduction of the Ag salts with a reducing agent to form Ag atoms, which cluster together to form colloidal Ag (Henglein and Giersig, 1999, Doty *et al,* 2005). $AgNO_3$ and sodium borohydride ($NaBH_4$) have widely documented in the literature as the most common agents used to produce AgNPs. Ag seeds are produced in the reduction of $AgNO_3$ (Figure 1.7) which agglomerates to form clusters that grow depending upon the controlled reaction conditions and addition of the capping agent (Pillai and Kamat, 2004).

It is particularly important that AgNPs are synthesised as small and as monodispersed as possible, due to AgNPs specific function for antibacterial purposes. Aggregation during synthesis will give larger polydispersed suspensions, and therefore the antibacterial action of the AgNPs is reduced as larger particles can't pass through bacterial cell membranes (Li *et al,* 2012). To avoid polydispersed suspensions, the particles are stabilised with capping agents which will have considerable effects upon the growth, aggregation and will determine the size of the particles produced (Henglein and Giersig 1999, Fabrega *et al,* 2011).

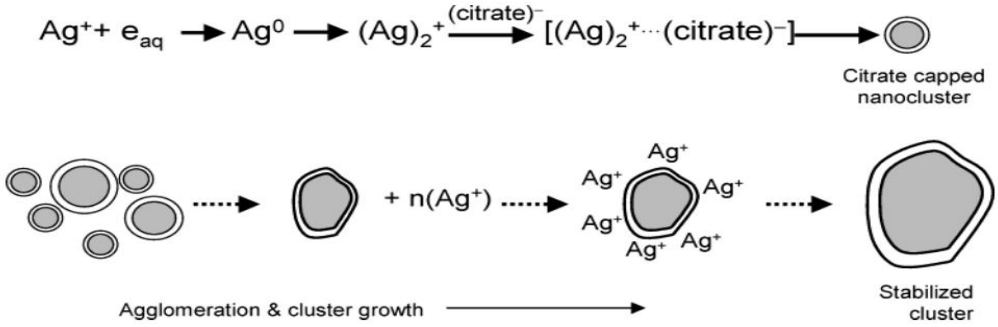

Figure 1.7: The mechanism of how silver nanoparticles are produced with a citrate stabilizer. Silver seeds are produced in the initial reduction step. With the addition of the charged ionic species (citrate) the seeds form a cluster encapsulated within the citrate coating. Figure extracted from Pillai and Kamat (2004).

1.4.2 Surface Coatings

The ultimate purpose of the capping agent is to increase stability by reducing the surface energy (Ju-Nam and Lead, 2008) and increase electrostatic and steric repulsion. Capping agents help to prevent and reduce NP interactions with the surrounding environment, avoid NP-NP interactions, and reduce aggregation by repelling neighbouring molecules from each other (Kvitek *et al,* 2008). Electrostatic repulsion occurs as charged ionic

species stabilise the particles to create a charged surface layer. The charged surface layer repels other NPs in suspension away and thus reduces aggregation in suspension. The extent of the strength of repulsion depends on how thick the particle is coated (Kvitek *et al,* 2008). Examples of such coatings include citrate (Henglein and Giersig, 1999, Doty *et al,* 2005, Cumberland and Lead, 2009, Fabrega *et al,* 2011) and sodium dodecyl sulfate (SDS) (Li *et al,* 2012). Steric repulsion occurs when non-ionic species or polymers coat the particle surface to stabilize the NP suspensions. Examples of polymer coatings include, poly(vinylpyrrolidons) (PVP), polyethylene glycols (PEG) (Radziuk *et al,* 2007), poly(vinylalcohols) (PVA) (Choi and Hu, 2008), and polyacrylamides. Tween has also been previously used as a surface stabilizer (Kvitek *et al,* 2008). Figure 1.8 illustrates the different types of stabilization mechanisms.

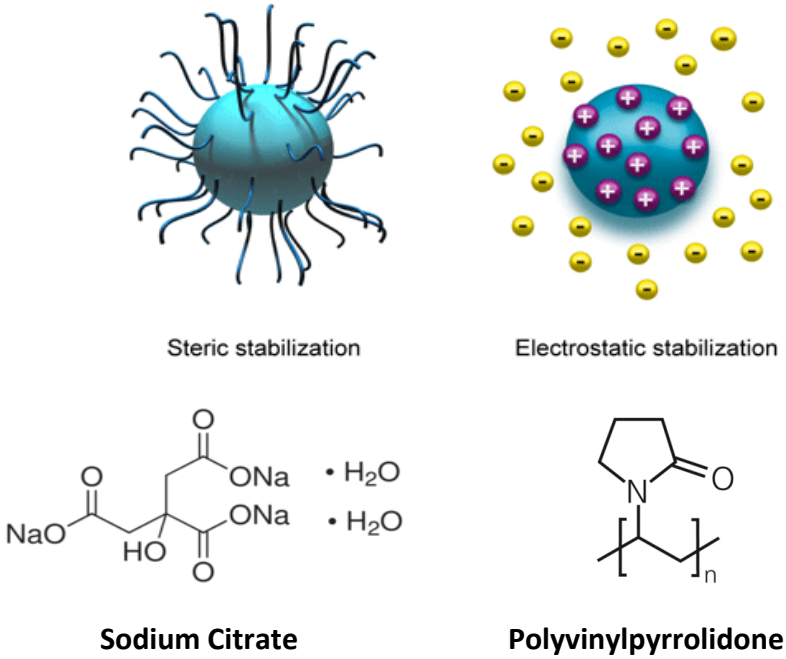

Figure 1.8: Particle stabilization differences with examples of chemical structures of steric and electrostatic capping agents.

Picture from: http://www.malvern.com/labeng/industry/colloids/dlvo_theory.htm

Citrate structure: http://www.sigmaaldrich.com, PVP Picture from: http://www.sigmaaldrich.com.

The strength of the interaction between the surface coating and the surface of the NP determines the behaviour and toxicity of NPs in the wider environment, especially when the NP comes into contact with substances such as NOM, which has the affinity to replace the existing surface coating (Fabrega *et al,* 2011). Little is known in the literature about how these surface coatings affect particle aggregation once released into the environment, or how they determine the fate of AgNPs. Although, a recent paper by Auffan *et al,* (2014) identified that with aging, citrate functional groups were de-protonated under illuminated conditions, suggesting that light sources can be likely co-factor in the degradation of the citrate surface coating.

1.5 Fate and Behaviour of AgNPs in the Environment

The fate and behaviour of NPs in environmental systems are determined by key factors such as dissolution, sedimentation, aggregation, deposition, phase transformation and NP surface properties. All of which may affect the colloidal stability and overall partitioning between environmental compartments. The fate and behaviour will help determine the bioavailability and toxicity of NPs (Farre *et al,* 2008). Below is a discussion of these key processes.

1.5.1 Dissolution

Dissolution refers to the release of ions from the NPs, and the dissolution rate refers to how fast they dissolve to produce the ions. Dissolution has an impact upon NP transportation and their overall environmental fate (Miao *et al,* 2009) which is dependent on size, shape, and surface chemical properties (such as surface coatings) (Zhang *et al,*

2011 b, Misra *et al,* 2012). The ionic form of the NP will also have a different fate, effect, and transport compared to the original NP (Li and Lenhart, 2012). Other physicochemical parameters from the surrounding aqueous medium such as pH, ionic strength (Baalousha, 2009, Elzey and Grassian, 2010, Ma *et al,* 2012), dissolved oxygen (DO) content (Zhang *et al,* 2011) and ligands, for example natural organic matter (NOM) chlorine (Cl) and sulfur (S) will also affect the dissolution rate.

The DO content is particularly important as AgNPs released into aerobic aqueous environments, such as surface natural water, will be subsequently oxidised (Li and Lenhart, 2012). High DO content combined with low pH provides optimal conditions (figure 1.9) for oxidation processes (Liu and Hurt, 2010). Oxidation of AgNPs results in the release of Ag^+ (Li and Lenhart, 2012) and will change the morphology of the NPs (Zhang *et al,* 2011). Therefore, the DO concentrations contribute to the dissolution via oxidation at the surface of the AgNPs as seen in figure 1.9.

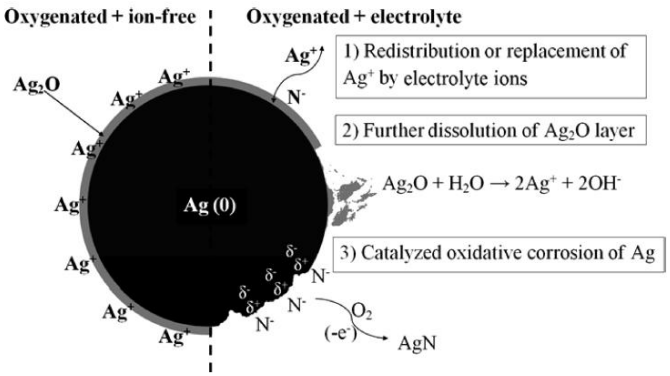

Figure 1.9: An example of an uncoated silver nanoparticle with a surface oxide layer showing how dissolution and surface oxidation occurs. Picture extracted from (Li and Lenhart 2012).

A further influencing factor on AgNP dissolution is in the presence and absence of light. Since Ag is light sensitive, photochemical oxidation in the presence of light can induce NP

dissolution (Kim *et al,* 2008 and Wodka *et al,* 2010). Studies by Wodka *et al* (2010) deposited AgNPs on a titania surface to act as a photocatalyst and observed that in the presence of light oxidation was facilitated. Literature suggests that depending on the media in which NPs are dispersed, exposure to NOM increases dissolution by acting as ligand. NOM can also reduce the dissolution process via steric protection due to re-capping (Misra *et al,* 2012). Liu and Hurt (2010) conducted ion release studies on AgNPs exposed to natural sea water in the presence and absence of humic and fulvic acids. They discovered that increasing temperature resulted in increased dissolution. In addition, increased pH in the presence of humic and fulvic acids, resulted in reduced dissolution (Liu and Hurt 2010).

Aggregation and agglomeration of the NPs in suspension will affect the dissolution rate as the surface area and dynamics of the NP will change, leading to increased size and reduced surface area (Hotze *et al,* 2010, and Misra *et al,* 2012). Many studies have looked at the dissolution of AgNPs in simple aquatic media and aggregation of citrate coated AgNPs with the influence of NOM and ionic strength (Bae *et al,* 2013). Further studies have focused on the dissolution of AgNPs to help identify differences between NP and ion specific toxicity (Zook *et al,* 2011, Linlin and Tanaka, 2013). However, there is still an absence of information on the AgNP dissolution behaviour in the presence of NOM (Linlin and Tanaka 2013) in a synthetic water standard.

Dissolution rates are important in assessing NP transport and behaviour of AgNPs, as the ionic species have been demonstrated to form NP surface complexes, particularly with chloride, sulphate and sulphide species (Ha and Payer, 2011). AgNPs can also form complexes with these electrolytes under environmental conditions which will alter the

dynamics of the NP species affecting the dissolution rate (Quadros and Marr, 2010, Levard *et al,* 2013). The dissolution of a particle is size dependant, the smaller the NP the higher the surface area and surface reactivity (Ma *et al,* 2012). Therefore, the tendency to dissolve increases, as particle size decreases (Misra *et al,* 2012). An important factor to consider is that AgNPs are typically synthesised with surface stabilisers, which can remain stable (depending on the type of coating) in solution and can reduce the dissolution rate, compared uncapped particles (Kvitek *et al,* 2008, Zhang *et al,* 2011b). Shape and crystalline structure will also affect how quickly the NPs dissolve.

1.5.2 Diffusion and Sedimentation

In stagnant water systems, NPs are transported by diffusion, and/or sedimentation. Diffusion occurs due to the difference of NP concentration between the different water compartments (surface, middle or bottom), whereas sedimentation occurs following NP aggregation. Ficks Laws of diffusion, which was first described in 1855, states that particles of a high concentration move to areas of a low concentration gradient until they are evenly distributed (Fick, 1855, Gorban *et al,* 2011). Diffusion is one transport mechanism used to describe the movement of NPs when exposed to an aqueous suspension. The movement can be explained by a diffusion coefficient which depends on particle size and viscosity of the media (Eq 1.1).

$$D = \frac{\mathrm{RT}}{3\mathrm{N_A}\,\pi\mu\,\mathrm{d}}$$

[Eq 1.1]

Where D is the diffusion coefficient (m^2s^{-1}), R is the gas constant (L.kPa K mol), T is temperature, N_A is Avogadro's number, viscosity of the solution μ (Pa.s) and d is the

particle diameter (m). Hinderliter *et al* (2010) described the sedimentation of NPs in cell culture systems. Together they produced a computer model that describes the speed at which NPs settle in order to predict the *in vitro* cellular dose of NPs as seen in figure 1.10. According Stokes Law:

$$U = \frac{g\,(\rho_p - \rho_f)\,d^2}{18\mu}$$

[Eq 1.2]

Where the sedimentation velocity of particles in solution is *U* (ms^{-1}), g refers to the gravitational force ($m\ s^2$), particle density is ρ_p ($km\ m^3$), fluid density is ρ_f, the particle diameter is d (m) and the viscosity of the solution media is termed μ (pa.s) (Hinderliter *et al,* 2010). The diffusion-sedimentation transport of NPs can be described by applying the partial differential equation (Eq 1.3) (Mason and Weaver 1924). The right hand side of the equation describes the diffusion and sedimentation of the particles as seen in Ficks Law (Socolofsky and Jirka, 2004) and is written as:

$$\frac{\partial c}{\partial t} = D\frac{\partial^2 c}{\partial z^2} + U\frac{\partial c}{\partial z}$$

[Eq 1.3]

Where *c* is the concentration of the solute ($g\ mL^{-1}$), *t* is time (s), *z* is distance from the source (m), D is the diffusion coefficient, and *U* is the sedimentation velocity (Mason and Weaver, 1924). The boundary condition and the solution of the diffusion-sedimentation equation are presented in chapter 2.

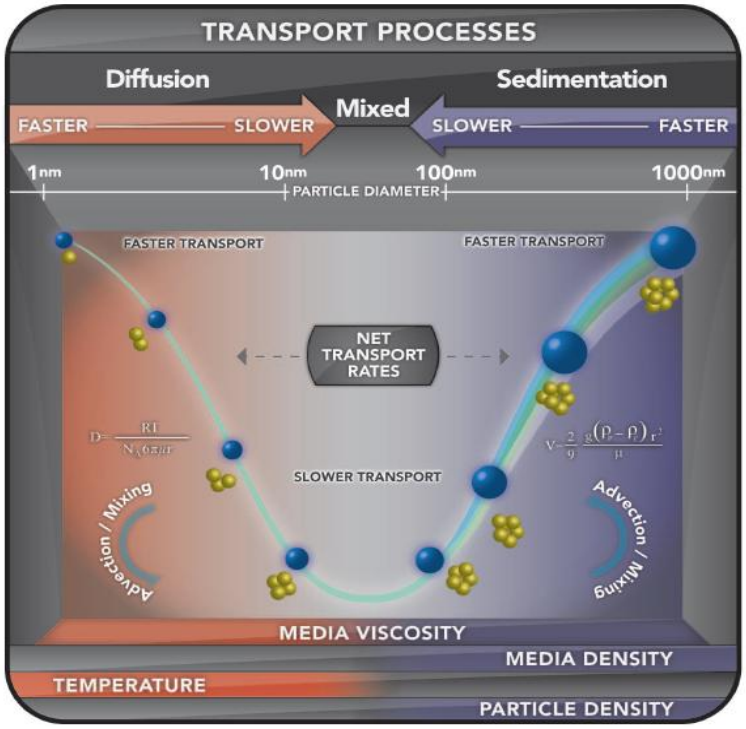

Figure 1.10: Diffusion and sedimentation transport processes of NPs, combined with the problems that affect transportation once exposed to an aqueous media. Figure courtesy of Hinderliter et al (2010).

As described in figure 1.10, the diffusion-sedimentation of the NPs will affect the transport process in terms of time and speed. The larger the NP the slower it will travel due to sedimentation. Equally, the smaller the NP, the faster it will move due to diffusion. Simple ionic exposure solutions have revealed that when NPs are exposed to aqueous environments they tend to aggregate which significantly affects their sedimentation and diffusion rates (Keller *et al,* 2010). Sedimentation and diffusion will further depend on the physicochemical properties of the AgNPs. In simple ionic solutions, polymer coated AgNPs have been demonstrated to remain stable (Tejamaya *et al,* 2012). Therefore, the aqueous conditions need to favour aggregation of AgNPs in order to have effects upon the sedimentation and diffusion rates.

Overall it is has been shown that the combined effects of adsorbed NOM (Li and Sun, 2011), pH, size, shape (Keller *et al,* 2010) and ionic strength (Li and Chen, 2012) all effect particle aggregation, which defines the diffusion/sedimentation rates and bioavailability of the nanoparticles**.** Eventually, in a natural water system sedimentation will determine the fate of these nanomaterials (Nowack and Bucheli 2007), especially aggregated particles, as they are less mobile and are more likely to be dispersed into sediments (Keller *et al,* 2010). Sedimentation creates potential problems as NPs can be taken up by small organisms feeding in the sediment, or accumulates in plants growing in this area (Nowack and Bucheli 2007).

1.5.3 Aggregation and Deposition

Aggregation is the interaction of two particles in suspension which occurs due to electrostatic forces of attraction, known as of van der Waals forces. Ionic species in solution which have a high valance occupancy, will be attracted to the NP surface charge (Grasso *et al,* 2002) which will allow them to agglomerate together to form larger structures (Navarro *et al,* 2008). Naturally occurring particles are dominated by the processes of aggregation and deposition, therefore it is essential that these processes are understood in order to define the behaviours of manufactured NPs (Lead and Wilkinson, 2006). Factors that can affect aggregation include solution chemistry such as pH, temperature, NOM presence/concentration, and salinity/ionic strength (Li and Lenhart, 2012). Fulvic and humic acids have the ability to absorb onto the NP surface and increase stability, resulting in reduced aggregation. Whereas, increasing ionic strength reduces the electrostatic diffuse double layer, resulting in increased aggregation (Romer *et al,* 2011).

According to Zhang *et al* (2011), the presence of DO in an aqueous system will have a significant effect on the aggregation rate of AgNPs. The researchers observed the AgNPs in the presence of DO aggregated at a rate of up to 8 times faster than those that were absent of DO and discovered that the hydrodynamic diameter decreased in size (Zhang *et al,* 2011). Other factors that dominate aggregation are the physicochemical properties of the NP such as their surface coatings. Surface stabilizers can enhance both electrostatic and steric repulsion, which reduce NP aggregation (Li *et al,* 2011). Once released into the environment many researchers have predicted that NPs will have a tendency to aggregate due to the effects of solution chemistry as discussed above (Liang *et al,* 2007).

Deposition is the connection and attachment of a moving particle to a static object (Navarro *et al,* 2008). Deposition is particularly useful when determining the transportation of NPs in a porous media, where NPs become embedded and re-entertained at a later period. The effects of deposition can be altered via solution chemistry such as pH changes and NOM. Particle deposition rates will increase as ionic strength increases (Li *et al,* 2011). When the ionic strength increases, the diffuse layers that surround the particles in suspension are reduced and the electrostatic repulsion is reduced. Adsorption of NOM onto the particle surface has been seen to reduce deposition of particles in suspension, and rate of re-entertainment of particles back into suspension has been shown to enhance in the presence of NOM (Franchi and O'Melia, 2003). Particle stability and surface interactions are described in the literature by the Derjaguin-Landau-Verwey-Overbeek (DLVO) theory, which defines the attractive and repulsive interaction energy between particles (Grasso *et al,* 2002).

1.5.4 DLVO Theory

The DLVO theory was first developed in the 1940s. It was traditionally used to describe the aggregation of spherical particles in an aqueous environment and define the interaction forces between charged particles (Li *et al,* 2012). Particles are surrounded by an electrostatic diffuse double layer, known as long range interaction forces. Combining forces of attraction (van der Waals) and the diffuse double layer of repulsion will determine particle stability (Liang *et al,* 2007, El Badawy *et al,* 2011). Assumptions are made that all the interacting surfaces are equally the same with a uniform surface charge distribution (Esmaeili *et al,* 2012) and the solution in which the particles are suspended contains only simple electrolytes (Li *et al,* 2012).

In principle, particles in solution are under Brownian motion, which describes the random movement of particles in solution. The DLVO theory applies when the electrolyte concentration of the solution is changed, resulting in the change in surface potential of the particles (Liang *et al,* 2007, Li and Chen, 2012). The change in surface potential changes electrostatic forces, which then overcome the repelling forces between the particles and thus aggregation occurs (Grasso *et al,* 2002). The DLVO theory sums up the total interaction energy between the surfaces of the particles and can be written as:

$$V_T = V_A + V_R \qquad \text{[Eq 1.4]}$$

Where V_T is the total interaction energy between the particles, V_A is the repulsive double layer energy, and V_R is the van der Waals energy. The force of V_R must be larger than V_A for aggregation to take place. V_R is mostly insensitive to changes to the solution chemistry such as pH and salinity (Liang *et al,* 2007). An example of the DLVO theory and the challenges encountered are illustrated in figure 1.11.

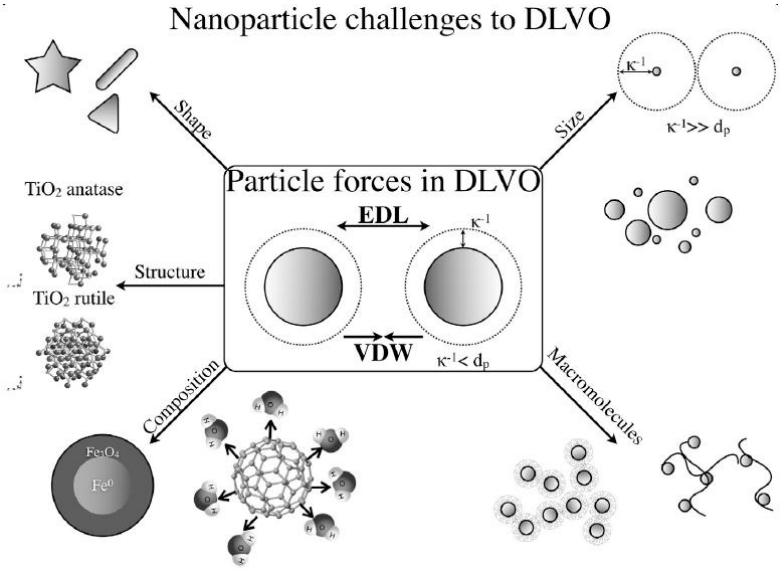

Figure 1.11: Extracted from Hotze et al (2010): Two spherical particles in suspension under van der Waals forces (VDW) and electrostatic double layer forces (EDL). Surrounding are the conditions that are presented additionally to these forces that affect the traditional DLVO theory (Hotze et al, 2010).

Changes in surface charge are caused by interactions between charged species on the NP surfaces. When ionic species adsorb onto the NP surface they cause additional physicochemical interactions between the two solid particle surfaces which are beyond the scope of the repulsion and attraction forces described by DLVO (Taboada-Serrano *et al,* 2005). Debye length (K^{-1}) (figure 1.11) defines the thickness of the diffuse electrical double layer surrounding the particle (Eq 1.5) which can be altered by changes in ionic strength.

$$K^{-1} = \left(\frac{\varepsilon_o \, \varepsilon_r k_g T}{e^2 2 N_A I} \right) \qquad \text{[Eq 1.5]}$$

Where ε_o is the vacuum permittivity, ε_r is the dielectric constant, k_g is the Boltzmann's constant, T is temperature (K), e is the elementary charge, N_A is Avogadro number and I is ionic strength. When the electrolyte concentration is increased, the Debye length is thus

reduced. For a 10 nm particle the Debye length is around equal to the particle diameter (10-12 nm), explaining why the hydrodynamic diameter over estimates particle size when analysed by DLS.

Additionally, further interaction forces are encountered in natural water such as hydration forces (Liang *et al,* 2007), hydrophobic forces and steric forces, otherwise known as non-DLVO forces (Lee *et al,* 2011), or extended DLVO theories (Boström *et al,* 2006). Steric repulsion occurs as a result of surface coating of the NPs by organic molecules or polymers (Kvitek *et al,* 2008). Non-DLVO forces are short ranged (Liang *et al,* 2007) as particles interact with each other based upon size, the smaller the particles the larger the NP-NP interactions.

1.5.5 Nanoparticle Surface Properties

Surface properties of NPs are one of the most important factors determining the stability and mobility of NPs (Navarro *et al,* 2008), including surface coatings and surface charge. These will dominate how the particles react when released into aquatic systems. Solution chemistry such as the pH, dissolved carbon, NOM, DO and the initial ionic/electrolyte strength of the water will also interact with the NP surface and affect NP behaviour (Baalousha, 2009, Romer *et al,* 2011). Surface charge provides a surface force which can be used to exploit surface stabilisers via steric and electrosteric forces, or provide a means of ligand interaction with artefacts such as NOM in the surrounding aqueous environment (Kvitek *et al,* 2008, and Fabrega *et al,* 2011). Surface stabilisers are used to provide and maintain stability of the metallic NPs, which can be either organic or in-organic (Navarro *et al,* 2008). The role of the surface coating is discussed in more detail

further in this chapter. The nature and surface chemistry of the NPs will largely effect which compartment the NPs are dispersed within the environment, e.g. surface water or sediment, each of these variable factors will contribute to the NP environmental behaviour, fate and toxicology (Farre *et al,* 2008).

1.6 Impact of Environmental Conditions on the Fate and Behaviour of AgNPs

Transformations of AgNPs will highly depend upon the local environment in which they are released. Depending on the aqueous conditions, the physicochemical properties of AgNPs will change in terms of surface structure, reactivity and composition (Levard *et al,* 2013). It is likely that AgNPs in the environment will become associated with NOM, or form complexes to sulfide (Lowry *et al,* 2012) and chloride compounds (Ha and Payer 2011). Therefore, the effects of the environmental conditions to which AgNPs are exposed needs to be assessed to help determine the overall transportation and fate of AgNPs.

1.6.1 Effects of Environmental Water Chemistry

Ionic strength of the aquatic system in which the NPs are dispersed is particularly important (Jiang *et al,* 2009). Increased ionic strength will result in the reduction in the diffuse double layer and alters surface charge, enabling NP aggregation (Navarro *et al,* 2008, Romer *et al,* 2011). Additionally, the presence of monovalent and divalent cations has been demonstrated to have a destabilizing effect on the surface charge of the NPs (Li and Sun, 2011), particularly that of divalent cations such as, calcium (Ca^{2+}) and

magnesium (Mg^{2+}) increase aggregation (Zhang and Oyanedel-Craver, 2012). Changes in pH will change in the NP surface charge and impact the rate at which particles aggregate. Acidic conditions have been shown to increase the rate off aggregation by reducing the surface charge density in citrate stabilized AgNPs (El Badawy *et al,* 2010).

In aqueous environmental systems, AgNPs form complexes with electrolytes such as sulphide groups and chloride by acting as an electron donor (Blaser *et al,* 2008, Allen *et al,* 2010, Quadros and Marr, 2010, Levard *et al,* 2013). Several studies have identified the effects of simple solution chemistry on particle behaviour and differences in capping agents (Romer *et al,* 2011 and Tejamaya *et al,* 2012). Other studies have concentrated on the effects of NOM on AgNP behaviour in presence of simple electrolytes (Akaighe *et al,* 2012, Bea *et al,* 2013). Until recently, studies were mainly unavailable that combined the complexity of a natural environmental system to observe the environmental transformations to AgNPs. Lowry *et al,* (2012) observed the changes and transportation of AgNPs when spread on terrestrial soils and surface natural waters using mesocosm studies in a natural wetland environment. The researchers identified around 50% of the AgNPs exposed to terrestrial soils and sediments were transformed to silver sulfhydryl compounds (Ag_2S), which reduced the amount of ionic silver in solution. Therefore, sulfidation of AgNPs was shown to reduce dissolution (Lowry *et al,* 2012).

Less complex studies have been conducted to identify the role of chloride in environmentally relevant conditions and its effects of AgNP transformations. AgNP transformations are hard to assess as there are many configurations of AgCl complexes that can be formed depending on the ratio of chlorine to silver in solution, which reduce

the toxicity and availability of the NP (Blaser *et al,* 2008). Ag can be oxidised in the presence of chloride in solution to form AgCl (Ha and Payer, 2011):

$$Ag + Cl^- = AgCl + e^- \quad \text{[Eq 1.6]}$$

Levard *et al,* (2013) attempted to assess the effects of chloride on AgNPs and discovered that the presence of chloride in small amount reduces AgNP dissolution.

1.6.2 Effects of Natural Organic Matter (NOM)

The presence of NOM can have effects on surface charge, particle aggregation, stability and influence the fate and transport of NPs (Manciulea *et al,* 2009). NOM describes all naturally occurring organic materials in the environments and can be distinguished by several different types of compounds. The first can be described as biopolymers, produced as biological waste by bacteria and algae. The second type is known as humic substances (Diegoli *et al,* 2008). Humic substances (HS) can be sub categorised into humic acids (HA) and fulvic acids (FA). HA are organic matter of soils and peats. FA is produced by the degradation process of plants and has higher oxygen contents than those of HAs (Adegboyega *et al,* 2013). The last sub-category refers to non-humic substances (Buffle *et al,* 1998).

Approximately 30-50% of NOM in natural aquatic systems is FA and has 50-60% total carbon content. FA is a mixture of high molecular weight organic matter which has several functional groups which can interact with metallic cations to increase their presence (Akaighe *et al,* 2012). The additional presence of the oxygen functional groups with the combination of high carbon content will influence the overall fate and behaviour of NPs as they move through natural environments (Li and Sun, 2011). It has been seen that NOM has the ability to coat the NP surface and enhance stability and persistence

(Cumberland and Lead 2009, Bae *et al,* 2011). Adsorption of the NOM on to the particle surface can take place by several different interactions such as hydrophobic interactions, electrostatic interactions and hydrogen bonding depending on the surface charge (Navarro *et al,* 2008).

Studies by Diegoli *et al* (2008) and Baalousha *et al* (2009) reported findings of surface interactions between nanomaterials and humic substances, and found the presence of humic substances resulted in the changed behaviours of the NPs and increased size. Surface adsorption of NOM is seen in figure 1.12 where HA is used as an example (Bae *et al,* 2011).

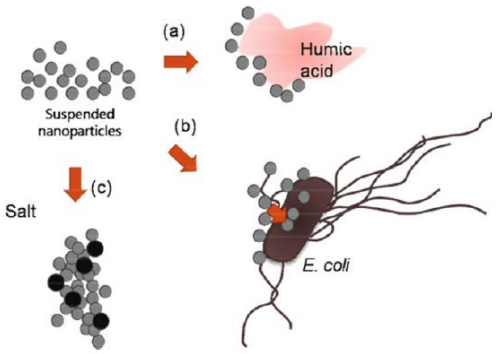

Figure 1.12: An example of NPs released into the environment and possible interactions with constituents found in natural aqueous environments. Suspended APs are exposed to a) humic acids, b) bacteria and other living organisms, and c) salt. Each exhibit a different behavioural reaction for the NPs. Humic acids adsorb on to the particle surface, reducing aggregation, whereas high salt concentrations induce aggregation. The humic acids NPs are attracted to the surfaces of living organisms and bacteria. Picture extracted from Bae et al (2011).

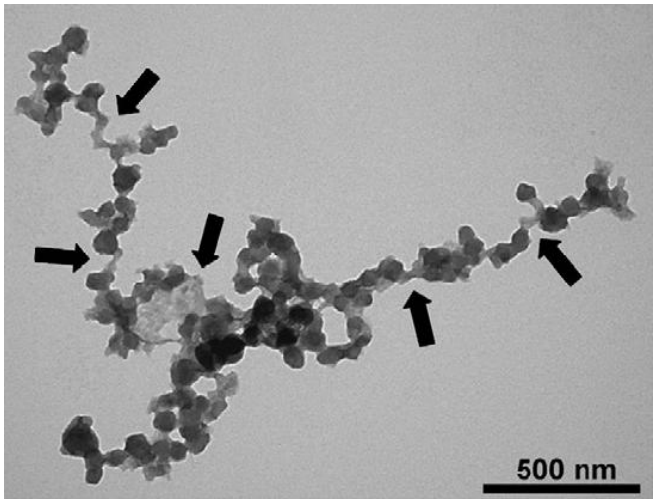

Figure 1.13: A TEM image of fullerene aggregates in the presence of 1 mg L^{-1} humic acid in a high ionic solution (40 mM) $CaCl_2$. The arrows indicate the humic acids linking the aggregates together. Picture source: Chen and Elimelech (2007).

Re-coating NPs reduces aggregation as the presence of the NOM on the particle surface increases the electrostatic repulsion. Increased stability of NOM coated NPs has also been demonstrated when in the presence of monovalent electrolyte environments such as chlorine (Cl^-) (Li and Sun, 2011). In complex mixtures that contain divalent electrolytes, such as Ca^{2+} and Mg^{2+}, NOM can either enhance the stability at low electrolyte concentrations, or decrease the stability at high electrolyte concentrations (Adegboyega *et al,* 2013). An example of destabilisation by humic acids in a high ionic solution is seen in figure 1.13.

As different aquatic systems have higher concentrations of NOM than others, once NPs are released into natural waters they will interact with NOM which will have a major effect upon their transport, fate and behaviour (Navarro *et al,* 2008). NP interactions with NOM such as polysaccharides with a higher molecular weight will cause the particles to be removed into the sediment.

1.7 Conclusion

The problem with laboratory studies is that they tend to expose the test subject to large quantities of the test solutions/media and realistically these are not relevant to environmental conditions or concentrations. Previous studies have been conduced based on small scale laboratory experiments that expose the test subject to large quantities of NPs which does not represent real environmental exposure concentrations. Once released, AgNPs will undergo a number of transformations such as aggregation, oxidation, sulfidation and chlorination depending on the surrounding solution chemistry (Hinderliter *et al,* 2010). Furthermore, AgNPs will interact with NOM (Bae *et al,* 2011) which will determine their stability. Each of these combined factors will decide which aquatic compartment the AgNPs will reside.

Further questions also arise as the effects that AgNPs could potentially have on ecosystems as a result of environmental releases (Miao *et al,* 2009). Few studies are available on how these NPs behave once dispersed into fresh water systems or how NP interactions with environmentally relevant conditions on a large scale. Little information exists about the stability, morphology or the kinetics of particles exposed to environmental waters over a long period of time (Fabrega *et al,* 2009b).

1.8 Research Aims and Objectives

The overall aim of the PhD is to understand the fate and behaviour of AgNPs in aquatic systems under environmentally relevant conditions, which will be achieved by meeting the following objectives:

1. To synthesize and characterise AgNPs with different surface coatings (for example citrate and PVP coated AgNPs).
2. To investigate the impact of surface coating on the behaviour and transport of AgNPs.
3. To understand the impact of NOM (SRFA) on the behaviour and transport of AgNPs in simple ionic media.
4. To investigate the behaviour and transport of AgNPs in natural lake water and identify patterns in behaviour in terms of the sedimentation and diffusion of AgNPs.

Objective 1 of this study will be to produce stable AgNPs that are monodispersed, using a reproducible methodology. To achieve stable particulates, parameters of the experimental procedure such as temperature, concentration of reducing agent and stabiliser concentration will be carefully controlled. Stable citrate and PVP AgNPs synthesised and characterised in chapter 3 were used for investigative studies in chapter 4 and 5.

Objectives 2-4 will be achieved by investigating the transport of AgNPs in mesocosms. The transport of the AgNPs in the column will be tracked by measuring the total Ag concentrations and UV absorbance, at different depths of the mesocosm (surface, middle and bottom) and at different time intervals. Chapter 4 will focus on the behaviour of AgNPs in simple synthetic waters and assess the effects of the FA on the stability of the NPs compared to studies without FA. Chapter 5 will determine the transport behaviour in seasonally changing lake water. Focuses will be on measuring and reporting the carbon content, and changing ionic strength of the water as the seasons change to assess differences or patterns in AgNP behaviour and transport in the mesocosms. Total and dissolved Ag concentrations will be measured in the different depths of the mesocosm to identify if AgNPs in the surface water behave differently to those at the bottom of the mesocosm.

Chapter 2 Methodology

2 Chapter Outline

This chapter presents the methods used for (i) the synthesis of AgNPs, (ii) the analytical methods used to identify the changes in physico-behaviour and stability of AgNPs, when exposed to simulated environmentally relevant conditions and (iii) the approaches used to study the stability transport of AgNPs in the aquatic environment. Citrate and PVP capped AgNPs were synthesized in house and fully characterised (described further in chapter 3). Since there are many different characterisation techniques available that have their own advantages and limitations, the best suitable techniques were used to perform the experimental analysis outlined in this thesis.

Purification of newly synthesized AgNPs was conducted by ultrafiltration and filtration techniques. Ultrafiltration was also used to determine the proportion dissolved Ag during dissolution measurements. Presence and movement of Ag in solution was determined by UV-visible spectroscopy (UV-Vis). Hydrodynamic size of the NPs was confirmed by dynamic light scattering (DLS) and flow field flow fractionation (Fl-FFF), while the core size was determined by atomic force microscopy (AFM) and transmission electron microscopy (TEM). Energy dispersive X-ray (EDX) and inductively coupled plasma mass spectrometry (ICP-MS) provided information on the elements present in solution, while ICP-MS gave further elemental concentrations. Total Ag concentrations were determined by flame atomic absorption spectrometry (FAAS). Natural water samples were further analysed for the total organic carbon content (TOC). The stability and

transport of the AgNPs was assessed using large scale mesocosms. AgNPs were exposed to simple ionic and NOM (SRFA) containing waters (chapter 4) followed by seasonally changing natural water discussed later in (chapter 5).

2.1 Materials

2.1.1 Chemicals and Reagent Storage

All chemicals used in this project were purchased from Sigma Aldrich and Fisher Scientific of analytical reagent grade. Table 2.1 lists all the chemicals used to make the solutions used in this thesis.

Table 2.1: Lists all the Chemicals and Reagents Used

Table 2.1: All chemicals and Reagents			
AgNP synthesis	**EPA Water**	**Natural Organic Matter (NOM)**	**Acid solutions**
Silver Nitrate ($AgNO_3$)	Sodium Bicarbonate ($NaHCO_3$)	Suwannee River Fulvic Acid (SWFA) Purchased from the International Humic Substance Society (IHSS)	Nitric Acid (HNO_3)
Sodium Borohydride $NaBH_4$	Calcium Sulfate Dehydrate ($CaSO_4.2H_2O$)		
Sodium Citrate	Magnesium Sulfate ($MgSO_4$)		
Polyvinyl pyrrolidone (PVP10)	Potassium Chloride (KCl)		

All solutions were made using ultrapure water (UPW) at a resistivity of 18.2 Ω. Glassware, ultrafiltration cells and polythene storage bottles were washed before and after use, by soaking them in a 10% nitric acid (HNO_3) solution for 24 hours and further soaking them for 24 hours in UPW. Simultaneously, cellulose membrane filters were soaked in a 2% HNO_3 solution for 24 hours and then soaked in UPW for a further 24 hours prior to usage. Washing steps were performed to remove any contaminating trace metals from the glassware, ultrafiltration cells, reagent storage bottles and membrane filters before

usage. $NaBH_4$ was stored in a desiccator to prevent any atmospheric water sorption and $AgNO_3$ was stored in dark container to stop natural and UV light photo-degradation. Materials were weighed out in fume cupboard containing a calibrated balance which has inspections every 6 months. Since AgNPs have been demonstrated to be light sensitive (Li and Lenhart, 2012), AgNP suspensions were stored in acid washed polythene bottles in a dark refrigerator at 4^oC until needed.

2.1.2 Silver Nanoparticle Synthesis

AgNPs were synthesized with citrate and PVP as capping agents, with an overall average core size of 11.5 ± 2.5 nm for both particle types. The purpose of different capping agents was to identify if the steric (PVP) and electrosteric (citrate) stabilization of the AgNPs, influenced the chemistry and transport in the water systems. Both citrate and PVP AgNPs were characterised by a multi-method approach discussed below and were used in the synthetic (Chapter 4) and natural water (Chapter 5) mesocosm studies.

2.1.2.1 Citrate Capped AgNPs

Citrate capped AgNPs were synthesized following the protocol presented in Cumberland and Lead (2009). A 100 mL (0.25 mM) $AgNO_3$ solution and 100 mL (0.25 mL) sodium citrate solution were added together in a 500 mL conical flask and mixed vigorously. A total of 6 mL (0.25m M) $NaBH_4$ was then added to the mixture, and mixed cold for 10 minutes before heating at 100^oC for 2 hours. Note that on the addition of the $NaBH_4$ the colourless solution changes to a pale yellow to indicate the formation of AgNPs. After 2

hours the reaction was taken off the stirrer counter, left to cool and then stored in polythene acid washed bottle in a dark refrigerator at 4^{o}C until needed.

NP suspensions were then filtered through a 100 nm cellulose membrane filter using a Millipore vacuum filtration system to remove any large aggregates formed during synthesis. Ultrafiltration, discussed specifically in more detail below, used a Millipore stirred cell ultrafiltration system with a 1 kDa cellulose membrane to ensure the suspension was free from ionic species. This procedure was performed 3 times to ensure the purity of the AgNP solution. The bottom up chemical approach to synthesise AgNPs produces Ag seeds from clusters which will grow depending upon the controlled reaction circumstances and addition of the capping agent (Pillai and Kamat, 2004). Additional experiments were conducted to identify the effects of temperature, citrate concentration and $NaBH_4$ concentrations upon the NP size/shape variations of citrate stabilized AgNPs. These experiments are outlined below and are discussed further in chapter 3.

2.1.2.1.1 Effects of Temperature

An experiment to identify the effect of temperature upon the size and morphology of AgNPs used a variety of temperatures between 20-100^{o}C. A 100 mL (1 mM) $AgNO_3$ solution, 100 mL (1 mM) sodium citrate, and 100 mL (8 mM) of $NaBH_4$ were used. The reagents were mixed in the same order as those by Cumberland and Lead (2009), by adding $AgNO_3$ and sodium citrate together first in a 500 mL conical flask followed by vigorously mixing, with the addition of $NaBH_4$. The suspensions were mixed cold for 10 minutes before heating at varying temperatures between 20-100^{o}C (see chapter 3) for 2 hours. After 2 hours the reactions were stopped, and left to cool. The suspensions were

stored in polythene acid washed bottles in a dark refrigerator at 4^{O}C overnight before analysis.

2.1.2.1.2 Effects of Sodium Citrate Concentration

The effects of citrate concentration were assessed using the same methodology, temperature variance, and $AgNO_3$ and $NaBH_4$ concentrations as section 2.1.2.1.1 to reduce the introduction of any other variables. The concentration of sodium citrate was doubled to 2 mM to assess the effects upon AgNP size and morphology.

2.1.2.1.3 Effects of Sodium Borohydride

The methodology of section 2.1.2.1.1 (including all concentrations) was followed with only changes to the amount of $NaBH_4$ used. The amount of $NaBH_4$ to be added was reduced from 100 mL to 6 mL to assess any changes the morphology and sizes of the AgNPs.

2.1.2.2 Polyvinyl Pyrrolidone (PVP) Capped AgNPs

PVP capped AgNPs were synthesized using methods previously developed by Tejamaya *et al* (2012). NP suspensions were made by cooling 2 mM $NaBH_4$ in a conical flask, whilst continuously stirred in an ice bath for 20 minutes. After the 20 minutes cooling phase the PVP10 solution was added to the $NaBH_4$ and additionally stirred for a further 5 minutes. $AgNO_3$ was then added to the stirred $NaBH_4$ and PVP10 solution by titration at rate 1 drop per second. The reaction was colourless and changed to a pale orange with the addition of $AgNO_3$. Once all the $AgNO_3$ had been added to the solution by titration the mixture is

left stirring on ice for an additional 10 minutes to ensure all ingredients are thoroughly mixed. Note, the solution is always stirred and remained in the ice bath until the reaction has finished (Tejamaya *et al,* 2012). The resulting AgNP suspension was stored in polythene bottles in a dark refrigerator at 4^{o}C. On refrigeration the pale orange colour changed to a darker orange colour over night. NP suspensions were filtered with a 1 kDa cellulose membrane to remove aggregates made during synthesis and purified using the Millipore stirred cell ultrafiltration system (Tejamaya *et al,* 2012). The filtration and ultrafiltration techniques are discussed in more detail below.

2.1.2.3 Characterisation of Nanoparticles

Characterisation is one of the most important aspects of analysis as it assesses what is present, for quality and quantification of the NPs (Darlington *et al,* 2009 and Fabrega *et al,* 2011). Appropriate characterisation helps describe the changing behaviour and physico-chemical properties of the NPs and helps to understand the environmental transformations (Lowry *et al,* 2012). The physicochemical properties of the AgNPs were characterised using a multi-method approach. Properties of interest included concentration, size, size distribution, morphology, stability, dissolution and solubility.

Ultrafiltration was used to remove dissolved Ag. The presence of Ag in solution was determined by UV-Vis. The size of the NPs was measured by DLS, Fl-FFF and AFM. Size and morphology was determined TEM. Elemental presence was determined by ICP-MS and EDX. ICP-MS was also used to determine elemental concentrations, whereas FAAS measured total Ag concentrations. Natural water samples were analysed for the

total organic carbon content (TOC). A brief description of the analytical techniques and their physical principles are outlined below in section 2.2.

2.1.3 Fate and Behaviour of AgNPs using Mesocosm Experiments

The fate and behaviour of 11.5 ± 2.5 nm citrate and PVP AgNPs in aquatic systems was investigated using mesocosm tubes (details in section 2.1.3.1) under the following conditions:

- UPW
- EPA moderately hard water
- EPA moderately hard water with Suwannee River Fulvic Acid
- Natural seasonally changing lake water
- Additionally the fate and behaviour of $AgNO_3$ was investigated in UPW, EPA moderately hard water and in natural lake water.

The purpose of the $AgNO_3$ exposed to UPW was to assess the diffusion of Ag throughout the mesocosms. Whereas the $AgNO_3$ exposed to EPA water was to determine both the transport and transformations of dissolved Ag exposed to simple electrolyte strength water such as AgCl formations. Exposure to the natural lake water enabled assessments of the transport and transformations that could be used to interpret AgNP behaviour.

To assess the behaviour of AgNPs, in simple water, exposures were set up releasing the AgNPs in UPW and were measured over time. Similarly, the AgNPs exposed to EPA water was conducted to assess the diffusion/sedimentation and the transformations of the AgNPs in the presence of simple electrolytes. In addition, the EPA water with added SRFA was to mimic a natural water system and address the additional

NOM effect on the AgNPs stability, transformation and transport in the mesocosm system.

Overall, the synthetic waters were used as a simple system to build and combine information of their interactions (water and NP-NP interactions), partitioning and sedimentation/diffusion rates, that can influence the NP behaviour as the waters become more complex. Information from the synthetic water studies was used as reference point to help build knowledge that could be used to interpret AgNP fate and behaviour in the natural water studies. Since a real life exposure of AgNPs to natural water will not occur as a single time point release situation, it is necessary to study the AgNP behaviour in seasonally changing water. During different times of the year natural water will have different concentrations of TOC, different components of NOM, and have different ionic strengths depending on the natural mixing and sedimentation of natural particulates. Natural mixing also occurs when the biological oxygen demands (BOD) of the water change, which is temperature dependant. Therefore the changing chemical makeup of the water conditions during the seasons will provide different conditions which will influence the AgNP transformations differently.

In total there were 6 mesocosm tubes, this enabled each particle coating to have three replicates for each of the water types. The replicates were also used to compare results to make sure they were statistically relevant and comparable like for like between the replicates. Therefore any outlying results could be identified with ease.

2.1.3.1 Mesocosm Design and Sampling

The mesocosms were composed of 6 tubes standing 100 cm high with a radius of 24 cm and had a liquid capacity of 43 L (Figure 2.1). Prior to experimental procedures a vigorous cleaning process was carried out in order to remove any previous trace metals, and other dirt contaminants that could interfere with experimental results. The cleaning procedure involved a disinfectant wash, followed by an overnight soak in 10% HNO_3 solution and a final wash with UPW. To check the washing procedure was adequate at removing all contaminates a test exposure was conducted before the main experiments. AgNPs were exposed to UPW in the mesocosm for 7 days, before the mesocosms were subsequently washed and left to soak in UPW over night. Water samples were taken from the top middle and bottom to assess if there was Ag present after the washing procedure. No Ag was reported after these washing steps.

A sieve which acts as a point of introduction for the AgNPs to the water is 24 cm wide, 2 inches deep and sits at the surface of the mesocosm (figure 2.1). The sieve contained 1 L of the water medium for the AgNPs to mix with on introduction. There was no air gap between the sieve and the water beneath in the mesocosm. There was no artificially mixing or stirring of the AgNPs in the columns, all experiments remained static. The sides and top of the external exterior of the mesocosms were covered in foil to prevent any light exposure and dust contaminates.

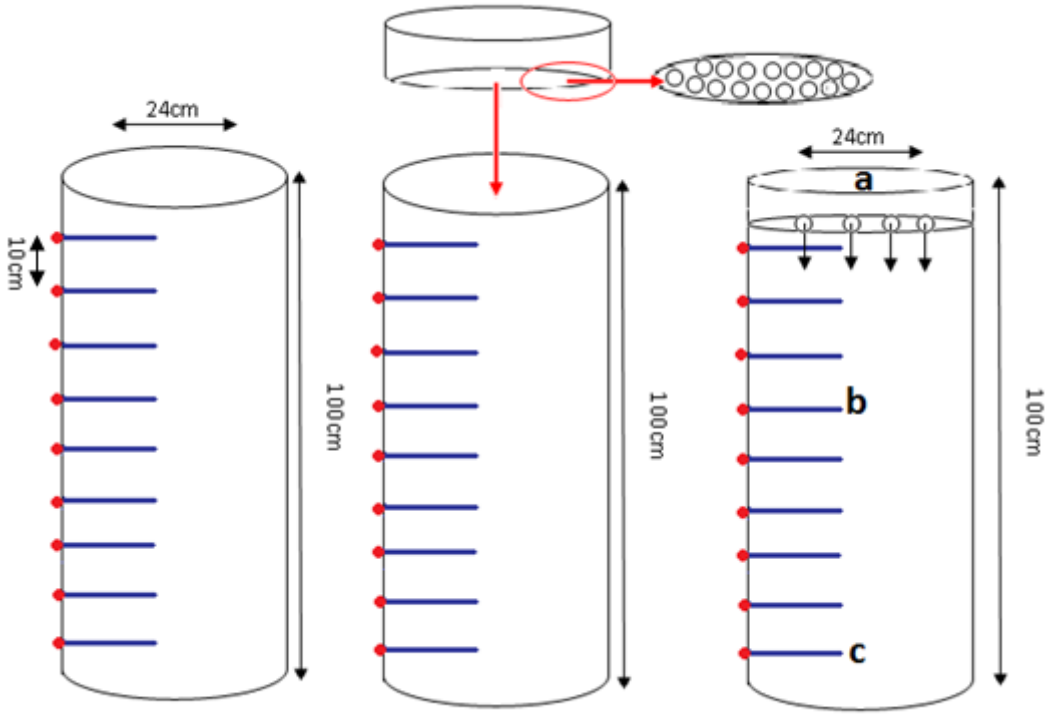

Figure 2.1: Schematic diagram of the mesocosm design. In total there are 9 injection points marked by rubber teats (red and blue on the diagram), located every 10 cm along the vertical side of the tank. The surface point is taken directly from the top of the tank to mimic surface water in contact with the air. The holding sieve fits the surface of the mesocosm and sits 2 inches deep inside, note this is not an extension of the total length of the mesocosm. Point a) marks the surface sampling point, b) marks the middle sampling point and c) marks the bottom sampling point.

Attached to the sampling points were rubber teats, where long (6 inches) stainless steel hypodermic needles are permanently injected to avoid perturbation of the water. These needles were inserted before the NPs were added to the mesocosms and were not removed during any point of the experiment. Attached to the hypodermics are 5 mL syringes which were used to withdraw the sample. Samples of 5 mL were taken on a daily basis for the first 14 days, then on days 21 and 28 of the experiment from the surface, middle (50 cm equally from the surface and bottom) and bottom area (90 cm

from the surface). The sampling point at the bottom was always sampled at a 45^{o} angle downwards in order to obtain samples that were directly from the bottom of the tank. The daily samples of 5 mL were assessed by the UV-vis for transportation and aggregation behaviour. Samples for TEM were taken at various time points between 24 and 120 hours after exposure.

To assess the dissolved Ag concentration, 10 mL samples were extracted from the surface and bottom areas between days 1-14 and again on days 21 and 28. Ultrafiltration of the 10 mL samples was used separate the dissolved and AgNP fractions, obtaining equal measures of 5 mL in the filtrate (below membrane) and retained (above membrane) portions. Samples were then analysed by FAAS to obtain the Ag concentration. The concentration of AgNPs added to the water columns needed to be as close to environmental predicted concentrations as possible as stated in the literature. Benn and Westerhoff (2008) studied the leaching of AgNPs from commercially available socks and discovered that the socks leached between 3-1300 ppb after the washing procedures. We also needed to consider the detection limits of the available equipment that was used to investigate the behaviour of the NPs. With this in mind, a series of dilutions were set up using known concentrations of the citrate AgNPs to test the limit detections of the UV-vis, as displayed in figure 2.2 below.

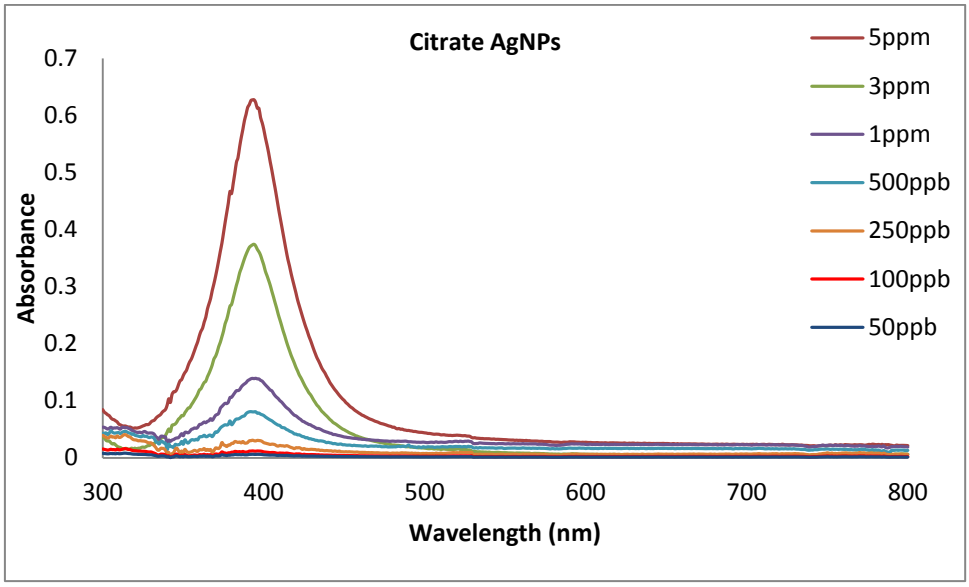

Figure 2.2: Limit detection test of the 10 cm long path cuvettes using known concentrations of citrate AgNPs.

At 50 ppb the citrate AgNPs were still detectable. Based on environmental releases (Mueller and Nowack, 2008) and UV-vis detection limits, a 100 ppb concentration (1 $X10^{-8}$ mol L) would be used assuming that the particles diffuse equally throughout the mesocosm. We added the citrate AgNPs at a starting concentration of 11 ppm and a volume of 390 mL and PVP AgNPs at a volume of 215 mL and a starting concentration 20 ppm (The difference in starting concentration volumes is due to the concentrations in which the NPs are first synthesised). Both solutions were calculated to have an even distribution of 100 ppb. To further investigate AgNP behaviour, a series of dilutions using citrate AgNPs in simple ionic solutions of sodium nitrate ($NaNO_3$) and calcium nitrate ($CaNO_3$) were also set up (figure 2.3).

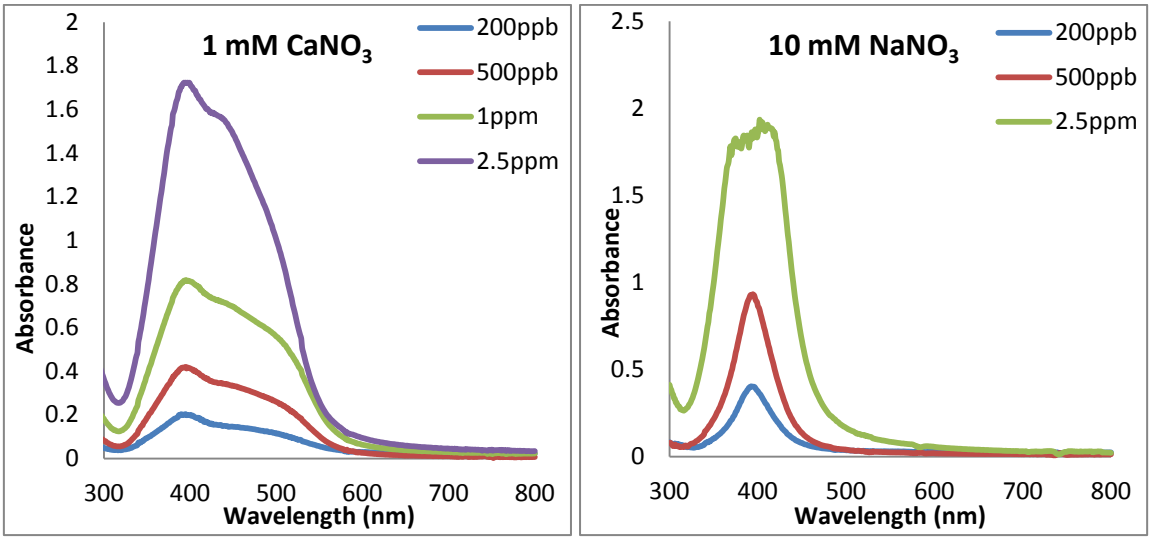

Figure 2.3: Serial dilutions of citrate AgNPs exposed to simple ionic solutions to test their behaviour and delectability.

These experiments were used as pre-investigative studies to identify the effects of different simple ionic media to the AgNPs. The results from the pre-investigative study were used to help interpret changes that occur from the complex water systems described further in section 2.1.3.2.

2.1.3.2 Preparation of Synthetic Waters

EPA standard moderately hard water was produced using guidelines from the United States Environmental Protection Agency (2002) using reagent grade chemicals shown in table 2.2. To mimic natural water Suwannee River fulvic acid (SRFA) was added at 1 mg L^{-1} to the synthetic waters. A stock solution of SRFA was prepared by dissolving 43 mg to 5 L of ultrapure water and stirred over night. The SRFA suspension was then added to make up the total water volume the mesocosm tube, pre-prepared with the EPA moderately hard water. To allow for natural settling, the suspensions were left for 24 hours to ensure even distributions of SWFA throughout the mesocosm.

Table 2.2: Composition of synthetic fresh water according to the US-EPA guidelines				
Water type	**Chemical added (mg L^{-1})**			
	$NaHCO_3$	**$CaSO_4.2H_2O$**	**$MgSO_4$**	**KCl**
Moderately Hard	96	60	60	4

2.1.3.3 Natural Water Collections and Preparations

Natural water samples were collected from the Vale Lake located the University of Birmingham campus (figure 2.4) during spring (April), summer (July), autumn (October) and winter (January). The water was collected in acid washed large heavy duty plastic containers (approximately 15 L). Transportation time took approximately 10-15 minutes between collecting the water from the lake and returning it to the lab. Prior to addition to the mesocosms, the water was filtered through muslin cloth to extract any large matter and left to settle for 48 hours before the AgNPs were added for study. An aliquot of the water was taken for characterisation purposes, including pH, elemental analysis, TOC and dissolved Ag.

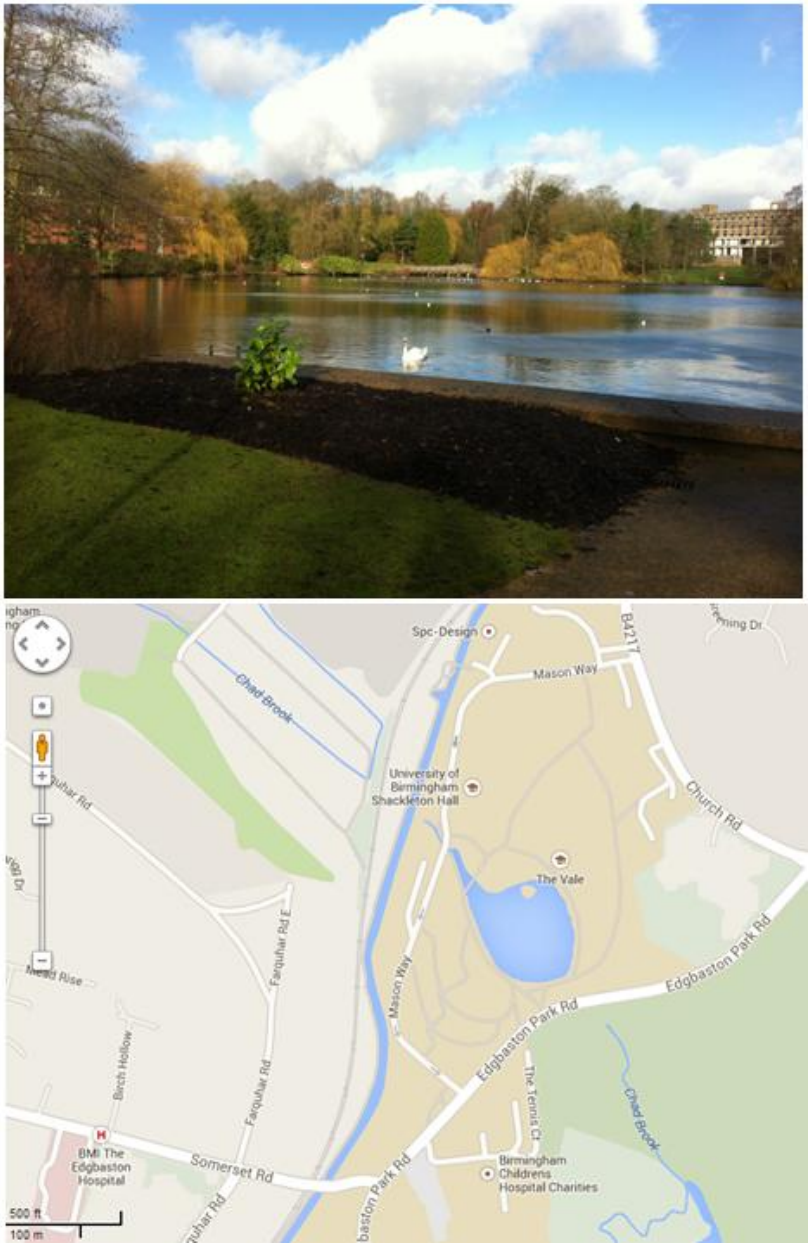

Figure 2.4: Top: The vale lake at the University of Birmingham. Bottom shows a map view of the Lake located next the Birmingham and Worcester canal line. Map coordinates: Latitude: 52.460403°, Longitude:-1.924152°. Map Image courtesy of Google maps: https://maps.google.co.uk/maps?q=Vale+Lake+at+the+university+of+birmingham&ie=UTF-8&ei=CXgDU7WwE8ve7AaFuIBg&ved=0CAoQ_AUoAg.

2.1.3.4 Diffusion-Sedimentation Model

To predict the fate and transport behaviour of the total Ag in the mesocosms, we devised a simple diffusion-sedimentation model using sedimentation and diffusion equations created by Hinderliter *et al,* 2010, with boundary conditions created by Socolofsky and Jirka 2004. Together we devised a mathematical model that we could introduce AgNP parameters such as size and starting concentration to predict the transport (in terms of total Ag concentration) over time in a 1 meter tall mesocosm column. Sedimentation and diffusion are independent processes that can be used in combination to describe the transport processes of NPs in solution. The following equation (Socolofsky and Jirka, 2004) can be applied to describe the transport phenomena using an Einsteinian notation combining Ficks Law of diffusion to produce the diffusion-advection equation (Eq 2.1):

$$\frac{\partial C}{\partial t} + \frac{\partial \mu_i C}{\partial \chi_i} = D \frac{\partial^2 C}{\partial \chi_i^2}$$

[Eq 2.1]

Equation 2.1 determines the sedimentation diffusion equation, where *D* is the diffusion coefficient (constant), *C* is concentration, *t* is time, and χ_i is the length of the mesocosm (m). We must consider our experimental conditions: a tall mesocosm column that stands 1 m tall, holds 43 L of fluids, NP dosing, gravitational pull, density of the NPs, temperature of the water, viscosity and density of the water. We also need to consider:

1- Concentration of Ag in the water column at time 0 = 0 (C_{Ag} = 0 at t = 0 for <0 x <L)

2- Introduction of Ag to the column (C_{Ag} = C_0 at t = 0 and x =0)

3- No flux at the bottom of the column (dC/dx= 0, at x=L).

The no-flux boundary is a surface that restricts the Ag concentration movement at the bottom of the mesocosm. The following equation account for the no-flux boundary condition using Ficks Law (Socolofsky and Jirka, 2004):

$$\left.\frac{\partial C}{\partial \chi}\right|_{\chi_b} = 0 \qquad \text{[Eq 2.2]}$$

Where, x_b is the no flux boundary condition at the bottom of the mesocosm measured in distance *L* (m). Under the previously mentioned boundary conditions, the following analytical solution of the diffusion-sedimentation equation can be used to fit the concentration of AgNPs in the water column:

$$C(x,t) = \frac{M}{A\sqrt{4\pi Dt}}\left(\exp\left(-\frac{(x-x_0)^2}{4Dt}\right) + \exp\left(-\frac{(x-x_i)^2}{4Dt}\right)\right) \qquad \text{[Eq 2.3]}$$

Where x_0 is the point where the NPs are introduced to the column, *D* is the diffusion coefficient of the NPs or their aggregates, *A* is the column cross sectional area of the mesocosm, *t* is the distance NPs travelled in terms of time, and *M* is the mass of the introduced NPs. The two solutions are then added together to describe the diffusion sedimentation equation:

$$C(x,t) = \frac{\left(\frac{M}{A}\right)}{\sqrt{4\pi Dt}}\left(\exp\left(-\frac{(x-\mathrm{U}x_0)^2}{4Dtx}\right)\right) \qquad \text{[Eq 2.4]}$$

The diffusion coefficient and sedimentation velocity can be described by equations 2.5 and 2.6 below (Fick, 1855, and Hinderliter *et al,* 2010):

$$D = \frac{\mathrm{RT}}{3\mathrm{N_A}\,\pi\mu\,\mathrm{d}} \qquad \text{[Eq 2.5]}$$

Diffusion is seen as *D* (m^2 s^{-1}), R defines the gas constant (L.kPa K mol), T refers to temperature (K), N_A is Avogadro's number, viscosity of the solution μ (Pa.s) the particle diameter is d (m). The diffusion-sedimentation transport of NPs can be described by applying the partial differential equation (Eq 2.6) (Mason and Weaver 1924). The right hand side of the equation describes the diffusion and sedimentation of the particles as seen in Ficks Law (Socolofsky and Jirka, 2004) and is written as:

$$\frac{\partial c}{\partial t} = D\frac{\partial^2 c}{\partial z^2} + U\frac{\partial c}{\partial z}$$

[Eq 2.6]

Where *c* is the concentration of the solute (g mL^{-1}), *t* is time (s), *z* is distance from the source (m), *D* is the diffusion coefficient, and the sedimentation velocity of particles in solution is *U* (m/s^{-1}) (Mason and Weaver, 1924). The equation can be completed by the following boundary conditions:

$$D\frac{\partial c}{\partial z} + sgc = 0$$

[Eq 2.7]

The sedimentation velocity of particles in solution is written by Stokes equation:

$$U = \frac{g\,(\rho_p - \rho_f)\,d^2}{18\mu}$$

[Eq 2.8]

Where g is the gravitational force ($m\ s^2$), particle density is ρ_p ($kg\ m^3$), fluid density is ρ_f, the particle diameter is d (m) and the viscosity of the solution media is termed μ (Pa.s) (Hinderliter *et al,* 2010). A limitation of the model is that it is unable to accurately account for the displacement of the capping agents which is a major driver of the aggregation/dissolution of the particles over time. These limiting factors will cause

changes to the total Ag concentrations in each depth over time as the particles sediment and diffuse throughout the compartments. Therefore once particles have settled the model is unable to predict the accumulation of Ag at the bottom of the mesocosm as the model assumes the bottom is infinite. A further limitation of this model is that it can only assume diffusion or sedimentation (depending on AgNP size) of the AgNPs with no dissolution processed involved.

Table 2.3 provides information for the model parameters used in chapters 4 and 5.

Table 2.3: Model Parameters		
Symbol	**Unit**	**Measurement**
Sedimentation (U)		
g	9.81	acceleration of gravity (m s^2)
Pp	10490	density of the particle (kg m^3)
Pf	998	density of the medium (kg m^3)
K	1.38E-23	Boltzman constant (m^2, kg s^{-2}, K^{-1})
T	293.15	Temperature (K)
µ	0.001	Viscosity of medium (Pa.s)
d	11.5	nm
Diffusion (D)		
A	0.049	Area of the column (m^2)
L	1	Column Length (m)
V=A*L*	43	Column volume (L)
V	0.215(PVP AgNPs) 0.391 (citrate AgNPs)	Dosing volume (L)
C_0	20 (PVP AgNPs) 11 (Citrate AgNPs)	Dosing concentration (ppm, mg L^{-1})
M	Determined from equation C_0*V	Mass of NPs (mg)
M*/V*	Determined from equation *M*/((*V*=A*L*)*1000)	C column based on diffusion (ppb)
D	Determined from equation	Diffusion coefficient (m^2 s^{-1})
U	Determined from equation	Sedimentation Velocity (m s^{-1})

2.1.4 Waste Disposal

For all nano-containing materials arrangements were made for a special waste disposal collection.

2.2 Analytical Techniques

This section describes the analytical methods that were used for characterisation and analysis of the AgNPs prior and during experimentation. An extensive range of techniques were used to produce a catalogue of data that obtained information about particle size, concentration, polydispersity and morphology. It is important to know this data before the NPs were used during experimentation, as it helps to understand the changing behaviour and dynamics of the AgNPs during the experimental analysis, compared to original AgNP suspensions.

2.2.1 Ultrafiltration and Filtration

Two types of filtration techniques were used in combination with specific pore sized membranes to remove dissolved Ag, and aggregates from the synthesized NP suspensions.

2.2.1.1 Ultrafiltration

Ultrafiltration was used to purify newly synthesized NPs. For characterisation purposes synthesized NP suspensions need to be 'cleaned', by removing impurities produced during the synthesis process. Such impurities include dissolved Ag and excess capping agent. The removal of these impurities will prevent any further AgNP growth in suspension.

The second process that ultrafiltration was used for was for the purpose of measuring dissolved Ag compared to nanoparticulate Ag. An estimation of how fast the AgNPs dissolved when exposed to the different water conditions, was assessed by

measuring the proportion of dissolved Ag in the filtrate, compared to the retained content inside the filtration cell.

2.2.1.1.1 Theory and Practice

Ultrafiltration uses a Millipore stirred ultrafiltration cell (figure 2.5) holding 350 mL of any desired liquid. A cellulose membrane with a pore size of 1 kDa (purchased from Sigma) under nitrogen (N_2) gas at approx 14 PSI was used to filter out impurities and retain pristine AgNP suspensions. For all experiments described in this thesis, the membrane size was chosen specifically to separate dissolved Ag and retain AgNPs in solution.

Prior to use, the cellulose membrane was washed in 2% nitric acid (NHO_3) for 24 hours and stored in UPW for 24 hours or until needed. The newly synthesized AgNP solution was poured to a volume of approx 200/250 mL, and topped up with 100 mL of a 0.25 mM solution of citrate solution for citrate particles or UPW for the PVP AgNPs. The gas was applied at 14 PSI to the stirred system until the volume was reduced to the original starting volume of the AgNP suspension. For example if 100 mL of the solution washing media was added, then the filtration would run until 100 mL was removed to ensure the original concentration of the NP suspension was not altered. The method was repeated for 5 times to ensure all impurities are removed. There is no prior sample preparation required for this method.

Figure 2.5*: 350 mL and 10 mL Amicon stirred ultrafiltration systems used in the present study.*

For measuring dissolved Ag, the experimental method uses the same procedure as previously described, using a 10 mL ultrafiltration cell (to reduce the amount of sample removed from the study) with a 25 mm diameter cellulose membrane. During the mesocosm experiments dissolved Ag concentrations were analysed by removing 10 mL aliquots directly from the surface and the bottom point of the tank. Ultrafiltration was conducted on a daily basis for 14 days and then again on days 21 and 28 of the study.

2.2.1.1.2 Ultrafiltration Membrane Viability Pre-tests

Ultrafiltration provides a good estimation of how quickly AgNPs dissolve, although the results cannot be assumed 100% reliable, as there is a possibility that AgNPs can stick to the walls of the container and ionic species can become bound to the filter membrane. To identify potential losses and test this theory a series of Ag standards were prepared and passed through the ultrafiltration system. The standards were measured using FAAS to confirm the concentrations and to ensure the FAAS was sufficiently calibrated. The

results are presented in table 2.4. New membranes were used for each experiment and the ultrafiltration cells were thoroughly washed using the HNO_3 washing steps (described earlier) between each test.

Table 2.4: Ultrafiltration Membrane Viability Tests					
Concentrations (ppm)					
Standard	**0.25ppm**	**0.5ppm**	**1ppm**	**3ppm**	**5ppm**
	0.25 ± 0.01	0.55 ± 0.04	1.29 ± 0.05	3.36 ± 0.98	5.52 ± 0.08
Solution in the cell (Retained)	0.25 ± 0.15	0.60 ± 0.08	1.19 ± 0.16	3.24 ± 0.11	5.41 ±0.09
Solution passed through membrane (Filtrate)	0.26 ± 0.08	0.46 ± 0.32	1.15 ± 0.22	2.94 ± 0.37	2.71 ± 0.03
Water wash after use	0.01 ± 0.25	0.02 ±0.02	0.03 ± 0.04	0.08 ± 0.13	0.15 ± 0.08

Once 50% of the standard was sufficiently filtered, the retained (everything above the membrane) was measured against the filtrate (everything that has passes though the membrane). The results identified that low concentrations of Ag that passed through the membrane had comparable retained and filtrate results, whereas losses occurred in the filtrate with higher Ag concentrations. After each experiment UPW was ultrafiltrated to identify if there was any Ag bound to the membrane after use. The results further confirmed that higher concentrations of the Ag standard produced losses via the membrane, as Ag was identified in the water wash.

2.2.1.1.3 Advantages and Limitations

Ultrafiltration has the major advantage of being able to enhance the stability of AgNP suspensions by removing impurities which can cause further growth of the NPs. A second advantage of ultrafiltration is that it can be used as estimation on how quickly AgNPs dissolve in a complex mixture. The disadvantage is that the filtration process is very slow and can take between 2-4 hours to filter out the ionic species, depending on the pore size

of the filter, the smaller the pore size the longer it takes to filter. A further disadvantage is that ionic species and AgNPs can become bound to the filter membrane and adhere to the surface walls to creating losses.

2.2.1.2 Filtration

A Millipore vacuum filtration system, complete with 0.1 µm cellulose nitrate filter paper was used to filter AgNP suspensions under vacuum conditions. The main purpose was to remove any large particulates and aggregates generated as by products during synthesis. The advantage of this method is that NP size differential fractionation can also be achieved by selecting the desired membrane pore sizes. A further advantage is that filtration only takes a couple of minutes to perform.

2.2.2 UV-Visible / Surface Plasmon Resonance (UV-Vis/SPR)

UV visible light can be used to give qualitative elemental data by its absorbance spectra (Darlington *et al,* 2009). Identification of NP properties are achieved according to their difference in light spectra, which can be used to describe size/shape changes by the addition of stretched SPR bands as seen in figure 2.6 (Li *et al,* 2010). Spherical AgNPs are mainly yellow/orange in colour and have SPR between 390-400nm (Pillai and Kamat, 2004).

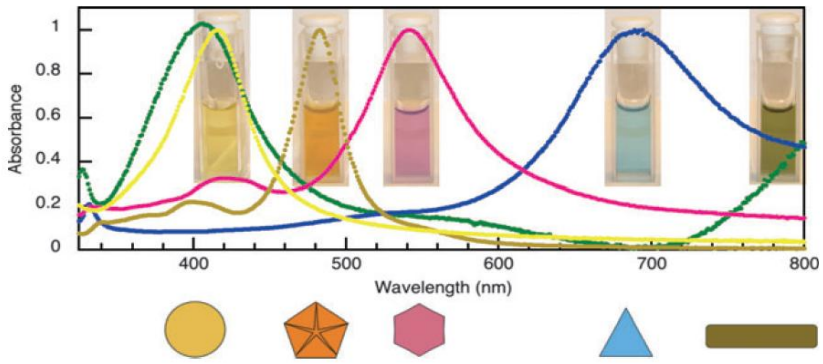

Figure 2.6*: Highlights the different morphologies of AgNPs with corresponding absorbance spectra. Extracted from Stamplecoskie and Scaiano (2012).*

2.2.2.1 Theory

An aliquot of the sample in question (in liquid form) is placed in to the machine along with a reference sample. A UV light source is then projected and split into two beams of by the monochromator. One of the beams passes through the sample and the other passes through the reference sample (Clark and Russell, 1993). As the beam passes through the sample the energy produced in the UV-visible region is enough to excite an electron into its higher orbital producing an excited state species. The excited electron becomes paired to an electron in another orbital, in its 'ground state' and drops back to a lower level. It is this electron energy state that causes a photon of light to be emitted back to the detector (Lakowicz, 2006). The more easily excited the electrons are, the longer the wavelength of light absorbed. The reference sample is used to reduce interference scatter and therefore the beam intensity has no absorbance (Clark and Russell, 1993).

2.2.2.2 Practice

All experimental analysis for this project was conducted on a Jenway 8300 double beam instrument. The basic instrumentation is made from a light source, a monochromator and a detector. A tungsten filament is used as the radiation source, and is fitted with a deuterium lamp. For characterisation of the pristine spherical AgNPs, UV-vis was used to confirm the presence of Ag. When measuring newly synthesized AgNPs, any unexpected additional peaks not in the region of 400nm confirmed contamination, size or shape deviations. Therefore the suspensions would not be used and were disposed of accordingly. UV-vis was also used to monitor how the AgNPs changed over time by tracking their movement in the mesocosm on a daily basis. The results obtained gave qualitative information on the concentration of nanomaterials in a particular area of the mesocosm (surface, middle, bottom) and aggregation state. The peak shape and width also described how polydispersed the NPs become over time (Li *et al,* 2010).

2.2.2.3 Advantages and Limitations

The advantages of this technique require little to no sample preparation, except some dilution in the case of very concentrated samples. Analysis is fast with results in just a couple of minutes (Clark and Russell, 1993). The limitations of this technique are that samples composed of complex matrixes are difficult to analyse. This is due to the samples containing lots of matter which have the ability to scatter more light and interfere with the true analysis of the species in question (Down and Lehr, 2005). Further limitations require the samples to be in a liquid solution for analysis.

2.2.3 Dynamic Light Scattering (DLS)

DLS, also known as photon correlation spectroscopy (PCS) provides a non-invasive technique to measure the size distribution of particles in suspension, and polydispersity by looking at particles under Brownian motion (Goldburg, 1999 and Murphy, 1997).

2.2.3.1 Theory

The theory behind DLS relates to the diffusion of the particles in a liquid (Murphy, 1997, Boyd *et al,* 2011) and the movement of the solvent molecules colliding with the particles (Malvern Instruments Ltd, 2004). Smaller particles move more rapidly due to the solvent molecule forces acting upon them and larger the particles move slower due to Brownian Motion (Murphy, 1997). DLS uses a laser light source to produce scattered light as the particles move in suspension (Goldburg, 1999 and Murphy, 1997), and measures the time between the fluctuations of the scattered light, which is used to produce a diffusion coefficient (Baalousha and Lead, 2012). The diffusion coefficient can then used to calculate the hydrodynamic particle size by using the Stokes-Einstein equation (Einstein, 1905 and Malvern Instruments Ltd, 2004) written as:

$$D = \frac{k_B T}{C\pi\eta\sigma} \qquad \text{[Eq 2.9]}$$

Where D is diffusion coefficient, η is the viscosity, k_B is a Boltzmann constant, T is temperature, C is a constant determined by hydrodynamic boundary condition and σ is the diameter of the particle (Boyd *et al,* 2011, Srivastava *et al,* 2009). The final report gives a *Z-average* which shows the intensity weighed average, the average of the particle

diameter sizing, polydispersity index and standard deviations for the percent distribution. The polydispersity index (PDI) assesses how polydispersed the sample is and gives a number between 0 and 1 (one being extremely polydispersed). DLS is a good indicator of the approximate size and size distributions, which can help set parameters for other modes of analysis, such as the Fl-FFF.

2.2.3.2 Practice

Particle sizing of newly synthesised pristine nanoparticles by hydrodynamic diameter was carried out using a Nanosizer 5000 Malvern instrument. A small 1 cm^3 disposable cuvette was filled with the AgNP solution to introduce the sample to the machine. Due to application limitations DLS method was not used in the mesocosm studies as there are many different components in the nano/macromolecule size region that is present in natural water. For this reason, the naturally occurring particles could cause multiple scattering effects (Xia *et al,* 2012) which would have been impossible to determine if the results were due to true AgNP readings or interferences.

2.2.3.3 Advantages and Limitations

The advantages of DLS are similar to that of UV-vis, as sample preparation is minimal (liquid form) except the dilution of concentrated samples and the results are produced within minutes (Xia *et al,* 2012). The disadvantage is that particulates need to be dispersed in liquid form to be analysed, and consideration also needs to be given to the viscosity and the tendency for the material to aggregate, which will influence the particle size distributions. Problems can occur in polydispersed samples, as larger particles scatter

more light than smaller particle, potentially masking them in solution which can give false readings of the actual average (Darlington *et al,* 2009). Therefore the limitation of DLS is that it works best with monodispersed samples in simple matrices (Xia *et al,* 2012).

2.2.4 Flow Field-flow Fractionation (Fl-FFF)

Often complex samples need to be separated to isolate the material of interest. Fl-FFF uses a sophisticated chromatographic technique in order to perform size fractionation, and analysis of particles ranging from 1 nm to 100 mm (Reschiglian *et al,* 2010 and Giddings *et al,* 1977). Linking FI-FFF to a UV detector can give qualitative analysis on what is present in the sample in question.

2.2.4.1 Theory

In principle Fl-FFF works with two liquid flows, the first is the cross flow running perpendicular to the channel, made up of a thin permeable membrane (Reschiglian *et al,* 2010). The second is the channel flow, which has a parabolic flow to the cross flow, as seen in figure 2.7. Typically flow rates are between 0.2-5 mL per minute (Gimbert *et al,* 2003). The sample is injected into an injection loop, where it is carried by the channel flow and focused near the membrane surface. This concentrates the particles into a narrow band near the inlet of the channel (Giddings, 1993). The cross flow forces the particles to collect near membrane surface and move towards the centre of the membrane (Giddings, 1993, Giddings, 1973). The combination of particle diffusion with cross flow will determine the particle distance from the membrane. Smaller particles will be located furthest away from the membrane, whereas larger particles will be closer to

the membrane surface shown in figure 2.7. Particles are then separated according to their diffusion coefficients and the hydrodynamic diameter can be calculated according to Stokes-Einstein equation (Einstein 1905, Reschiglian *et al,* 2010, Kalmykov and Denecke, 2011) as seen:

$$V_R = \frac{v_c w^2}{6D} = \frac{\pi \eta w^2 v_c}{kT} \times \frac{d}{2} \qquad \text{[Eq 2.10]}$$

Where V_R is the retention volume, v_c is the cross flow volume, w is the channel thickness, D is the particle diffusion coefficient, k is the Boltzmann constant, T is temperature, η is the viscosity of the solution, and d is the particle diameter (Kalmykov and Denecke, 2011). Smaller particles will elute first, if the sample has a well defined size difference a series of sharp peaks will be created. Polydispersed and complex mixtures can give boarder/bimodal peaks depending on the nature of the sample (Giddings, 1993).

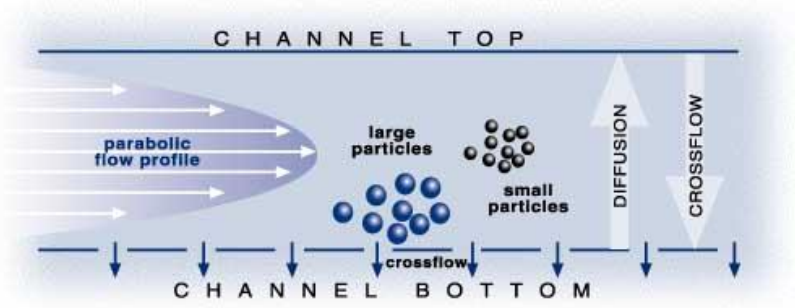

Figure 2.7: the parabolic channel flow focuses the particle near the membrane surface to concentrate the particles according to their sizes (Giddings, 1993). The cross flow forces the NPs towards the bottom of channel where they separate according to their diffusion coefficients. Image from :http://www.nanolytics.de.

2.2.4.2 Practice

After NP suspensions were synthesised, Fl-FFF was used to determine the hydrodynamic size diameter using an AF2000 postnova instrument with $NaNO_3$ mobile carrier solution. A volume of 0.5 mL injections of known standards were firstly determined in order to set the calibration. The standards were 20 nm, 30 nm and 60 nm polystyrene NPs. These were injected individually and the retention times/sizes were used to produce the size calibrations.

2.2.4.3 Advantages and Limitations

Fl-FFF can identify the hydrodynamic diameter of particulates as small as 1 nm into the macromolecule size, and has the ability to separate complex matrixes ranging from differences in molecular weight and size (Darlington *et al,* 2009). The limitation of Fl-FFF is the potential for aggregation to occur on the channel depending on the particle stability and the carrier flow liquid type. A further limitation is possible sample losses via membrane adsorption (Gimbert *et al,* 2003).

2.2.5 Transmission Electron Microscopy (TEM)

Accurate morphology and imaging is of the upmost important when characterising NPs (Darlington *et al,* 2009). Image analysis can show how the particles behave in solution i.e. aggregation/agglomeration states (Soto *et al,* 2005). TEM is one of best techniques to perform such analysis and can produce high resolution images of NMs (Oshida *et al,* 2013) A TEM can visualise images smaller than those of a light microscope (Rose, 2008)

and be equipped with energy dispersive X-rays (EDX) to give the chemical components of the sample.

2.2.5.1 Theory

A TEM is made up of a vertical column (figure 2.8) under vacuum conditions and uses an electron system, focused by various lenses to produce an image. Electrons are generated by an electron gun which creates an electron beam (Reimer and Kohl, 2008). The electrons are the focused to the illumination aperture to produce the picture (Bozzola and Russell, 1999).

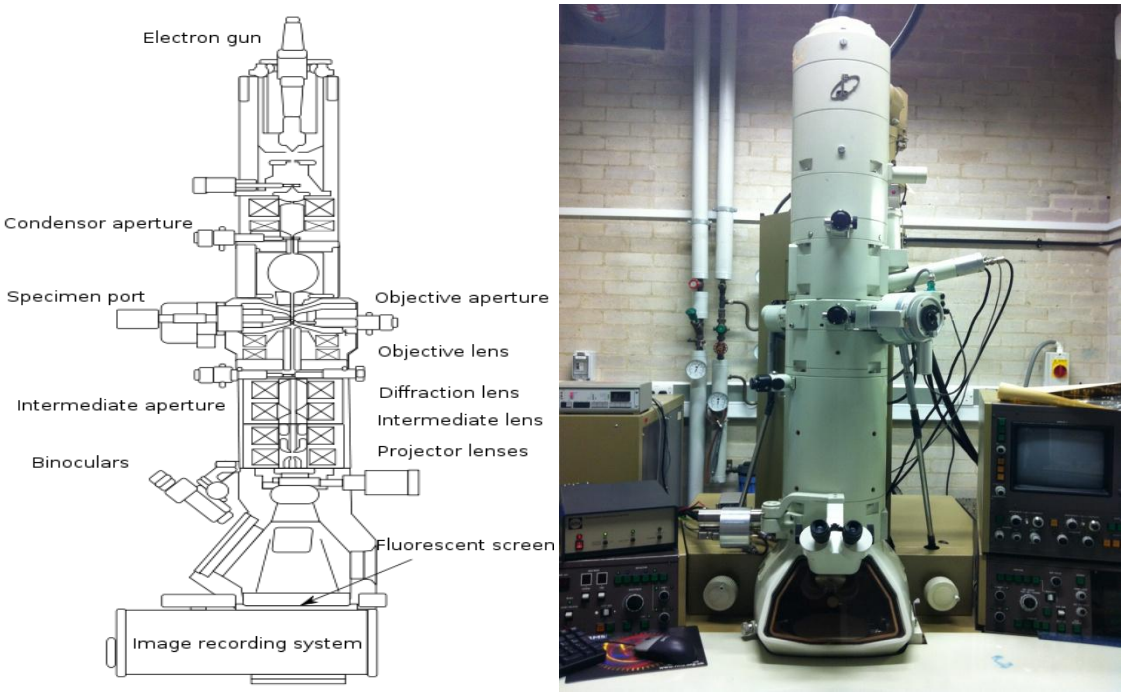

Figure 2.8: Left: A schematic view of the TEM courtesy of http://fgamedia.org/faculty/rdcormia/NANO53/TEM.htm. Right: A JEOL 1200EX 100kv located at the University of Birmingham materials and metallurgy Laboratory.

2.2.5.2 Practice

NP imaging was performed on a JEOL 1200EX 100kv Max system (figure 2.8). Sample preparation consisted of a 200 µL drop of the NP suspension onto a 300 copper mesh grid, with a carbon film disk purchased from Agar Scientific. The sample drop was left for approximately 30 minutes on the grid to allow the NPs to adhere to the surface. Note that the sample drop should not be dried on the grid, as the drying effect of the excess sample cause artefacts on the image, such as crystallization of any salts in solution. After the 30 minute sample drop adhesion, the carbon films were washed with UPW and left to dry over night before analysis.

2.2.5.3 Advantages and Limitations

The TEM is one of the most powerful microscopes that visualises materials in resolution to the order of several Angstroms. It is also possible to obtain elemental analysis by coupling to techniques such as EDX and electron energy loss spectroscopy (EELS). TEMs are relatively easy to use and can be used for a wide range of applications from nanotechnology to biological samples (Rose, 2008).

The limitation to TEM imaging, is that the sample needs to be dried on to the TEM grid before use. Sample preparation can also lead to contamination via other artefacts landing on the sample grid (Reimer and Kohl, 2008). A second limitation occurs due to the strength of the electron beam, which can alter the morphology of the sample in question, or destroy delicate samples (Soto *et al,* 2005, and Reimer and Kohl, 2008). A further limitation is the sample size which is analysed. Since there is only a tiny amount of material under observation, questions arise of how true the analysis is of representing

the whole sample. Therefore, for NP size analysis a large number of NPs need to be counted for good statistical representations.

2.2.6 Energy Dispersive X-Ray Analysis (EDX)

X-rays themselves were first discovered by Wilhelm Röntgen in 1895 (Tsuji *et al,* 2004, Garratt-Reed and Bell, 2003), since this discovery advances in technology has led to the use of X-rays for identifying crystalline solids, better known as x-ray diffraction (XRD) followed by x-ray fluorescence, and energy dispersive x-rays (EDX) in the 1960s (Garratt-Reed and Bell, 2003).

2.2.6.1 Theory

EDX is a semi-quantitative technique which can be coupled to a TEM or scanning transmission electron microscope (STEM) to use the electron beam as a source of excitation, to provide information on the chemical identity of a substance. If the substance is composed of a complex matrix, EDX can rapidly identify the individual materials (Loehman, 2010). The principle application works by using high energy radiation to ionize the atoms to excite the inner shell electrons, and shift between shells. The energy released during this process is emitted in the form of a photon x-ray that is unique to that atom. The more complex the atom, the more energy that will be released as the electron shells refill to stabilize the atom, (Brundle *et al,* 1992). The detector (usually lithium coated with silica) detects these photons and converts them electronic pulses (Loehman, 2010).

2.2.6.2 Practice

For experimental procedures EDX was coupled to a Tecnai TEM to determine elemental analysis of the newly synthesised NPs. EDX was also used to confirm the presence of Ag for AgNPs exposed to the natural and synthetic water systems.

2.2.6.3 Advantages and Limitations

EDX is a fast and non-destructive way of obtaining elemental analysis of an unknown sample (Carmona *et al,* 2010). The limitations of EDX are for elements with a low atomic number, for these samples detection limits are low. Therefore this type of analysis is better suited for the analysis of metals. A further limitation is that analysis needs to be done *in situ* coupled to other expensive equipment. EDX is not portable cannot be taken to the sample (Linke *et al,* 2004).

2.2.7 Atomic Force Microscopy (AFM)

The AFM was originally invented in 1986 and belongs to the family of scanning probe microscopes (Bowen and Hilal, 2009). AFM enables 3D visualisations of the shape and surface of any material (Stawikowska and Livingston, 2013) including liquid, cellular or hard materials visualised down to the nanometre scale (Baalousha and Lead, 2007).

2.3.7.1 Theory

AFM uses specialised sharp probes (better known as a tip) as a point force to contact or scan the sample (depending on the mode used) to produce a surface topography image (Haugstad, 2012). This is particularly useful for sizing nanoparticles, as the surface

information can be used to produce the size based upon the height of the sample (Baalousha and Lead, 2012). There are several modes in which this microscope can be used, the method depends greatly on the information in which one requires at the end point and what form the sample is in, i.e. liquid or solid state (Haugstad, 2012). The microscope can perform analysis in either contact or in non contact mode 'tapping mode'. The cantilevers are a detachable part of the microscope that engages with the sample and have a small tip which serves as the point of sample interaction. The laser beam is aligned with the tip and tip is brought into contact with the sample by use of a piezocrystal (Bowen and Hilal, 2009). Depending upon the mode, either the sample or the cantilever is moved in order to engage the surface of the sample with the tip at this point. When the sample and the cantilever are engaged the forces between the sample and the tip, better known as Van der Waals (Haugstad, 2012), cause the tip to move along the sample surface. This is generated into a feedback loop where the topography image is then produced (Haugstad, 2012).

2.2.7.2 Practice

For characterisation of the pristine AgNPs, an AFM XE-100 system in non contact mode was used. Sample preparation involved adhering the AgNPs to a flat mica sheet (Boyd *et al,* 2011) purchased from Agar Scientific. Sample adhesion to the mica sheet involved placing the mica sheet at the bottom of a Beckman test tube with the addition of 0.5 mL of the NP solution diluted in 4.5 mL of UPW. The samples were ultracentrifuged using a Beckman ultracentrifuge at 30,000 revolutions per minute (rpm) for 2 hours to adhere the NPs to the mica sheets. After this the mica was washed with UPW and left to dry

overnight before analysis. Image analysis was conducted using XEI software and particles analysis of average sizing was based on at least 100 particles height counts.

2.2.7.3 Advantages and Limitations

Unlike other scanning microscopy techniques such as scanning electron microscopy (SEM), AFM provides a 3D topography surface image (Stawikowska and Livingston, 2013). No sample pre-treatment is required which makes this technique suitable for (biological materials which can be in liquid form. The main limitation of this technique is the area which is analysed by the instrument is small. Specialised cantilevers are needed in order to perform a surface scan, this can introduce contamination via artefacts on the tip (Haugstad, 2012). A further limitation is that the sample needs to be adhered to a mica sheet for analysis, which can introduce other artefacts into the image such as contamination of drying (Baalousha and Lead, 2012).

2.2.8 Inductively Coupled Plasma Mass Spectrometry (ICP-MS)

ICP-MS is used for quantitative analysis and has a board detection limit from parts per trillion (ppt) to parts per million (ppm) concentrations (Thomas, 2008). Low concentrations are of particular interest in identifying trace elemental concentrations in natural water samples prior to nanoparticle exposure.

2.2.8.1 Theory

The method uses an inductively coupled plasma (ICP) source linked to a mass spectrometer (MS). The ICP is composed of a torch that which contains a frequency coil

which surrounds a flow of an inert gas, typically argon. This is a neutral gas that forms the plasma that is used to ionize the sample as it is introduced (Taylor, 2001 and Higson, 2003). The molecules of the sample in the gas phase are converted to ions by bombarding them with a stream of electrons, causing an electron to be knocked off, to produce a molecular ion with a positive charge. To stop these ions regaining an electron by collision, the instrument is kept under a high vacuum at approx 10^{-3} to 10^{-6} atmosphere. Ions are transported the MS part of the instrument where they are separated by their mass over charge (m/z) value (Higson, 2003).

2.2.8.2 Practice

ICP-MS was used to determine a 20 element semi-quantitative analysis on the natural water samples taken from the Vale Lake, before they were exposed to AgNPs. It was also used to determine the concentration of NPs after synthesis and subsequent washing by ultrafiltration.

2.2.8.3 Advantages and Limitations

ICP-MS has a large elemental detection range and low detection limits (Thomas, 2008). The limitation is that the argon can cause spectral interferences when detecting calcium and iron. Large ventilation systems are also required (Taylor, 2001 and Higson, 2003).

2.2.9 Flame Atomic Absorption Spectrometry (F-AAS)

2.2.9.1 Theory

Atomic absorption spectroscopy primarily looks at UV-visible radiation which is then absorbed by atoms in a gas phase. Specific wavelengths of radiation are absorbed which match the energies of electronic transitions within each atom giving a unique profile (Khopkar, 1998)

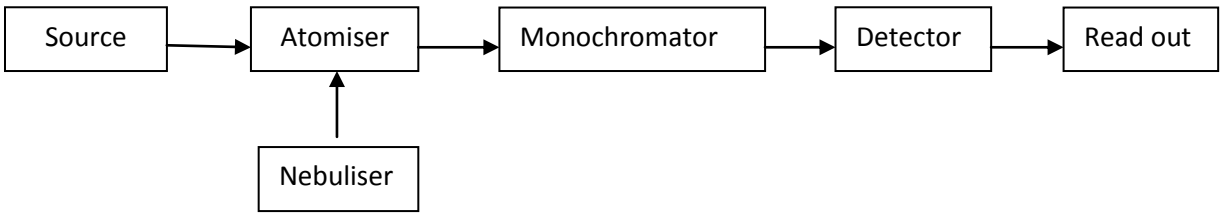

Figure 2.9: Perkin Elmer instrument AAnalyst 300 Atomic Absorption Spectrometer located in Public Health at the University of Birmingham. Underneath: schematic diagram of the principle instrumentation set up.

The source is usually a cathode lamp, where lamps of the known element can be added to emit radiation of that particular element. In this case an Ag lamp was attached. The sample is then introduced in the gas phase by the atomiser (introduced via a nebuliser)

where it mixes with an oxidant and fuel where it burns in the flame. The burning causes atoms and ions to form of the element which will give off a unique radiation wavelength (Cantle, 1982). The monochromator splits the light into its component wavelengths by a quarts prism or by diffraction grating (usually the preferred method as it gives greater resolution). The concentration can be given by measuring the loss of energy of the radiation passing through the flame (Nielsen, 2010).

2.2.9.2 Practice

To detect concentrations of Ag in the mesocosm studies, a PerkinElmer instrument AAnalyst 300 Atomic Absorption Spectrometer (figure 2.9) was used with an air-acetylene fuel oxidant. Total Ag concentrations from the mesocosm studies were measured using FAAS. An aliquot of 5mL from the direct surface, middle and bottom of the mesocosms were taken to obtain a total Ag concentration. Measurements of dissolved Ag using ultrafiltration were also measured using FAAS.

2.2.9.3 Advantages and Limitations

FAAS is a widely used technique that is used to determine concentration and element detection with high accuracy. The limitations are that this technique can only detect a single element concentration in a liquid sample, and the element of the sample must be known before analysis. FAAS doesn't distinguish if the element is bulk metal (NPs) or if the sample is in ionic form before the sample is atomised. Prior to analysis requires a calibration using known concentrations of the standard element in question. A further limitation is that a 1-4 mL volume of sample is required for analysis, and the sample is destroyed (Khani *et al,* 2011).

2.2.10 Total organic Carbon Analyser (TOC)

2.2.10.1 Theory

The sample in question is oxidised with an oxygen (O_2) carrier gas (Girard, 2010). The organic parts of the unknown sample will become oxidised to produce carbon dioxide (CO_2). The carrier gas flushes the oxidized carbon the detection system (Linskens and Jackson, 1999).

Figure 2.10: Shimadzu TOC-V CSH total organic carbon analyzer at the University of Birmingham.

2.2.10.2 Practice

The total organic carbon of the natural water samples were analysed on a Shimadzu TOC-V CSH total organic carbon analyzer, shown in figure 2.10. Initial standards were run prior to the samples for calibration purposes.

2.2.10.3 Advantages and Limitations

TOC measure the presence of carbon in a water sample irrespective of its source, i.e in/organic. The Limitations of this technique is that the more complex the sample material, such as high salt concentrations, the harder it is to oxidise high molecular weight compounds resulting in decreased sensitivity (Linskens and Jackson, 1999).

Chapter 3: Synthesis and Characterisation of Silver Nanoparticles

3. Chapter Outline

This chapter presents the synthesis and characterisation of silver nanoparticles (AgNPs) capped with citrate and polyvinylpyrrolidone (PVP). We were able to successfully produce novel synthesis methods by manipulating the temperature and reactant concentrations, to produce a size distribution of citrate AgNPs. The results found higher temperatures with higher citrate concentrations, produced more monodispersed AgNP suspensions, compared with controlling only the temperature. Additional citrate and PVP AgNPs have been suitably re-produced and characterised in correspondence to the original authors reported sizes and morphologies, which have been used for the fate and behaviour experiments in chapters 4 and 5 of this thesis.

3.1 Introduction

Traditionally the basic chemical synthesis of AgNPs involves a suitable solvent (there are many solvents available), to which the salt form of Ag is dissolved and reduced to a zero valence state. This methodology is known as the bottom up approach to synthesis AgNP suspensions (Tolaymat *et al,* 2010, Stamplecoskie and Scaiano, 2012). Problems of the bottom up method include aggregation of the particles over time, due to the short life of the atoms in solution. Therefore, an effective methodology needs to be produced to attempt perfect the stability of the AgNPs in suspension (Ju-Nam and Lead 2008). Citrate and PVP stabilised AgNPs are well documented in the literature (Doty *et al,* 2005, Tejamaya *et al,* 2012, El Badawy *et al,* 2013), and are described in further in chapter 1.

3.2 Aims and Objectives

The aim of this study was to produce stable citrate AgNPs using novel methods of synthesis, and successfully re-produce stable citrate and PVP AgNPs using published methodologies. Specific sub objectives were to:

i. To produce novel methods to synthesise citrate AgNPs by adjusting parameters of the experimental procedure such as temperature, concentration of reducing agent and stabiliser concentrations.
ii. Ensure citrate AgNPs were monodispersed and that the methodologies were reproducible to obtain the same size and morphology each time.

3.3 Citrate Capped Silver Nanoparticles

The effect of the synthesis conditions were manipulated to identify if systematic differences in controlling temperature, citrate concentration and sodium borohydride ($NaBH_4$) concentration could affect the physicochemical properties of AgNPs. A literature review found works by Asharani *et al* (2008) who capped AgNPs using soluble potato starch with an average reported size between 5-20 nm (TEM). Further investigation of the ingredients used 1 mM of $AgNO_3$ and 8 mM $NaBH_4$, with the addition of the potato starch as the stabiliser. With this in mind, a set of experiments were devised based on a combination of the same $AgNO_3$ and $NaBH_4$ concentrations (Asharani *et al,* 2008) assembled with reagent mixing methods produced in house by Cumberland and Lead (2009). Lists of the newly devised reactions are located in table 3.1. Particles produced using the new methods were characterised by a multi-method approach, while DLS and TEM measurements were taken over one year to assess the stability. Stable citrate AgNPs were also produced based on original works by Cumberland and Lead (2009), as described in chapter 2. Particle batches produced were also suitability characterised using a multi-method approach.

Table 3.1: Novel citrate AgNP experimental conditions. NOTE: Solutions are made up to 100 mL unless otherwise stated with*. *Denotes where 6 mLs of solution was used from the original stock solution. The "original" nanoparticles produced from Cumberland and Lead (2009) are listed for reference/comparison. Three different sets of reagents were set up with reference to the works of Asharani et al (2008) to produce method A, B and C. Each of the experimental conditions was altered to see if the temperature changes effected AgNP size and morphology. A total of 5 suspensions were produced from each method to assess the repeatability and the stability of the methods.

Table 3.1: Experimental Conditions for Synthesising Novel Citrate AgNPs					
Method Name	**$AgNO_3$**	**$NaBH_4$**	**Citrate**	**Heating time (hours)**	**Temp (^oC)**
	Molar Conc. (mM)	**Molar Conc. (mM)**	**Molar Conc. (mM)**		
(Cumberland and Lead, 2009)	0.25	0.25*	0.31	2	100
AgNP Method A					
A1	1	8	1	2	20
A2	1	8	1	2	30
A3	1	8	1	2	60
A4	1	8	1	2	70
A5	1	8	1	2	80
A6	1	8	1	2	100
AgNP Method B					
B1	1	8	2	2	20
B2	1	8	2	2	30
B3	1	8	2	2	40
B4	1	8	2	2	60
B5	1	8	2	2	80
B6	1	8	2	2	100
AgNP Method C					
C1	1	8*	1	2	30
C2	1	8*	1	2	60
C3	1	8*	1	2	80
C4	1	8*	1	2	100

An experiment to identify the effect of temperature (method A) kept variables including reagent addition the same for each experiment (table 3.1). Method B used a 2 mM

concentration of sodium citrate solution, with combined temperature variances to identify the effects upon particle size outcomes. Reagent mixing and addition were also kept the same to reduce the introduction of any random errors. A final experiment to identify the effect of the $NaBH_4$ concentration and temperature was conducted. Method C combines the use of Cumberland and Lead (2009) 6 mLs of sodium $NaBH_4$ from the original 8 mM stock solution previously used in the Asharani *et al* (2008) methodology.

As Cumberland and Lead (2009) produced AgNPs at average of 10 nm, it's possible to suggest that using a larger $AgNO_3$ and citrate concentration of 1 mM the particles produced should be >20 nm in size.

3.3.1 Characterisation and Analysis

AgNP imaging was performed on a JEOL 1200EX 100 kv Max system. Size distribution and morphology were analysed using Gatan Digital Micrograph imaging software. Samples were prepared by depositing a 100/200 µL drop of the AgNP suspension onto a 300 copper mesh grid with carbon film disk. The samples were left for 30 minutes to adhere to the grid before being washed with UPW, to remove excess solution. Details of sample preparation are discussed in chapter 2.

Particle size and size distribution were measured by DLS and Fl-FFF respectively. DLS was performed on a Nanosizer 5000 Malvern instrument and Fl-FFF used was an asymmetrical instrument purchased from Postnova Analytics. Optical properties of the synthesized AgNPs were measured by UV-Vis spectroscopy using a Janerway UV-Vis spectrophotometer. The concentrations of the AgNP suspensions were measured using

FAAS. Each of the experimental procedures was reproduced at least 3 times to assess their repeatability within the batches. Results given in all cases are an overall average over the replicates. Stability of the AgNP suspensions was monitored over a period of one year using UV-vis, DLS and TEM.

3.4 Polyvinylpyrrolidone (PVP) Capped Silver Nanoparticles

AgNP suspensions were synthesised and capped with PVP10. Hydrodynamic size determination was conducted using DLS and core sizes were determined by TEM and AFM. The SPR using UV-vis was used to confirm Ag, and concentration analysis was analysed using FAAS. Details of the preparation and methodology of these techniques are discussed in chapter 2.

3.5 Results and Discussion

3.5.1 Citrate stabilized AgNPs

3.5.1.1 Effects of Temperature

The results to assess the effects of varying temperature using fixed additions of the reagents are shown in table 3.2. It should be noted that the results for table 3.2 show the standard deviation for DLS to reflect the variability in the measured size between the replicates, not width of distribution. The PDI is the polydispersity of the particles in suspension. The standard deviation for TEM and Fl-FFF reflect the size distribution between the particles measured. Number of particles counted is determined as n and ND = not determined. ANOVA testing between the variations of each sample is defined by the *p* value for the TEM data.

Table 3.2: DLS, TEM and Fl-FFF results comparing the sizes obtained at 24 hours post synthesis compared to 1 year post synthesis for the effects of temperature controlled changes.

Table 3.2 AgNP Size Determination for Temperature Controlled Reactions									
Method A	**DLS Readings**						**TEM size (nm) 24hrs post synthesis**	**TEM size (nm) 1 yr post synthesis**	**Fl-FFF size (nm) 24hrs post synthesis**
	24 hours post synthesis		**1 month post synthesis**		**1 year post synthesis**				
	Z-average size (nm)	***PDI***	***Z-average size (nm)***	***PDI***	***Z-average size (nm)***	***PDI***			
A1 20°C	26 ± 1	0.3 ± 0.1	28 ± 4	0.3 ± 0.1	23 ± 1	0.3 ± 0.1	16 ± 7 (*n*=200)	18 ± 3 (*n*=200)	14 ± 2
Replicate 2	30 ± 10	0.3 ± 0.12	29 ± 7	0.3 ± 1.6	31 ± 6	0.3± 1.2	15 ± 3 (*n*=100)	17 ± 3 (*n*=100)	12 ± 1.7
Replicate 3	27 ± 8	0.1 ± 1.3	30 ± 2	0.3 ± 0.1	23± 0.5	0.3 ± 2.2	ND	ND	9 ± 0.02
Replicate 4	27 ± 1	0.3 ± 0.01	29 ± 1	0.3 ± 0.02	30 ± 0.8	0.3 ± 0.2	ND	ND	ND
Replicate 5	21± 0.5	0.3 ± 0.1	25 ± 2	0.3 ± 0.1	30± 0.6	0.3 ± 1.2	ND	ND	ND
							(*p* 2.75 E-14)	(*p* 0.78)	
A2 30°C	21 ± 1	0.4 ± 0.11	24 ± 1	0.6± 0.1	25 ± 3	0.4± 0.1	ND	ND	ND
Replicate 2	22 ± 3	0.3± 0.03	23 ± 0.5	0.5± 0.1	25 ± 0.4	0.6 ± 0.01	ND	ND	ND
Replicate 3	20 ± 0.7	0.4 ± 0.1	24 ± 2	0.5± 1.2	25 ± 3	0.29± 0.1	ND	ND	ND
A3 60°C	22 ± 1	0.5 ±0.06	23 ± 1	0.4± 0.07	24 ± 0.3	0.5 ± 0.06	ND	ND	ND
Replicate 2	25 ± 1	0.6 ± 0.2	30 ± 4	0.5 ± 0.12	24 ± 0.3	0.5 ± 0.1	ND	ND	ND
Replicate 3	24 ± 0.2	0.4 ± 0.01	25 ± 3	0.4 ± 0.01	26 ± 0.7	0.4± 0.01	ND	ND	ND
A4 70°C	23 ± 0.36	0.4 ± 0.004	23 ± 1	0.4± 0.009	26 ± 1	0.4 ± 0.01	ND	ND	ND
Replicate 2	25 ± 0.031	0.3± 0.1	26 ± 0.7	0.4 ± 0.03	26 ± 0.7	0.4 ± 0.02	ND	ND	ND
Replicate 3	25 ± 0.164	0.4± 0.03	24 ± 0.01	0.5 ± 0.1	27 ± 2	0.4 ± 0.1	ND	ND	ND
A5 80°C	28 ± 1	0.2 ± 0.03	25 ± 0.3	0.3± 0.05	25 ± 2	0.3 ± 0.05	ND	ND	ND
Replicate 2	28 ± 0.6	0.2 ± 0.02	26 ± 0.3	0.2± 0.02	27± 3	0.3 ± 0.02	ND	ND	ND
Replicate 3	25 ± 2	0.3± 0.1	27 ± 0.9	0.3 ± 002	26 ± 2	0.3 ± 0.01	ND	ND	ND
A6 100°C	23 ± 1	0.3 ± 0.01	25 ± 2	0.3 ± 0.05	24 ± 1	0.2 ± 0.03	17 ± 3 (*n*=100)	16 ± 3 (*n*=200)	18 ± 1
Replicate 2	25 ± 1.5	0.3 ± 1.2	24 ± 0.7	0.3 ± 0.07	24 ± 0.5	0.2 ± 0.1	16 ± 3 (*n*=100)	18 ± 2 (*n*=100)	12 ± 0.02
Replicate 3	24 ± 0.1	0.2 ± 0.4	30 ± 0.5	0.2 ± 0.1	24 ± 0.7	0.2 ± 0.3	17 ± 3 (*n*=200)	19 ± 3 (*n*=200)	ND
Replicate 4	21 ± 0.4	0.3 ± 0.1	32 ± 2	0.3 ± 1.2	25 ± 0.4	0.3 ± 0.1	17 ± 3 (*n*=100)	15 ± 2 (*n*=200)	ND
Replicate 5	28± 1	0.3 ± 1.08	26 ± 1	0.3 ± 0.7	25 ±0.003	0.3 ± 0.02	ND	ND	ND
							(*p* 1.28 E34)	(*p* 1.2E-24)	ND

The DLS revealed similar *Z*-average sizes between 20 and 30 nm for each experiment, with only small size growths and losses over time. Suspensions synthesised at 30^{o}C, 60^{o}C and 70^{o}C each had a PDI between 0.4 and 0.6 identifying polydispersity. Suspensions synthesised at 20^{o}C, 80^{o}C and 100^{o}C produced the most stable results over time, with smaller PDI's between 0.2 and 0.3. Monodispersed particles are defined by a PDI > 0.1 (Baalousha and Lead, 2012), with less than 5% coefficient of variation. Near monodispersed fractions are those which have less than 15% coefficient of variation (Baalousha and Lead, 2013). Suspensions at 20^{o}C had an average overall DLS size of 26 ± 4 nm and a TEM size of 16 ± 4 nm after 1 years post synthesis. AgNP suspensions at 80^{o}C produced an average DLS size of 26 ± 2.3 nm with a PDI of 0.2. Finally, suspensions produced at 100^{o}C were the most reliable with average DLS size of 23 ± 1 nm and a PDI of 0.2. The TEM sizes were 17 ± 3 nm 24 hours post synthesis, which were comparable at 17 ± 2 nm after 1 year with no significant difference between the NP sizes observed for the 100^{o}C replicates. Although, there was a significant difference between the TEM replicates for the particles synthesised at 20^{o}C post 1 year, suggesting the NPs became unstable over time introducing size variations.

As discussed in chapter one, AgNPs are produced Ag seeds in the presence of a reducing agent and grow to form NPs based on the reaction ingredients (Pillai and Kamat 2004). For this devised methodology (method A) the increased temperature should have acted as a catalyst to provide activation energy for the nucleation of the Ag seeds. Therefore one should have seen a difference in the sizes/shapes between the temperature variances, but instead observed increased stability, with increased

temperature over time. Due to the lower PDI results, AgNP suspensions synthesised at 20°C and 100°C were selected for further UV-Vis, TEM and Fl-FFF characterisation.

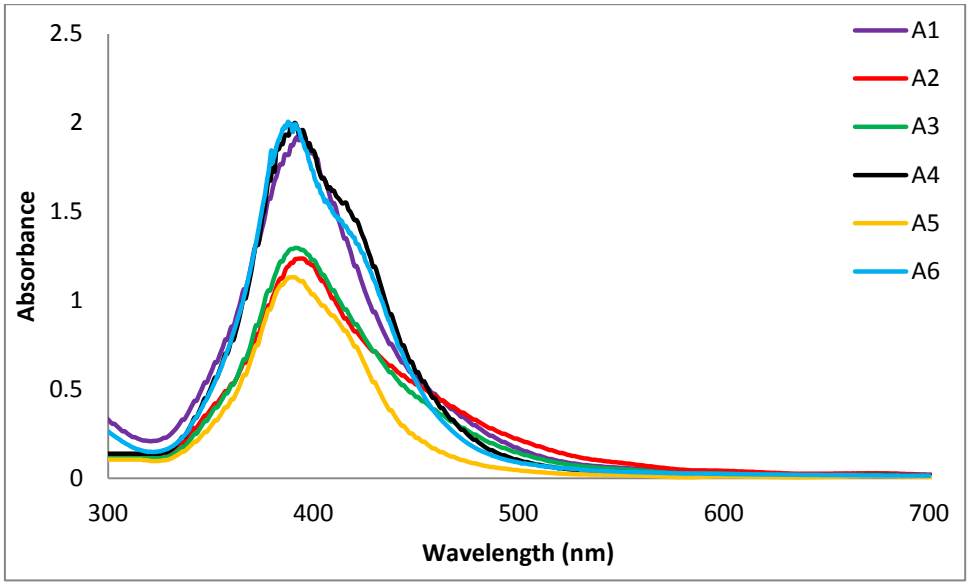

Figure 3.1: UV absorbance profiles for each of the temperature controlled conditions 24 hours post synthesis. The λ_{max} for each of the suspensions are as follows: A1 393nm, A2 393nm, A3 392nm, A4 390nm, A5 391nm, and A6 391nm. All solutions produced were orange in colour.

Suspensions synthesised at 20°C (A1), 70°C (A4), and 100°C (A6) have the highest AgNP concentrations (defined by the highest absorbance values). Suspensions synthesised at 30°C (A2) 60°C (A3) and 70°C (A4) exhibit peak boarding towards 600nm (figure 3.1). Peak boarding in this region is due to larger particles and non spherical aggregates present in the suspension. Particles synthesised at 80°C (A5) and 100°C (A6) have an average PDI of 0.2 but do not exhibit a board shoulder peak, showing they were less polydispersed than the other suspensions. Methods A5 and A6 also had a λ_{max} 391nm closest to the published literature for small citrate AgNPs. Smaller spherical Ag citrate monodispersed suspensions will give a sharper peak at around λ_{max} 390nm (Cumberland and Lead 2009, Tejamaya *et al,* 2012), to which all of NP suspensions had a λ_{max} within 390-396nm. To assess the stability of these synthesised particles the UV profile can

identify losses in concentration and shape changes. Particle suspensions A1 and A6 were deemed the best suspensions in terms of size, low PDI and were assessed after 1 year using UV-vis, which can be seen in figures 3.2 and 3.3.

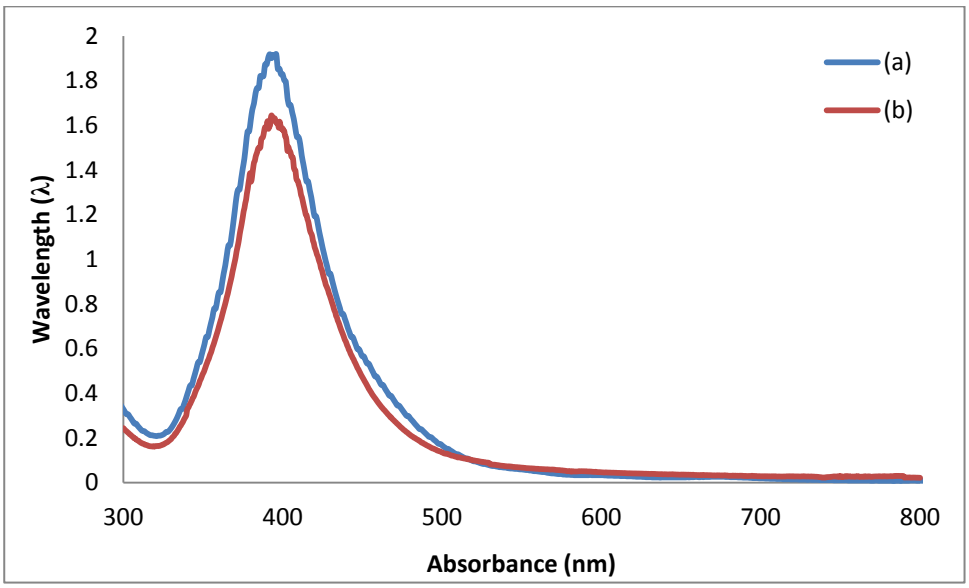

Figure 3.2: UV stability data for suspensions A1 synthesised at 20°C at 24 hours (a) and 1 year post synthesis (b).

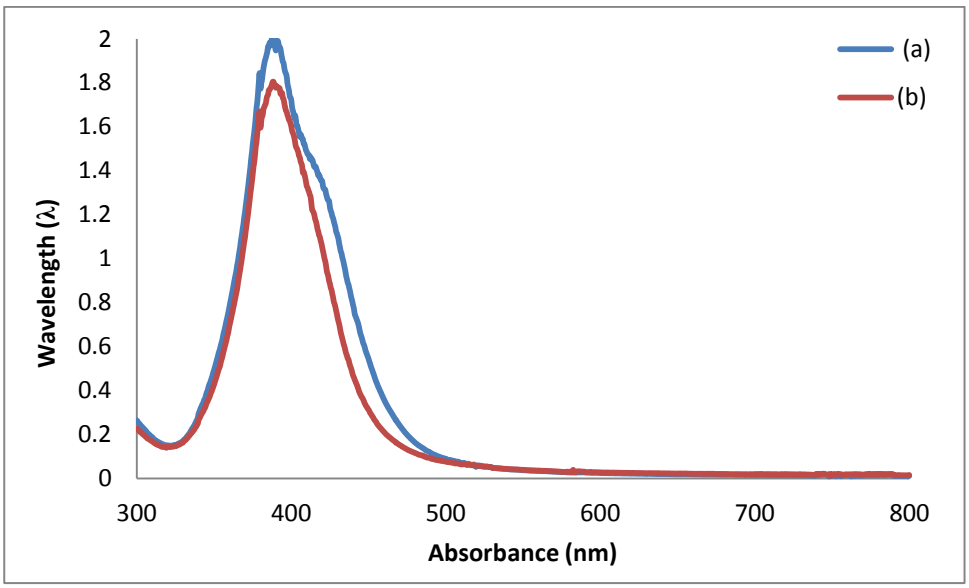

Figure 3.3: UV stability data for suspensions A6 synthesised at 100°C at 24 hours (a) and 1 year post synthesis (b).

Particle suspensions synthesised at 20^{o}C (figure 3.2) identified a small loss in Ag as a mass of total AgNP concentration, shown by the decrease in the SPR band after 1 year. Losses in NP concentration could have incurred from particle dissolution, which would account for the narrower band in the 400nm region. The peak max absorbance is 396nm after 24 hours post synthesis, compared to 393nm after 1 year. TEM analysis after 1 year post synthesis revealed large size differences between the batches, confirming the UV data of instability with batches synthesised at 20^{o}C.

The SPR bands in figure 3.3 identified small losses in AgNP concentration after 1 years post synthesis for AgNPs synthesised at 100^{o}C, which is comparable to the UV profiles obtained from the suspensions synthesized at 20^{o}C. Particle dissolution could further account for the reduction on the SRP band. Detailed analysis of the DLS results are presented in figures 3.4 and 3.5.

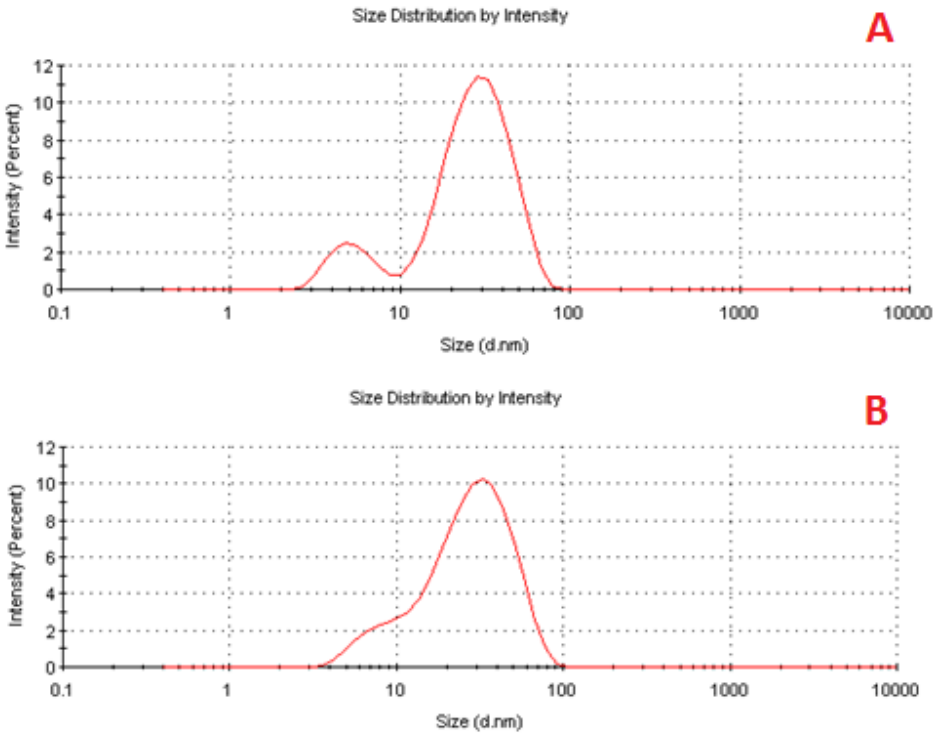

Figure 3.4: DLS size distribution intensity chart for suspension A1 20°C, A) 24 hours post synthesis and B) 1 year post synthesis.

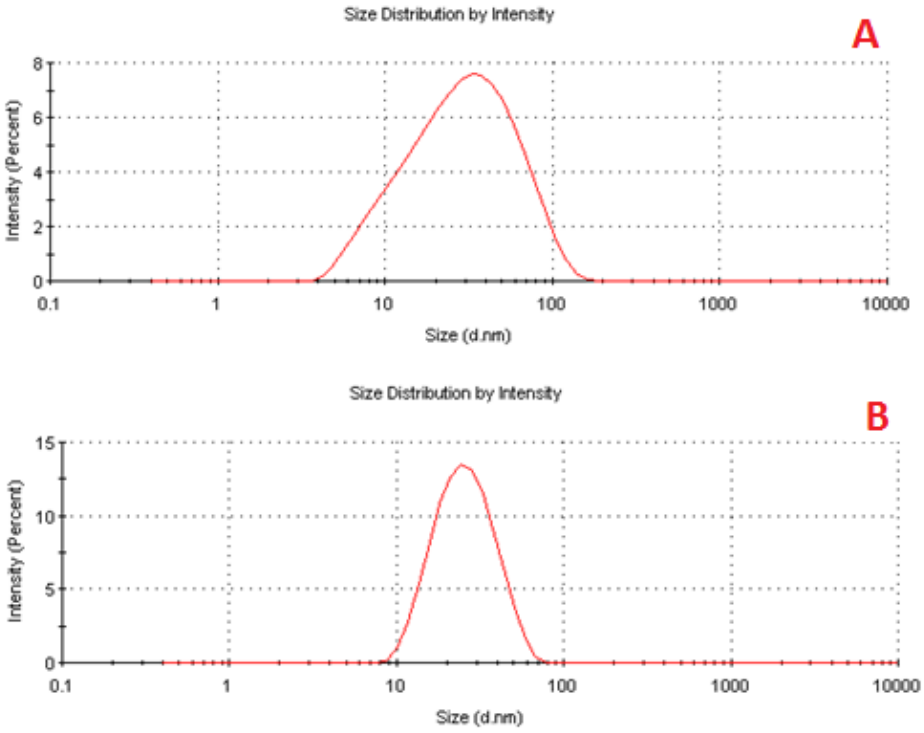

Figure 3.5: DLS size distribution intensity chart for suspension A6 100°C, A) 24 hours post synthesis and B) 1 year post synthesis.

Figure 3.4A identifies a bimodal peak distribution of size intensity represented by the two distinct peaks for particles synthesised at 20^{o}C. It is possible that the solution contains two uniform size ranges, one small and the other considerably larger. In comparison, after one year post synthesis (figure 3.4B), although there is little change in the PDI, the percentage intensity for the larger peak has dropped, followed by the two peaks merging. The information suggests particle dissolution has occurred over the 12 months to produce a wider distribution of sizes, which would account for formation of one large tailing peak.

For suspensions synthesised according to A6, the PDI is 0.3 for 24 hours and 6 months post synthesis, except after 1 year where it drops to 0.2. Figure 3.5A shows a board peak demonstrating a wide size distribution. However, figure 3.5B shows after 1 year the size distribution peak is narrower with a higher percentage intensity and reduced PDI. The TEM analysis also showed a slight reduction in average particles size over the year period. It's possible that the smaller particles dissolved over the year and the AgNPs have stabilised over time.

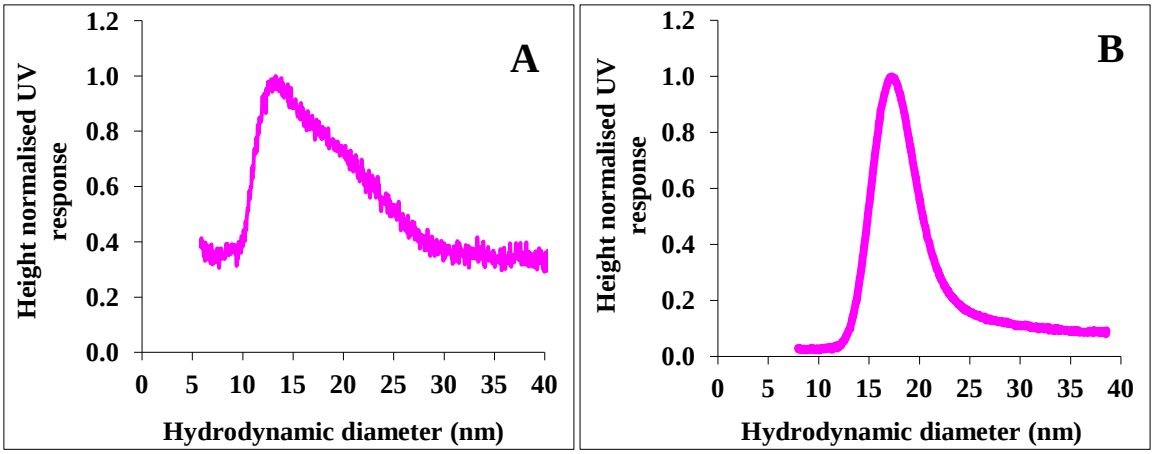

Figure 3.6: Fl-FFF size analysis of A: A1 20°C, a 500 µl injection for 30 minutes at a cross flow of 1 giving a reported size of 14 ± 2 nm. B: Method A6 100°C, a 500 µl injection for 30 minutes at a cross flow of 1 giving a size of 18 ± 1 nm. Both injection of size distributions were made 24 hours post synthesis.

Hydrodynamic size was determined by Fl-FFF, as shown in figure 3.6. The results for the Fl-FFF identified lower sizes than those given by the DLS. At 24 hours post synthesis for suspensions synthesised at 20°C, the DLS reported sizes of 26 ± 1 nm (replicate 1) compared to 14 ± 2 nm from the Fl-FFF. Similar findings were seen for those synthesised at 100°C, where Fl-FFF results produced 18 ± 1 nm compared to 23 ± 1 nm (replicate 1) from the DLS. It must be noted that the DLS over estimates size (details discussed in chapter 2) (Darlington *et al,* 2009), whereas the Fl-FFF measures size based on mass. Therefore, when the mass is converted to particle number the sizes are reported smaller (Baalousha *et al,* 2008).

Particles synthesised at 20°C give a boarder peak distribution compared to a well defined peak from particles synthesised at 100°C (3.6B). The information shows that the AgNPs from the A1 suspensions do not have well defined sizes, justified further by the broad UV peak presented in figure 3.3A. Well defined sizes will give a sharp defined peak like those seen in figure 3.6B for the Fl-FFF results.

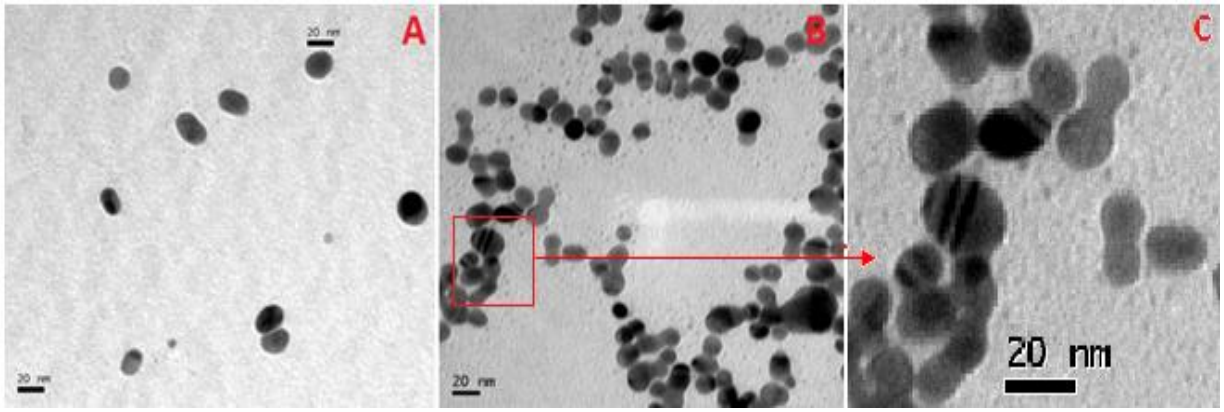

Figure 3.7: TEM images of suspensions (A) A1 20°C, (B) A6 100°C, and (C) shows particle surface dynamics zoomed in from image B (A6 100°C).

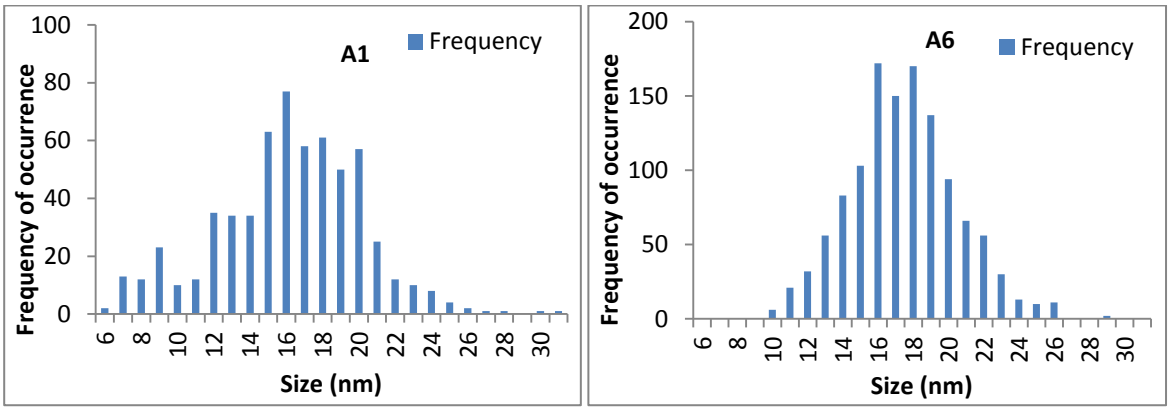

Figure 3.8: Corresponding TEM histogram size images of suspensions (A) A1 20°C and (B) A6 100°C.

For particles synthesised at 20°C, figure 3.7A show less concentrated particulates of non uniform spherical shapes. Towards the bottom right, two particles are agglomerating together, highlighting instability. TEM imagining revealed that the core size for NP suspensions synthesised at 20°C were 16 ± 7 nm for replicate 1 (based on the analysis of 200 particles), and 15 ± 3 nm for replicate 2 (based on 100 particles), compared to an average of 26 ± 1 nm (replicate 1) and 30 ± 10 nm (replicate 2) using DLS over the year period. As TEM measures core size this is expected to be lower than the reported hydrodynamic diameter measured by the DLS. The corresponding histogram in figure

3.8A identifies a wide distribution of obtained sizes showing a multimodal size distribution. The information presented from figures 3.7A and 3.8A support results obtained for the PDI (0.3 ± 0.1), DLS, Fl-FFF and UV-Vis band broadening, showing the particles are polydispersed for suspensions produced using method A at 20^{o}C.

However, figure 3.7B shows an image of more concentrated mixed particle sizes and morphologies compared to figure 3.7A. Core shell surface structures of vertically striated indentations can also been seen from these particles, as highlighted in figure 3.7C. The striations on the particle surface show the particles have a (1 1 1) formation as seen by similar images presented by Song *et al* (2011). The corresponding histogram in figure 3.8B shows an average size of 17 ± 3 nm counted from a combined total of 400 particles. Particles synthesized at 100^{o}C are less polydispersed and show a size normal distribution fit, with the most counted particle size between 16-20 nm. Similar size distributions for citrate AgNPs analysed by TEM were seen by Cumberland and Lead (2009). The information here corresponds to the defined Fl-FFF size peak and UV SPR bands, showing that the particles are more uniform in size compared to method A1.

Overall, there are no systematic trends between the heating temperature and size variations in this method. Although, the methodology did provide evidence that increasing the synthesis temperature increased the longer term stability of the AgNPs. As described in more detail in chapter one AgNPs are formed from silver seeds by the reduction of $NaBH_4$ in the presence of the stabiliser. Suspensions produced at 100^{o}C identified the most reliable results, producing stable, lees polydispersed AgNPs over a period of one year.

3.5.1.2 Effects of Citrate Concentration

The effects of doubling the citrate concentration during AgNP synthesis were assessed using fixed additions of the reagents with variable temperatures as seen in table 3.1. The results for the size determination are presented in table 3.3.

Table 3.3: DLS, TEM and Fl-FFF size results for 24 hours post synthesis compared to 1 year post synthesis for the effects of temperature and citrate controlled changes. The standard deviation for TEM and Fl-FFF reflects the size distribution between the particles measured. Number of particles counted is determined as n.*ND= not determined. ANOVA testing between the variations of each sample is defined by the p value for the TEM data.

Table 3.3: AgNP Size Determination for Citrate Controlled Reactions									
Method B	**DLS Readings**						**TEM size 24hrs post synthesis (nm)**	**TEM size 1 year post synthesis (nm)**	**Fl-FFF size (nm)**
	24 hours post synthesis		**1 month post synthesis**		**1 year post synthesis**				
	***Z-average* size (nm)**	**PDI**	***Z-average* size (nm)**	**PDI**	***Z-average* size (nm)**	**PDI**			
B1 20°C	23 ± 3	0.4 ± 0.1	21 ± 0.44	0.5 ± 0.08	25 ± 1	0.4 ± 0.1	ND	ND	ND
Replicate 2	22 ± 1.5	0.5 ± 0.03	23 ± 0.21	0.4 ± 0.02	25 ± 0.8	0.4 ± 0.1	ND	ND	ND
replicate 3	24 ± 4	0.4 ± 0.2	22 ± 0.28	0.4 ± 0.1	24 ± 5	0.4 ± 0.2	ND	ND	ND
B2 30°C	38 ± 4	0.2 ± 0.07	34 ± 3	0.2 ± 0.1	39 ± 7	0.1 ± 0.1	ND	ND	ND
Replicate 2	39 ± 7	0.11 ± 0.1	33 ± 0.9	0.1 ± 0.04	35 ± 3	0.1± 0.01	ND	ND	ND
replicate 3	36 ± 4	0.1 ± 0.05	35 ± 4	0.1 ± 0.1	38 ± 5	0.1 ± 0.1	ND	ND	ND
B3 40°C	37 ± 3	0.11 ± 0.01	34 ± 1	0.1 ± 0.01	34 ± 3	0.11 ± 0.1	ND	ND	ND
Replicate 2	34 ± 3	0.1 ± 0.04	34 ± 0.8	0.2 ± 0.2	32 ± 1	0.1 ± 0.3	ND	ND	ND
replicate 3	35 ± 2	0.1 ± 0.01	33 ± 3	0.1 ± 0.2	34 ± 4	0.1 ± 0.01	ND	ND	ND
B4 80°C	30 ± 1	0.3 ± 0.3	26 ± 3	0.3 ± 0.3	26 ± 0.3	0.3 ± 0.2	ND	ND	10 ± 0.5
Replicate 2	24 ± 2	0.3 ± 0.5	34 ± 1	0.3 ± 0.1	34 ± 4	0.3 ± 0.4	ND	ND	ND
replicate 3	26 ± 0.3	0.4 ± 0.1	29 ± 4	0.3 ± 0.2	30 ± 3	0.3 ± 0.02	ND	ND	ND
B5 100°C	24 ± 1	0.3 ± 0.3	23 ± 2	0.2 ± 0.2	24 ± 1	0.3 ± 0.2	15.5 ± 2.4 (*n*=100)	17± 3 (*n*=100)	13 ± 0.14
Replicate 2	24 ± 0.6	0.2 ± 0.01	25 ± 1	0.2 ± 0.1	32 ±4	0.3 ± 0.2	15.5 ± 3 (*n*=100)	16.6 ± 2.3 (*n*=100)	11 ± 0.08
replicate 3	24 ± 0.3	0.2 ± 0.2	23 ± 2	0.2 ± 0.4	24 ± 0.5	0.2 ± 0.1	16.2 ± 2.3 (*n*=100)	17 ± 2.6 (*n*=100)	12 ± 0.14
Replicate 4	25 ± 4	0.01 ± 0.05	24 ± 4	0.1 ± 0.02	25 ± 1.5	0.1 ±0.2	18 ± 3 (*n*=100)	17 ± 3 (*n*=100)	ND
Replicate 5	27 ± 2	0.1 ± 0.03	25 ± 3	0.2 ± 0.1	23 ± 0.7	0.2 ± 0.2	16 ± 3 (*n*=100)	18 ± 6 (*n*=100)	ND
							p= 0.001	p= 0.004	ND

The DLS data presented in table 3.3 identified a variation of sizes between the different batches of particulate suspensions. Information suggests that increased citrate concentration in combination with temperature variations, does see an effect to the particle size. Method B1 and B5 both represent the extreme ends of the temperature variances but yield similar sized particles, although B5 is less polydispersed than B1. In addition, the DLS results for B1 and B5 are also comparable to the results obtained for A1 and A6 for the same corresponding temperatures, although the PDI results were not comparable. The best particles produced from this method were those synthesised at 30^{o}C (B2), 40^{o}C (B3) and 100^{o}C (B5) as yielded particles that were less polydispersed than the other temperature variations with double citrate concentration.

Method B2 produced particles with a hydrodynamic diameter of 38 ± 4 nm 24 hours post synthesis and 39 ± 7 nm (replicate 1) when analysed 1 year later. The PDI was 0.11 ± 0.1 after 1 year, and had the sharpest SPR bands compared with the other temperature variations of this method of synthesis 24 hours post synthesis (figure 3.9). However, when compared to method A, AgNPs synthesised at 30^{o}C (B2) do see a larger difference between the hydrodynamic sizes. Information suggests temperatures between 30-40^{o}C do see a systematic difference in size and polydispersity when comparing the two methodologies. Further analysis of the suspensions using UV-Vis post 24 hours synthesis is described in figure 3.9.

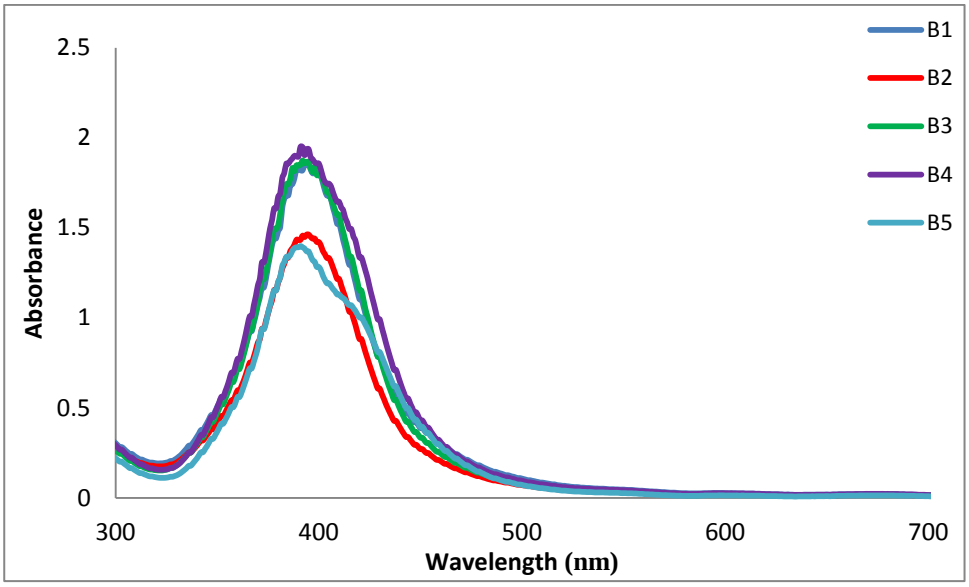

Figure 3.9: UV absorbance profiles for each of the citrate variant and temperature controlled conditions at 24 hours post synthesis. The λ_{max} for each of the suspensions are as follows: B1 394nm, B2 394nm, B3 392nm, B4 388nm, and B5 391nm. As with method A, all solutions were also orange in colour.

Figure 3.9 describes the UV-Vis profiles of each of the NP suspensions, all except B4 have a λ_{max} between 390-396nm, agreeing with reported literature results (Cumberland and Lead 2009, Tejamaya *et al,* 2012). Method B2 and B5 both show a decreased SPR band, showing that the total concentration of Ag in particulate form is lower compared to methods B1, B3 and B4. The UV-Vis was also measured for B5 after 1 year, which identifies a small loss in AgNP concentration shown in figure 3.10. Combined SPR and PDI data show that the particles synthesised by methods B2 and B3 are more stable and less polydispersed suspensions than B1, B4 and B5. Therefore the results show there is no linear pattern between temperature increases, with the addition of the double citrate concentration to the overall size distribution.

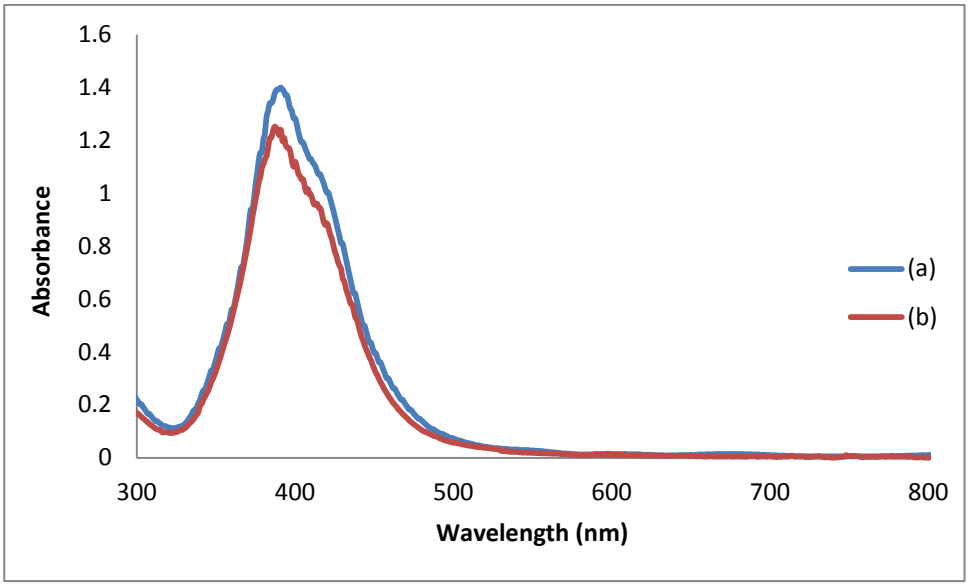

Figure 3.10: UV stability spectra (a) shows 24 hours post synthesis of the AgNPs and (b) shows the spectra at 1 years post synthesis for B5 at 100°C. The difference shows only a small loss in concentration after 1 year.

Figure 3.10 identifies the UV-vis SPR bands for 24 hours and 1 years post synthesis. Both absorbance peaks shows slight band stretching in the 500-600nm region, indicating the presence of larger particulates. These results confirm polydispersity with mixed PDI results between 0.1 and 0.3 for the replicates. The results are comparable to method D5 synthesised at the same temperature, to which particle dissolution could account for the reduction on the SRP band after 1 year post synthesis. Analysis by DLS and TEM provided information that these particles remained stable over a period of one year. The ANOVA test was used to identify that there was no significant difference between TEM sizes, for each of 100°C replicates measured at 24 hours post synthesis (*p* 0.001) and 1 year post synthesis (*p* 0.004).

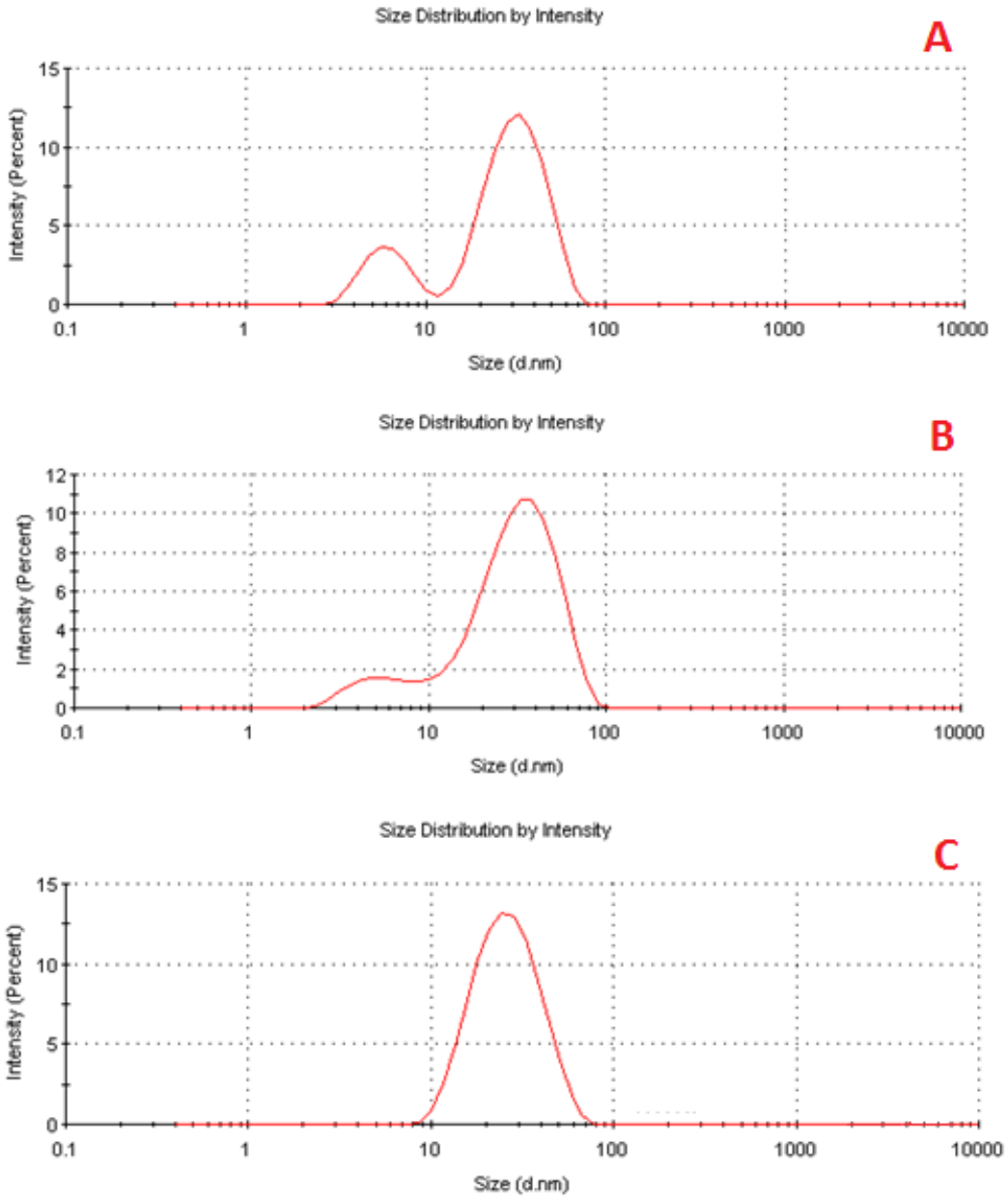

Figure 3.11: DLS size distribution intensity chart for A) B2 30°C, B) B3 40°C and C) B5 100°C, all measured at 24 hours post synthesis.

Although method B2 produced a small PDI between 0.1 and 0.2 over the year period, DLS size intensity identified a bimodal distribution, showing a presence of smaller particulates in suspension. When the temperature is further increased to 40°C shown in figure 3.11B, the two peaks combined to show a mixed distribution of sizes despite the PDI being lower

at 0.1. The DLS results for method B5 (figure 3.11C) have a better size distribution compared to B2 and B3, despite having a higher PDI which could have been over estimated. In comparison, AgNPs synthesised by method A6 at the same temperature, were more evenly distributed than those produced by method B5. Both methods of synthesis (A and B) yielded particles of similar sizes with an average of 24 ± 3.2 nm for A6, and 24 ± 1.5 nm for B5, 24 hours post synthesis. After 1 year the sizes were comparable at 24 ± 0.5 nm for A6 and 25 ± 1.5 nm for B5 at 1 years post synthesis. The reported *Z*-averages were also similar, despite method B5 having a smaller size distribution (figure 3.11).

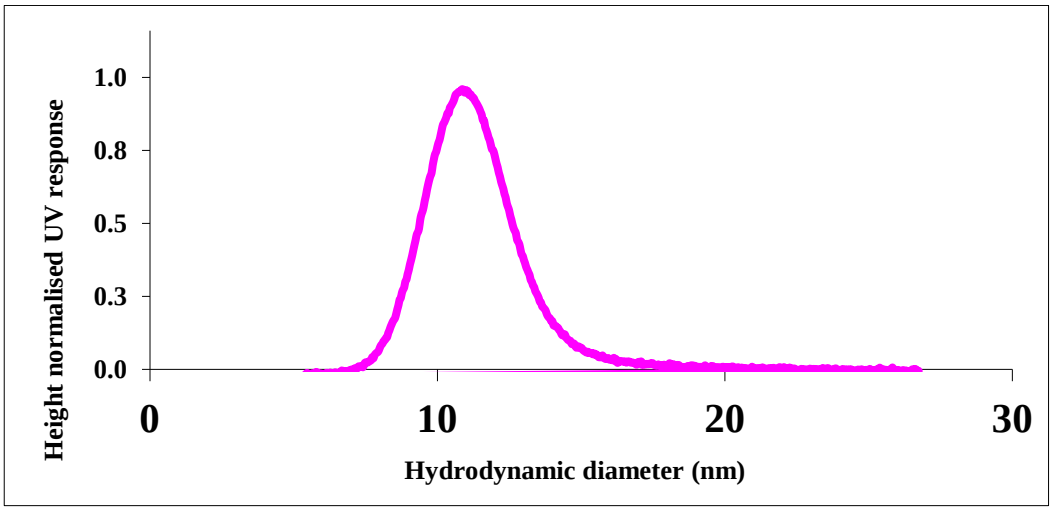

Figure 3.12: Fl-FFF hydrodynamic diameter for method B5 produced at 100°C using a 500 µl injection for 30 minutes at a cross flow of 1 giving a size of 13 ± 0.14 nm (replicate 1). (Standard deviation represents the deviation between the sizes as an average).

The Fl-FFF identified the average AgNP size to be at 13 ± 1 nm for method B5, which is smaller than the reported Fl-FFF size of 18 ± 1 nm for method A5 produced at the same

temperature. The information presented here also agrees with the DLS results presented in figure 3.11C, that both methods of synthesis produce a normal distribution of size.

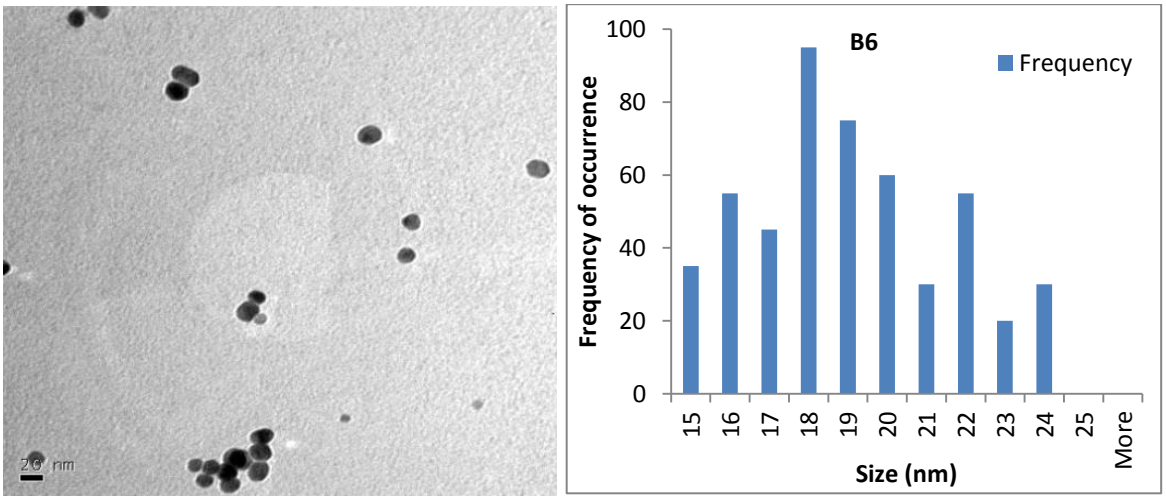

Figure 3.13: TEM image and corresponding histogram for particles synthesised at 100°C Replicate 1 (B5) 1 year post synthesis.

Particles synthesised using method B5 produced an average core size of 16 ± 3 nm 24 hours post synthesis based on a combined count of 500 particles. The suspensions 1 year later also yielded a comparable size of 17 ± 3 nm based on a 500 particle count (figure 3.13). The TEM image (figure 3.13, left) shows irregularly sized particles of a spherical form, and identifies particles similar to the NPs presented in figure 3.7B synthesized by method A6. The corresponding histogram shown in figure 3.13 (right) indentifies a size distribution between 15-24nm, compared to method A6 which had a range between 10-26 nm.

Overall, according to the DLS figures NP suspensions synthesized at lower temperatures were less polydispersed. Closer analysis of the size intensity revealed that they had a bimodal size distribution, which was comparable to results obtained for method A at lower temperatures. The best method of synthesis produced by this method

were those NPs produced at 100^{o}C, they were consistently stable and TEM analysis revealed no significant changes in sizes between the replicates over a period of 1 year. The results defined at there were systematic differences between the NP sizes obtained between the lower temperature variations when the citrate concentration was doubled, compared to the uniform sizes obtained from those of method A. Particulates synthesised at 30^{o}C and 40^{o}C produced larger sized NPs between 32-38 nm (DLS) from method B, compared to higher temperatures producing smaller sizes between 22-27 nm. Therefore with the exception of suspensions made at 20^{o}C, as the temperature increased, the AgNP size decreased.

3.5.1.3 Effects of Sodium Borohydride Concentration

Method C used fixed concentrations of $AgNO_3$ and $NaBH_4$, as presented by Asharani *et al* (2008), but used a 6 mL aliquot of $NaBH_4$, from the 8 mM concentration (table 3.1) as inspired by Cumberland and Lead (2009). A 1 mM concentration of sodium citrate was used to cap the NPs as used in method A. The temperatures were also varied to compare with methods A and B, to identify any linear effects upon particle size, morphology and stability.

Table 3.4: DLS and TEM size results at 24 hours post synthesis compared to 1 year post synthesis for the effects of temperature and sodium borohydride concentration controlled changes. Number of particles counted is determined as n *ND= not determined. ANOVA testing between the variations of each sample is defined by the p value for the TEM data.

Table 3.4: AgNP Size Determination for $NaBH_4$ Controlled Reactions							
Method C	**DLS Readings**						**TEM Sizes (nm)**
	1st reading 24 hours post synthesis		**2nd readings one month post synthesis**		**3rd readings 1 year post synthesis**		
	Z-average size (nm)	***PDI***	***Z-average size (nm)***	***PDI***	***Z-average size (nm)***	***PDI***	ND
C1 30°C	18 ± 0.7	0.6 ± 0.02	18 ± 0.4	0.6 ± 0.04	41 ± 0.5	0.6 ± 0.04	ND
Replicate 2	22 ± 0.1	0.6 ± 0.01	40 ± 0.5	0.6 ± 0.04	27 ± 2	0.6 ± 0.03	ND
Replicate 3	17 ± 0.5	0.6 ± 0.1	29 ± 0.4	0.6 ± 0.03	22 ± 0.2	0.6 ± 0.02	ND
C2 60°C	33 ± 0.2	0.6 ± 0.003	24 ± 0.7	0.5 ± 0.01	36 ± 0.8	0.6 ± 0.3	ND
Replicate 2	21 ± 0.3	0.6 ± 0.01	24 ± 0.7	0.6 ± 0.04	28 ± 0.5	0.5 ± 0.02	ND
Replicate 3	36 ± 0.8	0.6 ±0.1	33 ± 0.9	0.5 ± 0.02	32 ± 1	0.6 ±0.2	ND
C3 80°C	23 ± 0.8	0.5 ± 0.03	23 ± 0.6	0.5 ± 0.02	27 ± 1	0.5 ± 0.02	27 ± 7 (n=100)
Replicate 2	44 ± 1	0.5 ± 0.02	31 ± 0.7	0.5 ± 0.1	35 ± 1	0.5± 0.01	33 ± 12 (n=100)
Replicate 3	29 ± 0.6	0.5 ± 0.01	31 ± 1	0.5± 0.03	38 ± 0.5	0.5 ± 0.02	27 ± 8 (n=100)
							p= 1.96E-09
C4 100°C	22 ± 0.3	0.6n ± 0.05	18 ± 0.7	0.6 ± 0.04	28 ± 0.2	0.6 ± 0.04	ND
replicate 2	40 ± 0.1	0.6 ± 0.4	107 ± 1.5	0.6 ± 0.1	55 ± 0.6	0.6 ± 0.1	ND
Replicate3	35 ± 0.2	0.5 ± 0.02	30 ± 0.4	0.5 ± 0.01	51 ± 1	0.6 ± 0.04	ND

Table 3.4 identified that all of the suspensions were unstable after 1 year post synthesis and each suspension had a PDI between 0.5 and 0.6, showing high polydispersity. As method C3 exhibited a small growth over the year using DLS, further TEM observations of

the sample was conducted. No further analysis was governed for the rest of the samples as they were deemed unstable over time with large PDI numbers. It should be noted that the solution colours were not orange like the previous batches, but instead produced a dark green/brown coloured solution. AgNP studies by Stamplecoskie and Scaiano (2012) reported AgNPs that are a dark green/brown colour to have large particulates with a rectangular shape. Therefore these samples were imaged under using TEM to identify any differences in morphology.

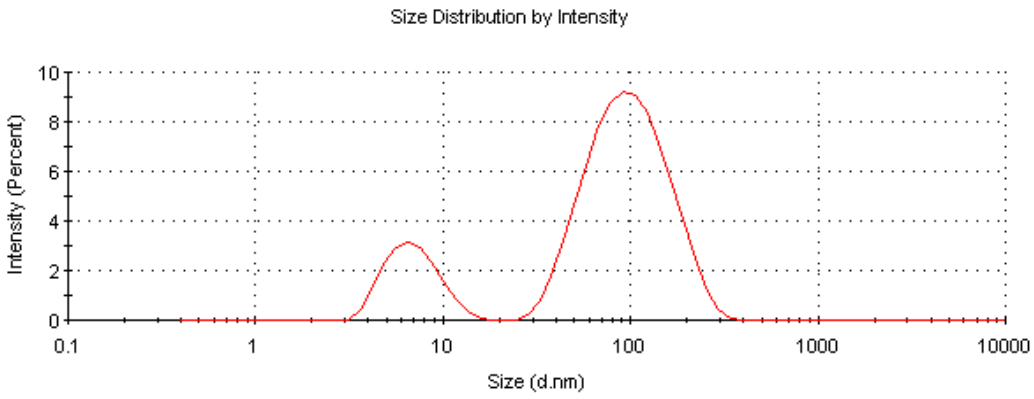

Figure 3.14: DLS hydrodynamic size profile for method C4 synthesised at 80°C 24 hours post synthesis.

The DLS size report in figure 3.14 identifies a bimodal distribution represented by the two peaks from the same sample. The double peaks correspond to different sizes of AgNPs in suspension showing that the particles are polydispersed which was also indicated by the high PDI number.

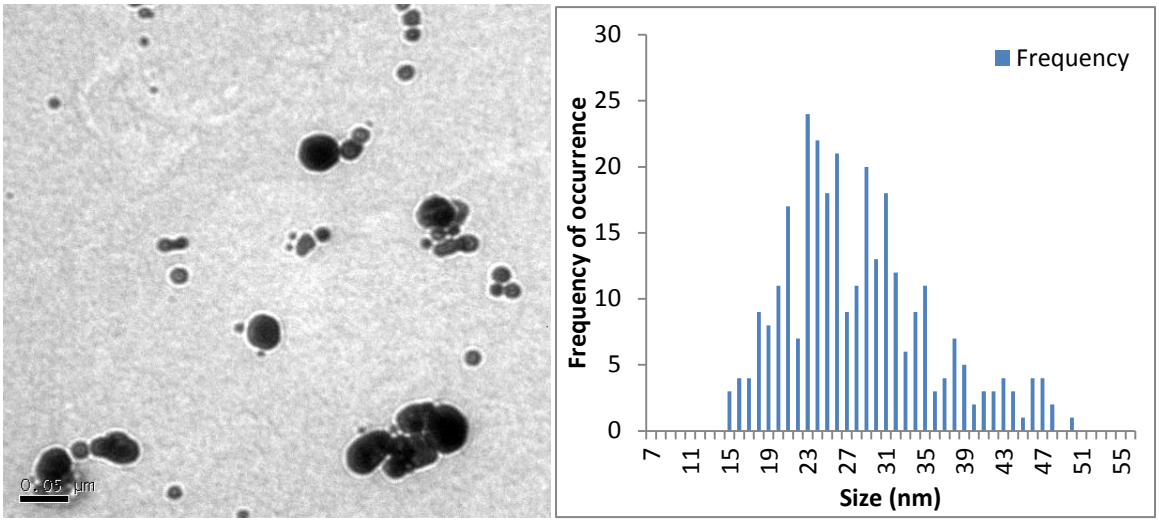

Figure 3.15: Example TEM image of particles synthesised at 80°C for method C.

Figure 3.15 (left) presents a TEM image which shows a multitude of size and shape variations with particle aggregation. Some particles appear slightly rectangular/tube shaped, agreeing with literature reports for the suspension colouring in relation to size and shape (Stamplecoskie and Scaiano, 2012). The peak distribution in the corresponding histogram shows a bimodal distribution, consistent with the DLS size distribution and reported PDI. Using a 300 particle count the average core size was reported at 29 ± 9 nm. The TEM results show the largest proportion of particles are between 15-30 nm, with a small number of particles larger than 40 nm as shown in figure 3.15. Whereas, the DLS identifies the largest peak contribution to be assigned from larger particulates shown in figure 3.14. As previously discussed larger particles scatter more light than the smaller particles to give an abnormal estimation of the larger particulates % intensity in suspension (Darlington *et al,* 2009). Since each of the suspensions synthesised in method C produced similar sizes and PDI numbers, it is confirmed that there are no differences between the batches made at varying temperatures.

Overall, three methods of particle synthesis was conducted to produce citrate capped AgNPs. DLS, TEM, Fl-FFF and UV-Vis (except method C) were used to study the stability of the particles over one year. Fl-FFF was used to determine the hydrodynamic diameter 24 hours post synthesis for methods A and B. The effects of temperature for all variations of method A, identified no linear size differences as the temperature increased. Although each of the NP suspensions were similar in size, the best AgNP suspensions were produced from method A6, with an overall average PDI of 0.2, DLS size of 23 ± 1 nm and TEM sizes of 17 ± 3 nm (24 hours post synthesis) and 17 ± 3 nm (1 year post synthesis).

The effects of doubling citrate concentration were observed in method B. The results identified that the AgNP suspensions did show size systematic differences between the batches, with the exception of solutions produced at 20^{o}C. The remaining solutions decreased in size as temperature increased. Suspensions synthesized by method B also had lower PDI between 0.1 and 0.3 than those produced by method A. Therefore higher citrate concentrations with the temperature variances produced less polydispersed particles than those produced by method A. The increased citrate concentration will have increased the amount of free citrate in solution, and would have occupied all sites on the NP surface where the coating and surface attractive forces bind. Therefore, higher citrate concentrations produced higher electrostatic repulsion between nanoparticles to prevent NP-NP interactions and reduced aggregation during synthesis. It is also possible that if the ingredients had of been added in a different way, such as $AgNO_3$ and $NaBH_4$ first to allow the silver seeds to grow, with varied time frames before the addition of citrate, there may have been better size variations within the batches

produced in method A and B. Nonetheless, the best AgNPs were produced using method B5 which gave an overall average PDI of 0.1, a DLS size of 23 ± 1 nm, and TEM sizes of 16 ± 3 nm (24 hours post synthesis) and 17 ± 3 nm (1 year post synthesis).

Method C and its variants were used to assess the amount of $NaBH_4$ effects upon particle sizing. Each of the reported *Z* averages of the solutions shifted upon analysis suggesting they were unstable over time. The suspensions produced were very polydispersed with a PDI on average between 0.5 and 0.6. TEM imaging revealed irregular size and shapes of the particles therefore these particles will not be used in further analysis.

In 2009 our group were able to produce monodispersed pristine citrate AgNPs which were published by Cumberland and Lead (2009), with an average core size of 13.7 ± 6.2 nm (TEM) and an average hydrodynamic diameter of 35 ± 8 nm. The methodology was later modified my Romer *et al* (2011) who produced these particles at a published DLS size of 20nm. The researchers based their methodology on the reduction of Ag salts in the presence of sodium citrate with $NaBH_4$ as a reducing agent, originally devised by the works of Doty *et al* (2005). Tejamaya *et al* (2012) produced PVP stabilised AgNPs of a similar size. Both the citrate and PVP particles described have been previously documented for their well known behaviour, stability, size and morphology in different media and therefore will be used in the long term mesocosm studies presented in chapters 4 and 5.

3.5.1.4 Synthesis of Stable Citrate AgNPs

AgNP suspensions were produced using methodology created by Cumberland and Lead (2009) to provide particles for further studies. The batches of particles were grouped as the following:

- Spring batch (used in the spring natural water and UPW experiments).
- Summer batch (used in the summer water and EPA moderately hard water experiments).
- Autumn batch (used in the autumn water and EPA moderately hard water with SRFA).
- Winter batch (used only in the winter natural water).

Particles synthesised at these time points were split between the seasonal variations of the natural waters and the synthetic water simulations discussed in more details in later chapters.

Table 3.5: DLS, AFM and TEM size results comparing the sizes and concentrations obtained for each technique for previously published citrate AgNPs. The number of particles per count is referred to as n.

Table 3.5: Multi-Method Characterisation of Stable Citrate AgNPs					
Technique	**Size (nm)**				**Overall**
	Spring	**Summer**	**Autumn**	**Winter**	**Average**
TEM	12 ± 2	11 ± 3	11 ± 3	12 ± 2	11.5 ± 2.5
n=	260	326	350	236	1172
					p 3.92E-14
AFM	11 ± 3	12 ± 3	12 ± 4	11 ± 3	11.5 ± 3.25
n=	138	154	208	193	693
					p 0.004
DLS (Z-average)	22 ± 1	21 ± 2	22 ± 2	18 ± 0.7	20.75 ± 1.4
Zeta Potential (mV)	20.5 ± 2	20 ± 2	22 ± 3	24 ± 2	21.6 ± 2
PDI	0.1 ± 0.02	0.1 ± 0.09	0.2 ± 0.05	0.1 ± 0.03	0.1 ± 0.04
FAAS (Concentration ppm)	11.32 ± 0.07	12.44 ± 0.03	12.87 ± 0.05	11.73 ± 0.03	11.5 ± 0.45

Results presented in table 3.5 identify a variation of sizes between the different methods of characterisation. DLS results were on average 10 nm larger than those that reported the core size, which is expected for the hydrodynamic diameter size measurement (Darlington *et al,* 2009, Xia *et al,* 2012). Methods that measured core size (TEM and AFM) produced results which were comparable to each other. Simultaneously, ANOVA testing for the variance between AgNP sizes for TEM and AFM revealed no significant differences between the batches. The only difference between the batches was introduced in the autumn particulates which had a higher PDI of 0.2 compared to 0.1 for spring, summer and winter NP suspensions. Therefore all batches were reproducible in terms of size and stability, reducing any systematic error and bias between the suspensions when they were used in later studies described in chapters 4 and 5.

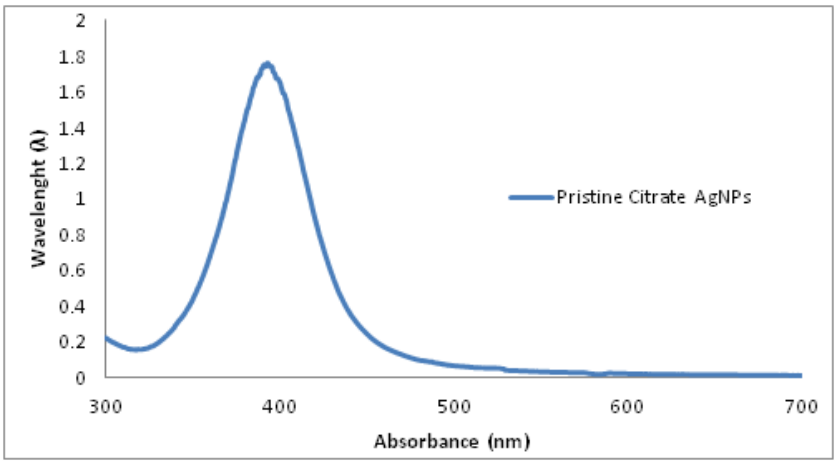

Figure 3.16: UV absorbance spectra for pristine stable citrate capped AgNPs.

Figure 3.16 identifies an example UV SPR peak for citrate AgNPs. The literature states that monodispersed suspensions of spherical citrate AgNPs will give a sharp peak at around 390-396nm (Cumberland and Lead, 2009, Tejamaya *et al,* 2012). Particles produced using this method had a reproducible SPR peak of 396nm which confirmed literature results. Further analysis of the citrate particles identified an average (DLS) hydrodynamic diameter of 20 ± 1 nm between the batches (Table 3.5).

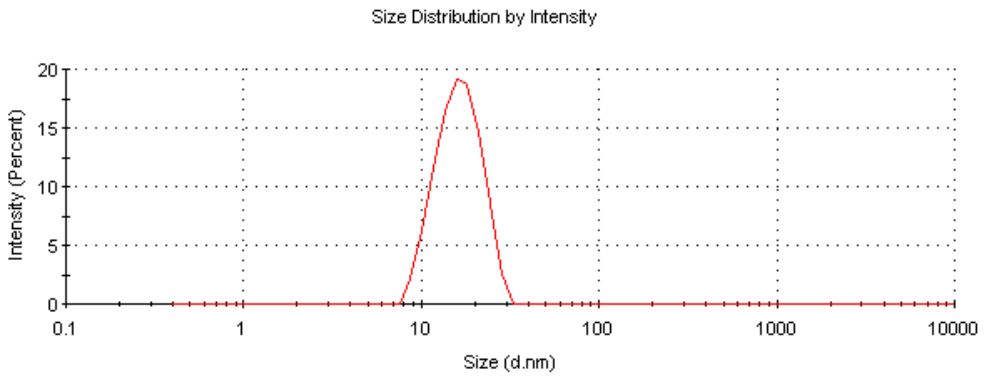

Figure 3.17: An example of a DLS size intensity distribution for citrate AgNPs.

The size distribution identified (figure 3.17) a small narrow peak showing monodisperse AgNPs, agreeing with the average PDI overall of 0.1 ± 0.04 as shown in table 3.5.

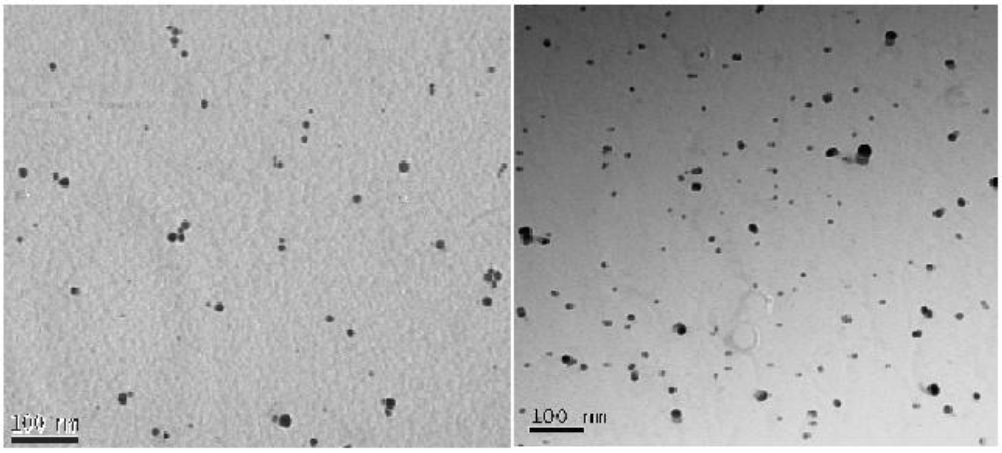

Figure 3.18: Example TEM images of pristine citrate AgNPs, left image shows AgNPs from the spring batch, and right shows particles from the autumn batch.

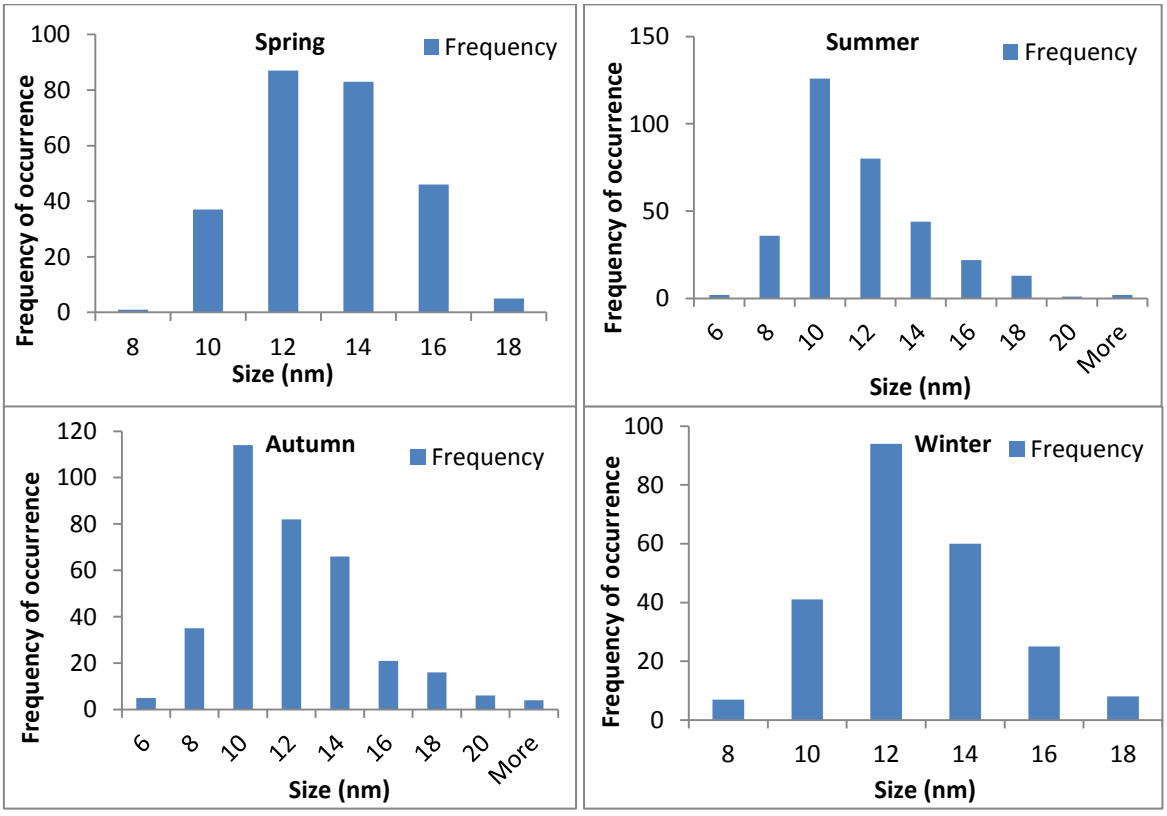

Figure 3.19: TEM histograms of the size occurrence for the different batches of citrate AgNPs suspensions.

Figure 3.18 shows example TEM images of particles made from two separate batches. Particles are small and spherical with the some slightly larger in the autumn batch. Particles made in the spring had an average core size was 12 ± 2 nm, and the corresponding histogram identified that the most frequent core particle size was 12 nm. The histogram represented a bell shaped distribution between the sizes of particles measured. The summer batch of particles had an average core size of 11 ± 3 nm, with the most occurring size of 10 nm. The representing histogram for the summer particles has a right screwed distribution with a tailing peak from a few larger outliers in the size range, however these are still normal distributed sizes. According to the histogram for the autumn batch of particles, a small increase in the size distribution in the representing histogram would account for the elevated the PDI number of 0.2. Despite the presence of some larger particulates the average core size was 11 ± 3 nm with the most frequent size being 10 nm, which compares to the previous particle suspensions. Finally, the particle suspensions synthesised in winter had a bell shaped curve distribution with an average size of 12 ± 2 nm, with the most occurring size of 12 nm.

All of the particle batches synthesised were evenly distributed size and were reproducible between the suspensions. The results obtained match that of the UV profile with a sharp SPR peak between 380-296nm determining small spherical particles. TEM analysis of the citrate AgNPs show the combined size distributions reported to be agreement and match those produced by Cumberland and Lead (2009).

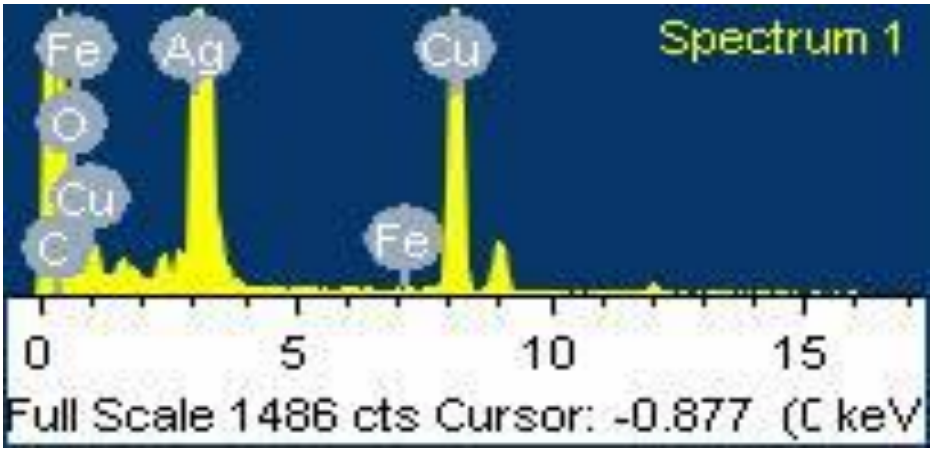

Figure 3.20: EDX spectra for pristine citrate AgNPs.

To determine the elemental presence of Ag and check the purity of the suspensions, EXD was conducted as shown in figure 3.20. The large Ag peak confirms Ag in the sample and the copper signal is from copper mesh grid used to mount the sample. There is a small iron peak which could be due to contamination of the grid from inside the TEM.

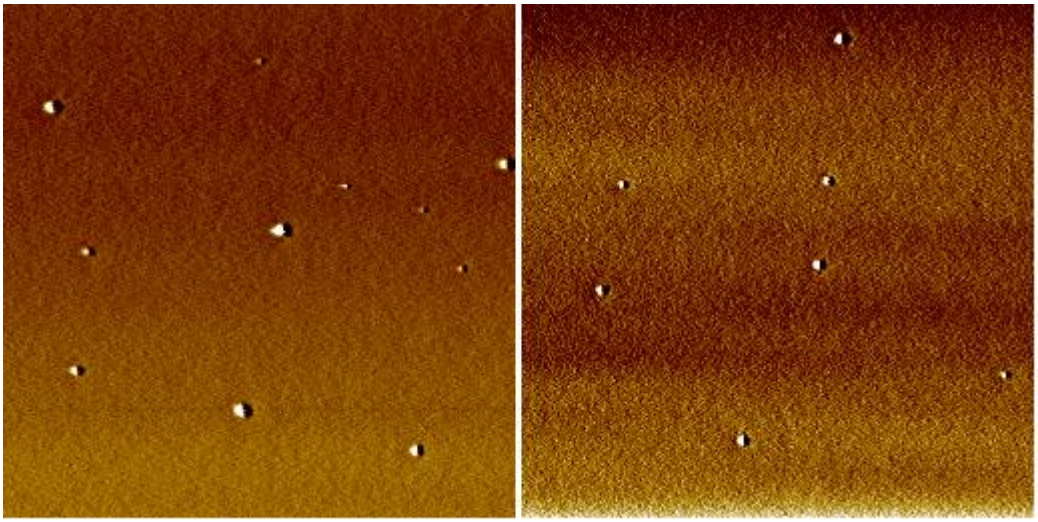

Figure 3.21: Example AFM images of pristine citrate AgNPs mounted on to a silica mica sheet, left autumn batch and right autumn batch.

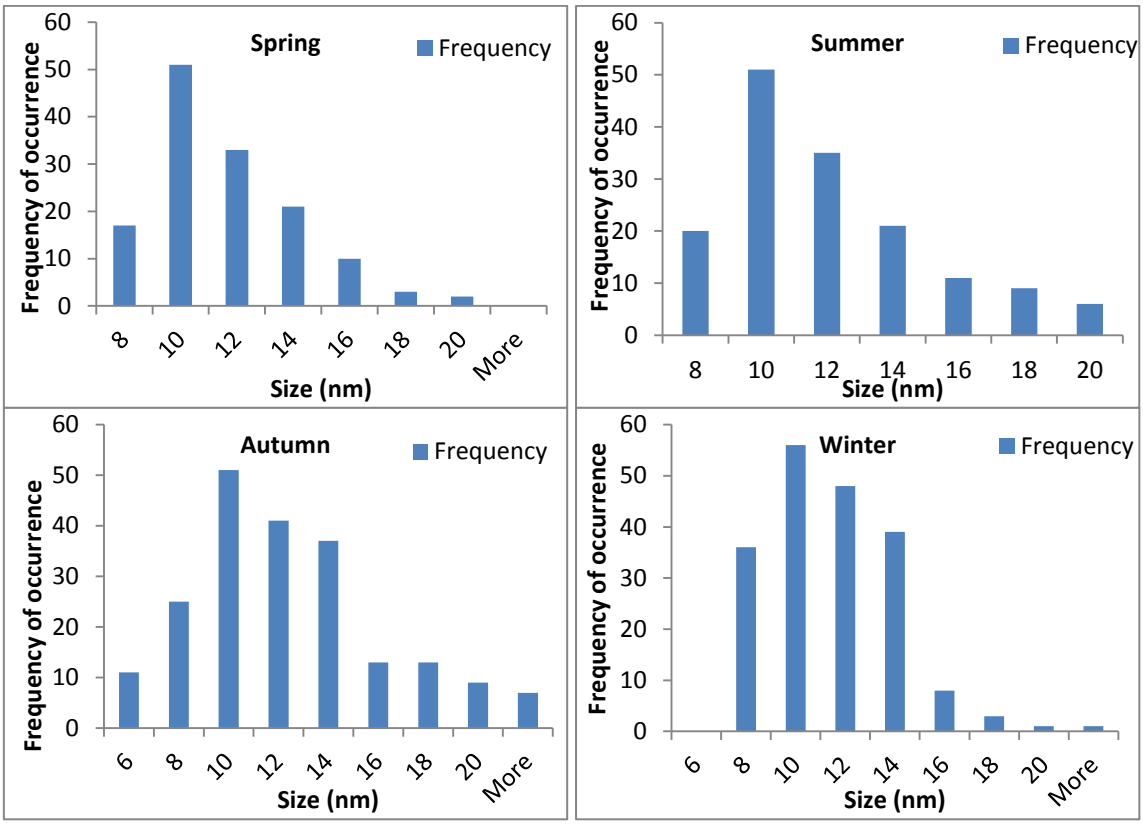

Figure 3.22: AFM histograms of the frequency of size occurrence for the different batches of citrate AgNPs suspensions.

Citrate AgNPs were analysed by AFM as another method to determine the core size which was comparable to the data obtained from the TEM. Figure 3.21 highlights two different batches of citrate AgNPs from the spring and autumn. Both images show small, less concentrated AgNPs on the mica surface. For the spring batch of particles the reported TEM size was 12 ± 2 nm (n=260), compared to 11 ± 3 nm (n=138) when analysed by AFM. When comparing the AFM histogram (figure 3.22) there is a small presence of NPs larger than 20 nm, which was not observed with TEM. Since AFM measures the surface topography compared to the morphology observed from the TEM, consideration of possible dust particulates adhering to the mica sheet could account for the presence of larger particulates.

The AFM histogram for the summer batches of particles shows the same right screwed distribution as those presented in the figure 3.19. Both histograms sets for TEM and AFM analysis identify the most frequently sized particle to be 10nm, with the average TEM size of 11 ± 3 nm (n=326) and AFM size of 12 ± 3 nm (n=154). Therefore, both sets of data are in agreement to each other. Analysis of the autumn batches of particles show both sets of histograms from the TEM and AFM to have the same size distribution, with the most frequently occurring size of 10 nm respectively. Although the average core size for the winter suspensions were 12 ± 2 nm (n=236) by TEM and 11 ± 3 nm (n=193) by AFM, the corresponding histograms were dissimilar. The AFM histogram revealed a higher distribution of 8 nm particles when measured compared to TEM. There was also presence of particulates larger than 18 nm when analysed by AFM.

To conclude, the overall results show that the citrate particles produced AgNPs that were reproducible in terms of size between the batches. NP suspensions had an

average hydrodynamic diameter of 20.75 ± 1.4 nm (DLS) and a core size of 11.5 ± 3 nm (TEM and AFM) between the batches. Despite the PDI of 0.2 for the autumn batch of NPs, the overall PDI was 0.1 ± 0.04 between each of the batches made. The EDX of the sample confirms the particles are Ag and no contaminates were present.

3.5.2 PVP Stabilized AgNPs

PVP stabilised AgNPs were specifically synthesised to be used for further fate and behaviour studies discussed in later chapters. Batches of particles were produced and compared for their reproducibility and PDI in accordance to the literature (Tejamaya *et al,* 2012). The particle batches were classified into the following groups in accordance with the citrate AgNP suspensions:

- Spring batch (used in spring natural water and UPW experiments).
- Summer batch (used in summer water and EPA moderately hard water experiments).
- Autumn batch (used in autumn water and EPA moderately hard water with SRFA).
- Winter batch (used only in the winter natural water).

Particles synthesised at these time points were split between the seasonally changing waters and the synthetic waters simulations, discussed in more details in later chapters.

Table 3.6: Table 3.6: DLS, AFM and TEM size comparison data, with polydispersity index and concentration for the previously published PVP synthesised AgNPs.

Table 3.6: Multi-method characterisation of stable PVP AgNPs					
Technique	**Size (nm)**				
	Spring	**Summer**	**Autumn**	**Winter**	**Overall Average**
TEM	11 ± 2	11 ± 3	12 ± 2	12 ± 3	11.5 ± 2.5
n=	172	107	274	244	797
					p 0.0007
AFM	12 ± 3	11 ± 3	12 ± 3	12 ± 3	11.75 ± 3
n=	226	197	125	123	671
					p 0.014
DLS (*Z-average*)	21 ± 0.4	19 ± 2	19 ± 0.2	21 ± 6	20 ± 2.15
Zeta Potential (mV)	-27.7 ± 4	-31 ± 3	-38.5 ± 5	-28 ±3	-31.3 ± 3.75
PDI	0.2 ± 0.01	0.2 ± 0.08	0.2 ± 0.05	0.3 ± 0.05	0.2 ± 0.04
FAAS (Concentration ppm)	19.39 ± 0.01	19.57 ± 0.01	19.47 ± 0.04	19.34 ± 0.03	19.44 ± 0.02

Results presented in table 3.6 show the size determinations for each of the characterisation methods. As with the citrate particles, the DLS results were an average 10 nm larger than those of the core size. TEM and AFM produced results which were almost identical to each other within ± 1 nm and ANOVA analysis determined no significant difference between the batches made. With the exception of the winter batch with a PDI of 0.3, each set of particle suspensions had an average PDI of 0.2, showing that they are less polydispersed. Overall, all batches were reproducible for size, stability and concentration.

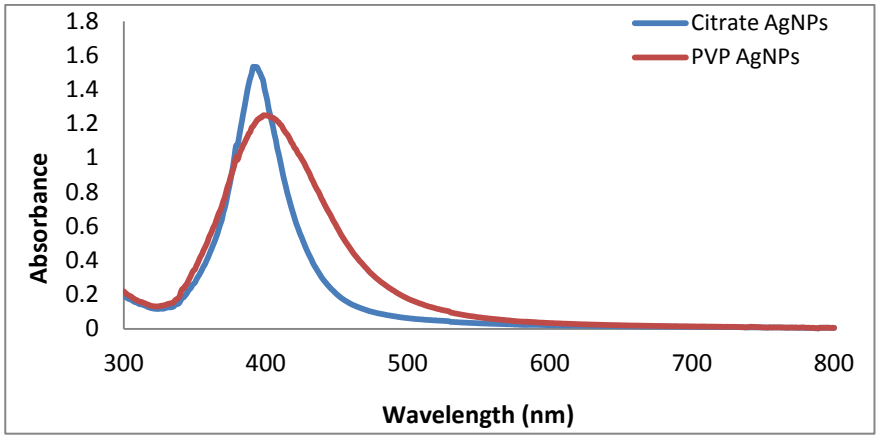

Figure 3.23: UV absorbance spectra for pristine PVP stabilised AgNPs compared to the absorbance spectra obtained to AgNPs stabilised with citrate.

PVP AgNPs were yellow/orange in colour and had an SPR absorption peak max at 400nm compared to citrate particles at 390nm (Tejamaya *et al,* 2012). Figure 3.23 compares the citrate SPR band, to the PVP SPR band. Note that the concentration of PVP AgNPs was reported higher at 20 ppm, but in order to get the profiles to fit on the same spectra the AgNPS were diluted; citrate 1:2 and PVP 1:4. The citrate AgNPs peak is much narrower than the PVP AgNP peak, showing that the particles are less polydispersed. The PVP particles have a stretched tail in the 500-600nm region identifying the presence of slightly larger particulates than the citrate suspension. The PDI given by the DLS in table 3.6 also confirms mixed particulates in suspension.

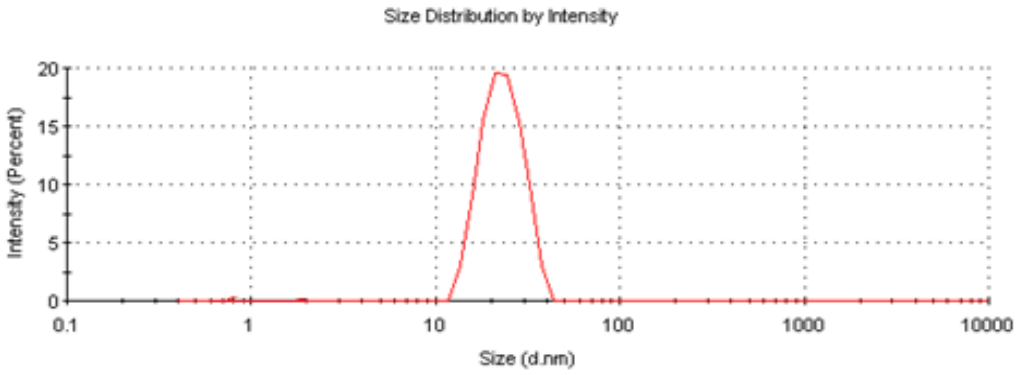

Figure 3.24: DLS size intensity for pristine PVP AgNPs.

The DLS size intensity is similar to those produced by the stable citrate particles. Although on closer inspection the percent (%) size intensity is slightly higher and the peak is shifted slightly more to the right, when compared to the citrate particles in figure 3.17 (DLS), identifying the NPs are slightly larger.

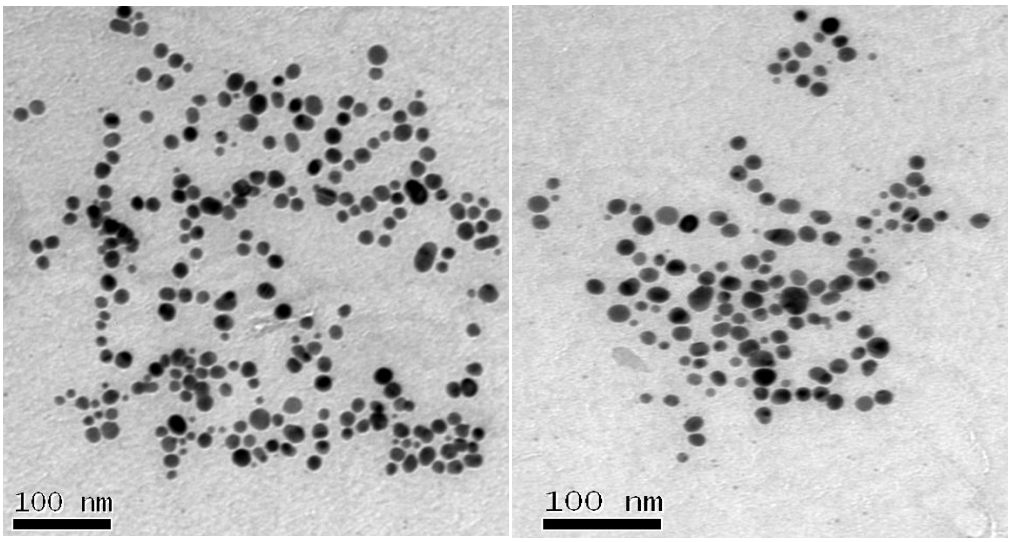

Figure 3.25: TEM images of pristine PVP produced AgNPs.

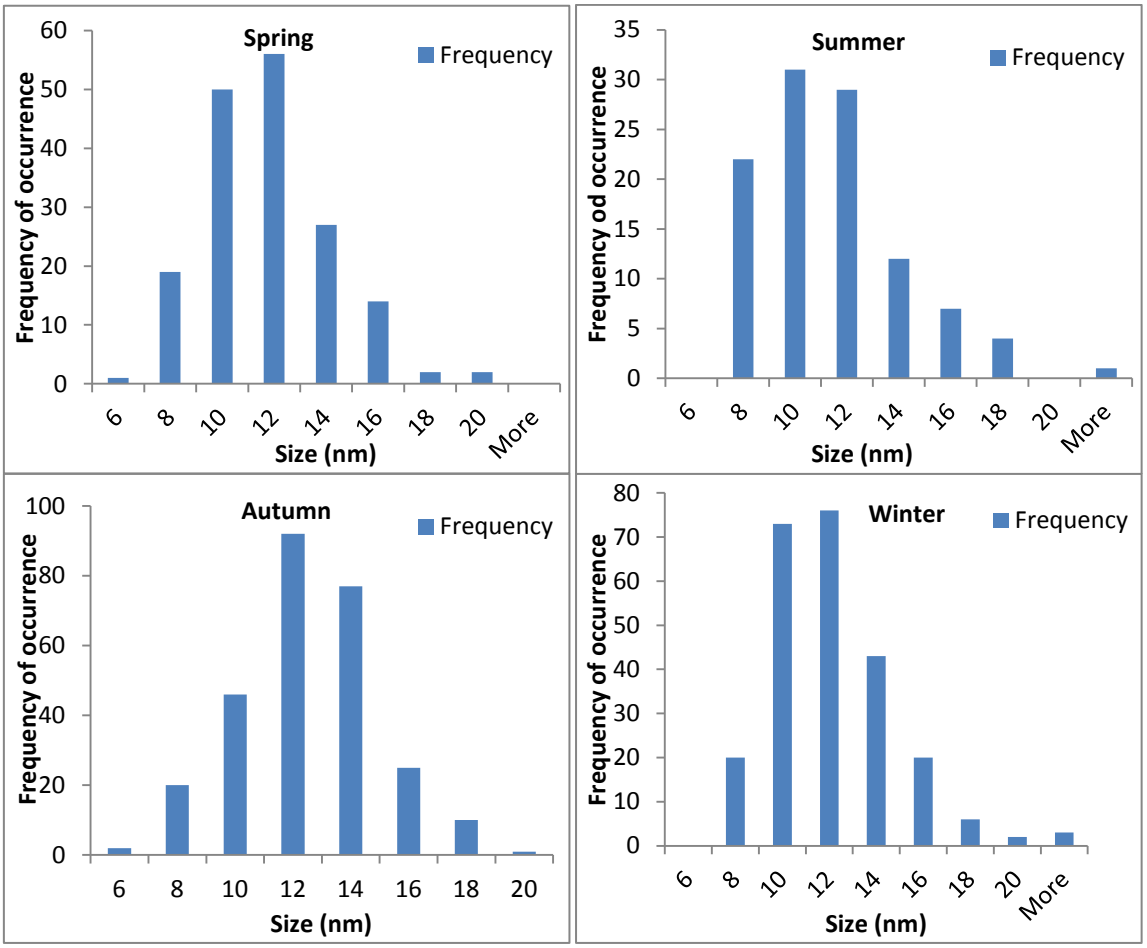

Figure 3.26: TEM histograms of the frequency of size occurrence for the different batches of pristine PVP AgNPs suspensions.

The TEM images (figure 3.25) revealed high concentrated areas of spherical PVP particles of slightly differing sizes, which corresponded to the reported PDI, although the average size overall was 11.5 ± 2.5 nm. Particles produced in the spring batch produced an average core size of 11 ± 2 nm, comparable with the citrate AgNPs of 12 ± 2 nm. The corresponding histogram (figure 3.26) identified the most frequent sizes were between 10-12 nm, and the size distribution was between 6-20 nm, with one outlier larger than 20 nm. As the PDI was 0.2 the size distribution from the TEM correlates to the results obtained from the DLS, and describes why the SPR banding has a wider peak than the citrate particles. The summer batch of particles was also comparable to those produced

in spring. The most occurring size was also between 10-12 nm and the distribution of sizes ranged from 8-18 nm with a few outliers larger than 20 nm.

Particles produced in the autumn batches show a bell shape curve of size distribution, with particles sized between 6-20 nm. The most frequently occurring sizes were 12 nm which corresponds to the average size produced for this batch of 12 ± 2 nm. The TEM results within each of the batches produced gave consistent results identifying that the methodology is reproducible. The reproducibility of the particles gives confidence that the particles can be compared between the batches, especially when exposed to more complex environments. Therefore the transformations that could occur to the NPs once exposed to complex environments will be due to solution chemistry, and not bias from the difference in synthesised batches.

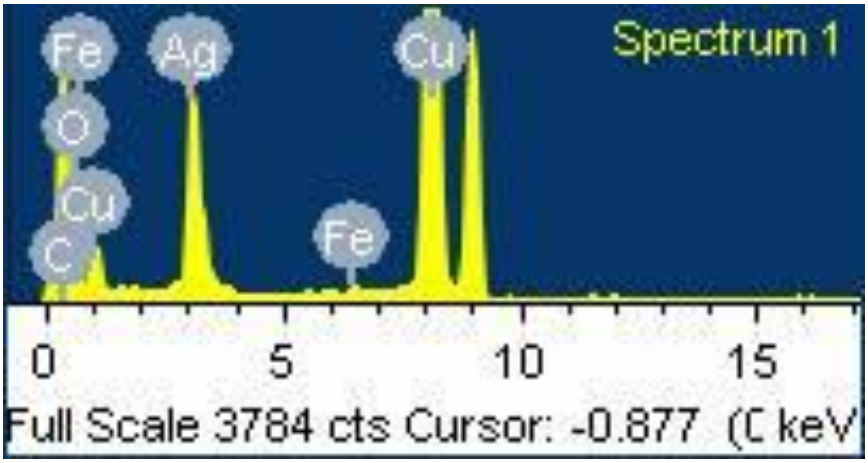

Figure 3.27: EDX spectrum of PVP capped AgNPs.

Figure 3.27 describes the elemental analysis of the PVP AgNPs. The copper peak is due to background noise from the copper mesh grid in which the sample is mounted. The large Ag peak shows the particles are Ag and the iron peak is from background noise of the TEM.

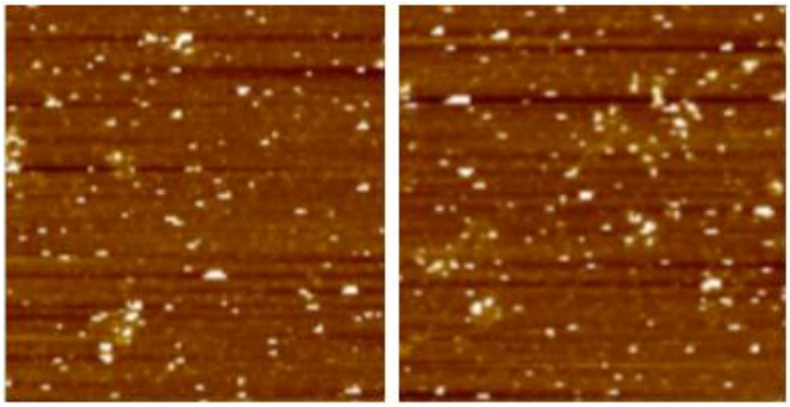

Figure 3.28: Example AFM images for pristine PVP AgNPs

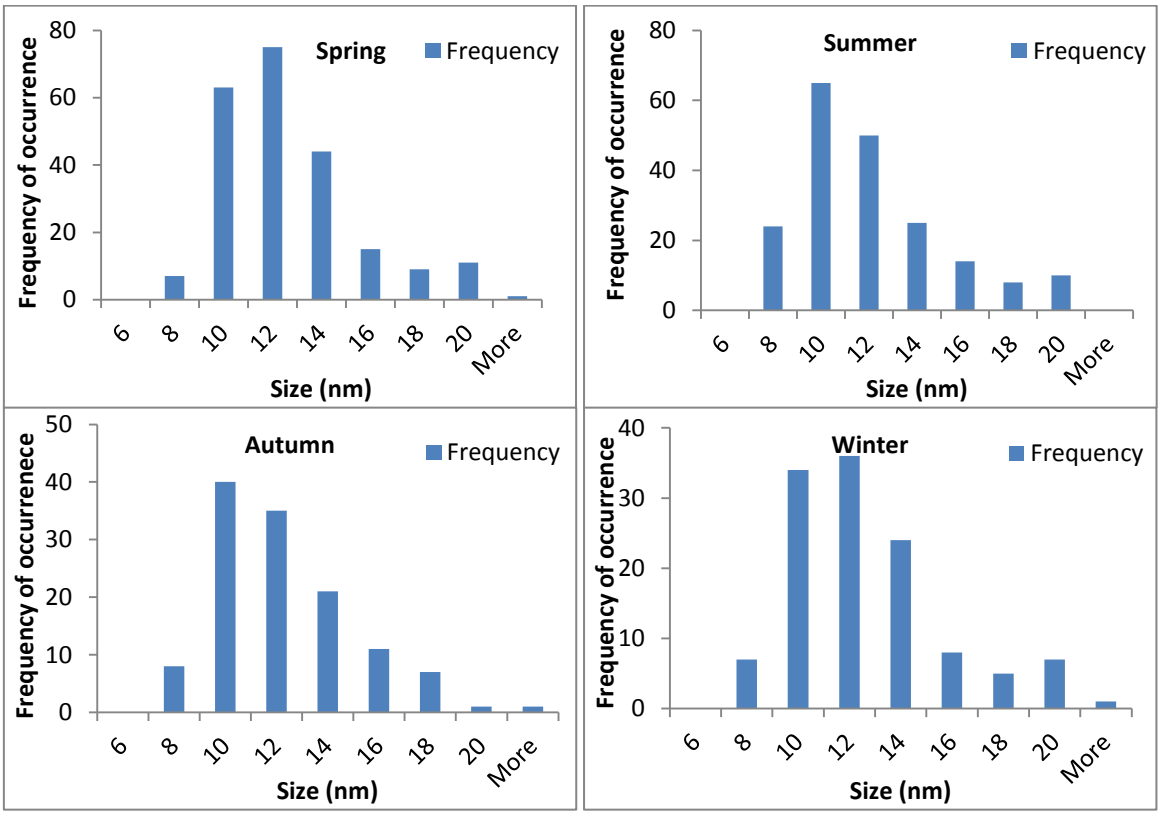

Figure 3.29: AFM histograms of the frequency of size occurrence for the different batches of PVP AgNPs suspensions.

As with the TEM images presented in figure 3.25, the AFM images (figure 3.28) show highly concentrated areas of particulates adhered to the mica sheet. The topography images show the presence of smaller and larger particulates, which futher correlates to the average PDI and broardened SPR peak. The results for the AFM between the

seasonal batches of particles were almost identical to those obtained with the TEM in terms of average size. The only difference were some slight vairations in the size fequency histograms, where the AFM results tended to have a small presence of larger particlulates than those measured by TEM.

3.6 Conclusion

Overall there were three different methods were used to attempt to produce novel sized stable citrate AgNPs. From the three methods of synthesis the best results were obtained from method B3 synthesised at 40^{o}C. These suspensions had an average hydrodynamic diameter of 35 ± 2 nm with a PDI of 0.1, and were on average more stable over 1 year. Method B5 produced and overall average PDI of 0.1, DLS size of 23 ± 2 nm and a TEM size of 17 ± 3 nm. Although the particles produced in method B3 and B5 were stable over a period of 1 year, more time was needed to assess their ageing and long term effects once exposed to various ionic solutions at environmentally relevant conditions. These further investigations would ensure that the stability and transformations were due to changing environments rather than AgNP instability.

Due to the lower polydispersity, size, documented stability and associated transformational behaviour in different media, the citrate stabilised AgNPs by Cumberland and Lead (2009) and PVP capped AgNPs by Tejamaya *et al* (2012) have been re-produced for further experimental procedures in this thesis. These particles have been suitably characterised in correspondence to the original authors, reported literature sizes and morphologies.

Chapter 4

Fate of Silver Nanoparticles in Synthetic Aquatic Media: Impact of Surface Coating and Natural Organic Matter

4 Chapter Outline

The present study assessed the transport and behaviour of AgNPs once released into large scale water systems. Citrate (11.5 ± 2.5 nm by TEM) and PVP (11.5 ± 2.5 nm by TEM) coated AgNPs as described in Chapter 3, were exposed to three simple water types and monitored over a period of 28 days. Large scale mesocosm studies were set up to mimic real life exposures where particles were introduced in a holding sieve to surface waters, to allow the NPs to diffuse through the water at their own rate. Particle movement throughout the system was monitored using marked injection points along the side of the mesocosm column (as seen in Chapter 2). During the first 14 days the stability of the AgNPs was assessed by measuring total Ag and dissolved Ag, then again on days 21 and 28. TEM imaging was carried out where possible on the samples to assess changes in size and morphology. The movement of the particles between the compartments was assessed using UV-Vis spectroscopy.

4.1 Introduction

Little information is currently known about the transport and behaviour of AgNPs in the wider environment. Factors that are known to influence particle fate are natural organic matter (NOM), ionic strength of the water and aggregation of the particles in solution. Particle aggregation will increase particle size, reduce surface area and slow down the process of dissolution (Hotze *et al,* 2010). Capping agents are designed to increase stability of the AgNPs by reducing the surface energy (Ju-Nam and Lead, 2008), which prevent interactions with the surrounding environment and avoid NP-NP interactions reducing aggregation rates (Kvitex *et al,* 2008). Therefore the chemistry, fate and transportation mechanisms of AgNPs are required in order to assess the risks that are posed to the environment and human health as a result (Bea *et al,* 2013, Kittler *et al,* 2010).

Despite the presented information in the literature (see chapter 1), most studies were conducted using small scale laboratory experiments, not large realistic release measurements. The purpose of this study was to conduct large scale mesocosm column experiments and mimic realistic exposure points which are monitored at controlled depth heights. Large mesocosm experiments incorporated two different surface coated AgNPs exposed to simple synthetic water and electrolyte concentrations, building to more complex waters with natural organic matter (NOM) to assess the chemistry, behaviour and transportation of AgNPs. A diffusion-sedimentation model was devised on the works of Socolofsky and Jirka, (2004) and Hinderliter *et al* (2010) to allow us to predict the transportation of the total Ag in the mesocosms.

4.2 Aims and Objectives

The aims of this chapter were to identify the behaviour and transformations of AgNPs similar size with different capping agents in simple aquatic media. AgNPs were spiked at the top of tall mesocosm columns standing 1 meter in length, with a holding capacity of 43 L containing either UPW, EPA standard moderately hard water or EPA moderately hard water with SRFA. Specific sub-objectives were:

i. To assess the behaviour of Ag^{+} using control studies of $AgNO_3$ released in UPW and EPA moderately hard water.
ii. Identify the transportation of AgNPs and assess patterns in behaviour such as diffusion and sedimentation.
iii. Assess any surface coating specific differences in the behaviour, transformations and transport of the AgNPs.

Overall the combined objectives will help understand AgNP fate and behaviour in simple waters, which will help to predict the interactions that AgNPs will encounter in natural aqueous environments.

4.3 Experimental

Synthesis of citrate and PVP stabilised AgNPs are discussed in chapter 2 and are characterised in chapter 3. The preparation of EPA waters and SWFA are discussed in chapter as are the mesocosm design and dosing. The presence and movement of AgNPs in solution was determined by UV-Vis (detailed in chapter 2, section 2.2.2). TEM was used to identify size the morphological transformations of the AgNPs (chapter 2, section 2.2.5). EDX was used to provide information on the elements present in solution (chapter 2, section 2.2.6). Total Ag concentrations were determined by FAAS (chapter 2, section 2.2.9).

In order to predict and validate the transport mechanisms followed by the AgNPs once released, we devised a simple diffusion-sedimentation model (Socolofsky and Jirka 2004, and Hinderliter *et al*, 2010). Further details of the model, including definitions, parameters and equations are presented in chapter 2. Total Ag concentrations obtained from the studies were plotted with the modelled concentrations and the differences were discussed. Prior to analysis, $AgNO_3$ pilot studies were conducted in UPW and EPA water, to assess the transport of Ag in the mesocosm. Samples of total Ag were taken over 12 days from each of the surface, middle (0.5 m depth) and bottom (1 m depth) and analysed by FAAS.

4.4 Results and Discussion

4.4.1 $AgNO_3$ Exposures

4.4.1.1 $AgNO_3$ in Ultrapure Water

To assess the diffusion of Ag throughout the mesocosms, a control study using $AgNO_3$ in UPW was spiked at the surface. $AgNO_3$ concentrations were calculated based on an equilibration concentration of 100 ppb and the study ran for 12 days. The total Ag results from each depth are presented figure 4.1, as an average of 3 replicates and are plotted alongside the modelled predicted concentrations of Ag in each depth in figure 4.2, with the model parameters outlined in table 4.1.

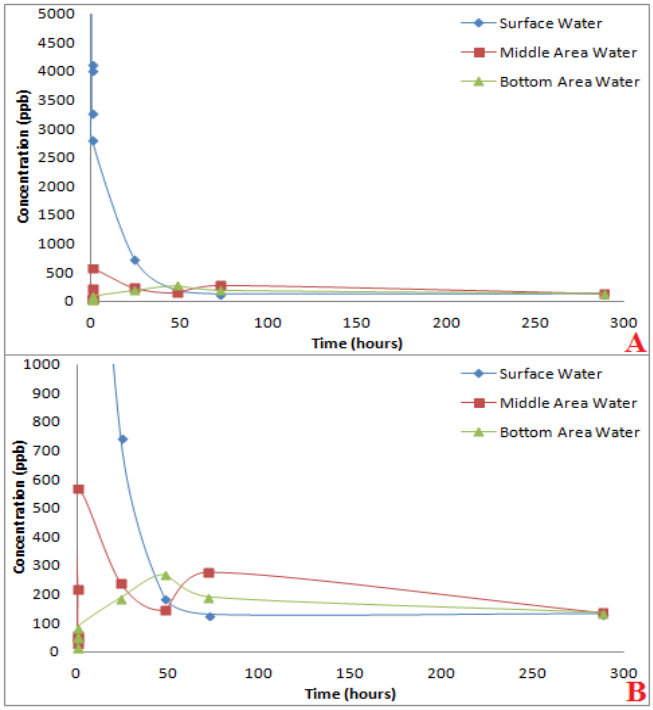

Figure 4.1: Total Ag recovery concentration (ppb) measured by FAAS for $AgNO_3$ exposed to UPW over a period of 12 days, showing the concentration changes at the different depths of the column. A) All samples and B) shows a zoomed image of those samples less than 1000 ppb.

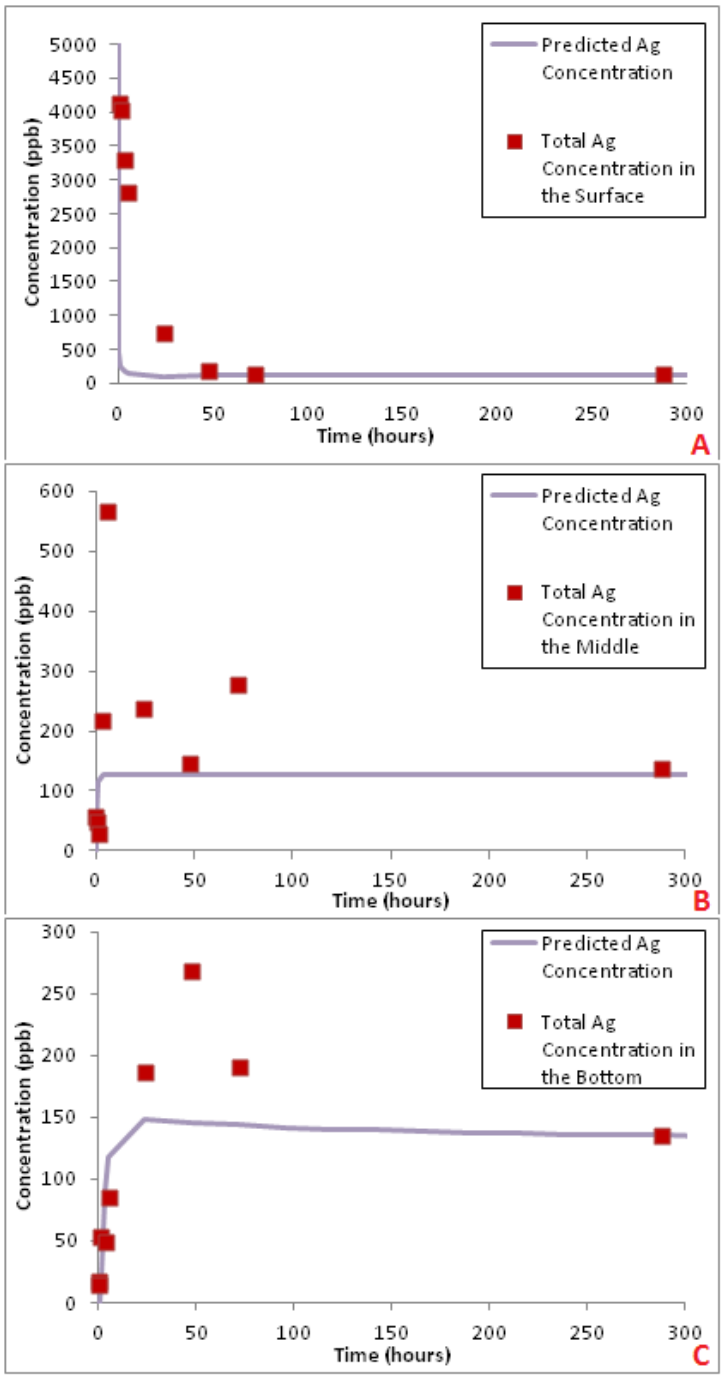

Figure 4.2: Model predicted concentrations over time plotted against the average total Ag concentrations obtained for $AgNO_3$ in UPW at, A) the surface water, B) the middle depth and C) the bottom of the mesocosm. The model parameters are presented in table 4.1.

Table 4.1: Model Parameters for $AgNO_3$ in Ultrapure and EPA Water			
Parameter	**Symbol**	**Unit**	**Measurement**
Diameter of Ag atom	d	nm	0.288
Cross section area of the column	A	m^2	0.049
Column Length	*L*	m	1
Column volume	*V*=A*L*	L	43
Dosing volume	*V*	L	0.391
Dosing concentration	C_0	ppm	11
Mass of Ag	M	mg	4.3
C column based on diffusion	M/*V*	ppb	100
Diffusion coefficient	*D*	$m^2 s^{-1}$	1.49.E-5
Sedimentation Velocity	*U*	$m\ s^{-1}$	4.30E-13

To successfully model the dissolved Ag transport (Socolofsky and Jirka 2004, and Hinderliter *et al* 2010) in the mesocosm, parameters of the model were adjusted to fit the diameter of Ag atom (0.288 nm) (Sellers *et al,* 2009) in place of the AgNP diameter (d). The diffusion coefficient and sedimentation velocity are described using equations 4.1 and 4.2 below (Hinderliter *et al,* 2010):

$$D = \frac{\mathrm{RT}}{3\mathrm{N_A}\,\pi\mu\,\mathrm{d}}$$

[Eq 4.1]

Where R defines the gas constant (L.kPa K mol), T refers to temperature (*K*), N_A is Avogadro's number, viscosity is μ (Pa.s) and the particle diameter is d (m). The partial differential equation and boundary conditions for this equation are explained in chapter 1 section 1.5.2 equations 1.1 and 1.2. The sedimentation velocity is as:

$$U = \frac{\mathrm{g}\left(\rho_\mathrm{p} - \rho_\mathrm{f}\right)\mathrm{d}^2}{18\mu}$$

[Eq 4.2]

Where the sedimentation velocity of particles in solution is U (m s^{-1}), g refers to the gravitational force, particle density is ρ_p (km m^3), fluid density is ρ_f, the particle diameter is d (m) and the viscosity of the solution media is termed μ (pa.s) (Hinderliter *et al,* 2010).

The diffusion-sedimentation equation used to predict Ag concentrations is described:

$$C(x,t) = \frac{\left(\frac{M}{A}\right)}{\sqrt{4\pi Dt}} \left(\exp\left(-\frac{(x - \mathrm{U}x_0)^2}{4Dtx}\right)\right) \quad \text{[Eq 4.3]}$$

Where x_0 is the point where the NPs are introduced to the column, and *t* is the distance of the NPs travelled in terms of time (Socolofsky and Jirka 2004, and Hinderliter *et al,* 2010). Further details are presented in chapter 2.

As AgNPs were not used in this study we assume that the dissolved Ag travels through the mesocosms via the process of diffusion under Brownian motion. As the $AgNO_3$ was spiked at the top of the mesocosms, according to Ficks Law the Ag will move from the surface (high concentration), to the bottom (low concentration) until the Ag is evenly distributed (Fick, 1855, Gorban *et al,* 2011). Therefore, as time increases if diffusion is the only transport mechanism, the concentration profiles will become flat when the concentrations at each depth reach equilibration. Evidence in figure 4.1 shows the concentrations for each depth are equal by 288 hours (12 days), with concentrations between 131 ± 0.06 ppb in the surface, 136 ± 0.05 ppb in the middle and 135 ± 0.08 ppb in the bottom.

To determine how well the observed data fits with the modelled data we can use a Pearsons correlation coefficient to determine the R^2 value which ranges from 0 to 1. The closer to 1 the R^2 values are indicates less variance between the two sets of data

(Moriasi *et al,* 2007). The observed and expected concentrations were plotted against each other and the R^2 values were determined (see appendix) as follows; surface 0.87, middle 0.43 and the bottom 0.91. Values for R^2 larger than 0.5, are generally considered as acceptable for showing a reasonably good correlation (Moriasi *et al,* 2007). Values lower than 0.5 would be considered to show little/no correlation between our modelled and expected data. For this thesis, we will consider values of $R^2 \leq 0.7$ to show strong correlations between our modelled and observed data sets. Based on the R_2 values for the $AgNO_3$ exposures, the surface and bottom data sets show a large linear association between the observed and expected Ag concentrations, compared to the middle which determined weak associations between the two sets of data.

In terms of transport behaviour, when the $AgNO_3$ concentrations are compared to the predicted modelled Ag concentrations in figure 4.2, it can be seen that the total Ag the surface water profile (figure 4.2A) follows the modelled fits after 48 hours with a concentration of 187 ± 0.07 ppb, maintaining a concentration gradient to comply with diffusion behaviour. The total Ag concentrations for the middle and bottom are higher than those predicted by the model at the beginning of the study, between 146 ± 0.05 ppb (48 hours) and 277 ± 0.09 ppb (72 hours), and 268 ± 0.09 ppb (48 hours) and 190 ± 0.07 ppb (72 hours) in the bottom. The difference in concentration from the expected at these time points would account for the deviations to the R^2 values, which is sensitive to outliers (Moriasi *et al,* 2007). Despite the concentrations of Ag being higher in the lower depths, the transportation behaviour still followed the expected outcome for diffusion as the Ag moves down the mesocosm. The R^2 values are acceptable for the surface and

bottom to accept that the observed data fits those of the model predictions, and follows diffusion behaviour.

4.4.1.2 $AgNO_3$ in EPA Water

In accordance with the ultrapure water study, a further control study using $AgNO_3$ released into EPA moderately hard water was observed over 12 days. The total Ag results from each depth are presented figure 4.3, and are plotted alongside the modelled Ag concentrations in each depth in figure 4.4.

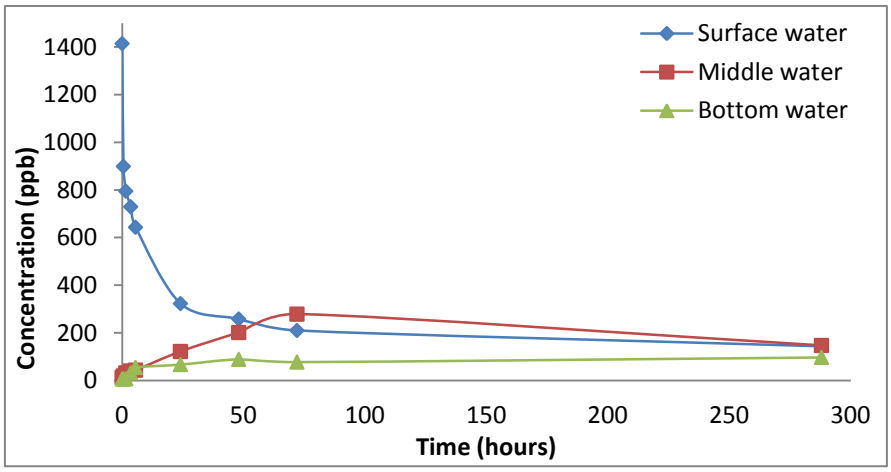

Figure 4.3: Total Ag recovery concentration (ppb) measured by FAAS for $AgNO_3$ exposed to EPA moderately hard water over a period of 12 days showing the concentration changes at the different depths of the column.

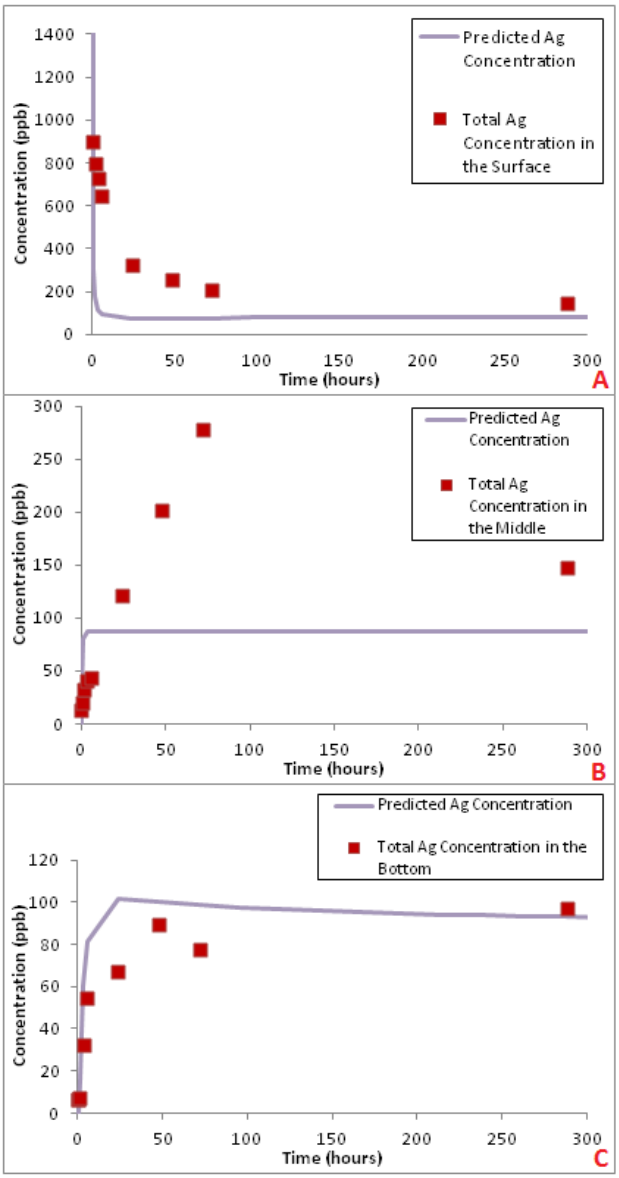

Figure 4.4: Model predicted concentrations over time plotted against the average total Ag concentrations obtained for $AgNO_3$ in EPA moderately hard water in, A) the surface water, B) the middle depth and C) bottom of the mesocosm. Model parameters are described in table 4.1.

Figure 4.3 compares the average Ag concentration movements in each depth after being released into EPA moderately hard water. When the total Ag concentration is plotted against the modelled predicted concentrations for each depth, assumptions of the transport mechanisms can be made. As with the previous $AgNO_3$ study in UPW, the assumption is that the concentration of Ag will follow diffusion through the mesocosm

according to Ficks Law (Fick, 1855). If sedimentation occurs the concentration of the Ag will move down the mesocosm in a 'cloud like' formation. This pattern was identified by showing a gradual elevation from 26 ± 0.91 ppb after 0.5 hours release, to 279 ± 0.92 ppb at 72 hours, followed by a gradual decline back to measurable concentrations between the surface and bottom at 147 ± 0.57 ppb for 288 hours to create a peak (Figure 4.4B). Therefore, Ag is no longer moving by the random movement of Brownian motion alone and has possibly transformed to produce AgNPs, (or other Ag complexes) to which other forces such gravity, will affect the transport behaviour (Navarro *et al,* 2008). The R^2 value of 0.79 also identified small differences between the observed and the modelled data.

Figures 4.4A and 4.4C for the surface and bottom, show the total Ag concentrations follow the modelled concentration pattern, and demonstrate Ficks law of diffusion, by displaying concentrations profiles that eventually become flat, showing equilibrium concentrations around 288 hours (day 12). The R^2 value for the surface was 0.93 and the R^2 value for the bottom was 0.97, evidencing strong correlations between the modelled and observed Ag concentrations.

When compared to the $AgNO_3$ UPW study, differences between the chemical make-up of the water and the transport behaviour of the Ag can be observed. Evidence from the model suggests that the diffusion of Ag in the surface water (figure 4.4A) is slower than those observed in the surface of the UPW studies (figure 4.2A), demonstrated by the higher concentrations retained in the surface over time when compared to the lower depths (figures 4.4B and 4.4C) and previous results. It is possible that the chemical constituents of the EPA moderately hard water are interacting with the dissolved Ag to cause the changes transport behaviour. As sedimentation behaviour was

observed in the middle depth (figure 4.4B), information suggests that small NPs may have formed and thus, gravitational pull of the NPs resulted in sedimentation. Zook *et al* (2011) previously identified that Ag^+ in solution can complex with chlorine (Cl) to form AgCl and AgCl NPs in natural aqueous environments. Since Cl was part of the constituents that make up the EPA moderately hard water standard, it is agreeable that small AgNPs have formed in solution and explain the sedimentation behaviour observed.

Overall, the purpose of the $AgNO_3$ studies in the UPW and EPA moderately hard water were to assess the transport mechanisms of the dissolved Ag, which can be used to interpret and compare the AgNP transport later in this chapter. The results identified that in the presence of simple electrolytes, the transport behaviour of dissolved Ag was altered, resulting in the combined diffusion of Ag and sedimentation of small NPs formed in solution. The information in the present study can also be used to predict the NP fate and behaviour when exposed to complex water systems.

4.4.3 AgNP Exposures

4.4.3.1 Ultrapure Water

4.4.3.1.1 Modelled and Dissolved Ag Concentrations

The transport of citrate (12 ± 2 nm TEM) and PVP (11 ± 2 nm TEM) AgNPs in UPW, was assessed over 28 days. Measurements were made during the first 5.5 hours on day one of exposure, daily for 14 days and then again on days 21 and 28. The tables for the total Ag and dissolved Ag concentrations for each water condition, are displayed in the appendix. The data obtained for the total Ag concentrations were plotted against modelled predicted Ag concentrations over time (Socolofsky and Jirka 2004, and Hinderliter *et al*, 2010), and are presented in figure 4.5.

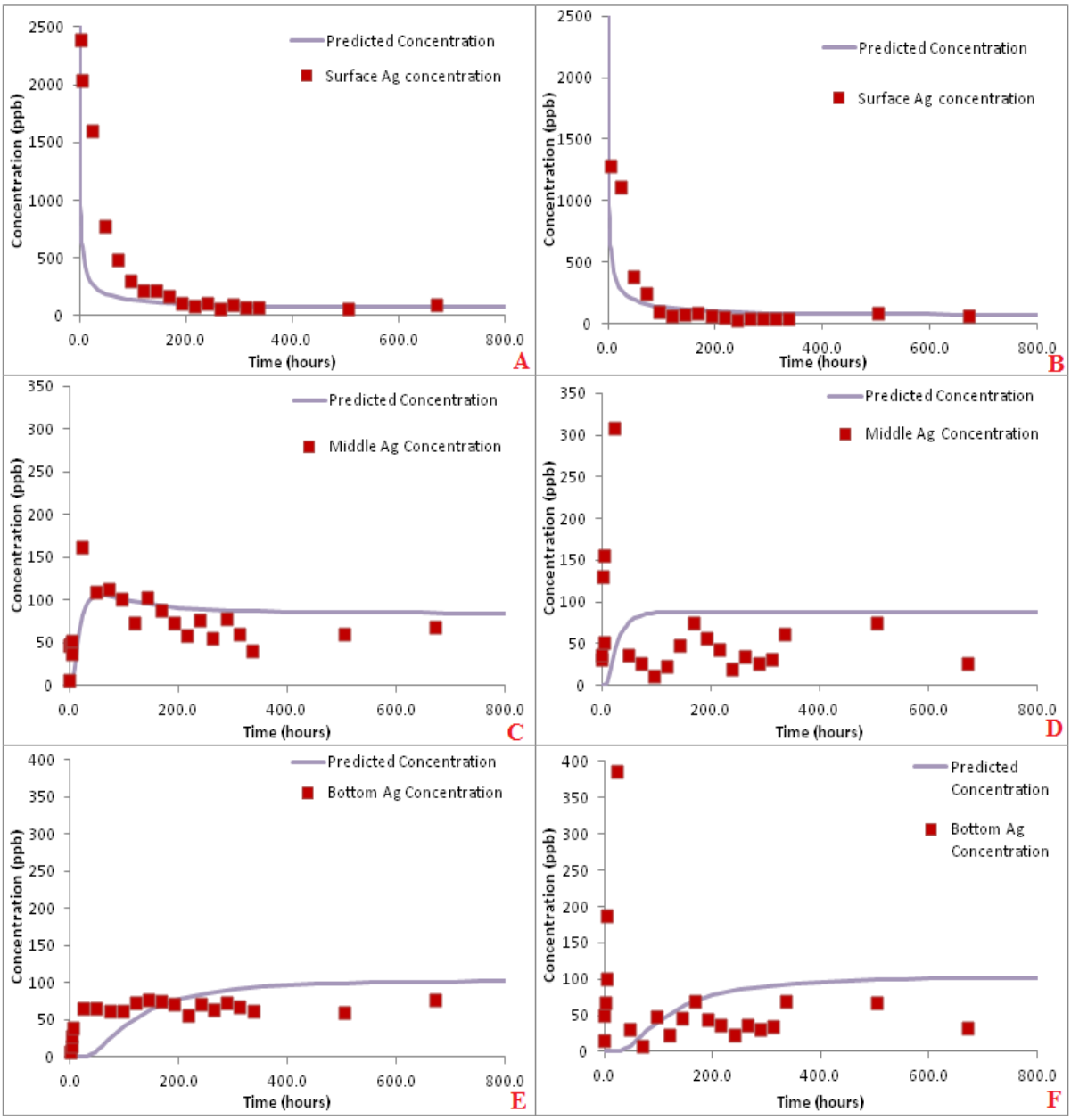

Figure 4.5: Model predicted Ag concentrations over time plotted against the average total Ag for, A) citrate AgNP study in the surface, B) PVP AgNP study in the surface, C) citrate AgNP study in the middle, D) PVP AgNP study in the middle, E) citrate AgNP study in the bottom, and F) PVP AgNP study in the bottom of the mesocosm containing UPW. Note, actual concentrations are presented as a function of total Ag. Model parameters are presented in table 4.3.

Table 4.2: Model Parameters for Citrate and PVP AgNPs in UPW				
Parameter	**Symbol**	**Unit**	**Citrate AgNPs**	**PVP AgNPs**
Diameter of AgNP	d	nm	11.5	11.5
Cross section area of the column	A	m^2	0.049	0.049
Column length	*L*	m	1	1
Column volume	*V*=A*L*	L	43	43
Dosing volume	*V*	L	0.391	0.215
Dosing concentration	C_0	ppm	11	20
Mass of Ag	M	mg	4.3	4.3
C column based on diffusion	M/*V*	ppb	100	100
Diffusion coefficient	*D*	$m^2 s^{-1}$	3.743E-7	3.743E-7
Sedimentation Velocity	*U*	$m s^{-1}$	6.8E-10	6.8E-10

Analysis of the citrate AgNP study in figure 4.5 shows that the Ag concentration follows the predicted concentrations for each depth. The surface water profile (figure 4.5A) shows that the total Ag was slightly higher than those modelled for the first 48 hours of analysis at 770 ± 0.15 ppb. Stabilisation of the Ag concentrations in the surface water begins after 192 hours (8 days) at 111 ± 0.02 ppb (Table A1.3 additional information) which then follow the modelled concentrations. A Pearsons correlation coefficient (Moriasi *et al,* 2007) between the modelled and observed Ag concentrations determined the R^2 value of the surface water to be 0.93, showing a strong correlation between the two sets of data.

However, small deviations in the total Ag concentration for the middle depth (figure 4.5C) resulted in an R^2 value of 0.45, showing weak associations between the model and observed Ag concentrations. As the model doesn't account for deviations in concentration due aggregation/settling we can identify that the citrate AgNPs have aggregated and follow sedimentation due to the differences between the observed and modelled data. A further suggestion for the deviations between the modelled and observed concentration, may be due to Ag^+ from NP dissolution and/or smaller AgNPs

diffusing back into the middle area, as a stable concentration gradient establishes between the depths.

The total Ag in the bottom of the mesocosm (figure 4.5E) shows a stable concentration gradient from 24 hours (day 1) at 66 ± 0.01 ppb, comparable to 74 ± 0.03 ppb on day 7 and 77 ± 0.02 ppb on day 28, agreeing with Ficks Law (Fick, 1855). However the R^2 value is 0.49 in the bottom, suggesting large variances due to observed concentrations falling bellowed the predicted. If we change the model parameters we can fit the model data to the observed (figure 4.6) which will give us a better understanding of the behaviour and transport of the Ag. We can set the parameters to account for small losses of Ag due to sample removal during experimentation, losses of Ag from sedimentation of particles settling at the bottom, and changes of AgNP size due to aggregation as seen in the TEM imaging (figure 4.10/4.11).

When we adjust the model parameters (figure 4.6) the R^2 value for the middle increase to 0.56 and 0.57 in the bottom. Although these figures still determine an average fit between the modelled and observed concentrations, we can argue that the R^2 number is sensitive to outliers and the data presented in the model is valid due to small deviations in the observed concentrations.

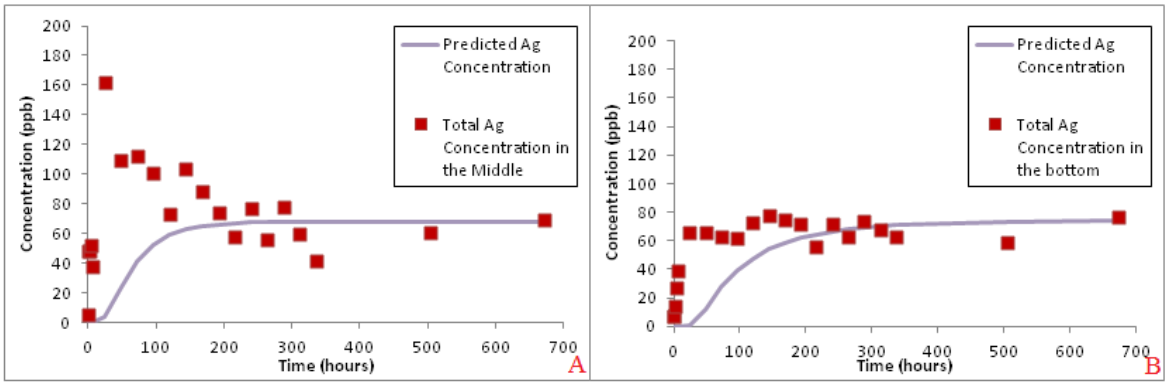

Figure 4.6: Adjusted model fits for the middle and bottom water for citrate AgNPs exposed to ultrapure water. New model parameters are listed in table 4.3.

Table 4.3: Adjusted Model Parameters Citrate AgNPs in UPW

Parameter	Symbol	Unit	Middle	Bottom
Diameter of Ag atom	d	nm	27	19
Cross section area of the column	A	m^2	0.049	0.049
Column Length	*L*	m	1	1
Column volume	*V*=A*L*	L	43	43
Dosing volume	*V*	L	0.391	0.391
Dosing concentration	C_0	ppm	8.5	8
Mass of Ag	M	mg	3.3	3.1
C column based on diffusion	M/*V*	ppb	77.3	72.7
Diffusion coefficient	*D*	$m^2 s^{-1}$	1.59.E-07	2.26.E-7
Sedimentation Velocity	*U*	ms^{-1}	3.8 E-09	4.2E-10

Analysis of the PVP AgNPs shows the (figure 4.5B) total Ag concentrations in the surface water follow those predicted by the model. Stable Ag concentrations are seen in the surface water after 96 hours (day 4) in the range of 96 ± 0.04 ppb (Table A1.4 additional information) agreeing with Ficks law. The correlation coefficient for the modelled and observed Ag concentrations produced an R^2 value of 0.97, showing a strong relationship between the two sets of data. However, the total Ag concentrations in the middle and

bottom (figures 4.5D and 4.5F) of the mesocosm do not show evidence of a constant concentration gradient within the first 240 hours (10 days), and do not agree with Ficks Law (Fick, 1855). The R^2 value for the middle and bottom are 0.23 and 0.16 further evidencing little correlation between the modelled and observed data.

In accordance with the citrate AgNPs, if we change the model parameters we can fit the observed data around the model (figure 4.7) to account for losses of Ag due to sample removal during experimentation, and losses of Ag due to particles settling. If the size of the PVP AgNPs are increased to 15 nm as seen in the TEM imaging (figure 4.12/4.13) and the concentration is reduced to 11 mg L^{-1} (table 4.4) to account for Ag losses, the R^2 value for the bottom increases to 0.86. The higher R^2 value shows there is a stronger correlation between the model and observed concentrations, and validates that PVP AgNPs settle as demonstrated by the changes in concentration profiles. Due to poor quality and variations of the observed data in the middle the model parameters could not be adjusted around the data to increase the R^2 value and produce a good correlation between the two.

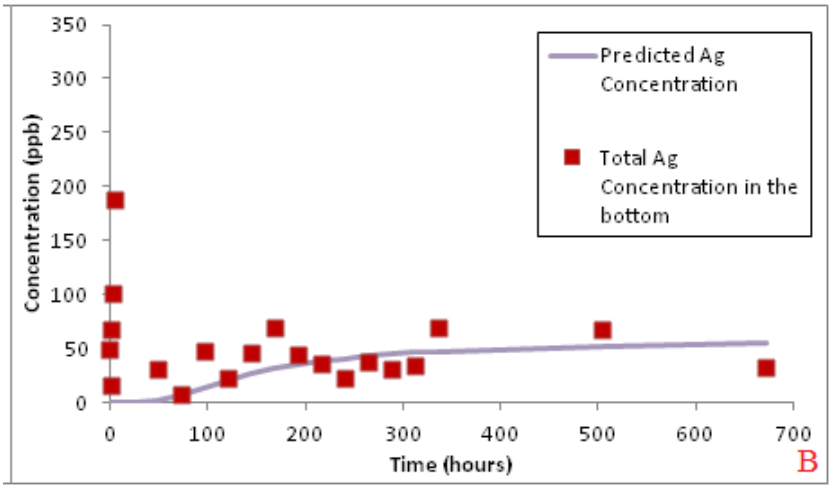

Figure 4.7: Adjusted model fits for the bottom water for PVP AgNPs released in UPW. New model parameters are listed in table 4.4.

Table 4.4: Adjusted Model Parameters for PVP AgNPs in UPW for the Middle and Bottom			
Parameter	**Symbol**	**Unit**	**Bottom**
Diameter of Ag atom	d	nm	15
Cross section area of the column	A	m^2	0.049
Column Length	*L*	m	1
Column volume	*V*=A*L*	L	43
Dosing volume	*V*	L	0.215
Dosing concentration	C_0	ppm	11
Mass of Ag	M	mg	2.4
C column based on diffusion	M/*V*	ppb	55
Diffusion coefficient	*D*	$m^2 s^{-1}$	2.8 E-7
Sedimentation Velocity	*U*	ms^{-1}	1.2 E-9

To compare, both the observed concentrations for the citrate and PVP AgNPs followed the predicted concentrations as modelled in the surface water (Socolofsky and Jirka 2004, and Hinderliter *et al,* 2010). The transport difference between the citrate and PVP AgNPs are evidenced in the lower depths, to which we can adjust the model to identify and validate. The total Ag for the citrate AgNP study mainly followed diffusion and maintained a concentration gradient, whereas the PVP AgNP study demonstrated some sedimentation behaviour in the middle depth. Since the model does not account for an accumulation of particles at the bottom of the mesocosm, it is possible that the PVP

AgNPs settled at the bottom which would account for the loss of an observed equilibration in the bottom and the poor correlation as seen by the small R^2 values. Further samples were taken for the first 14 days and again on days 21 and 28 to attempt to assess what proportion of the AgNPs had dissolved.

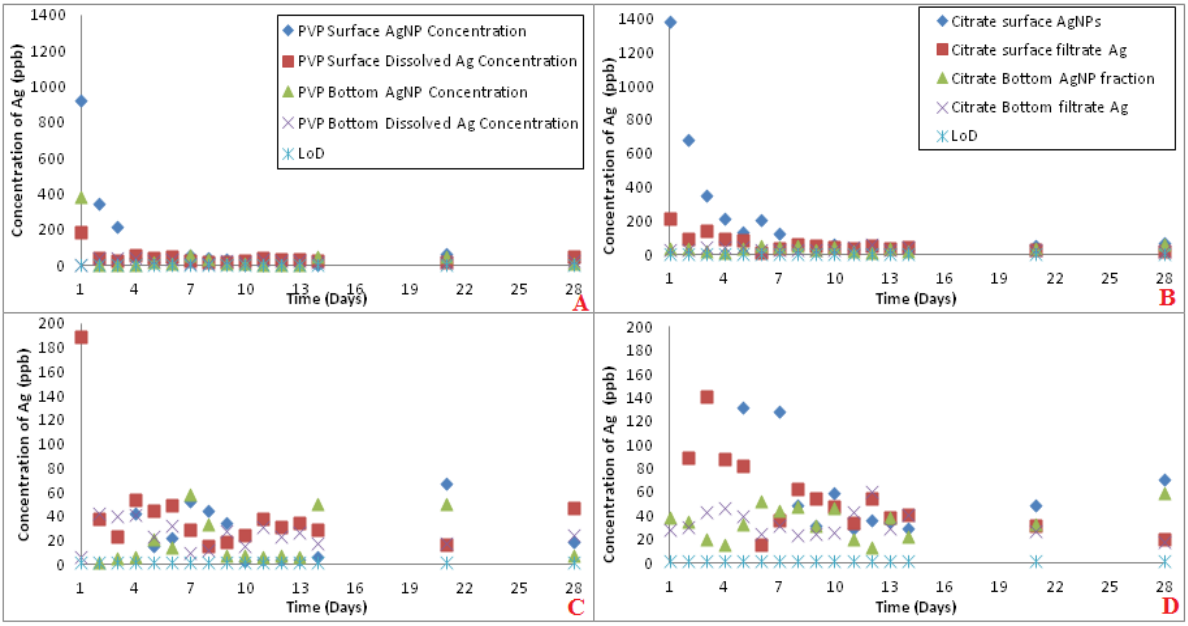

Figure 4.8: Dissolved and AgNP concentrations (ppb) using ultrafiltration in UPW: A) citrate AgNP and Ag^+ concentrations in the surface and bottom depth water for each day, B) PVP AgNP and Ag^+ concentrations in the surface and bottom depth water for each day, C) shows the same graph as A for concentrations below 200 ppb, D) shows the same graph as B for concentrations below 200 ppb. Note the LoD = Instrumentation limit of detection at 2 ± 0.2 ppb.

As described in chapter 2, ultrafiltration only provides an estimation of how quickly NPs dissolve, and the results cannot be assumed 100% reliable. Therefore all of the dissolved Ag (Ag^+) and AgNP concentration data presented in this chapter is used as an estimation of the AgNP behaviour. Using ultrafiltration to obtain the Ag^+ concentration, we were then able to calculate an estimated AgNP concentration as follows:

$$C_{AgNP} = (T_{Ag} - D_{Ag}) \qquad \text{[Eq 4.4]}$$

Where C_{AgNP} is the AgNP concentration, T_{Ag} is the total Ag concentration and D_{Ag} is the Ag^{+} concentration. Limits of detection for the FAAS instrumentation were tested by running a set of blanks as samples and devising the average result.

The total Ag^{+} was calculated by measuring the Ag concentration in the filtrate (figure 4.8). AgNP fractions were devised from the sum of the total Ag (units presented in the appendix) minus the Ag+ concentration. Limits of instrumentation detection were tested by running a set of blanks (ultrapure water) as samples and devising the average result. The major disadvantage of ultrafiltration is that the data is not 100% reliable as there is a possibility that AgNPs can stick to the walls of the container and ionic species can become bound to the filter membrane. Therefore this data is presented as an estimation of the NP behaviour once released into UPW. The concentrations of Ag^{+} and AgNPs in the surface and bottom depths of the mesocosm over time are described in figure 4.8. The information can be used to determine the AgNP stability and assess difference in behaviour via surface coating.

Analysis of the citrate AgNP study reveals that the highest concentrations of Ag^{+} were recorded in the surface water between 1383 ppb and 201 ppb during days 1-6. Simultaneously, as the AgNP concentration in the surface water reduces the AgNP concentration in the bottom rises, corresponding to the concentration data presented in figure 4.5. The results presented in figure 4.8 also demonstrate that the citrate AgNPs are persistent in particulate form for the duration of the study with AgNP concentrations of 91 ppb on day 28.

Investigations of the PVP AgNP dissolution and transport are seen figure 4.8C and 4.8D. The graphs show that PVP AgNPs travel to the bottom of the mesocosm at

facilitated speed compared to the citrate AgNPs, as evidenced by the increased AgNP concentration of 380 ppb in the bottom on day 1. The information also confirms the total Ag concentration movement seen in figures 4.5D and 4.5F. After 28 days the PVP AgNPs were still detected at a concentration of 19 ppb in the surface and 8 ppb in the bottom demonstrating their persistence for the duration of the study.

Comparisons between the citrate and PVP coated AgNPs in UPW revealed behavioural differences as previously seen in the modelling data. As PVP AgNPs have previously been documented from their colloidal stability over citrate AgNPs (El Badawy *et al,* 2011, Li *et al,* 2013, and Li *et al,* 2013b), citrate AgNPs in the present study were not expected to have lower Ag^{+} fractions and higher AgNP concentrations than those observed in the PVP AgNP study. Therefore it possible to suggest that a) the samples extracted (10 mL) were not good representatives of the whole area, b) losses of Ag occurred or C) our data is correct (based on 3 replicates) and disagrees with previous literature.

Losses of Ag could be due to removal of 5 mL per sampling area at each time point to record the total Ag. Particles were taken out of the system, never replaced and samples from areas of high concentrations of Ag would be permanently removed from the study. AgNPs may have been lost by depositing on to the mesocosm walls and settling at the bottom. Although ultrafiltration separates the dissolved Ag through a porous 1 nm sized membrane, losses could have occurred by the ionic species and NPs sticking to the membrane channel (Zook *et al,* 2011).

To summarise, when the AgNP concentrations in the surface decline, the AgNP concentration in the bottom increases, demonstrating particle movement by measuring

concentration. Furthermore, when the concentration of Ag^+ increases the AgNP concentration decreases, providing evidence of AgNP particle dissolution, evidenced in both the surface and bottom water depths for both AgNP types. The overall results can be used as an indication to show that citrate and PVP AgNPs persist in particulate form for 28 days, and dissolve over time to produce Ag^+, which has been seen to be highly toxic to many organisms (Levard *et al*, 2013).

4.4.3.1.2 UV Analysis

Nanoparticles display strong absorption in the visible light region of the electromagnetic spectrum, due to the oscillation frequencies of the electrons located at the surface of the NPs. The oscillation frequencies are known as the surface plasmon resonance (SPR) and account for the yellow/orange colouring of AgNPs in solution (Burda *et al,* 2005). The size and the shape of the particles will also determine the strength of the SPR emitted (Stamplecoskie and Scaiano, 2012). Other factors that will affect the strength of the SPR are the dielectric constant of the surrounding solution in which the particles are exposed (Bhui *et al,* 2009). The SPR, using UV spectroscopy was observed hourly for the first day (up to 8.5 hours) and then daily thereafter. The SPR peak (λ_{max}) for spherical pristine citrate AgNPs as characterised in chapter 3 was 392nm, and 400nm for those coated with PVP. Figure 4.9 (A-F) describe the SPR profiles for both citrate and PVP particles exposed over time at the surface, middle and bottom points of the mesocosm tanks.

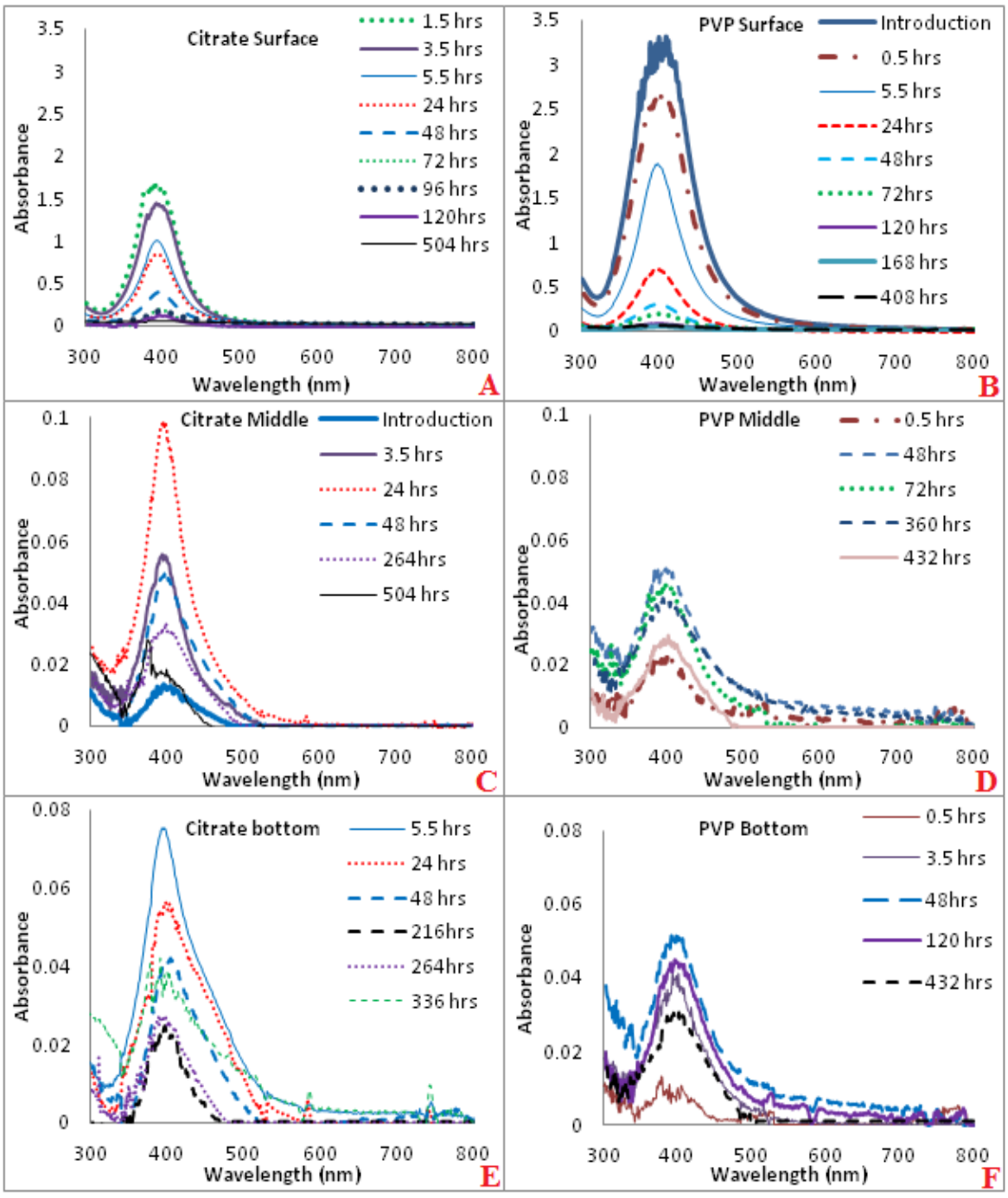

Figure 4.9: UV SPR profiles taken from different depths of the mesocosm column when released in UPW, A) Citrate coated AgNPs at the surface, B) PVP AgNPs at the surface, C) citrate AgNPs from the middle, D) PVP AgNPs from the middle, E) Citrate AgNPs from the bottom and F) PVP AgNPs from the bottom. Note that the Y axis for the graphs are not presented in the same scale for each of the depths, as detail from the lower regions would be lost.

Once released in UPW the citrate AgNP SPR banding patterns gave one uniform peak in the region of 392nm (figure 4.9) matching the absorbance values as characterised pre-release in chapter 3, and confirmed the literature data (Cumberland and Lead, 2009 and Romer *et al*, 2011). After 24 hours post release the SPR bands appear to gradually reduce in size and become narrower as shown by their reduced absorbance intensity in the middle depth. Explanations for the reduction in size and shape of the SPR peaks maybe due to the transport of the AgNPs as they diffuse down towards the bottom of the mesocosm (Lowry *et al,* 2012). Narrowing SPR bands overtime also indicates size reduction via dissolution of the AgNPs (Li *et al,* 2010). After 22 days there were no measurable citrate AgNPs in the surface water using UV spectroscopy, although the dissolution studies (figure 4.8) identified concentrations AgNPs on day 28 at 71 ppb. Suggestions may be that the sample size was not a representative of the whole area.

Analysis of the PVP AgNPs using the SPR data also revealed one single peak in the region of 400nm, comparable to the results pre-release in chapter 3 and literature data (Tejamaya *et al,* 2012). The SPR bands appeared slightly wider in the middle for PVP AgNPs at 48 hours, with slight band stretching into longer wavelengths of 600nm region, indicating size and possible shape changes (Stamplecoskie and Scaiano, 2012). Larger AgNPs will give a wider peak band between 500-800nm (Li *et al,* 2010), which would account for the sedimentation behaviour patterns observed in figures 4.5D and 4.5F. As band stretching was not observed when the PVP AgNPs were first characterised (chapter 3) it can be assumed that instability resulting in larger AgNP formation occurred after release into the mesocosms.

Overall, UV data is particularly important as it shows differences in peak shifts, and can be used trace NP movement and aggregation (Chinnapongse *et al,* 2011), which help to confirm the model data. As the intensity of the SPR peaks reduce in the surface water, the intensity of the SPR peaks increase in the lower depths, showing AgNP compartmental movement. In addition, the SPR bands for both citrate and PVP AgNPs became narrower over time, suggesting the presence of less concentrated smaller particles (Li *et al,* 2010). The reduced SPR intensity as displayed for both the citrate and PVP AgNPs after 24 hours can be used to provide information about particle dissolution, as Ag^{+} does not have an SPR absorbance (Zook *et al,* 2011). Therefore as the SPR bands decrease, particle dissolution may be occurring during the transportation processes. We know dissolution occurs as figure 4.6 provided good estimations of the concentrations of Ag^{+} released over time in solution, and correspond to the reduced SPR peaks over time in each depth.

4.4.3.1.3 Transmission Electron Microscopy (TEM) Analysis

To explore the size and morphological changes of the citrate (12 ± 2nm) and PVP (11 ± 2 nm) AgNPs, TEM imaging was conducted. Aims were to identify differences between the AgNPs in the surface compared to the bottom of the mesocosm, and define behavioural patterns between the different surface coated AgNPs.

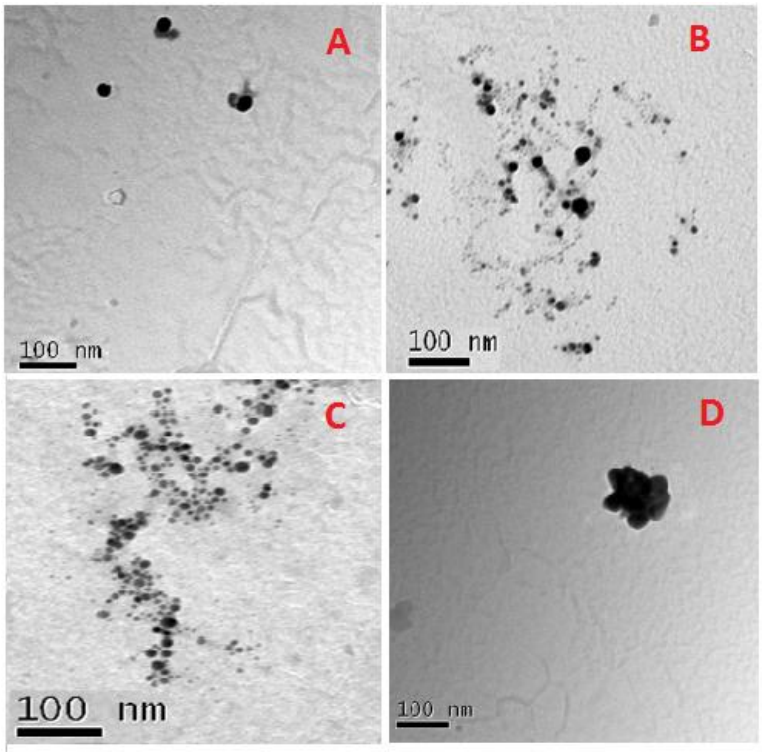

Figure 4.10: TEM images comparing citrate AgNPs at the surface and bottom of the mesocosm at, A) 24 hours surface, B) 24 hours bottom, C) 72 hours surface, and D) 72 hours bottom.

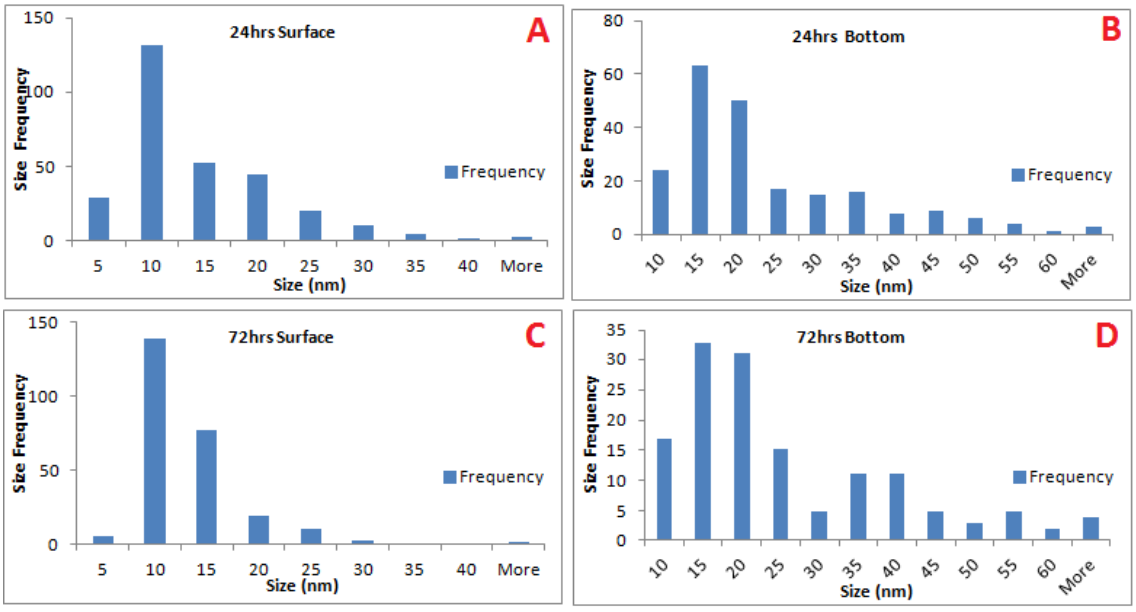

Figure 4.11: TEM histograms highlighting the number and frequency of occurrence, for citrate stabilised AgNPs for 24 hours and 72 hours exposures. A) 24 hours at the surface, B) 24 hours from the bottom, C) 72 hours from the surface, and D) 72 hours from the bottom.

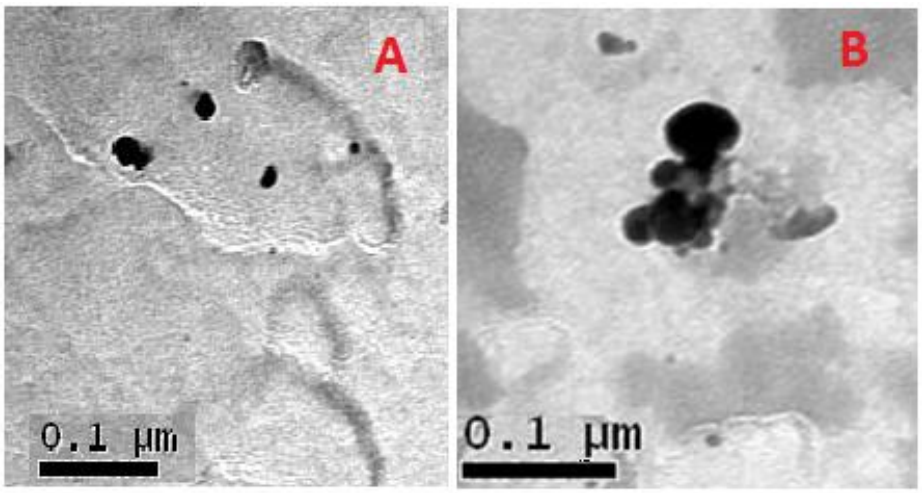

Figure 4.12: TEM images comparing PVP AgNPs at the surface and bottom of the mesocosm at A) 72 hours surface, and B) 72 hours in the bottom.

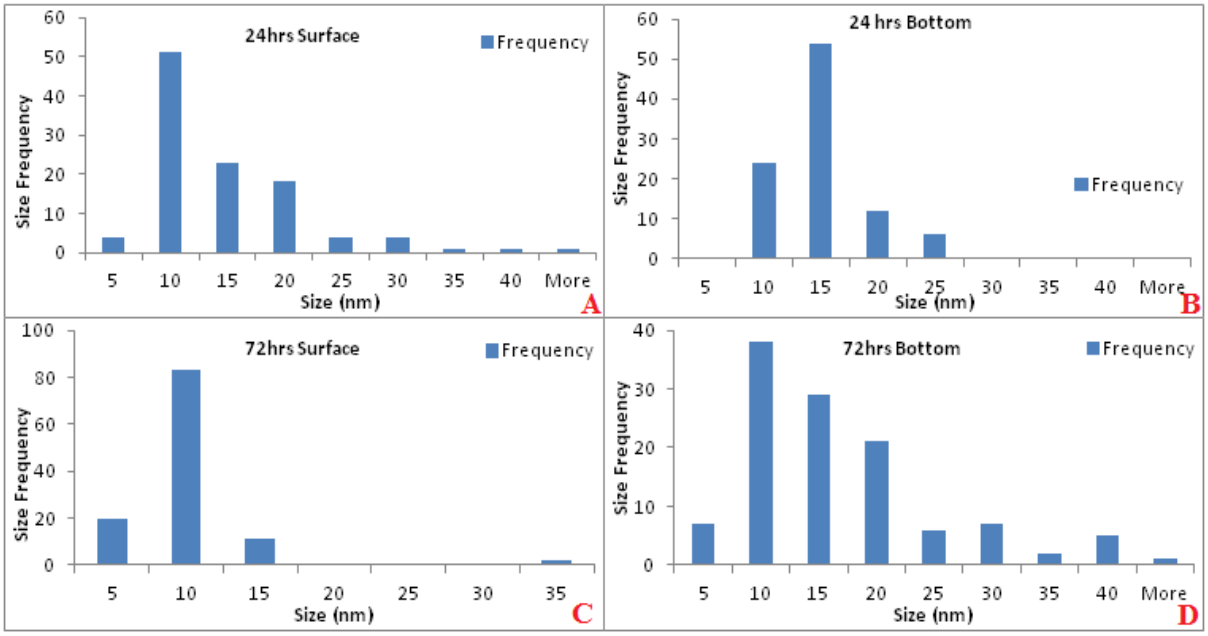

Figure 4.13: TEM histograms describing the number and frequency particle occurrence, for PVP AgNPs at 24 hours and 72 hours exposures. A) 24 hours at the surface, B) 24 hours from the bottom, C) 72 hours from the surface, and D) 72 hours from the bottom.

Table 4.5: TEM sizes (nm) at different time points for citrate and PVP AgNPs exposed UPW.
A t-test was performed to identify differences from the observed compared to the original AgNPs sizes before release. *n= number of particles counted*ND= Not Determined. A p value <0.05 highlights that the observed particle size using the t-test is significantly different to the size of the original particles before release, at a 95% confidence level.

Table 4.5: Average Size by TEM					
Time (hours)	**24**		**72**		**168**
Area Analysed	**Surface**	**Bottom**	**Surface**	**Bottom**	**Surface**
Particle type	**Citrate AgNPs**				
Size (nm)	13 ± 8	22 ± 13	11 ± 6	25 ± 17	23 ± 8
p-Value	0.845	2.45E-26	0.001	1.69E-24	2.93E-64
n	296	215	257	141	121
Particle Type	**PVP AgNPs**				
Size (nm)	13 ± 7	14 ± 4	8 ± 4	15 ± 9	ND
p-Value	0.007	8.48E-8	1.20E-11	5.82E-7	ND
n	108	97	120	117	ND

Table 4.5 identifies citrate AgNPs to be 13 ± 8 nm after 24 hours in the surface water (*p* 0.845), which shows no significant difference when compared to the sizes at 12 ± 2 nm pre-release. The most frequently counted citrate AgNPs had a core size of 10 nm (figure 4.11A), providing evidence that smaller particles were retained in the surface water. However, the citrate AgNPs increased significantly in size over time at the bottom of the mesocosm. After 24 hours the sizes increased from 12 ± 2 nm (original) to 22 ± 13 nm (*p* 2.45E-26) and 25 ± 17 nm (*p* 1.69E-24) after 72 hours in the bottom of the mesocosm. Larger particles found at the bottom of the mesocosm may be due to settling and aggregation (Hinderliter *et al,* 2010). Histogram 4.11B and 4.11D further confirms a larger size frequency located in the bottom of the mesocom, compared to the surface. Morphological presentations of citrate AgNPs from the surface water at 72 hours (figure 4.10) show that the AgNPs are uniform in shape with some larger particles present. In

addition, at 72 hours at the bottom of the column (Figure 4.10D) the citrate AgNPs are aggregating together (it's visible to see these particles were once individual by their outer shape).

PVP AgNPs in the surface water remained comparable to the original size of 11 ± 2 nm after 24 hours exposure to 13 ± 7 nm (p 0.007). The corresponding TEM histograms show similar size distribution frequencys for PVP AgNPs in the surface water at 24 hours (figure 4.13A) and 72 hours (figure 4.13C). Figure 4.12B shows PVP AgNPs at the bottom of the column were large and aggregated, which compares to the morphological results for the citrate particles at this time point. TEM analysis revealed that for both citrate and PVP AgNPs, larger particles sediment to the mesocosm leaving smaller AgNPs suspended in the surface water.

To summarise for this section, it has been shown that the citrate AgNPs followed close to the modelled concentrations (figure 4.5), demonstrating stable concentration gradients following diffusion when released in UPW. Whereas, PVP AgNPs follow the modelled transportation rates over 28 days in the surface water only, and displayed sedimentation behaviour in the lower depths. According to figure 4.8 both the citrate and PVP AgNPs dissolve over time and are still present in NP form for 28 days duration of the study. Further evidence from the TEM data shows that smaller AgNPs remain in the surface water, compared to larger AgNPs at the bottom and was true for both AgNP types.

4.4.3.2 EPA Moderately Hard Water

4.4.3.2.1 Modelled and Dissolved Ag Concentrations

Total Ag was modelled (Socolofsky and Jirka 2004, and Hinderliter *et al,* 2010) to assess the transport of citrate (11 ± 3 nm TEM) and PVP AgNPs (11 ± 3 nm TEM) in EPA moderately hard water. Total Ag samples were extracted from the surface, middle and bottom water areas of the mesocosms. Samples were taken over a period of 5.5 hours for the first day of exposure, daily for 14 days, and again on days 21 and 28. The data obtained for the total Ag concentrations were plotted against a modelled predicted total silver concentration. The results are presented in figure 4.12.

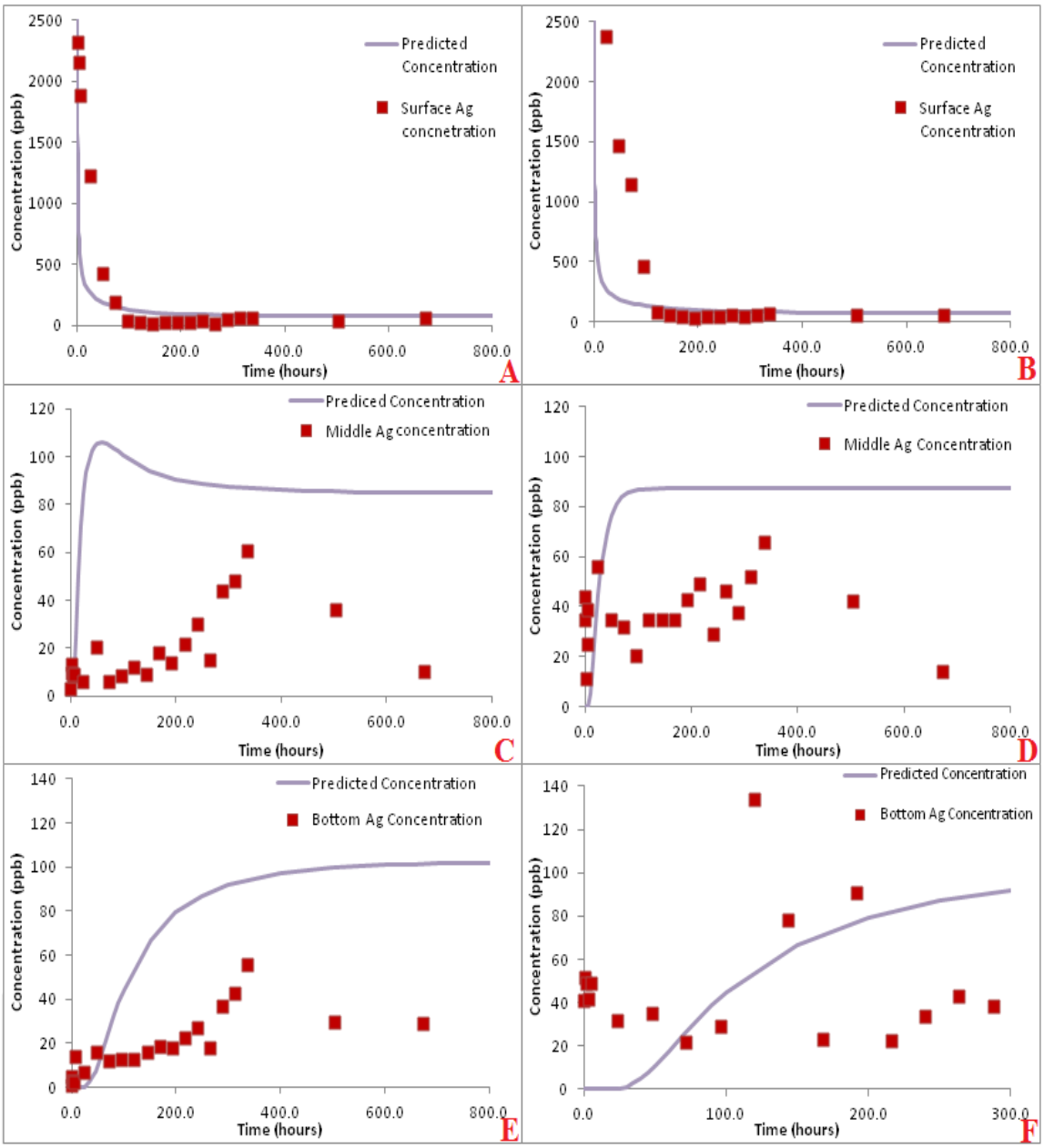

Figure 4.14: Model predicted concentrations over time plotted against the average total Ag obtained from the study for, A) citrate AgNPs in the surface, B) PVP AgNPs in the surface, C) citrate AgNPs in the middle, D) PVP AgNPs in the middle, E) citrate AgNPs in the bottom, and F) PVP AgNPs in the bottom of the mesocosm containing EPA moderately hard water. The model fits were based on a single 11 nm AgNP transporting through the mesocosm based on parameters in table 4.4. The model was then optimised to fit the total Ag concentration data for the citrate AgNPs to account for aggregation and sedimentation, as seen in figure 4.13 with the new parameters listed in table 4.6.

Table 4.6: Model Parameters for AgNPs in EPA Moderately hard Water				
Parameter	**Symbol**	**Unit**	**Citrate AgNPs**	**PVP AgNPs**
Diameter of AgNP	d	nm	11	11
Cross section area of the column	A	m^2	0.049	0.049
Column length	*L*	m	1	1
Column volume	*V*=A*L*	L	43	43
Dosing volume	*V*	L	0.391	0.215
Dosing concentration	C_0	ppm	11	20
Mass of Ag	M	mg	4.3	3.4
C column based on diffusion	M/*V*	ppb	100	100
Diffusion coefficient	*D*	$m^2 s^{-1}$	3.904.E-7	3.904.E-7
Sedimentation Velocity	*U*	ms^{-1}	6.3E-10	6.3E-10

To assess the transport mechanisms of the AgNPs, the total Ag concentrations were plotted against predicted modelled concentrations over time for each depth of the mesocosm as displayed in figure 4.14. Analysis of the citrate AgNP study revealed that only the surface water profile (figure 4.14A) followed the model predictions for the total concentration of Ag. A Pearsons correlation coefficient (Moriasi *et al,* 2007) between the modelled and observed Ag concentrations determined the R^2 value of the surface water to be 0.99, showing strong correlation between the two sets of data. The surface water profile shows the total Ag to be slightly higher than those modelled for the first 96 hours of analysis (4 days). On day 4 the total Ag concentrations was 43.2 ± 0.04 ppb, where they remained lower than the predicted 100 ppb concentration for the duration of the study. By day 13 the surface water Ag concentrations were 62 ± 0.02 ppb where they remained comparable for the duration of the study showing equilibration.

The total Ag in the middle depth for the citrate AgNP study does not follow the predicted modelled concentrations and has an R^2 value of 0.29, showing no correlation between the two sets of data. A gradual rise in concentration followed by a decline in

concentration show aggregation behaviour as the citrate AgNPs sediment to the bottom (Hinderliter *et al,* 2010). Further evidence to support aggregation of the citrate AgNPs were observed in the SPR data (figure 4.18A, 4.18C and 4.18E) and TEM imaging (figures 4.19B and 4.19D).

To test the hypothesis that the citrate AgNPs aggregate under the conditions of EPA moderately hard water, parameters of the model were adjusted to increase the fit between the total Ag concentration data obtained. As the model does not account for accumulating Ag concentrations at the bottom of the mesocosm (Socolofsky and Jirka 2004, and Hinderliter *et al,* 2010), we can assume the overall concentration reduces as the AgNPs aggregate, sediment and settle. Therefore, if we replace the original AgNP diameter (d) of 11 nm with a larger size such as 230 nm seen from TEM imaging (aggregated), and reduce the dosing concentration (previously calculated to account for settling losses), the new model parameters for the middle and bottom of the mesocosm fit the total Ag concentration data obtained as presented in figure 4.15. Figure 4.15A shows a better visual fit for the total Ag in the middle for the citrate AgNPs and the R^2 value previously 0.29, has increased with the new parameters to 0.66. The parameters for the model were difficult to fit for the Ag concentrations obtained from the bottom samples due to large aggregates settling at the bottom at the beginning of the study which gave an original R^2 value of 0.79, which the model is not designed for. Adjustments in the parameters increased the R^2 value to 0.89 showing stronger correlations between the modelled data and the observed data

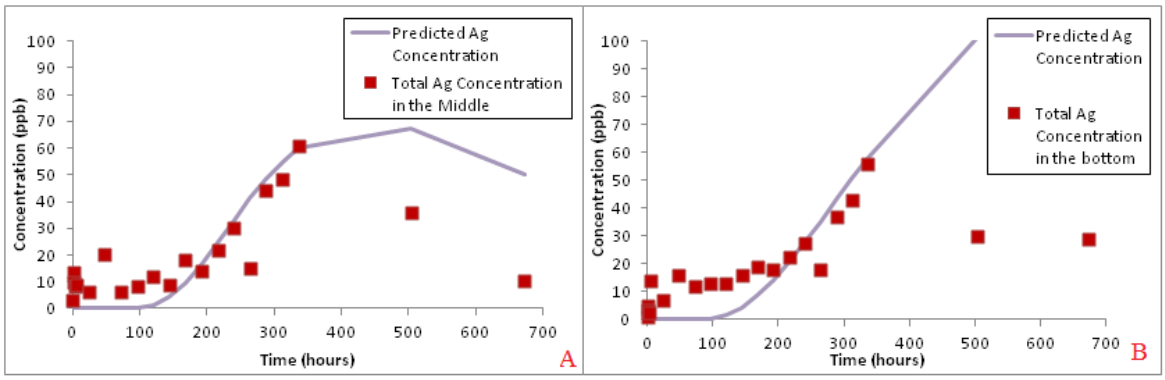

Figure 4.15: Adjusted model parameters to account for larger aggregated citrate AgNPs (table 4.7) for the predicted concentrations over time, plotted against the average total Ag obtained from the study for, A) citrate AgNPs in the middle, and B) citrate AgNPs in the bottom of the mesocosm.

Table 4.7: Adjusted Model Parameters for aggregated citrate AgNPs in EPA water for the Middle and Bottom

Parameter	Symbol	Unit	Middle	Bottom
Diameter of Ag atom	d	nm	230	47
Cross section area of the column	A	m^2	0.049	0.049
Column Length	*L*	m	1	1
Column volume	*V*=A*L*	L	43	43
Dosing volume	*V*	L	0.391	0.391
Dosing concentration	C_0	ppm	2	15
Mass of Ag	M	mg	0.8	5.9
C column based on diffusion	M/*V*	ppb	18.2	136.4
Diffusion coefficient	*D*	$m^2 s^{-1}$	1.867.E-8	9.137E-7
Sedimentation Velocity	*U*	ms^{-1}	2.7E-7	1E-8

In comparison, analysis of the PVP AgNPs show the surface water total Ag concentrations follow those predicted by the model giving a strong R^2 correlation of 0.98, although deviations occur from the modelled concentrations in the lower depths. The total Ag concentrations in the middle (figures 4.14D) and of the mesocosm show evidence of a constant concentration gradient from 5.5 hours at 56 ± 0.05 ppb after 24 hours to 42 ± 0.04 ppb on day 21. A drop in concentration to 14 ± 0.01 ppb was seen on day 28. Although values that are larger than 0.5 are generally considered as acceptable (Moriasi *et al,* 2007), the middle R^2 values between the observed and modelled concentrations

was 0.57. If we adjust the model parameters (figure 4.16 and table 4.8) to account for losses of Ag concentration of approximately 50% from settling and sample losses(previously calculated) we can increase the R^2 value for the middle to 0.98, showing that the model is acceptable to predict the concentration of the PVP AgNPs over time.

After 24 hours the concentration in the bottom of the mesocosm was 32 ± 0.08 ppb, comparable today 28 at 28 ± 0.05 ppb (figure 4.12F) agreeing with Ficks Law (Fick, 1855). Although the R^2 value was 0.27 showing there was weak correlation between the observed and the modelled data. As the middle does not equate for AgNP settling on the floor of the mesocosm, if we input the reduced concentration in the modelled parameters (figure 4.16 and table 4.8) we can increase the R^2 value to 0.99.

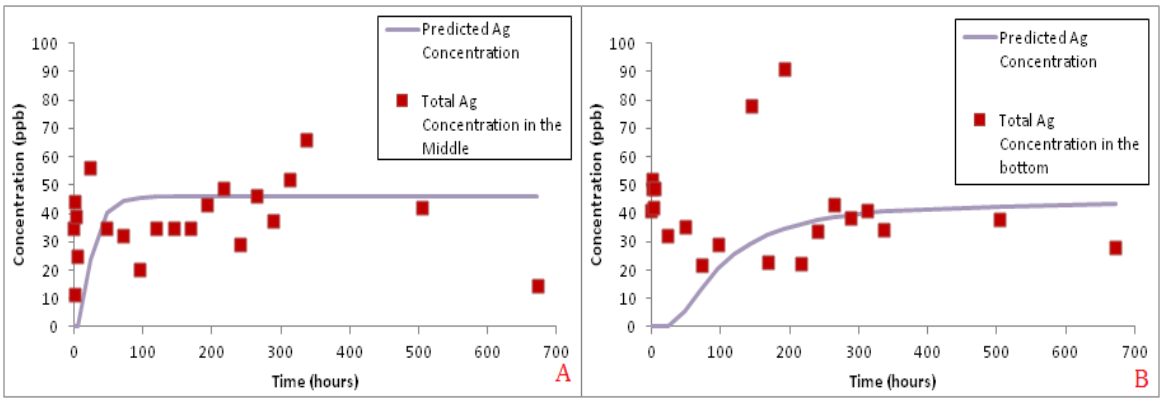

Figure 4.16: Adjusted model parameters to account for PVP AgNPs (table 4.5) for the predicted concentrations over time, plotted against the average total Ag obtained from the study for, A) citrate AgNPs in the middle, and B) citrate AgNPs in the bottom of the mesocosm. New model parameters are listed in table 4.8.

Table 4.8: Adjusted Model Parameters for PVP AgNPs in EPA water for the Middle and Bottom				
Parameter	**Symbol**	**Unit**	**Middle**	**Bottom**
Diameter of Ag atom	d	nm	10.5	10
Cross section area of the column	A	m^2	0.049	0.049
Column Length	*L*	m	1	1
Column volume	*V*=A*L*	L	43	43
Dosing volume	*V*	L	0.215	0.215
Dosing concentration	C_0	ppm	10.5	8.5
Mass of Ag	M	mg	2.3	1.8
C column based on diffusion	M/*V*	ppb	52.5	42.5
Diffusion coefficient	*D*	$m^2 s^{-1}$	4.090E-7	4.294E-7
Sedimentation Velocity	*U*	ms^{-1}	5.7E-10	5.2E-10

As with the results from the UPW exposures, both citrate and PVP AgNPs follow the predicted concentrations that were modelled in the surface water (Socolofsky and Jirka 2004, and Hinderliter *et al,* 2010). Deviations between the particle types and transport differences were shown in the lower depths. Differences from the previous study compared to the present study show that the PVP AgNPs diffuse, where as the citrate AgNPs aggregate and sediment, highlighting that differences in the water chemistry are accountable for the observations to the NP behaviour (Levard *et al,* 2013). Overall the modelled data shows that, the PVP AgNPs are more stable over the citrate AgNPs and are transported by diffusion to the bottom when released into EPA moderately hard water. Evidence of non-aggregated spherical AgNPs was shown in figure 4.18 to support the stability and diffusion of the PVP AgNPs over the citrate AgNPs.

To distinguish between the dissolved and AgNP concentrations, samples were taken for ultrafiltration from the surface and bottom of the mesocosm for the first 14 days and again on days 21 and 28. Total Ag^+ was calculated by measuring dissolved Ag using ultrafiltration. AgNP concentrations were calculated using equation 4.4 and the results are presented in figure 4.14.

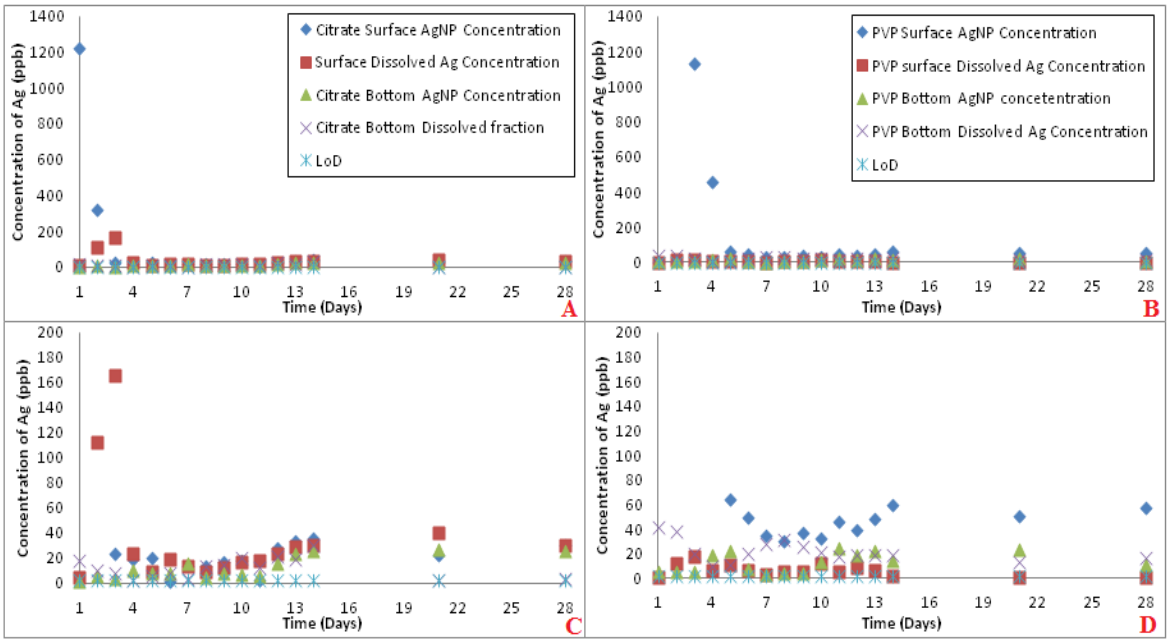

Figure 4.17: Dissolved and AgNP concentrations (ppb) using ultrafiltration in EPA moderately hard water: A) citrate AgNP and Ag^+ concentrations in the surface and bottom depth water for each day, B) PVP AgNP and Ag^+ concentrations in the surface and bottom depth water for each day, C) shows the same graph as A for concentrations below 200 ppb, D) shows the same graph as B for concentrations below 200 ppb. Note the LoD = Instrumentation limit of detection at 2 ± 0.2 ppb.

The information in the graphs 4.17 can be used to confirm the total Ag data presented in figure 4.14, determine the AgNP stability and assess predominate behavioural differences between the two different surface coated AgNPs when compared to the UPW study. The transport mechanism of Ag follows those of the previous study and agrees with the modelled data (figure 4.14). Investigation of the citrate AgNPs revealed that the concentration of AgNPs in the surface water rapidly declined from 1266 ppb on day 1 to 24 ppb on day 3, whereas 6 days were required to see a decline in AgNP concentration the UPW studies. The highest concentrations of Ag^+ were recorded in the surface water between days 1-3, (216-141 ppb) which exceeded those seen in the UPW study, indicating rapid instability of the citrate AgNPs when introduced to the EPA moderately

hard water. Evidence suggests that the differences in the water chemistry have a major effect upon the stability of the AgNPs (Jiang *et al,* 2009). Despite the instability of the citrate AgNPs when introduced to the water, AgNP concentrations were still detected in both the surface at 71 ppb and bottom of the mesocosm at 59 ppb on day 28 of the study.

Observations of the PVP AgNPs revealed that the AgNP concentrations were higher in the surface water when compared to the UPW study. At 24 hours the concentrations of PVP AgNPs were 2380 ppb, compared to 924 ppb in the previous study. Concentrations of PVP AgNPs were also higher on day 28 at the end of the study, at 57 ppb compared to 19 ppb in the UPW study, highlighting PVP AgNP stability. As with the pilot $AgNO_3$ studies presented in figure 4.3 and 4.4, the EPA water shows reduced transport of the Ag to the bottom of mesocosms. In terms of transport between the compartments, the PVP AgNPs in the surface were 64 ppb on day 5, which was comparable 58 ppb at the end of the study and corresponds to Ficks Law (Gorban *et al,* 2011), where the PVP AgNP concentration is 64 ppb on showing an equilibration. In the bottom the AgNP concentration was 6 ppb on day one, where the concentration was comparable on day 28 at 11 ppb.

The information in figure 4.17 can be used to compare the AgNP behaviour between the citrate and PVP coated particles. The Ag^+ concentrations in the citrate study were higher than the Ag^+ concentrations for the PVP study, showing the stability of the PVP AgNPs over the citrate AgNPs, and highlighting behavioural differences in the presence of simple electrolytes. Since citrate is an electrostatic surface coating (Doty *et al,* 2005, and Fabrega *et al,* 2011) it is more susceptible to changes in ionic strength,

resulting in behavioural changes such as dissolution via oxidation (El Badawy *et al,* 2010). Similar results were seen for An Huynah and Chen (2011), who observed the facilitated dissolution of citrate AgNPs compared to PVP AgNPs in the presence of simple electrolyte media.

However, both the citrate and PVP AgNP studies appear to have lower dissolved concentration rates than those previously observed in the UPW. Consideration needs to be made for the ionic species reforming NP complexes with Cl and the other electrolytes in solution (Zook *et al,* 2011). These complexes cannot be distinguished from the original AgNPs that were introduced to the aqueous system, as FAAS, like other conventional methods of analysis, only detects total Ag and doesn't distinguish between the different forms, for example, AgCl. Therefore the time frame in which these studies were conducted was more than a sufficient amount of time for AgCl complexes to form, resulting in lower concentration of Ag^{+} compared to the UPW study.

4.4.3.2.2 UV-Visible Analysis

Figure 4.18 (A-F) describes the SPR profiles for both citrate and PVP particles exposed over time at the surface, middle and bottom points of the mesocosms.

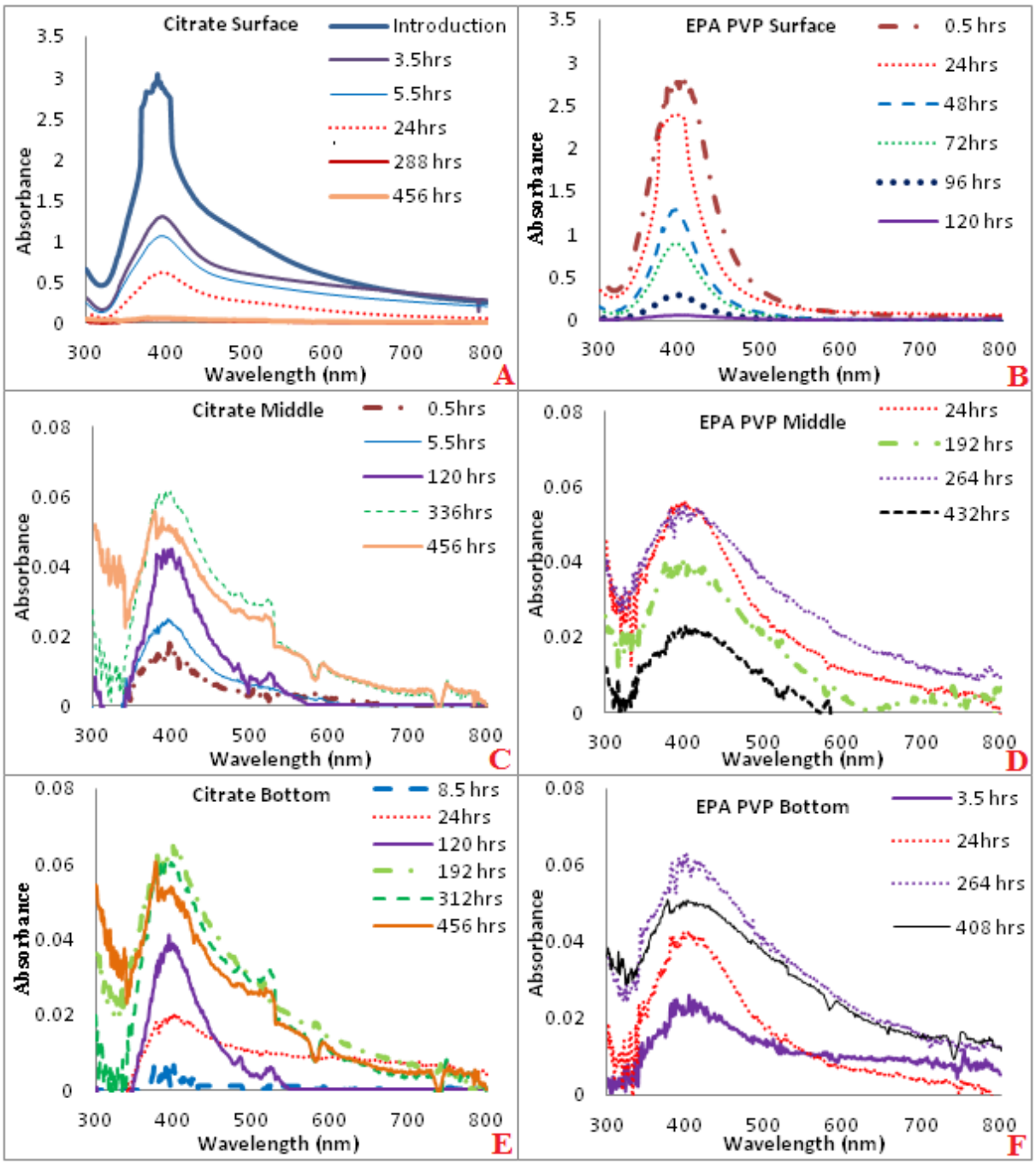

Figure 4.18: UV SPR profiles of citrate and PVP coated AgNPs released in EPA standard moderately hard water taken from different depths of the mesocosm column. A) Citrate coated AgNPs at the surface, B) PVP AgNPs at the surface, C) Citrate AgNPs from the middle, D) PVP AgNPs from the middle, E) Citrate AgNPs from the bottom and F) PVP AgNPs from the bottom. Note that the Y axis for the graphs are not presented in the same scale for each of the depths, as detail from the lower regions would be lost.

On introduction to the surface water it should be noted that upon mixing the yellow/orange colour of the citrate NPs changed to a dark brown/orange colour, which became colourless over time as particles diffused throughout the mesocosm tanks. Colour changes were not observed in the UPW study. Stamplecoskie and Scaiano (2012) indicated that a brown colouring to an AgNP suspension indicated large irregularly shaped particles. Therefore the transition of citrate AgNPs forming aggregates is indicated by the colour change.

UV-Vis results obtained for the EPA water show that citrate particles see a completely different SPR banding pattern obtained for the EPA water compared to those exposed to UPW, which is agreeable with similar results obtained by Chinnapongse *et al* (2011), who observed the same band tailing when citrate AgNPs were exposed synthetic waters. Many other studies have also identified the direct relationship with the SPR peak shift with the size and shape (Hao and Schatz, 2004, and Kelly *et al,* 2003). The widening of the SPR peaks is known to be caused by dipole and quadrupole red shifting of the SPR, causing a change in the surface electrons light scattering. When particles change size, shape, or aggregate together, the electrons on the surface of the particles scatter light differently depending on the particle properties. Smaller particles scatter light more quickly (Bhui *et al,* 2009). The changes in the SPR banding patterns would account for the colour changes observed on introduction. Depending on the polydispersity, capping agent and the size, the more polydispersed the AgNPs are, the wider the peak will be (Liu and Hurt, 2010). Therefore the wider peak between 500-800nm for the citrate particles in figures 4.18A, 4.18C and 4.18E, is due to large shape changes caused by aggregation (Li *et al,* 2010).

The typical aggregation profile for the citrate AgNPs follows the Derjaguin-Landau-Verwey-Overbeek (DLVO) theory, which describes the aggregation of spherical particles in an aqueous environment and the forces between charged particle surfaces. These forces are the van der Waals forces of attraction and the electrostatic repulsion between the two particles in solution (Esmaeili *et al,* 2012). When the particles were in UPW the electrostatic forces between the particles prevented them from aggregating, whereas the introduction to an ionic solution reduces these forces and aggregation occurs (Bae *et al,* 2013). Evidence from the SPR graphs confirms the transportation of the citrate AgNPs to follow sedimentation, due to the aggregated AgNPs as seen in the modelled data (figures 4.14 and 4.15).

Once the citrate particles are introduced to the EPA water, a small red shift is observed from 392nm (original) to 395nm is observed. Although the shift is small, the shifting to a larger wavelength is known as the red shift effect (Hao and Schatz, 2004). The red shift effect occurs from the AgNP interactions with the surrounding water molecules and its dielectric constant. Particles display a red shift effect when the AgNPs shift towards the red end of the spectrum, increasing the wavelength of light emitted, which is dependent on the size and shape of the AgNPs (Li *et al,* 2010). A change in SPR is due to changes in electromagnet wavelengths that move parallel to the particle surface. Therefore, when molecules adsorb on to the NP surface, the change in oscillations cause light to emit at higher wavelengths, thus, observing the red shift effect (Pinchuk *et al,* 2004). The larger the red shift the more interactions that are present between the water molecules and the AgNPs. A red shift in wavelength can also occur when there is an oxide layer on the surface of the NP (Li and Sun, 2011). Therefore the red shifting of the

SPR signal further supports AgNP aggregation caused from interactions of the surrounding EPA water.

Overall the differences in the observed behaviour seen in the two different water types (UPW and EPA water) for the citrate particles are due to the AgNP interactions with the electrolytes. The addition of electrolytes in the EPA water system, caused immediate behavioural changes. Unlike the PVP polymer stabilised particles, citrate is electrosterically attached to the AgNP surface. The addition of ionic species in the EPA water has caused a change in the surrounding charge in solution, which may have caused the citrate coating to have been removed from the NP surface or partially removed. As described by the DLVO theory, the electrostatic repulsion between two particles in conjunction with van der Waals attraction will determine particle aggregation (Bae *et al,* 2013). A partial removal of the citrate surface coating and a change in the surface charge, induced by the ionic strength of the water will reduce the electrostatic diffuse double layer, resulting in increased aggregation as there are reduced charges to prevent NP-NP interactions (Romer *et al,* 2011). Evidence of aggregation is determined by the tailing peak between 500-600nm (Stamplecoskie and Scaiano, 2012) and the colour changes observed on introduction. Simultaneously, the lack of charge repulsion between the NP surfaces would have caused decreased NP stability, making them susceptible to dissolution and to form Ag complexes with the electrolytes in solution, such as AgS and AgCl complexes.

At the point of introduction, the PVP AgNPs remained orange until they diffused out of the area and the water became colourless. In comparison, the PVP particles show the same sharp SPR bands as observed in the UPW study for the surface water. After 24

hours the PVP particles sampled in the middle and the bottom areas of the mesocosm tanks observed small band broadening where the peaks tailed between 600-800nm, showing small size or shape changes (Li *et al,* 2010). At day 18 there was only a small board peak between 300-600nm, with no tailing in the 800nm region. Evidence suggests by day 18 all the larger particles had settled to lower region, as the bands for the PVP particles at the bottom also exhibit the same stretching in the 600-800nm region. The results confirm findings observed in the modelled data, which shows a steady concentration gradient in the surface and middle. A small elevation and decline of Ag concentration in the bottom of the mesocosm, confirm the PVP AgNPs move mainly by the process of diffusion. As PVP is a polymer coating attached via steric forces, the particles were more stable in ionic solutions as they do not interact fully with the surrounding water chemistry.

4.4.3.2.3 Transmission Electron Microscopy (TEM) Analysis

The size and morphological changes to the citrate and PVP AgNPs were investigated using TEM. As discussed in chapter 3 the original citrate AgNPs were sized at 11 ± 3 nm (TEM), and the PVP AgNPs were sized at 11 ± 3 nm (TEM). Size results after release to the EPA moderately hard synthetic water are located in table 4.9, and Imaging of the particles are displayed in figures 4.19 (citrate) and 4.21 (PVP).

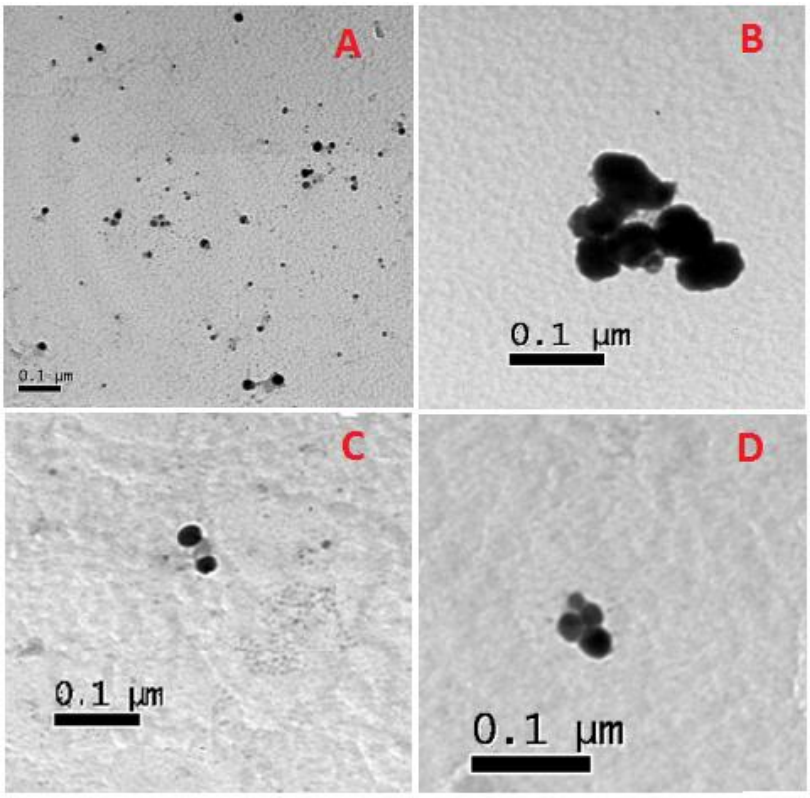

Figure 4.19: TEM images of citrate AgNPs exposed to EPA moderately hard water at A) 24 hours surface, B) 24 hours bottom, C) 96 hours surface, and D) 96 hours bottom.

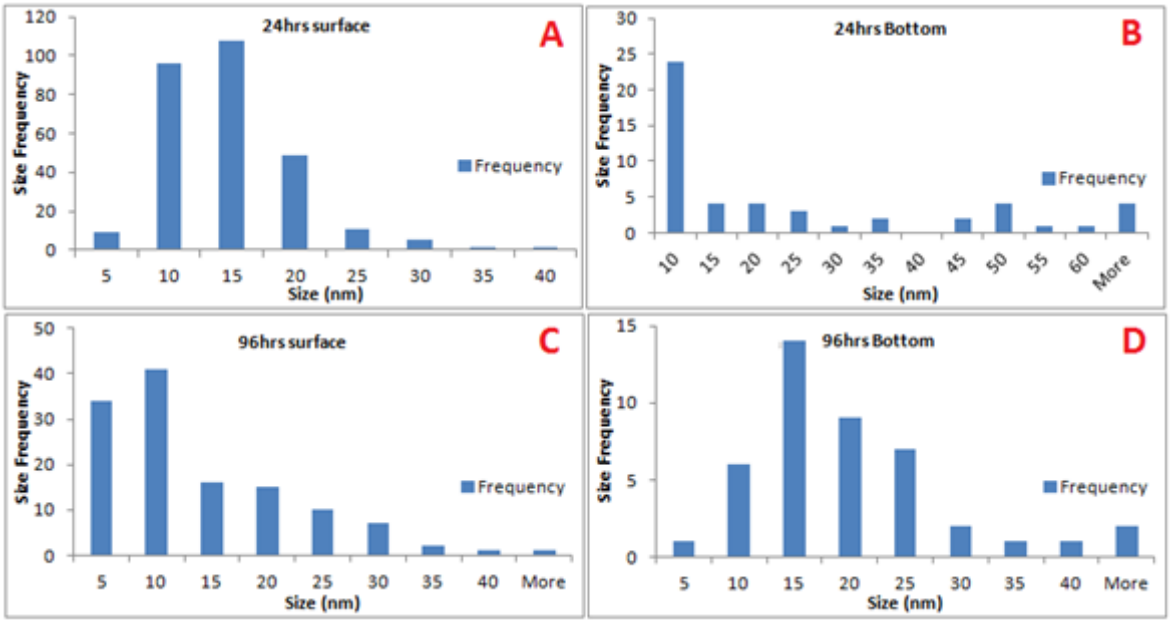

Figure 4.20: TEM histograms showing the core size occurrence frequency for citrate AgNPs in EPA moderately hard water, A) 24 hours surface, B) 24 hours bottom, C) 96 hours surface, and D) 96 hours bottom.

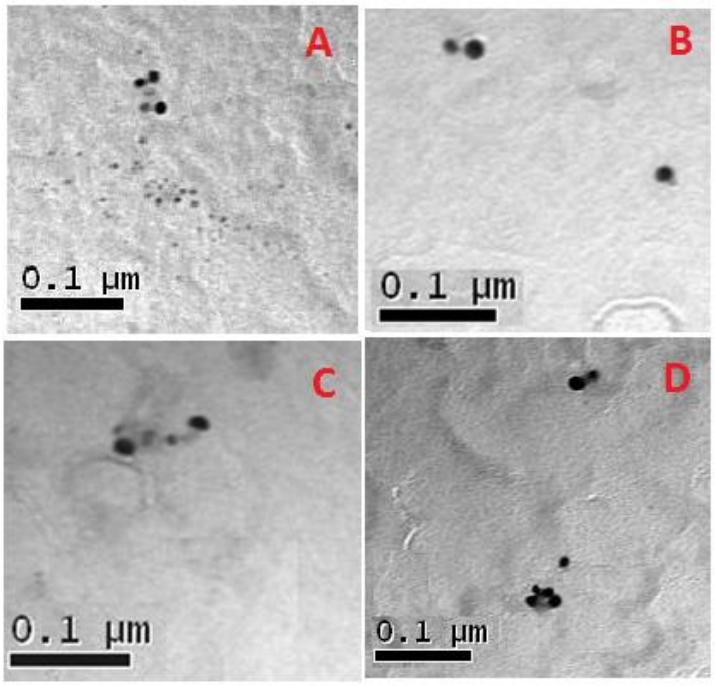

Figure 4.21: TEM images of PVP AgNPs exposed to EPA moderately hard water at A) 72 hours surface, B) 72 hours bottom C) 120 hours surface and D) 120 hours bottom.

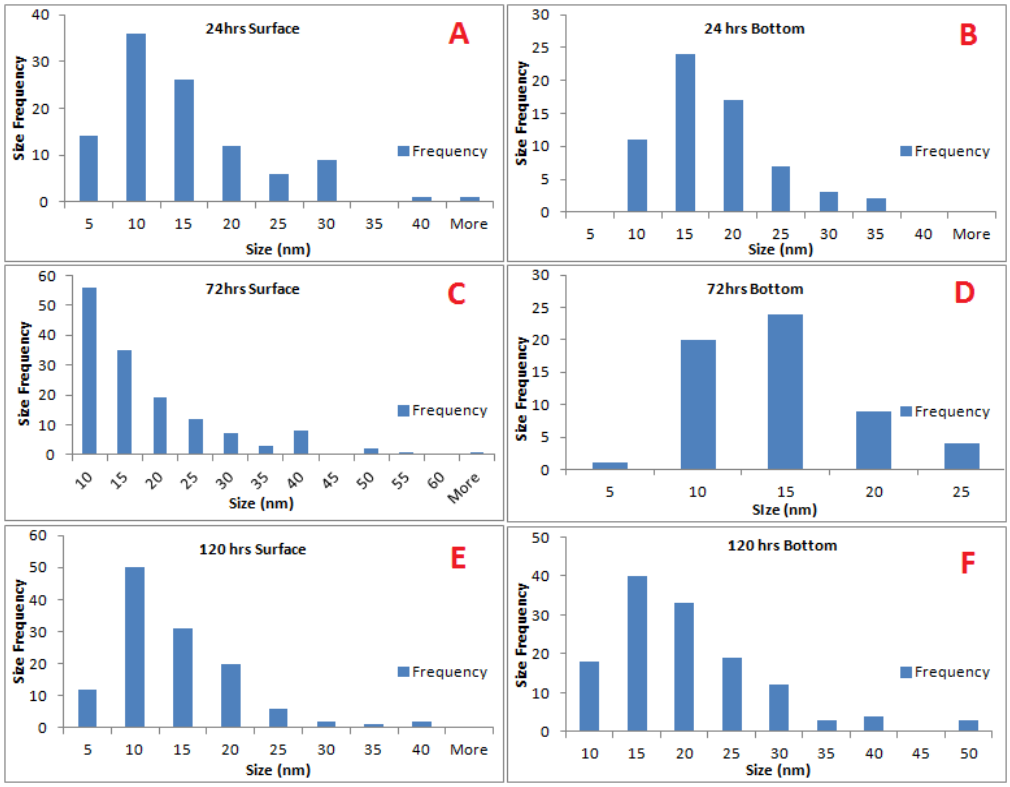

Figure 4.22: TEM histograms of PVP AgNPs exposed to EPA moderately hard water. A) 24 hours in the surface water. B) 24 hours in the bottom water, C) 72 hours in the surface waters, D) 72 hours in the bottom water, E) 120 hours in the surface water and F) 120 hours in the bottom water.

Table 4.9: TEM sizes (nm) at different time points for citrate and PVP particles exposed EPA moderately hard water. A t-test was performed to identify differences from the observed compared to the original AgNPs sizes before release. *n= number of particles counted*ND= Not Determined. A p value <0.05 highlights that the observed particle size using the t-test is significantly different to the size of the original particle before release, at a 95% confidence level.

Table 4.9 Average Core Size by TEM								
Time (hours)	**24**		**72**		**96**		**120**	
Area Analysed	**Surface**	**Bottom**	**Surface**	**Bottom**	**Surface**	**Bottom**	**Surface**	**Bottom**
Particle type	**Citrate AgNPs**							
Size (nm)	13 ± 5	23 ± 23	ND	ND	12 ± 8	18 ± 10	ND	ND
n	279	65			127	45		
P-Value	4.84E-7	4.34E-17			0.171	3.83E-21		
Particle Type	**PVP AgNPs**							
Size (nm)	13 ± 8	16 ± 6	16 ± 11	13 ± 4	ND	ND	12 ± 7	18 ± 7
n	105	64	144	59			124	132
P-Value	0.013	3.93E-12	2.21E-6	0.001			0.082	2.65E-15

After 24 hours the citrate AgNPs show the particle sizing is significantly different from the original citrate AgNPs before release (11 ± 3 nm), at 13 ± 5 nm (*p* 4.84E-7) at 24 hours and 12 ± 8 nm (*p* 0.171) for 96 hours (table 4.9) in the surface water. Additionally, the citrate AgNPs sampled from the bottom of the mesocosm were larger than those at the surface at 24 hours at 23 ± 23 nm (*p* 4.34E-17 compared to original), and reduced in size after 4 days to give an average size of 18 ± 10 nm (*p* 3.83E-21 compared to original). The reduction in size over time may be due to dissolution and/or breakage of aggregates.

Analysis of the citrate AgNPs in figure 4.19 show a high concentration of NPs with varying size from the surface water at 24 hours. In comparison figure 4.19C shows particles in the surface after 96 hours post release, are less concentrated, of unequal sizes. Similarly, the images that represent citrate AgNPs from the bottom of the

mesocosm at 24 hours and 96 hours identify shape changes and aggregation, which corresponds to the SPR shape changes on exposure (figure 4.18A, 4.18C, and 4.18E). As particles were in lower concentration from the bottom samples, they required extensive searching on the microscope grids in order to image particles, and explain why the number of particles analysed is lower than those for the surface.

The corresponding size frequency histograms in figure 4.20 identify that citrate AgNPs exposed to EPA moderatly hard water become immediantly unstable in solution, evidenced by the polydispersity of the size frequencies. Larger particles sediment to the bottom, evidenced further in the modeling data (figure 4.14C, 4.14E and 4.14). The modeled data shows concentrations of Ag follows sedimetation of the citrate AgNPs, which corresponds to the settling of larger aggergates. When comparing to the previous UPW studies, the citrate AgNPs exposed to the EPA moderately hard water produced a larger size frequency for the surface at 24 hours. The size frequency changed from 10 nm (UPW) to 15 nm (EPA water), providing further evidence of NP instability when released into simple ionic solutions.

PVP AgNPs in the surface water are slightly larger than the original (11 ± 3 nm) at 13 ± 8 nm (p 0.013), which was also true for the UPW study. Morphological analysis of the PVP AgNPs presented in figure 4.21 at 72 hours in the surface water, show a mixed abundance of small spherical particles present in high concentration, as seen with the citrate particles at 24 hours (figure 4.19A). To compare with the bottom water samples, at 72 hours (figure 4.21B) and 120 hours (figure 4.21D) the PVP AgNPs show spherical and non-aggregated particulates.

The corresponding size frequency histograms (figure 4.22) for the PVP AgNPs when compared to the UPW at 24 hours in the surface region, show a higher abundance of particles larger than 25 nm. Although PVP AgNPs are renowned for their stability over citrate AgNPs (El Badawy *et al,* 2011, and Li *et al,* 2013), instability has been demonstrated via the increased sizes. Despite this, the most frequently counted particle core size was 10 nm (at 24 hours), showing smaller particles favoured retention in the surface waters. Simultaneously, at 72 hours for the surface water there was evidence of polydispersity compared to the UPW studies. PVP AgNPs in the surface water at 72 hours (figure 4.22C) show a decline in the number of particles that larger than 20 nm, compared to 24 hours, showing larger particles sediment to the bottom. Larger PVP AgNPs are evident in figure 4.22F, where there is higher frequency of large particles settled in this area. Information further corresponds to the slight SPR band tailing in the 500-600nm region in the UV profiles for the bottom area, further evidencing instability when AgNPs are exposed to the electrolytes in the EPA water. However, the unstable effects are only slight when compared to the changes and transformations observed to the citrate particles in EPA water.

Overall combined evidence from the TEM histograms and the UV SPR peaks show a surface coating difference in behaviour to the AgNPs once released to EPA moderately hard water, although both citrate and PVP AgNPs were persistent for the duration of the study (figure 4.17). On introduction to the EPA moderatly hard water citrate AgNPs immdiately aggregate and demonstrate shape and size changes. Larger citrate AgNPs sediment quicky, and smaller AgNPs are retained in the surface and slowly diffuse down the mesocosm, as evidenced by the model (figure 4.14C, 4.14E and figure 4.14). In

comparison, PVP AgNPs exhibit maintained stability when introduced to the EPA water. Unlike the citrate AgNPs, there was no evidence of aggergation in the SPR profiles in the surface water, and the total AgNP fraction was higher in concentration for the duration of the study. Equally the dissolved Ag proportion was also lower in concentration compared to the citrate AgNP study. Overall, all particles analysed had *p-values* below *p* 0.05, showing EPA moderately hard water had a significant effect to the sizes when compared to the original particles pre-release.

4.4.3.3 EPA Moderately Hard Water with Suwannee River Fulvic Acid (SRFA)

To make realistic comparisons to natural water, a final synthetic water study using fulvic acid (SRFA) was added at a concentration of 1 mg L^{-1} to EPA moderately hard water.

4.4.3.3.1 Total and Dissolved Silver Concentrations

To assess the effects of adding SRFA to the EPA moderately hard water, the total Ag concentrations for the citrate (11 ± 3 nm TEM) and PVP AgNP (12 ± 2 nm TEM) studies were measured. Samples were taken in coherence with the previous studies over a 28 day period. The tables for the results are displayed in the additional information section and the total Ag concentration data has been plotted alongside the predicted modelled concentrations (Socolofsky and Jirka 2004, and Hinderliter *et al,* 2010).

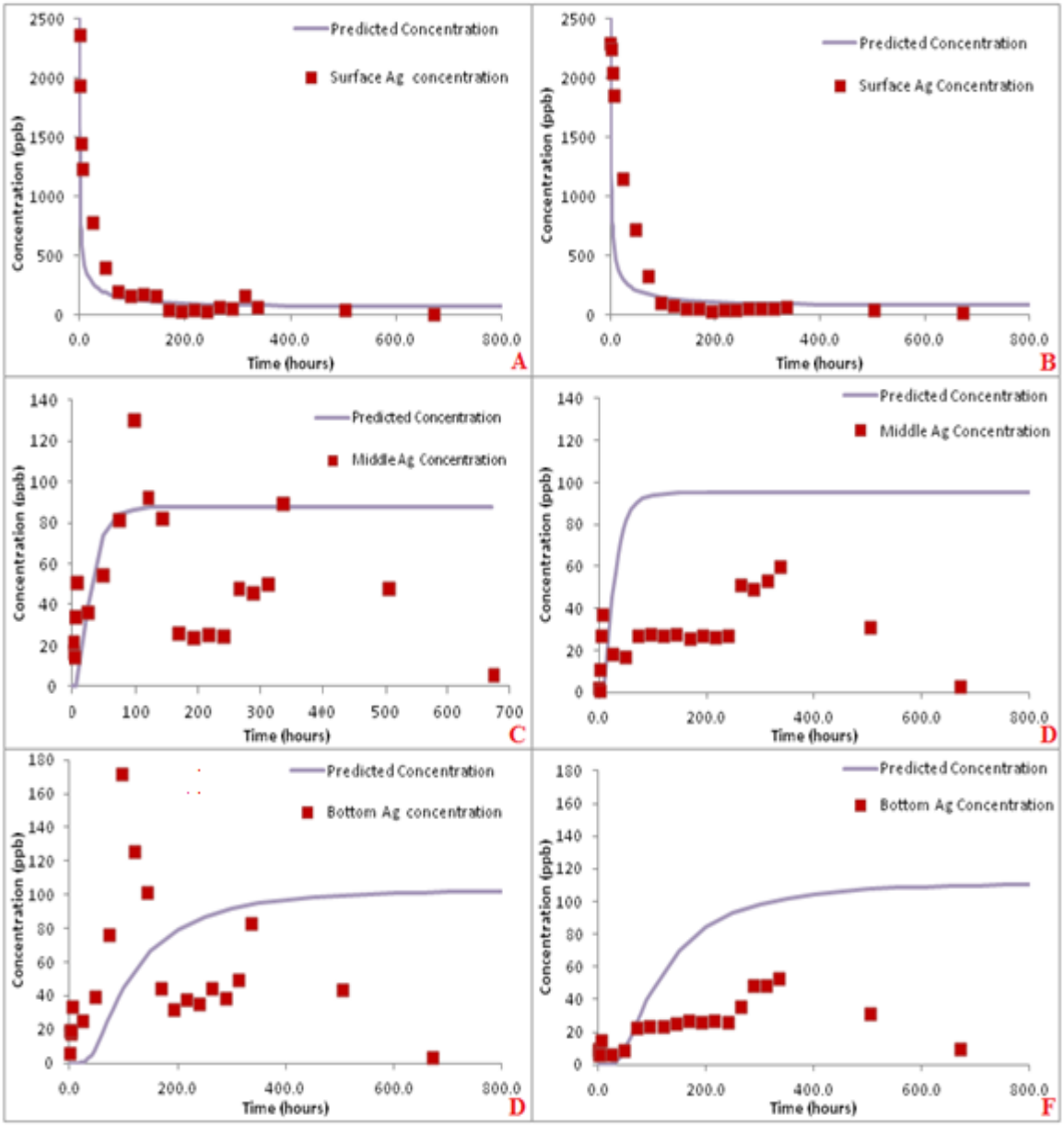

Figure 4.23: Model predicted concentrations over time plotted against the average total Ag obtained from the study for, A) citrate AgNPs in the surface, B) PVP AgNPs in the surface, C) citrate AgNPs in the middle, D) PVP AgNPs in the middle, E) citrate AgNPs in the bottom, and F) PVP AgNPs in the bottom of the mesocosm containing EPA moderately hard water with SRFA. Model conditions are the same as those presented in table 4.6.

The total Ag concentrations for the citrate and PVP AgNP studies were plotted against the predicted modelled Ag concentrations over time, for each depth of the mesocosm as displayed in figure 4.23. Analysis of the citrate AgNP study revealed that only the surface

water profile (figure 4.23A) followed the model predictions for the total Ag concentrations. We conducted a Pearsons correlation coefficient between the modelled and observed Ag concentration determined the R^2 value of the surface water to be 0.99, showing a strong correlation between the two sets of data. Results are also in accordance to all the previous water outcomes for the surface waters.

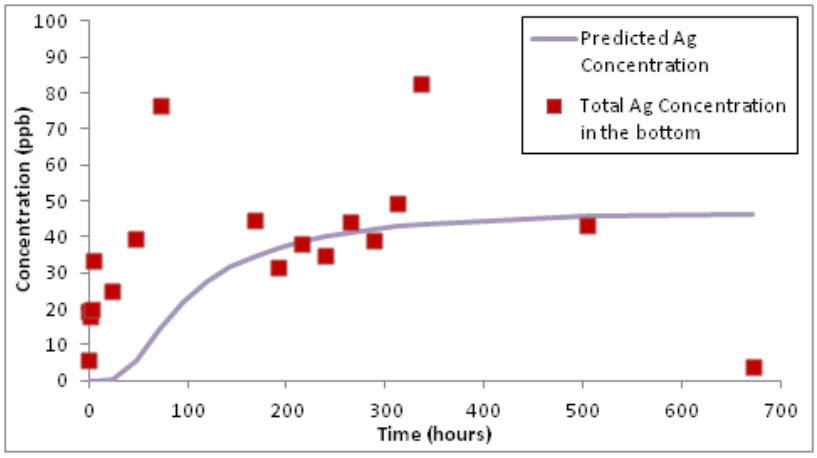

Figure 4.24: Adjusted model fits for the bottom water for citrate AgNPs exposed to EPA SRFA water. New model parameters are listed in table 4.10.

Table 4.10: Adjusted Model Parameters for citrate AgNPs in EPA SRFA water for the Bottom depth

Parameter	Symbol	Unit	Bottom
Diameter of Ag atom	d	nm	10
Cross section area of the column	A	m^2	0.049
Column Length	*L*	m	1
Column volume	*V*=A*L*	L	43
Dosing volume	*V*	L	0.391
Dosing concentration	C_0	ppm	8.5
Mass of Ag	M	mg	2
C column based on diffusion	M/*V*	ppb	45.5
Diffusion coefficient	*D*	$m^2 s^{-1}$	4.294E-7
Sedimentation Velocity	*U*	ms^{-1}	5.2E-10

The middle and bottom depth demonstrates a series of elevations and declines in the Ag concentrations, consistent with aggregation and sedimentation of larger particulates (Hinderliter *et al,* 2010) evidenced in the TEM imaging. The R^2 value for the

middle was determined at 0.71 and the R^2 value for the bottom was determined at 0.49. We adjusted the model parameters to assess the cause of the reduced R^2 value in the bottom of the mesocosm as seen in figure 4.24 and table 4.10. As aggregation will cause the citrate AgNPs to settle in the bottom, if we reduce the Ag concentration to fit the model and observed data the R^2 value increases to 0.96. Aggregation of the citrate AgNPs is due to the electrolytes in solution as established in the previous EPA water study (Zhang and Oyanedel-Craver, 2012). Further explanations maybe due to AgCl NPs formations which can attach to the citrate AgNP surface (Baalousha *et al,* 2013). Aggregation of the citrate AgNPs is also evidenced in the SPR profiles presented in figure 4.22, confirming sedimentation (figure 2.20). When compared to the previous EPA water study, increased sedimentation of the aggregates was seen in the present study for the citrate AgNPs. Explanations of the may be due to NOM re-coating the NP surfaces, or AgNPs bonded with other NOM coated AgNPs resulting in larger aggregates to influence their fate and transport. Overall, investigations of the total Ag concentration for the citrate AgNP study reveals that the AgNPs aggregate and sediment to the bottom.

Analysis of the total Ag recorded for the PVP AgNP study identified a strong correlation between the model and the observed data with an R^2 value of 0.99. The total Ag concentrations observed for the PVP study identifies behavioural differences between the two surface coated AgNPs and infers a difference in the transportation mechanisms in the lower depths. After 24 hours there is a plateau in Ag concentration in both the middle and bottom depths, agreeing with Ficks Law (Fick, 1855). Evidence shows that the movement of Ag is stable and slowly diffuses in to the lower depths compared to rapid sedimentation and diffusion observed in the citrate AgNP study. Because the observed

concentrations in the middle and bottom are lower than the modelled concentration the R^2 value in the middle is 0.46 and 0.44 in the bottom. To account for losses of Ag during the study as calculated from sample removal and settling, the model parameters can be adjusted accordingly to fit non-aggregated 10-12 nm PVP AgNPs (TEM), as seen in figure 4.25 and table 4.11. After the model adjustments have been made the R^2 values in the middle rise to 0.62 and 0.67 in the bottom (see appendix), showing stronger correlations between the modelled and observed data.

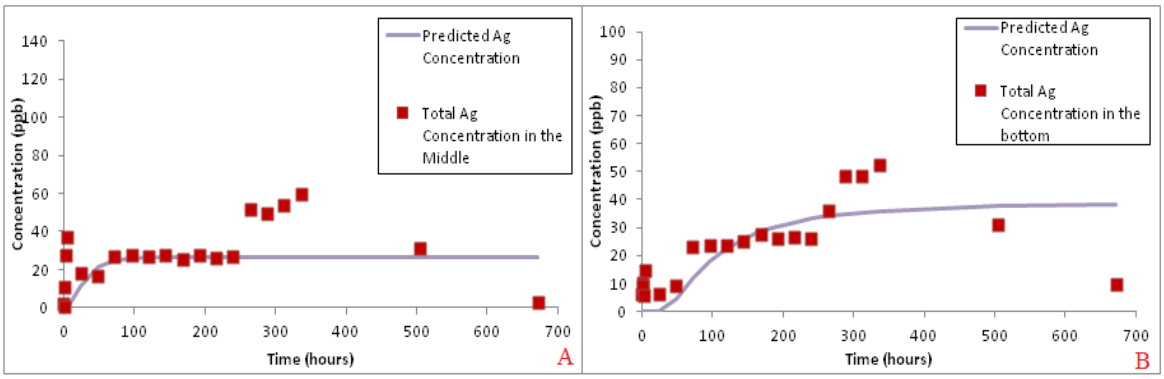

Figure 4.25: Adjusted model fits for the middle and bottom water for PVP AgNPs exposed to EPA SRFA water. New model parameters are listed in table 4.11.

Table 4.11: Adjusted Model Parameters for PVP AgNPs in EPA SRFA water for the Middle and Bottom

Parameter	Symbol	Unit	Middle	Bottom
Diameter of Ag atom	d	nm	12	10
Cross section area of the column	A	m^2	0.049	0.049
Column Length	*L*	m	1	1
Column volume	*V*=A*L*	L	43	43
Dosing volume	*V*	L	0.215	0.215
Dosing concentration	C_0	ppm	6	7.5
Mass of Ag	M	mg	1.3	1.6
C column based on diffusion	M/*V*	ppb	30	37.5
Diffusion coefficient	*D*	$m^2 s^{-1}$	3.579E-7	4.294E-7
Sedimentation Velocity	*U*	ms^{-1}	7.4E-10	5.2E-10

As with the previous studies, assessments of the dissolved Ag proportions compared to the AgNP proportions were analysed. Samples were taken for the first 14

days and again on days 21 and 28 AgNP fractions were devised from the sum of the total silver (units presented in the appendix) minus the dissolved fraction number obtained using ultrafiltration methods.

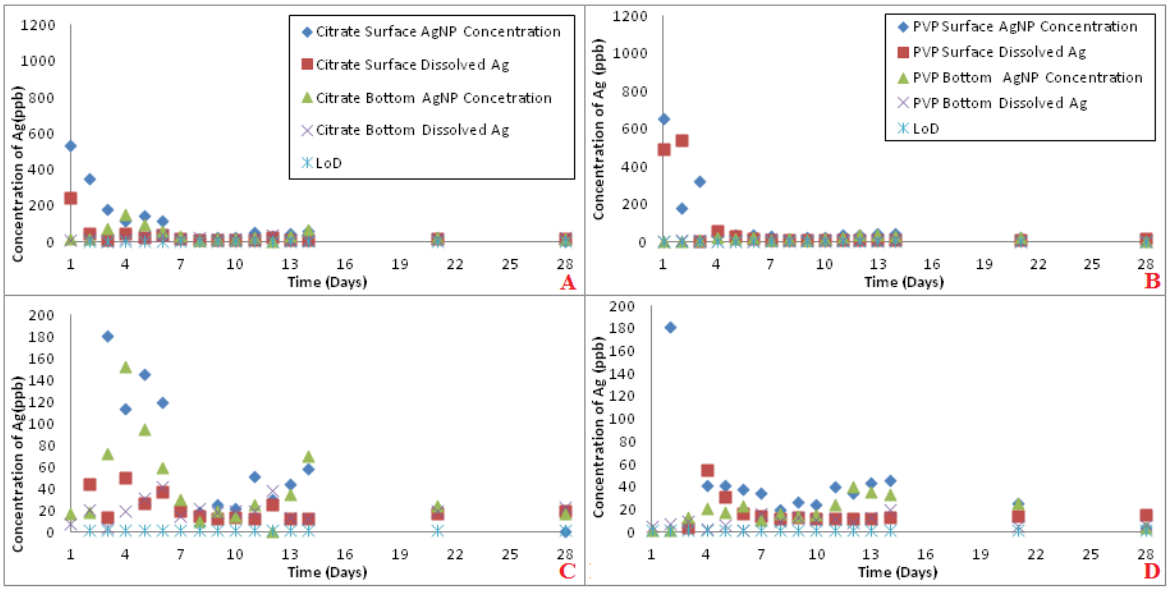

Figure 4.26: Dissolved and AgNP concentrations (ppb) using ultrafiltration in EPA moderately hard water with added SRFA, A) citrate AgNP and Ag^{+} concentrations in the surface and bottom depth water for each day, B) PVP AgNP and Ag^{+} concentrations in the surface and bottom depth water for each day, C) shows the same graph as A for concentrations below 200 ppb, D) shows the same graph as B for concentrations below 200 ppb. Note the LoD = Instrumentation limit of detection at 2 ± 0.2 ppb.

The Ag concentrations in the modelled data suggested that aggregation had taken place for the citrate AgNPs, due to the sedimentation patterns of the observed concentrations in the lower depths of the mesocosm. Suggestions for the reduced dissolution rate for the citrate AgNPs may be explained by the increased aggregation rate, by reducing the surface area that can be oxidised (Li *et al,* 2010, Zhang *et al,* 2011). As citrate is an electrostatic surface coating (Fabrega *et al,* 2011) changes in ionic strength (El Badawy *et al,* 2010) reduces the diffuse double layer of repulsion (Liang *et al,* 2007) and thus,

aggregation occurs. A reduced oxidation state will result in less ionic Ag being released. It has been well documented that NOM has been known to re-coat the NPs, resulting in aggregation changes (Lowry *et al,* 2012) which have been observed in this study when compared to a simple water system. It's also important to note that organic macromolecules can absorb on to the NP surface (Lowry *et al,* 2012). Therefore, suggestions for the reduced dissolution of the citrate AgNPs, may be due to NOM adsorbing onto the NP/aggregate surface and creating a new surface coating (Bae *et al,* 2013).

EPA moderately hard water standard is made up of a mixture of salts that contain of monovalent cations such as potassium (K^+) and sodium (Na^+) and divalent cations such as calcium (Ca^{2+}) and magnesium (Mg^{2+}). Each has the potential to interact with the AgNPs and the free SRFA in solution (Akaighe *et al,* 2012). Ha and Payer (2011) observed that in the presence of Cl in solution dissolution of Ag was reduced resulting in small amounts of Ag^+ released. Further consideration for the ionic Ag species reforming NP complexes with the other electrolytes in solution cannot be overlooked. Therefore, it is possible that AgCl complexes have formed, thus increasing the NP concentration, and reduced dissolution as observed in the present study. Similar results were also obtained by Akaighe *et al,* (2012) who exposed AgNPs to a series of individual solutions containing calcium chloride ($CaCl_2$) magnesium chloride ($MgCl_2$), sodium chloride (NaCl) potassium chloride (KCl). The researchers found that the exposure to divalent cations (Ca^{2+} and Mg^{2+}) increased sedimentation due to reduced electrosteric and steric forces between the particles. These studies were conducted using small scale laboratory experiments using UPW (Linlin and Tanaka, 2013) and simple electrolyte solutions with larger NPs (>50

nm). Unlike the present study none of the previous literature studies used a mixture of electrolytes in solution to create a moderately hard water standard with the addition of NOM added to the solution.

We suggest that the introduction of citrate AgNPs to the EPA water with SRFA induces immediate particle aggregation in solution. We further pose, that the citrate AgNP surfaces attract the functional groups of the SRFA, which adopts a surface coating function to retain particle stability and reduce dissolution. In addition, the electrolytes in solution can also ionize the exposed functional groups of the SRFA on the particle surface creating an electrostatic charge, further stabilising the particles. The newly adopted charge can attract other surrounding particles that have been transformed by NOM to further induce sedimentation of the aggregated particles. These combined theories account for why the citrate AgNPs aggregate and sediment, shown by the increased presence of larger particles in the bottom areas compared to the previous studies. Evidence also shows that the water chemistry has a major effect upon the stability of the AgNPs (Jiang *et al,* 2009).

Analysis of the PVP AgNPs demonstrated similar behaviour to the EPA water absent of NOM and remained stable. PVP AgNPs were detected for the duration of the study of 28 days, and the dissolved Ag concentrations observed for the PVP AgNP study were comparable to those from the previous studies.

4.4.3.3.2 UV Analysis

Figure 4.27 (A-F) describes the SPR profiles for both citrate and PVP particles exposed over time at the surface, middle and bottom points of the mesocosm tanks.

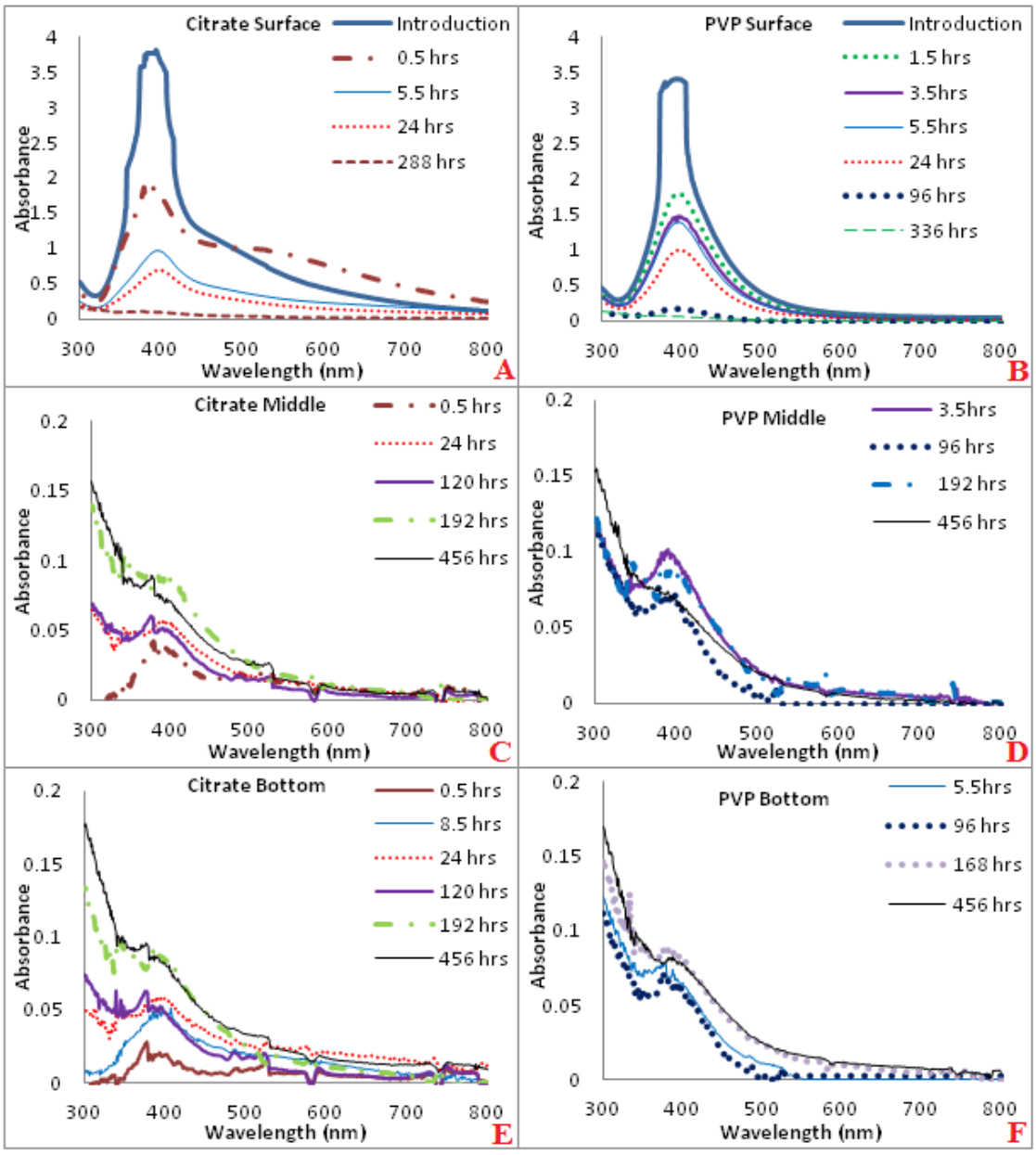

Figure 4.27: UV SPR profiles of citrate and PVP coated AgNPs exposed to EPA standard moderately hard water with added SRFA, taken from different depths of the mesocosm column. A) Citrate coated AgNPs at the surface, B) PVP AgNPs at the surface, C) Citrate AgNPs from the middle, D) PVP AgNPs from the middle, E) Citrate AgNPs from the bottom and F) PVP AgNPs from the bottom Note that the Y axis for the graphs are not presented in the same scale for each of the depths, as detail from the lower regions would be lost.

When compared to the previous studies, the addition of SRFA to the EPA water shows a completely new SPR time profile for the middle and bottom water areas for both AgNP

type. In the previous studies the SPR bands drop after 320-350nm back towards the baseline, whereas the present study sees a continuous rise after 350nm. Differences in SPR bands are due to out of plane quadrupole resonance, (Kelly *et al,* 2003, Zou *et al,* 2007, and Kawaguchi *et al,* 2011). Since out of plane quadrupole resonance was not observed in the previous waters effects are due to the addition of SRFA, information suggests that the addition of SRFA transforms NP behaviour at lower depths once diffusion and sedimentation had taken place.

The SPR profiles for the citrate AgNPs demonstrate strong differences for the aggregation state, when compared to the previous EPA water study. A dominate second peak in the 500-600nm region provides evidence of a strong bimodal size distribution for the citrate AgNPs. The extent of aggregation is further evidenced in the model transport data in figures 4.23C and 4.23E. SPR analysis of the PVP AgNPs reveals no aggregation as shown by the absence of SPR band stretching between 500-600nm, which confirms the mechanism of transport followed is diffusion as shown in the model.

4.4.3.3.3 TEM and EDX Analysis

Original citrate AgNPs were sized at 11 ± 3 nm (TEM), and PVP AgNPs were 12 ± 2 nm (TEM) before release in the the EPA water with added SRFA. Average particle sizes from the surface and bottom water in the present study are shown in table 4.12. EDX analysis of the citrate AgNPs was also conducted from a sample extracted at 24 hours post release in the surface water.

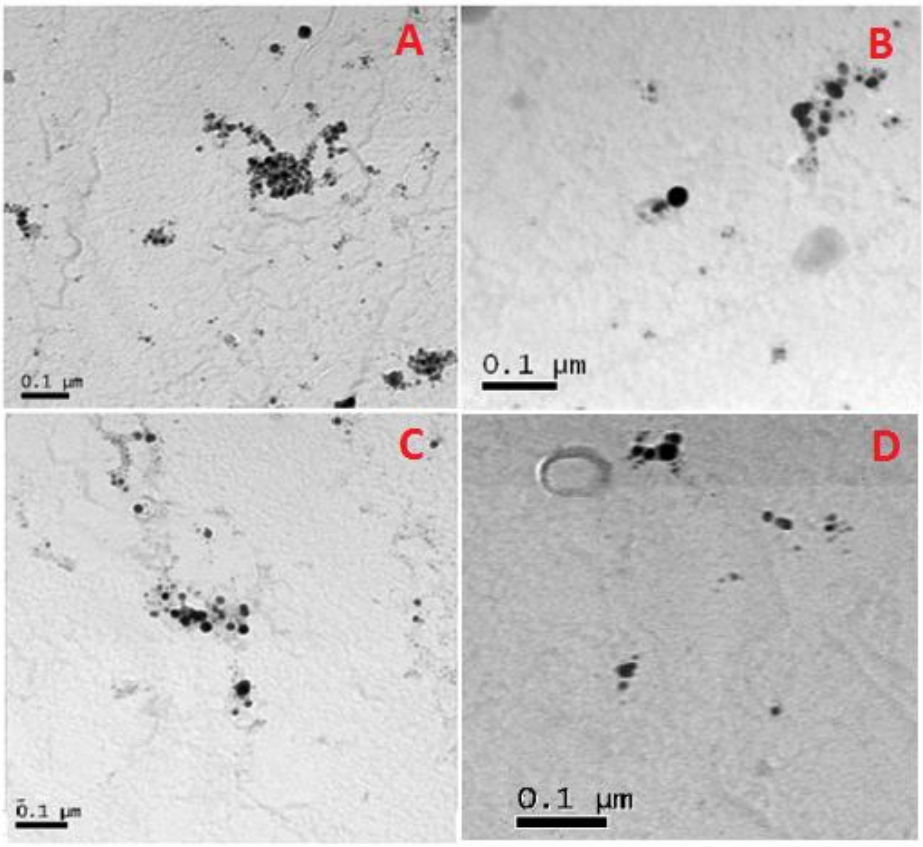

Figure 4.28: TEM images of citrate particles exposed to EPA moderatly hard water with SRFA at A)surface 24 hours, B) bottom at 24 hours, C) 96 hours surface and D) 96 hours bottom.

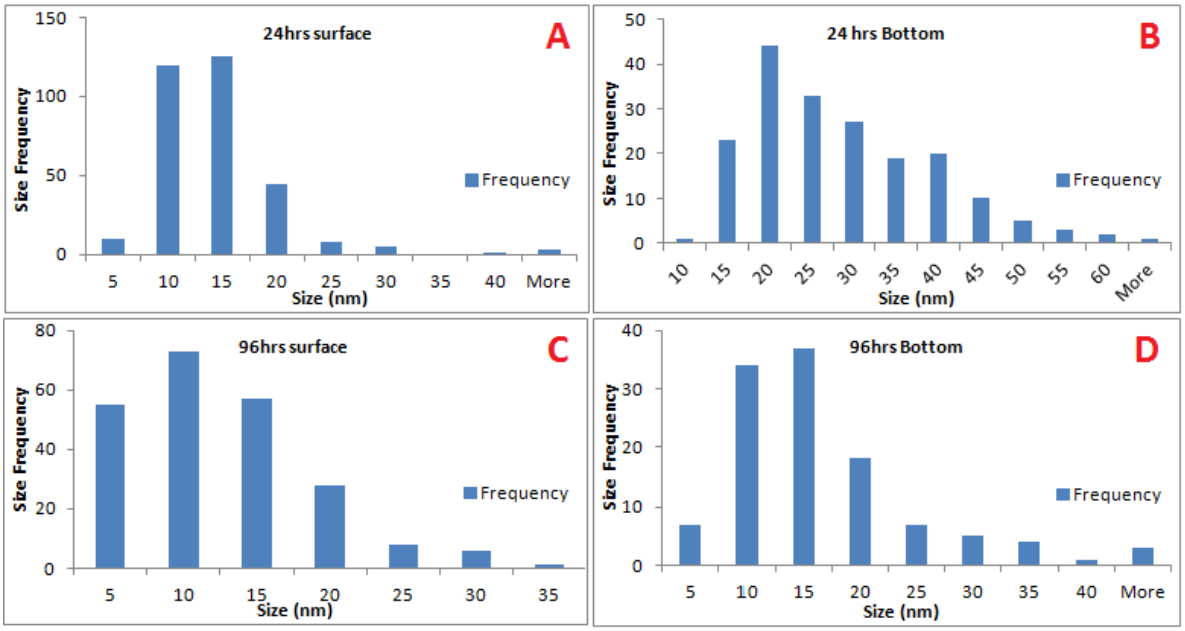

Figure 4.29: TEM histograms of citrate AgNPs exposed to EPA moderately hard water with SRFA. A) 24 hours in the surface water, B) 24 hours in the bottom water, C) 96 hours in the surface waters, and D) 96 hours in the bottom water.

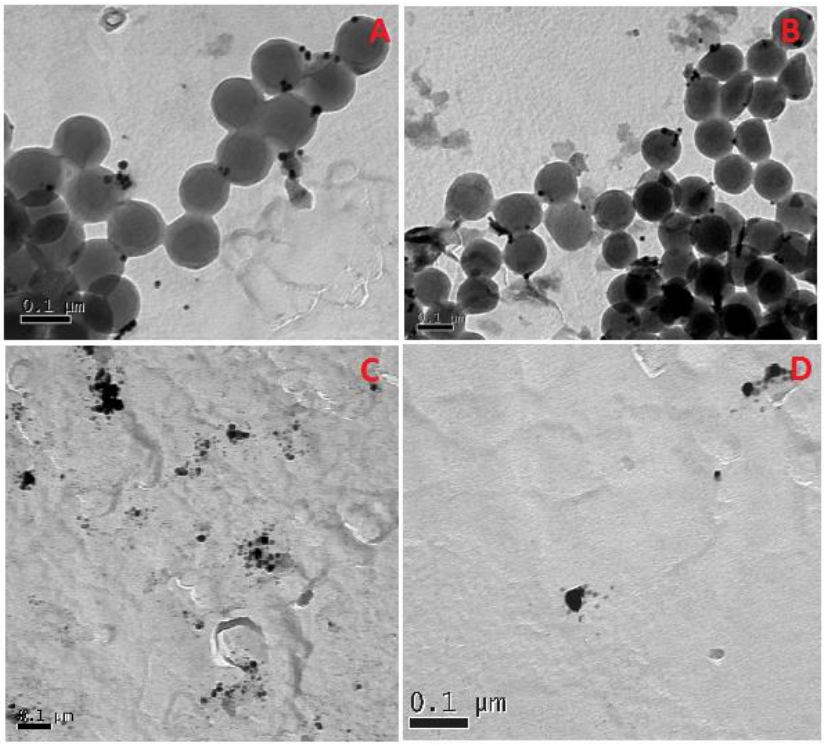

Figure 4.30: TEM images of PVP AgNPs exposed to EPA moderately hard water with SRFA at A) 24 hours surface, B) 24 hours bottom, C) 96 hours surface and D) 96 hours bottom.

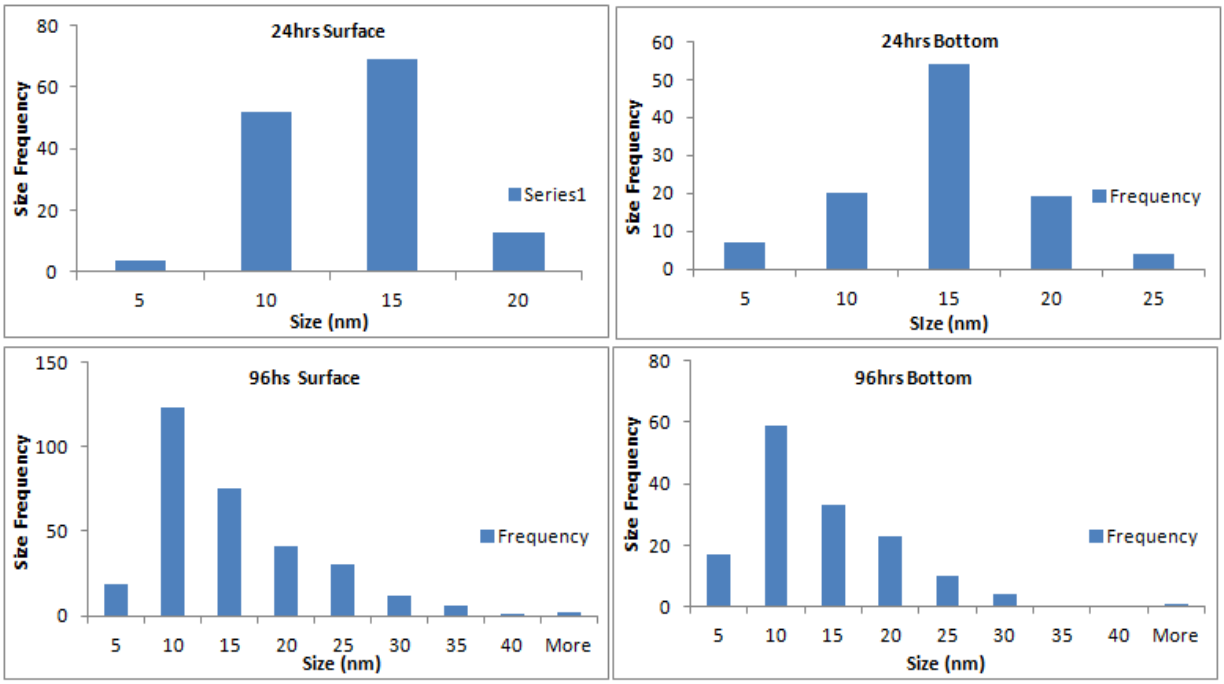

Figure 4.31: TEM histograms for PVP AgNPs exposed to EPA moderately hard water water with SRFA at A) 24 hours surface, B) 24 hours bottom, C) 96 hours surface and D) 96 hours bottom.

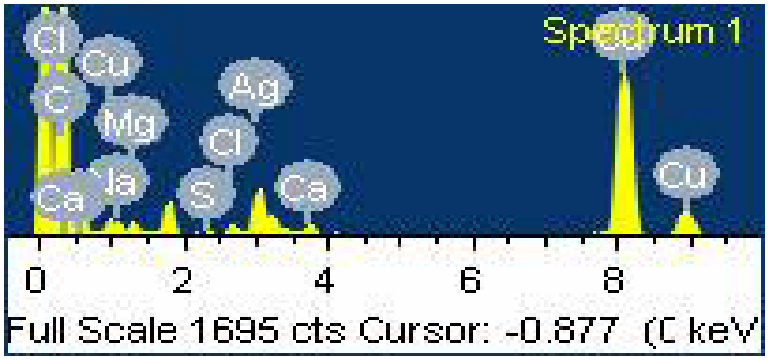

Figure 4.32: EDX spectrum for citrate AgNPs located in the surface water after 24 hours exposure to EPA moderately hard water with SRFA.

Table 4.12: TEM sizes (nm) at different time points for citrate and PVP particles exposed EPA moderately hard water with SRFA. A t-test was performed to identify differences from the observed compared to the original AgNPs sizes before release. *n= number of particles counted*ND= Not Determined. A p-value <0.05 highlights that the observed particle size using the t-test is significantly different to the size of the original particle before release, at a 95% confidence level.

Table 4.12: Average Core Size by TEM				
Time (hours)	**24**		**96**	
Area Analysed	**Surface**	**Bottom**	**Surface**	**Bottom**
Particle type	**Citrate AgNPs**			
Size (nm)	12 ± 6	27 ± 10	11 ± 6	15 ± 9
n	316	187	227	116
p - Value	0.012	2.64E-92	0.061	1.14E-8
Particle Type	**PVP AgNPs**			
Size (nm)	ND	11 ± 3	13 ± 7	6 ± 12
n		137	308	146
p-Value		0.012	0.005	0.462

After 24 hours the citrate AgNPs in the surface water show a significant growth of 12 ± 6 nm (*p* 0.012), when compared the original citrate AgNPs pre-release At 11 ± 3 nm. No significant difference was observed for the citrate AgNPs in the surface water at 96 hours at 11 ± 6 nm (*p* 0.061). Additionally, the citrate AgNPs sampled from the bottom of the mesocosm were larger than those at the surface at 24 hours at 27 ± 10 nm (*p* 2.64E-92), and reduced in size over time to give an average size of 15 ± 9 nm (*p* 1.14E-8) at 96 hours.

Reduced size with increased time may be due to dissolution and/or breakage of aggregates, and were comparable to the size results obtained from the previous studies (EPA water study). The majority of the particle sizes analysed had *p-values* below *p* 0.05, identifying that water chemistry had a significant effect to the behaviours and transformations, when compared to the original particles pre-release. Figure 4.28 identifies citrate AgNPs aggergated together at different time points and depths, confirming the modled data (figure 4.23), and the SPR profles (Figure 4.27A, 4.27C and 4.27E). The TEM histograms for the surface water (figure 4.28A) at 24 hours had a similar profile to that of the previous study in the absence of SRFA (figure 4.19A). As SRFA has a high molecular weight it is possible that the NP-NOM interactions occured at lower depths, explaining why the citrate AgNPs in the bottom of the mesocosm displayed a higher concentration of NPs in the presence of SRFA. As the citrate AgNPs demonstrated persistance and reduced dissolution rates, EDX was performed on an additional sample from the surface water at 24 hours (figure 4.32). Well documented literature states that in simple aqueous environments AgNPs have been known to form ligands with cholride and sulfide groups (Ha and Payer, 2011, Levard *et al,* 2013, Zook *et al,* 2011). The EPA water used in the present study contained electrolytes that could form complexes with the AgNPs. The presence of copper (Cu) and carbon (C) shown in the EDX spectrum (figure 4.32) are accountable for background noise from the carbon film, copper mesh grid used to mount the sample. The presence of calcium (Ca), magnesium (Mg), sulfur (S) and sodium (Na), are all expected interactions with the AgNPs, as they are part of the EPA water chemistry. Since Cl is present in the spetrum it is possible that AgCl complexs may have formed, and explain why there are higher AgNP fractions were present in the

dissoluton studies (figure 4.26) compared to previous studies. The results from the present study were also similar to an EDX profile obtained by Ha and Payer (2011) who exposed Ag to a sodium chloride solution (NaCl).

Analysis of the PVP AgNPs from figure 4.30A and 4.30B identifies large colloidal structures with NPs attached, since these structures were not seen previously they are believed to be SRFA structures. At 96 hours the SRFA structures were not seen leading to assumptions that they may have sedimented to the bottom of the tank. The addition of SRFA to the EPA water shows a different TEM histogram profile for the PVP AgNPs, compared to the citrate AgNPs. PVP AgNPs were smaller size distribution with the highest size frequency size of 15 nm in the bottom region of the coloumn at 24 hours (11 ± 3 nm), compared to 10 nm 2 days later at 96 hours (6 ± 12 nm). When compared to the previous EPA water study, the PVP AgNPs in the presence of SRFA, are more stable and less polydispersed in terms of size frequency. PVP AgNPs were smaller overall in each depth compared to the citrate AgNPs, further confirming the modelled data for the sedimentation and diffusion transport mechanisms.

Overall the combined characterisation techniques demonstrated that the addition of SRFA had stabilising effects to both the citrate and PVP AgNPs. The modelled concentration data revealed that the citrate AgNPs transported via sedimentation, compared to diffusion for the the PVP AgNPs. In addition to the previous EPA water study, the citrate AgNPs had a reduced dissolution rate in the presence of SRFA, where as the dissolution rate for the PVP AgNPs was comparable to the previous study. The SPR data revelaed the highest extrent of aggergation compared to the previous water studies for the citrate AgNPs, confirming the sedimentation profiles in the modelled data.

4.5 Conclusion

Overall we have been able to study the behaviour and transport of AgNPs with two different capping agents in a mix of simple waters. We have also been able to successfully use a mathematical model (Socolofsky and Jirka 2004, and Hinderliter *et al,* 2010) to predict and validate the AgNP transport and behaviours.

The information from the preliminary and main studies identified that the changes in the surrounding solution chemistry had a major impact upon NP stability and behaviour. As the water chemistry becomes more complex, the physicochemical interactions and behaviours of the AgNPs change. On release to the simple ionic water, citrate AgNPs were unstable and immediately aggregated, whereas, the PVP AgNPs remained stable and saw no reduced effects to dissolution. However, the addition of SRFA in the presence of a simple ionic water demonstrated stabilising effects, particularly to the citrate AgNPs. Increased aggregation was observed for the citrate AgNPs (as shown in the SPR data) but the dissolution rate was reduced. The reduced dissolution of the citrate AgNPs could be due to aggregation reducing the surface area and possibly by the re-formation of AgCl NPs (Baalousha *et al,* 2013), further stabilised by re-coating the newly formed NP surface with NOM (Cumberland and Lead 2009, Bae *et al,* 2011).

When modelling the transport behaviour of the AgNPs, the lower depths proved problematic when fitting the model parameters as the model can only be set for one concentration value and one size value, when realistically the concentrations and sizes of the AgNPs will change as the transformations change. Nonetheless, when the parameters of the model were adjusted according to the behavioural patterns observed, we were

able to validate that AgNP behaviour is surface coating specific and polymer coated AgNPs are more stable than steric coated AgNPs regardless of the absence or presence of NOM, confirming similar findings in the literature (El Badawy *et al,* 2011 and Li *et al,* 2013b). Nonetheless, both citrate and PVP AgNPs dissolve to produce ionic species, although the rate is dependent upon the water chemistry (Ma *et al,* 2012). Therefore, based on these studies, predictions of AgNPs released in a real environmental situation will see elevated concentrations of Ag^{+} and AgNPs. Citrate AgNPs will aggregate and sediment, whereas PVP AgNPs will maintain stability and diffuse thorough environmental waters.

Chapter 5

Fate and Transport of Silver Nanoparticles in Seasonally Changing Natural Lake Water

5 Chapter Outline

Chapter 4 focused on understanding the fate and behaviour of citrate and PVP capped silver nanoparticles (AgNPs) in simple aqueous media. In the present chapter, we assess the behaviour and transport of the citrate and PVP AgNPs in natural lake water. To explore the temporal variability of AgNP fate and behaviour after potential discharge to the environment, natural water was collected at four different times of the year to account for seasonal variations.

During the first 14 days the stability of the AgNPs were assessed by measuring total silver (Ag) and identifying the dissolved concentration using ultrafiltration and FAAS. TEM imaging was carried out where possible to assess changes in size and morphology. The transportation of the AgNPs was assessed using UV-Vis spectroscopy, and predicted total Ag concentrations of each depth was calculated using a mathematical model described in chapter 2 (Socolofsky and Jirka 2004, and Hinderliter *et al,* 2010).

5.1 Introduction

AgNPs are widely used in many consumer goods due their antibacterial properties. The Project on Emerging Nanotechnologies Consumer Products Inventory (2014) states that there is over 1400 nano-silver containing products on the market, ranging from medicinal health care to textiles. Therefore it is inevitable that AgNPs will be released into the wider environment via waste water exposures (Muller and Nowack, 2008). Once released to the aqueous environment little information is available on how these particles transform or where their ultimate fate ends. Studies have attempted to investigate the possible fate of AgNPs by identifying the effects of ionic strength of media and effects of NOM to AgNP suspensions, (Bae *et al,* 2013, Linlin and Tanaka 2013). It has been said that once AgNPs are released into the environment it is highly likely that the NPs will be oxidised, dissolve, interact with NOM, and form complexes to sulfide and chloride compounds (Levard *et al,* 2013). AgNPs released into aerobic aqueous environments, can be oxidised leading to NP dissolution (Li and Lenhart 2012) and the dissolution rate will determine NP presence in the environment (Ma *et al,* 2012). Interactions with NOM can reduce dissolution via steric protection due to re-capping and enhance NP stability (Misra *et al,* 2012). Environmental concentrations of Ag can also form complexes with chlorine to form AgCl, which reduce the bioavailability of the NPs (Blaser *et al,* 2008). Sulfidation is also a likely transformation of AgNPs once released into natural surface waters. Research has identified that exposing AgNPs to sodium sulfide (Na_2S) leads to the formation of sliver sulfide (Ag_2S) structures (Levard *et al,* 2011). The problem with these studies is that they

only provide estimations of the fate of AgNPs in natural aqueous environments, and lack the real complexity of the chemical make-up of natural water.

Lowry *et al* (2012) constructed studies using mesocosms directly in a fresh water environment over 18 months, using manufactured polydispersed (30-80 nm and aggregated species in the range of 200 nm) PVP coated AgNPs. The researchers identified that AgNPs were subject to sulfidation and resided in the sediment areas. The present study used small in-house synthesised AgNPs with two types of capping agent, citrate and PVP. The fate and behaviour of the AgNPs was assessed using *in situ* compartmental analysis of the mesocosms over 28 days (per study) in different seasonal variations of natural water.

5.2 Aims and Objectives

The aims of the present study were to determine the transformations, fate and behaviour of citrate and PVP coated AgNPs in seasonally different variations of natural lake water. Specific sub objectives were to:

1) Identify if AgNPs remain as isolated particles, aggregate or dissolve to produce Ag^{+} under natural aqueous conditions.
2) Identify if water from the varying seasons influences changes to AgNP behaviour, for example changing total organic carbon content.
3) To assess the surface coating specific behavioural differences/patterns in each of the water types.

5.3 Experimental

Synthesis of citrate and PVP stabilised AgNPs are discussed in chapter 2, section 2.1 and are characterised in chapter 3. Mesocosm design and dosing are discussed in chapter 2, specifically section 2.1.3.1. The collection and preparation of natural water is described in chapter 2 section 2.1.3.3. Diffusion-sedimentation modelling calculations are presented in chapter 2. The occurrence and transport of AgNPs in solution was determined by UV-visible spectroscopy (UV-Vis), discussed in chapter 2, section 2.2.2. Transmission electron microscopy (TEM) was used to identify size and morphological transformations of the AgNPs. TEM is further discussed in chapter 2, section 2.2.5. Energy dispersive X-ray (EDX) was used to provide information on the elements present in the water samples, which is also discussed further in chapter 2 sections 2.2.6. Total Ag and Ag^+ concentrations were determined by flame atomic absorption spectrometry (FAAS) detailed in chapter 2 section 2.2.9. A diffusion-sedimentation model (Socolofsky and Jirka 2004, and Hinderliter *et al,* 2010) was used to calculate the predicted total Ag concentrations for the surface, middle and bottom, calculations are presented in chapter 2.

Prior to analysis, $AgNO_3$ pre exposures were conducted in the natural water and samples for total Ag, were taken to assess the transport mechanism in the natural water. Natural water samples from the seasonally changing waters were analysed for total organic carbon (TOC) content, discussed in chapter 2 section 2.2.10, and analysed by inductively coupled plasma mass spectrometry (ICP-MS) for their chemical makeup, discussed in chapter 2, section 2.2.8. These studies were all conducted in laboratory setting where the temperatures were all kept at a constant room temperature.

5.4 Results and Discussion

Table 13: Overview/Summary of the Seasonal Constants and Variables between Experimentation

	Citrate AgNPs	PVP AgNPs
Spring water pH: 7.5 TOC: 12.59 mg L^{-1} Ionic Strength: High	• Surface modelled size 12 nm (R^2 0.92). • Transport mechanism: diffusion. • SPR: single sharp peak in region of 394nm, band extensions to 500-700nm in the lower depths, evidence of some larger NPs. • TEM: sizes at 24 hours in the surface 19 ± 12 nm and bottom of 46 ± 23 nm. After 120 hours in the surface 18 ± 7 nm and bottom 15 ± 7 nm. • EDX: C, Cu, S, Si, Cs, Co, Fe, Al, Cu, C and Ag.	• Surface modelled size 11 nm (R^2 0.94) • Transport mechanism: diffusion/sedimentation • SPR: single sharp peak in region of 400nm in the surface, band extensions to 500-700nm in the lower depths, evidence of some larger NPs. • TEM: after 24 hours, large size distributions in both surface 28 ± 15 nm and bottom 11 ± 6 nm. • EDX: C, Cu, Ag, Cl, Ca, O, P, S, and Si.
Summer pH: 7.6 TOC: 31.70 mg L^{-1} Ionic Strength: Low	• Surface modelled size 11 nm (R^2 0.94), middle (60 nm R^2 0.55), and 35 nm in the bottom (R^2 0.54). • Transport mechanism: sedimentation • SPR: sharp peak in region of 394nm with band extensions to 500-700nm in the lower depths, evidence of larger NPs. • TEM: 24 hours in the surface 13 ± 6 nm, 72 hours in the surface 16 ± 8 nm. • EDX: Not determined.	• Surface modelled size 11 nm (R^2 0.92), middle 15 nm (R^2 0.59), and 12 nm in the bottom (R^2 0.66). • Transport mechanism: diffusion. • SPR: single sharp peak in region of 400nm in the surface. • TEM: difficult to obtain lots of artefacts: 10 ± 3 nm after 24 hours in surface and 18 ± 7 nm after 72 hours in bottom. • EDX: Cu, C, Cl, Ca, O, P, S, Si, Fe, K, Mg, Ag and Na.
Autumn pH 7.4 TOC =28.31 mg L^{-1} Ionic Strength: Low	• Surface modelled size was 11 nm (R^2 0.96) and 30 nm in the middle (R^2 0.52) and bottom (R^2 0.47). • Transport mechanism: sedimentation. • SPR: bimodal peak in regions of 394nm with, band extensions to 500-700nm. • TEM: sizes at 24 hours in the surface 25 ± 8 nm and bottom of 125 ± 81 nm. After 120 hours in the surface 13 ± 6 and bottom 35 ± 38 nm. • EDX: C, Cu, Ag, Br, Cl, Ca, O, S, Mg, and Si.	• Surface modelled size 12 nm (R^2 0.94) 15 nm in the middle(R^2 0.21) and 20 nm in the bottom (R^2 0.97). • Transport mechanism: diffusion. • SPR: single sharp peak in region of 400nm. • TEM: after 24 hours in the surface 15 ± 8 nm, not determined in the bottom. After 72 hours 8 ± 2 nm in the surface and 17 ± 11 nm in the bottom. • EDX: C, Cu, Ag, Cl, Mg, Si, S, O, Ca, K, C, Fe, Cu, Na, and P.
Winter pH 7.2 TOC = 4.3 mg L^{-1} Ionic Strength: High	• Surface modelled size was 12 nm (R^2 0.77), 30 nm in the middle (R^2 0.76) and 20 nm in the bottom (R^2 0.76). • Transport mechanism: sedimentation. • SPR: bimodal peak in regions of 394nm with, band extensions to 500-700nm. • TEM: sizes at 24 hours in the surface 16 ± 5 am and 19 ± 7 nm in the bottom. At 168 hours the surface size was comparable to 24 hours at 17 ± 6 nm. • EDX: C, Cu, Fe, Si, S, Ag, Cl,Ca, Na and O.	• Surface modelled size was 12 nm (R^2 0.79), 11 nm in the middle (R^2 0.62) and 11 nm in the bottom (R^2 0.66). • Transport mechanism: diffusion. • SPR: single sharp peak in region of 400nm. • TEM: sizes at 24 hours in the surface were 16 ± 5 nm and 17 ± 5 nm in the bottom. • EDX: Not determined.

5.4.1 $AgNO_3$ Control Study in Natural Lake Water

A pilot study using silver nitrate ($AgNO_3$) was assessed for transport mechanism through the mesocosms over 5 days (figure 5.1C). The concentration of $AgNO_3$ added to the mesocosms was based on a 100 ppb equilibration. Assessments were only made for the transportation behaviour of Ag throughout the mesocosm. Therefore, analysis of the natural water for TOC and elemental analysis were not conducted. The total Ag results from each depth are presented figure 5.1, are plotted alongside the modelled predictions for the total Ag concentration over time (Socolofsky and Jirka 2004, and Hinderliter *et al,* 2010) for each depth in figure 5.2.

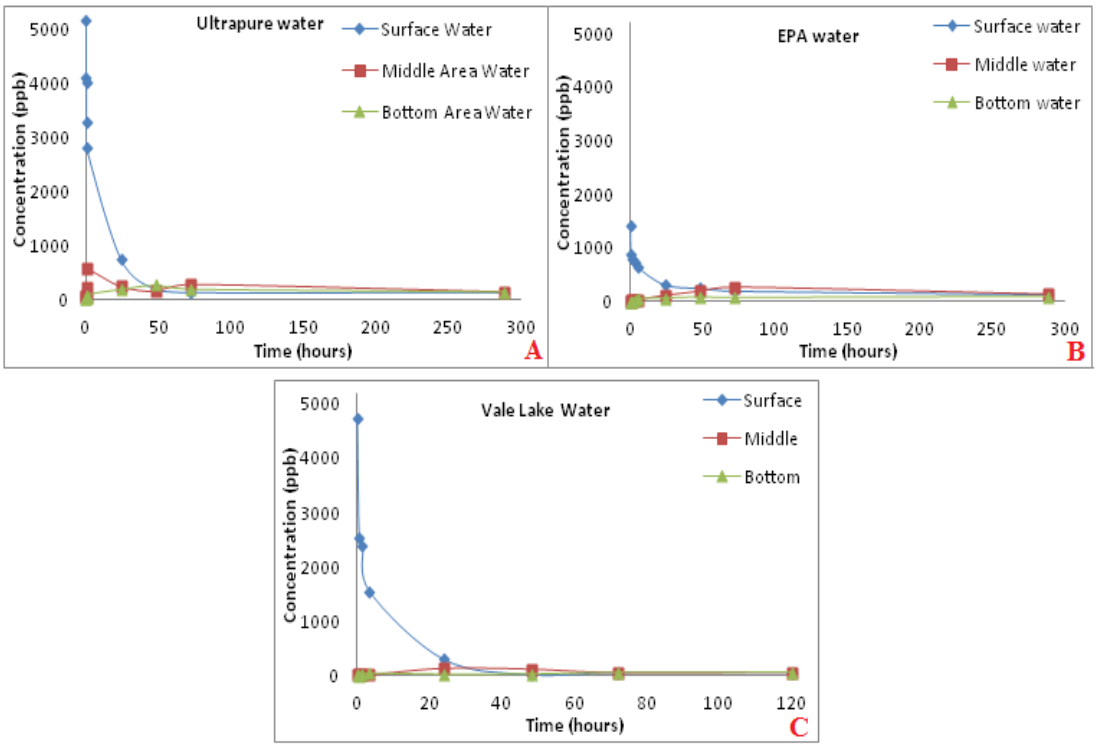

Figure 5.1: A) Total Ag recovery concentration (ppb) for $AgNO_3$ exposed to UPW (extracted from chapter 4), B) Total Ag recovery concentration (ppb) for $AgNO_3$ exposed to EPA moderately hard water (extracted from chapter 4) and C) total Ag recovery concentration (ppb) for $AgNO_3$ exposed to Vale Lake water over 5 days. Each graph shows the concentration changes for the different depths of the column.

A uniform concentration of $AgNO_3$ can be seen in figure 5.1 after 72 hours (3 days), which was comparable to the previous UPW and EPA moderately hard water studies (chapter 4).

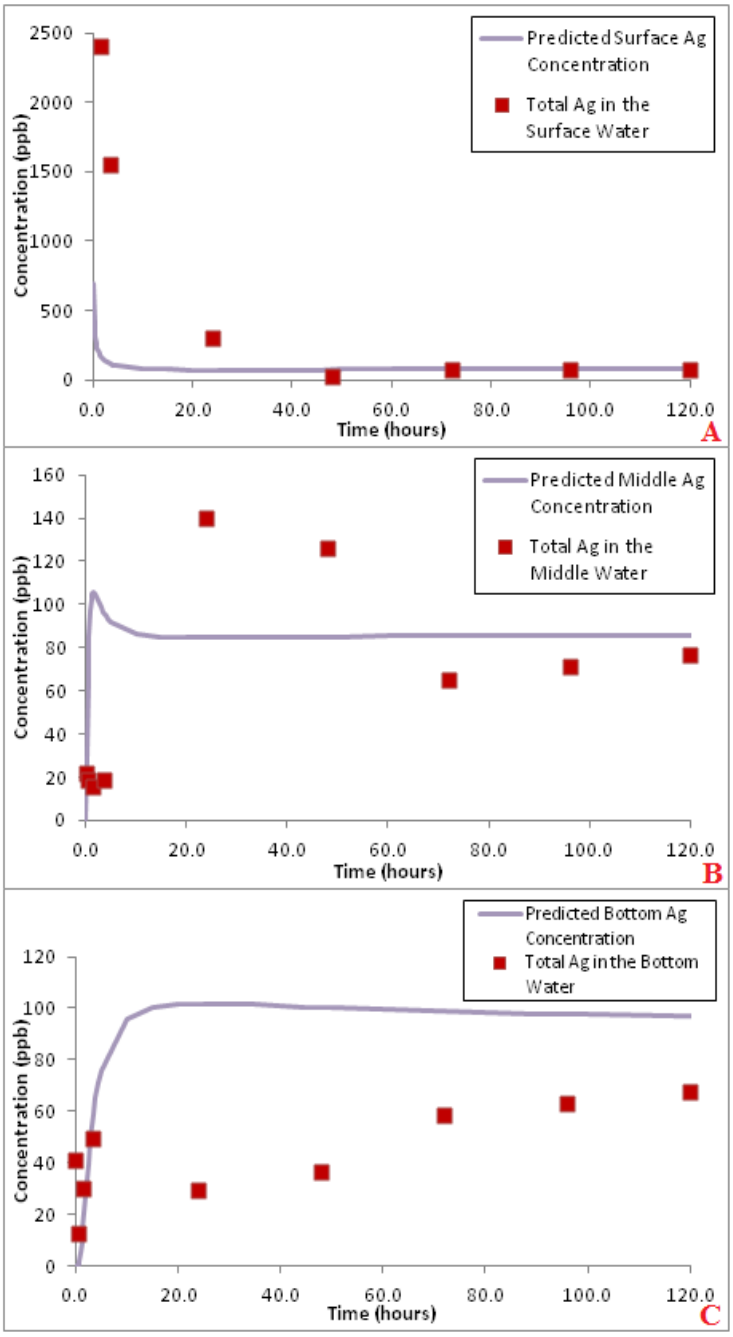

Figure 5.2: Model predicted Ag concentrations over time plotted against the average total Ag concentrations obtained for $AgNO_3$ in natural lake water for A) the surface water, B) the middle depth and C) at the bottom of the mesocosm. The model parameters are presented in table 5.1.

Table 5.1: Model Parameters for $AgNO_3$ in Natural Lake Water			
Parameter	**Symbol**	**Unit**	**Measurement**
Diameter of Ag atom	d	nm	0.288
Cross section area of the column	A	m^2	0.049
Column Length	*L*	m	1
Column volume	*V*=A*L*	L	43
Dosing volume	*V*	L	0.391
Dosing concentration	C_0	ppm	11
Mass of Ag	M	mg	4.3
C column based on diffusion	M/*V*	ppb	100
Diffusion coefficient	*D*	$m^2 s^{-1}$	1.431.E-5
Sedimentation Velocity	*U*	ms^{-1}	4.70E-13

The predicted Ag concentrations are shown by the blue lines in figure 5.2 and the average observed Ag concentrations recorded from the study are shown in red. The predicted Ag concentrations for each depth are modelled using a combination of sedimentation and diffusion equations, with the main 3 defined by Eq 5.1, Eq 5.2 and Eq 5.3 as repeated from chapter 2 and 4 (Socolofsky and Jirka 2004, and Hinderliter *et al,* 2010):

$$D = \frac{RT}{3N_A \pi \mu \, d}$$

[Eq 5.1]

R defines the gas constant (L.kPa/K/mol), T refers to temperature (K), N_A is Avogadro's number, viscosity is μ (Pa.s) and the particle diameter is d (m). The partial differential equation and boundary conditions for this equation are explained in chapter 1 section 1.5.2 equations 1.1 and 1.2 (Hinderliter *et al,* 2010).

$$U = \frac{g\,(\rho_p - \rho_f)\,d^2}{18\mu}$$

[Eq 5.2]

Where the sedimentation velocity of particles is *U* (ms^{-1}), g refers to the gravitational force ($m\ s^2$), particle density is ρ_p ($km\ m^3$), fluid density is ρ_f, the particle diameter is d (m) and the viscosity of the solution media is termed μ (pa.s) (Hinderliter *et al,* 2010). The diffusion-sedimentation equation used to produce the predicted Ag concentrations is described as:

$$C(x,t) = \frac{\left(\frac{M}{A}\right)}{\sqrt{4\pi Dt}} \left(\exp\left(-\frac{(x - \mathrm{U}x_0)^2}{4Dtx}\right)\right) \quad \text{[Eq 5.3]}$$

x_0 is the point where the NPs are introduced to the column, and *t* is the distance of the NPs travelled in terms of time (Socolofsky and Jirka 2004, and Hinderliter *et al,* 2010). Further details are presented in chapter 2.

The parameters of the model were adjusted to account for $AgNO_3$ in this instance, using the diameter of silver atom (0.288 nm) (Sellers *et al,* 2009), in place of the AgNP diameter (d). We assume that Ag^+ travels through the mesocosms via the process of diffusion under Brownian motion. To model the Ag^+ transport (Socolofsky and Jirka 2004, and Hinderliter *et al* 2010), samples from the surface, middle and bottom were measured for their Ag concentration at specific time points. Measuring the Ag concentration at each depth enabled us to identify how fast the Ag was travelling, by comparing the changes/similarities in concentrations from the surface to the bottom. According to Ficks Law, Ag will move from the surface (high concentration), to the bottom (low concentration) until evenly distributed (Fick, 1855). Therefore, as time increases the concentration profiles will become flat indicating equilibration.

To determine how well the observed data fits with the modelled data we used a Pearsons correlation coefficient to determine the R^2 value ranging from 0 to 1. The closer to 1 the R^2 values are, the more comparable the two sets of data were (Moriasi *et al,* 2007). The observed and expected concentrations were plotted against each other and the R^2 values were determined (see appendix) as follows; the surface R^2 value was 0.94, middle R^2 was 0.26 and the bottom R^2 value was 0.31. Values larger than 0.5 are generally considered in statistics as acceptable when showing a reasonable fit between observed and expected data. Values lower than 0.5 are not acceptable as they do not show a good correlation between the two sets of data (Moriasi *et al,* 2007). If the R^2 values are below 0.5, we can assume that the model parameters will need to be adjusted to fit the observed data, i.e. larger particle sizes seen from TEM imaging are needed to account for aggregation. This enabled us to make correct interpretations of the Ag behaviour, transport and increase the correlation between the observed and expected data to validate our model. We considered values of $R^2 \leq 0.7$ to show large linear associations between our observed and expected data (Moriasi *et al,* 2007).

Figure 5.2 shows only the surface water data points having a large linear association between the observed and expected Ag concentrations, compared to the middle and the bottom. To show stronger correlations between the data in the middle and bottom depths, we adjusted the parameters of the model to fit the observed data, which helped to describe and interpret the behaviour of the $AgNO_3$ in the natural water. Figure 5.2B provided evidence of sedimentation in the middle (at approx 0.5 m depth) over the first 48 hours (2 days), by showing a gradual increase in concentration over time followed by a decrease, which eventually plateaus. Studies by Akaighe *et al* (2011)

observed the formation of AgNPs from Ag^+ in the presence of a simple ionic media with NOM after 2-4 days exposure at room temperature, which helps to support our conclusions of AgNP formations under environmental conditions. Ag^+ can also complex with Cl^- (found in the natural water by EDX determination), which may indicate the formation AgCl particles (Ha and Payer 2011). Since the concentration of Cl^- was not determined it was not possible to calculate the solubility product for the formation of AgCl precipitates, although evidence from the model strongly suggests that sedimentation has occurred, thus small solid precipitates have formed. Therefore when adjusting the model parameters to account for the formation of small AgNPs in the lower regions, as seen in the TEM size frequency histograms, and reducing the concentration to account for settling, the R^2 value for the middle is increased to 0.67 and 0.76 at the bottom. Therefore it is possible that AgNPs are formed in natural water from the ionic source, and would validate the sedimentation patterns in total Ag concentration. Figure 5.3 and table 5.2 shows the adjusted model fits and parameters for $AgNO_3$ released into natural water for the middle and bottom depths.

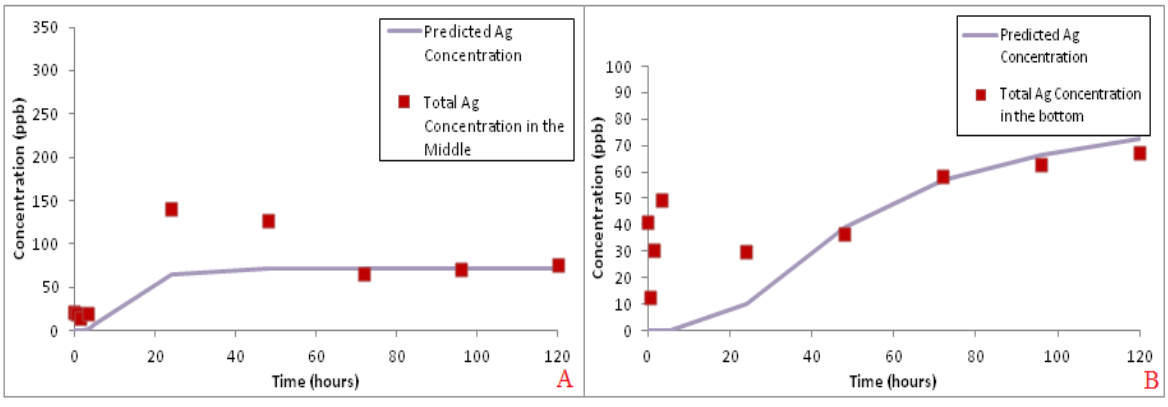

Figure 5.3: Adjusted model predicted concentrations over time plotted against the average total Ag concentrations obtained for $AgNO_3$ in natural lake water for A) the middle depth and C) at the bottom of the mesocosm. The new model parameters are presented in table 5.2.

Table 5.2: Adjusted Model Parameters for $AgNO_3$ in Natural Lake Water in the middle and Bottom of the Mesocosm			
Parameter	**Symbol**	**Unit**	**Measurement**
Diameter of AgNP	d	nm	5
Cross section area of the column	A	m^2	0.049
Column Length	*L*	m	1
Column volume	*V*=A*L*	L	43
Dosing volume	*V*	L	0.391
Dosing concentration	C_0	ppm	5
Mass of Ag	M	mg	3.5
C column based on diffusion	M/*V*	ppb	81.8
Diffusion coefficient	*D*	$m^2 s^{-1}$	8.59E-7
Sedimentation Velocity	*U*	ms^{-1}	1.30E-10

Overall, the average total Ag concentrations follow the modelled concentration pattern, and demonstrate Ficks law, by showing the Ag concentration profiles become flat and stabilise after 72 hours (day 3). The actual concentrations observed at 72 hours were 72 ± 0.61 ppb in the surface, 66 ± 0.03 ppb in the middle and 59 ± 0.03 ppb. After 5 days exposure to the natural water the Ag concentrations were as follows: 72 ± 0.03 ppb in the surface, 76 ± 0.01 ppb in the middle and 67 ± 0.02 ppb in the bottom. Concentrations of Ag were comparable between each depth of the mesocosm at 72 hours, 96 hours and 120 hours showing equilibration, and agreeing with the model output for the surface and bottom depth. As the control study was originally used to assess the movement of Ag through the mesocosms only, no further analysis was conducted to thoroughly support our claim of AgNP formation/complexes.

5.4.2 Spring Natural Vale Lake Water

5.4.2.1 Modelled and Dissolved Silver Concentrations

To assess the transport and stability of AgNPs in suspension, total Ag concentrations were measured from samples extracted from the surface, middle and bottom water areas of the mesocosms. Samples for total Ag concentrations were extracted over a period of 5.5 hours for the first day of exposure, daily for 14 days, and on days 21 and 28. The data obtained for the total Ag concentrations was plotted against modelled predictions of the total Ag concentration. Measurements of Ag^+ were sampled from the surface and bottom areas only from days 1-14 and days 21 and 28. Results tables for total and Ag^+ concentrations are displayed in the additional information section and the data has been presented in figures 5.4, 5.5 and 5.5.

To assess the transport mechanisms followed by the AgNPs when released, we modified a simple diffusion-sedimentation model (Socolofsky and Jirka 2004, and Hinderliter *et al,* 2010) to predict the transport of the total Ag in the mesocosm. Further details of the model are presented in chapter 2. The limitation of this model is that it is doe not account for AgNPs settling and accumulating at the bottom which may show as potential losses. The model also assumes no dissolution, therefore these parameters need to be factored and adjusted according to the observed data.

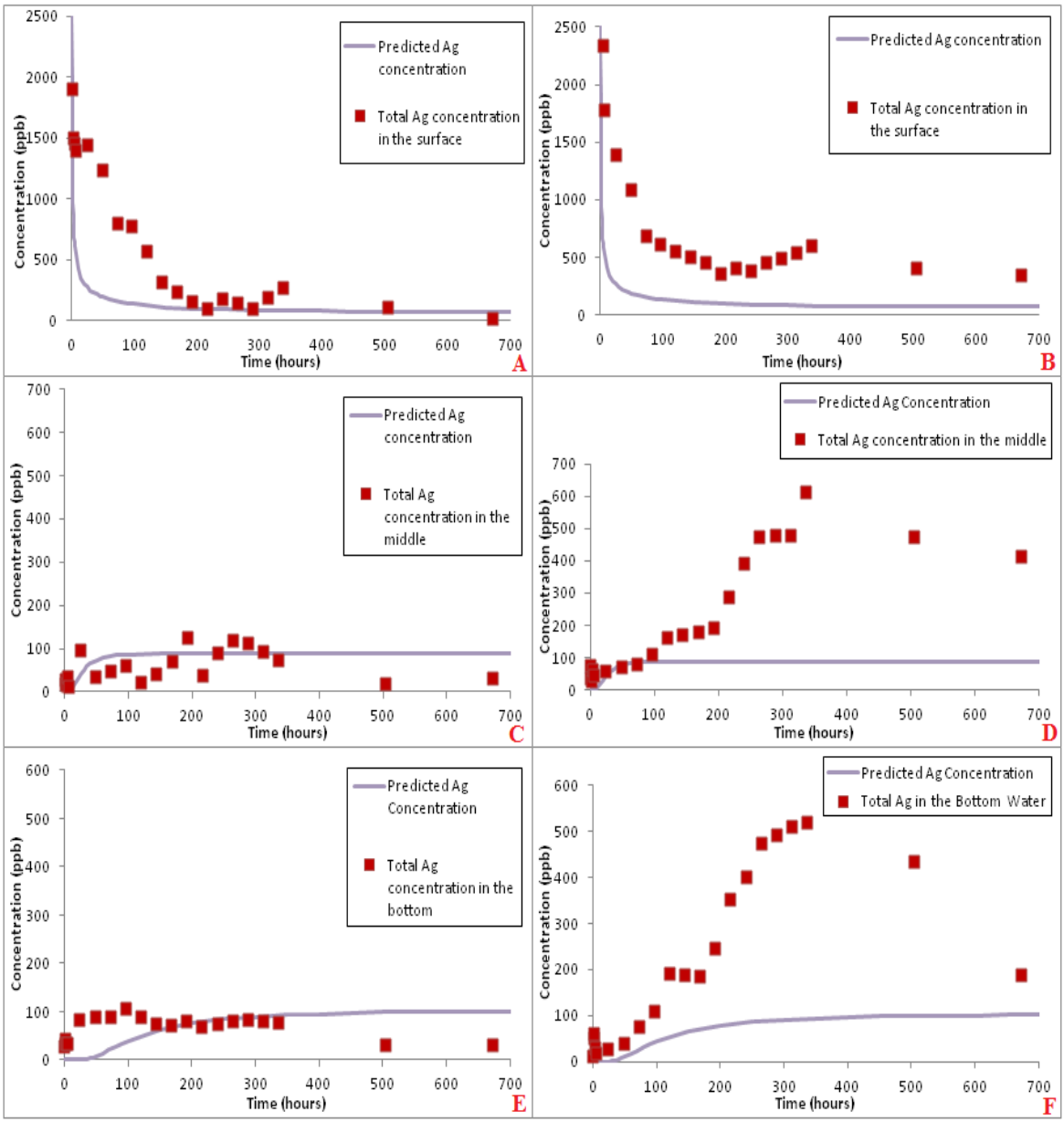

Figure 5.4: Model predicted Ag concentrations over time plotted against the average total Ag concentration obtained from the study for, A) citrate AgNPs in the surface, B) PVP AgNPs in the surface, C) citrate AgNPs in the middle, D) PVP AgNPs in the middle, E) citrate AgNPs in the bottom, and F) PVP AgNPs in the bottom of the mesocosm containing spring natural water. The model fits were based on a single 11 nm (citrate) and 12 nm (PVP) AgNP travelling through the mesocosm based on parameters in table 5.3. The model was then optimised to fit the concentration data for the PVP AgNPs to account for sedimentation, as seen in figure 5.5 with the new parameters listed in table 5.4.

Table 5.3: Model Parameters for AgNPs in Spring Natural Lake Water				
Parameter	**Symbol**	**Unit**	**Citrate**	**PVP**
Diameter of AgNP	d	nm	12	11
Cross section area of the column	A	m^2	0.049	0.049
Column length	*L*	m	1	1
Column volume	*V*=A*L*	L	43	43
Dosing volume	*V*	L	0.391	0.215
Dosing concentration	C_0	ppm	11	20
Mass of Ag	M	mg	4.3	4.3
C column based on diffusion	M/*V*	ppb	100	100
Diffusion coefficient	*D*	$m^2 s^{-1}$	3.743.E-07	3.743.E-07
Sedimentation Velocity	*U*	ms^{-1}	7.40E-10	6.40E-10

To compare the total Ag concentrations and the model predictions from citrate AgNP study, we used a Pearsons correlation coefficient to determine how well the two sets of data fit (Moriasi *et al,* 2007). The R^2 values were determined as 0.92 in the surface, 0.28 in the middle and 0.49 in the bottom. Several attempts were made to increase the R^2 values in the middle and the bottom to optimise the fits but were unsuccessful. As the R^2 values are sensitive to outliers from poor data this could have reduced the R^2 number in our data sets. Nonetheless, the total Ag concentration for the citrate AgNP study follow the modelled pattern in the surface, middle and bottom depths for a 12 nm AgNP based upon a 100 ppb equilibrium.

By day 9 the concentration in the surface stabilises around 108 ± 0.13 ppb, followed by the middle on day 11 at 118 ± 0.07 ppb, producing a stable concentration gradient agreeing with Ficks Law between the depths (Fick, 1855). By day 12 the total Ag concentration for the surface was 107 ± 0.05 ppb, 113 ± 0.03 ppb in the middle and 83 ± 0.06 ppb in the bottom, falling within ± 20% of the modelled predicted concentrations.

Some deviations to the predicated Ag concentrations for the citrate AgNPs study were seen in middle depth for first 120 hours (5 days). Figure 5.3C shows small elevations

and declines in the concentration which could suggest small amount of sedimentation (Hinderliter *et al,* 2010). The sedimentation of Ag maybe explained by reduced R^2 correlation and the settling of aggregates. Evidence to support aggregation of the citrate AgNPs is seen in the SPR data figure 5.7A, 5.7C and 5.7E, demonstrated by band tailing to longer wavelengths (Li *et al,* 2010). However, since the changes in the total Ag concentration only produce small elevations and declines, it is possible that of Ag^+ (produced via dissolution) maybe moving back into the middle water depth under Brownian motion. Between days 21 and day 28 the total Ag was equally distributed throughout the mesocosm for the citrate AgNP, and the concentrations fell below the predicted concentrations observed in the model. Explanations for the reduced observed Ag concentrations compared to the predicted, is due to the model not account for Ag accumulation at the bottom of the mesocosm, or losses such as Ag sticking to the walls.

Observations of the PVP AgNP study demonstrates differences in concentrations between the middle and bottom depths when compared to the citrate AgNP study. The Pearsons correlation coefficient (Moriasi *et al,* 2007) determined the R^2 values to be 0.94 in the surface, 0.39 in the middle and 0.76 in the bottom. These produced stronger correlations than those observed in the citrate AgNP study, indicating surface coating specific differences. The total Ag in the surface water for the PVP AgNP study shows evidence between days 12-14 (288-384 hours) that Ag diffuses back into the surface area which may be due to Ag^+ or small AgNPs. The Ag movement for the PVP AgNPs in the middle of the mesocosm produced a steady continuous rise in Ag concentration, followed by a steady decline, which do not fit the modelled parameters or follow Ficks Law (Fick, 1855). It is possible to suggest that that PVP AgNPs have aggregated in the natural water.

We tested this theory by altering parameters of the model (Socolofsky and Jirka 2004, and Hinderliter *et al,* 2010) to fit the Ag concentration data obtained for the middle and bottom of the mesocosm to account for larger AgNPs and increase the correlation R^2 value. Due to the differences in concentration observed between the middle and bottom it was difficult to fit the parameters of the model to optimise the predicted concentration in both depths. This is most likely a data error. Therefore the model was optimised by changing the size of the PVP AgNPs to fit the concentrations presented in the middle of the mesocosm. The new parameters are described in table 5.3 and the new model graphs are presented in figure 5.5.

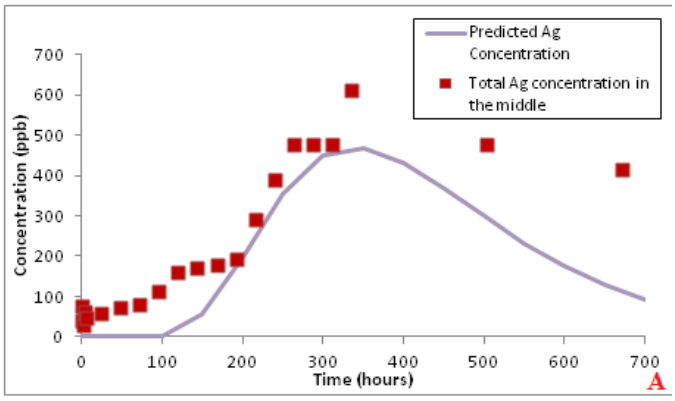

Figure 5.5: Adjusted model parameters to account for larger aggregated AgNPs (table 5.4) for the predicted concentrations over time, plotted against the average total Ag obtained from the study for PVP AgNPs in the middle of the mesocosm.

Table 5.4: Adjusted Model Parameters for PVP AgNPs in the middle depth in Spring Natural Lake Water

Parameter	Symbol	Unit	Measurement
Diameter of AgNP	d	nm	300
Cross section area of the column	A	m^2	0.049
Column length	*L*	m	1
Column volume	*V*=A*L*	L	43
Dosing volume	*V*	L	0.215
Dosing concentration	C_0	ppm	20
Mass of AgNPs	M	mg	4.3
C column based on diffusion	M/*V*	ppb	100
Diffusion coefficient	*D*	$m^2 s^{-1}$	1.431E-8
Sedimentation Velocity	*U*	ms^{-1}	4.7 E-7

Once the model conditions have been adapted for aggregation (Figure 5.4) the actual concentrations obtained followed the model predictions. This increased the correlation between the observed and predicted concentrations produced an R^2 value of 0.67 for the middle depth. Larger PVP AgNPs were also observed in the SPR data (figure 5.7D and 5.7F) in the lower depths of the mesocosm which supported and validated the modelled data. The PVP AgNP study shows that there were larger concentrations of total Ag in each of the measured depths (compared to citrate AgNPs), which could indicate surface coating differences in the transport mechanisms, or losses of Ag from the citrate AgNP study.

The large concentration of Ag in the middle depth for the PVP AgNP study may be explained by the formation of factual aggregates with large pore sizes. Therefore the density of the aggregate decreases as the aggregate size increases (Tang *et al,* 2002). As PVP AgNPs have previously been well documented from their stability over citrate AgNPs (El Badawy *et al,* 2011, Li *et al,* 2013) the model data showing aggregation only in the PVP AgNPs was not expected. Uncertainties in the model predictions, poor quality of the PVP data, or losses of Ag from the citrate study may be of explanation to the unexpected results. In order to assess AgNP stability, ultrafiltration was conducted to identify Ag^+ and AgNPs concentrations. The information obtained is presented in figure 5.6.

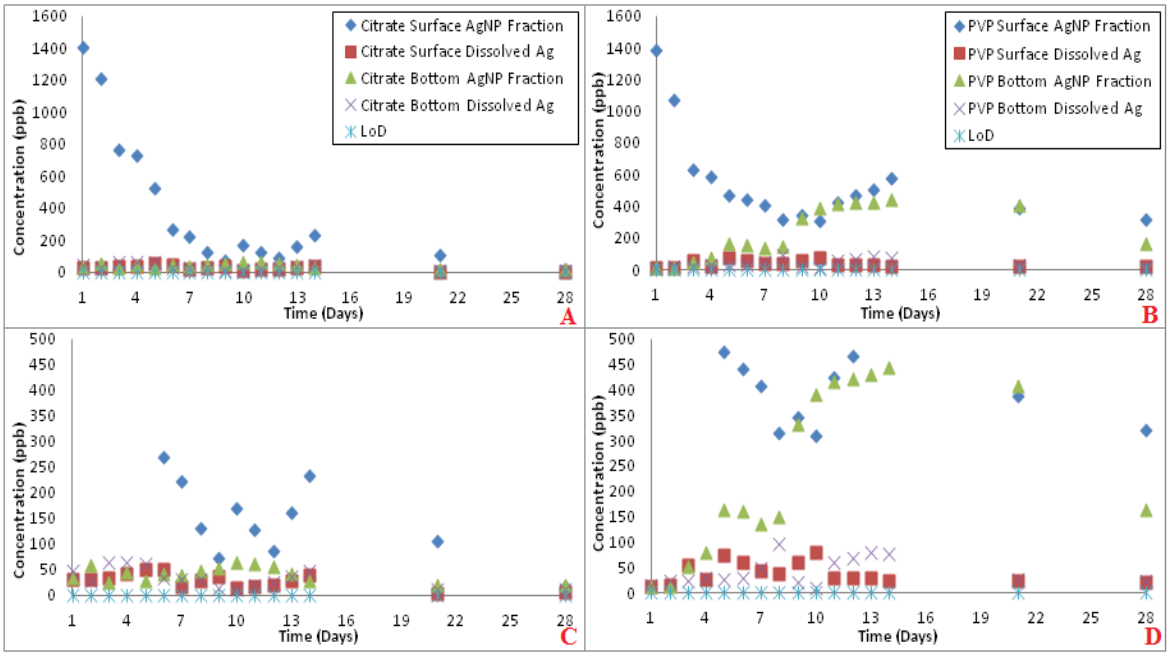

Figure 5.6: Dissolved and AgNP concentrations (ppb) using ultrafiltration in the spring lake water: A) citrate Ag^+ and AgNP concentrations in the surface and bottom depth water for each day, B) PVP Ag^+ and AgNP concentrations in the surface and bottom depth water for each day, C) shows the same graph as A for concentrations below 500 ppb, D) shows the same graph as B for concentrations below 500 ppb. Note the LoD = Instrumentation limit of detection at 2 ± 0.2 ppb.

Ultrafiltration provides a good estimation of how quickly NPs dissolve, although the results are not 100% reliable as there is a possibility that AgNPs can stick to the walls of the container and ionic species can become bound to the filter membrane, as seen in the ultrafiltration membrane viability tests in chapter 2. Therefore, all the dissolved and AgNP concentration data presented in this chapter was used only as an estimation of the AgNP behaviour once released into natural water. We were able to calculate an estimated AgNP concentration as follows (repeated form chapter 4):

$$C_{AgNP} = (T_{Ag}\text{-}D_{Ag}) \qquad \text{[Eq 5.4]}$$

Where C_{AgNP} is the AgNP concentration, T_{Ag} is the total Ag concentration and D_{Ag} is the Ag^{+} concentration. Limits of detection for the FAAS instrumentation were tested by running a set of blanks as samples and devising the average result.

Analysis of the citrate AgNPs show a steady decline in concentration in the surface water from 1410 ppb on day 1, until day 8 where the concentration began to stabilise around 130 ppb and agree with Ficks Law (Fick, 1855) and validate the observed and expected model parameters. The citrate AgNP concentration elevated between days 7-14 in the bottom of the mesocosm (figure 5.3) due to the sedimentation of aggregates evidenced in the total Ag data for the middle depth and in all the SPR profiles (figures 5.7A, 5.7C and 5.7E). The Ag^{+} concentration remained stable throughout the duration of the study, with ranges between 32 ppb on day 1, and 40 ppb on day 14. Overall the citrate AgNPs remain persistent as particulates for the duration of the study (28 days).

In comparison the PVP AgNP study shows high concentrations of AgNPs in both the surface and bottom of the mesocosm, which validates observations of high Ag concentrations presented in the model. The PVP AgNP concentrations in the surface water shows evidence of a small plateau consistent with diffusion, with smaller declines in concentration between days 4-8. Concentrations of PVP AgNPs between days 12-14 show diffusion back to the surface area, which was also seen in the surface total Ag concentrations in figure 5.4. To compare, both the citrate and PVP AgNPs show elevated AgNPs concentrations in the surface and bottom, possibly due to the breakage of aggregates and releases smaller NPs that move via diffusion (Li *et al,* 2013). When the concentrations of PVP AgNPs in the bottom of the mesocosm elevate, the surface AgNP concentration declines, which is constant with AgNP settling. Similar findings were seen

by Lowry *et al,* (2012) using PVP AgNPs, who saw small declines in total Ag concentration over the first 8 days after AgNP introduction to their mesocosm system. There is clear evidence from figures 5.6C/D that the PVP particles remain in NP form in higher concentrations, for longer periods of time when compared to the citrate AgNPs (figure 5.6A/B). This information demonstrates surface coating specific stability and supports literature claims of PVP AgNP stability over citrate AgNPs (El Badawy *et al,* 2011, Li *et al,* 2013, and Li *et al,* 2013b). Further evidence of surface coating specific behaviours were evidenced in the SPR profiles (figure 5.7) where the PVP AgNPs show persistency in AgNP form in the surface water 28 days post release.

The persistency, stability and surface coating specific differences of the PVP AgNPs may be explained by the effect of Cl on PVP dissolution based on identified presence of Cl in EDX spectrum (figure 5.13). Studies by Levard *et al* (2013) identified the direct relationship between the Cl concentration and the dissolution of PVP AgNPs in an aqueous environment. The researchers identified that a small amount of chloride in the media significantly decreased the amount of Ag^+ produced compared to a chloride free media. It was suggested that PVP AgNPs become coated with AgCl maintaining stability, and that AgCl particles can nucleate on surface scratches on the NP surfaces, reducing Ag^+ (Levard *et al*, 2013). Reduced Ag^+ was observed in the present study when compared to citrate AgNP study. After 24 hours exposure the concentration of A^+ in the surface water for the citrate study was 32 ± 0.04 ppb, compared t0 14 ± 0.02 ppb for the PVP AgNP study. Results for the Ag^+ concentration in the bottom revealed after 24 hours was 49 ± 0.06 ppb for the citrate study and 16 ± 0.04 ppb for the PVP study, highlighting surface coating specific stability.

The results from the present study were also similar to those presented in chapter 4 for the EPA synthetic waters present and absent of NOM. Both studies in chapter 4 identified that the Ag^+ concentration for the PVP AgNP studies were smaller than the Ag^+ concentrations for the citrate AgNP studies. Therefore the Cl in solution from the natural water only had destabilising effects to the citrate AgNPs in the present study. A continued explanation of the stability of the PVP AgNPs in suspension may also be due to the presence of sulfur in the natural water. Sulfur was detected in the EDX profiles (figure 5.13) which could account for possible AgS complexes. Previous work conducted by Levard *et al* (2011) suggested that AgNPs are subject to sulfidation under environmental conditions. Their work discovered that it was possible for the PVP surface coating to re-adsorb back on to the AgS complex, confirmed by the presence of PVP in their X-ray photoelectron spectroscopy (XPS) analysis. PVP is a strong high molecular weight coating (Li *et al,* 2013), when combined with other properties such as the organic carbon content. Although not likely, the PVP re-adsorption theory (Levard *et al,* 2011), could explain why the PVP AgNPs stay stable in particulate forms compared to the citrate AgNPs.

As described in chapter 4, original calculations were based on 100 ppb equilibrium of Ag, losses have occurred from the measured concentrations. A 5 mL sample was extracted per sampling area (surface, middle and bottom) at each time point to record the total Ag. Particles were taken out of the system and not replaced. Therefore, sampling from areas of high concentrations could have affected the overall concentration in the mesocosms. A total of 21 samples for each of the 3 sampling points were extracted at 5 mL each time, plus an additional 10 mL of sample was taken from the surface and the bottom area daily for 14 days, and on days 21 and 28. Additional losses may have

occurred from Ag sticking to the mesocosm walls and settling at the bottom. Instrumentation error of the FAAS is within the linear range for silver between 0-4 mg L^{-1}. The exact detection limit was obtained by running 11 blanks (UPW) as samples, and obtaining the standard deviation between the results to give a detection limit of ± 0.2 ppb

5.4.2.2 UV Analysis

SPR peak (λ_{max}) for spherical pristine citrate AgNPs as characterised in Chapter 3 was 392nm, and 400nm for those stabilised with PVP. Figure 5.7 (A-F) shows the SPR profiles for both citrate and PVP particles exposed over time at the surface, middle and bottom points of the mesocosm tanks.

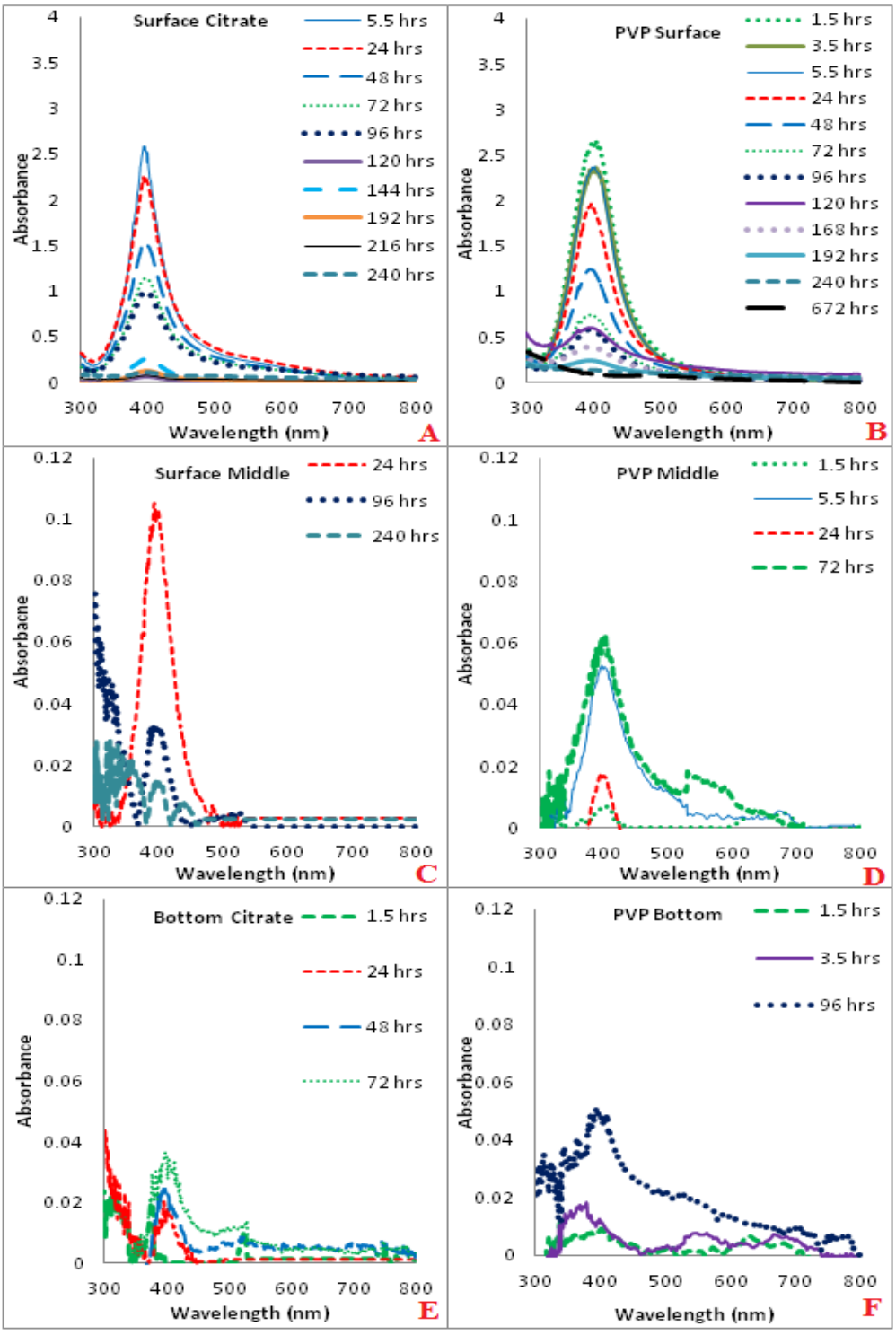

Figure 5.7: UV SPR profiles taken from different depths of the mesocosm column when exposed to natural Vale Lake water in spring. A) Citrate coated AgNPs at the surface, B) PVP AgNPs at the surface, C) citrate AgNPs from the middle, D) PVP AgNPs from the middle, E) citrate AgNPs from the bottom and F) PVP AgNPs from the bottom. Note that the Y axis for the graphs are not presented in the same scale for each of the depths, as detail from the lower regions would be lost.

The results for the UV-vis data show that the citrate AgNPs were retained in the surface water for up to 24 hours, before transporting to the lower depth. Evidence of high Ag concentrations retained in the surface water was also demonstrated in the modelled data between 0-168 hours (up to 7 days) (figure 5.4A). The dissolution data presented in figure 5.5 also confirmed high concentrations of citrate AgNPs retained in the surface water for up to 7 days. The stability of the citrate particles in the surface water is possibly due to the NOM concentration in the natural water. NOM has been previously documented to increase the stability of AgNPs in environmental systems and reduce aggregation (Baalousha *et al*, 2008, Zhang *et al,* 2009), by displacing the citrate surface coating (Diegoli *et al,* 2008). The present study had a higher NOM concentration recorded at 12.59 mg L^{-1}, as a function of total organic carbon (TOC). If we compare the results from the present study to the results seen in the EPA moderately hard water study (chapter 4), we can see that the presence of NOM in the natural water has demonstrated stabilising affects to the citrate AgNPs.

After 24 hours release the citrate AgNPs in the present study retained a high concentration of citrate AgNPs at 1410 ppb (table A2.4 additional information) in the surface water, compared to 35 ppb in the bottom, determined by a slight drop in concentration shown between the SPR peak at 5.5 hours and 24 hours (figure 5.7). At 5.5 hours the λ_{max} was 394nm for the citrate AgNPs in the surface water, compared to 24 hours where the λ_{max} red shifts to 398nm. The SPR remained at 398nm λ_{max}, until day 6 where it red shifts again to 401nm for the citrate particles. After day 6 the λ_{max}, continued to blue shift in a liner pattern until there was no observable peak on day 11. Although the red shifting observed was small, the red shift effect occurs when particles become

polydispersed and/or when they are oxidised at the surface (Li *et al,* 2010, Li and Sun, 2011), further demonstrating aggregation and instability of the citrate AgNPs. A narrowing of the SPR band was visible for both particle types in the 390-450nm region, and is also consistent with an oxidised layer on the surface (Li *et al,* 2010).

The UV graphs present small band tailing in the 500-700nm region for the citrate AgNPs in the surface (Figure 5.7A), identifying that the suspension is heterogeneous with the presence of larger particulates (Chinnapongse *et al*, 2011, and Li *et al,* 2010). Since these bands in the 500-700nm region were not observed when the citrate AgNPs were first characterised (see chapter 3), it can be determined that aggregation has occurred. Aggregation also confirms the sedimentation of the AgNPs to the middle water area in the modelled citrate Ag concentration data (figure 5.4C). After 11 days post release, no observable SPR peak was seen to determine the presence of citrate AgNPs in the surface water. Therefore, citrate AgNPs were assumed to have diffused/sediment to lower compartments of the mesocosm, as further determined by the model (figure 5.4).

Analysis of the SPR data for the PVP AgNPs provided evidence of surface coating specific differences. PVP AgNPs remained suspended in the surface water for 672 hours (28 days) when compared to 240 hours (10 days) for the citrate AgNPs. High Ag concentrations retained in the surface water was also shown in the modelled data for the duration of the study (28 days). The dissolution data presented in figure 5.6 confirmed high concentrations of PVP AgNPs retained in the surface with the lowest concentration of PVP AgNPs recorded at 309 ppb on day 10 (240 hours) in the surface water (Table A2.5 additional information). Analysis of the lower depths (middle and bottom) show after 48 hours exposure, evidence of band stretching in the 500-700nm region indicated the

presence of large particulates (Chinnapongse *et al*, 2011). Larger particulates in the lower depths of the mesocosm confirmed sedimentation and validated the modelled data (figure 5.5).

Analysis of the PVP and citrate AgNPs in the middle water depth identified out of plane quadrupole resonance. This was caused by the differences in NOM charges, resulting in electron and ion decoupling when excited and band interference between 300-350nm (Kawaguchi *et al,* 2011, Kelly *et al,* 2003 and Zou *et al,* 2007). In the EPA water studies (ultrapure and EPA water only) the SPR bands drop back to the base line after 320-350nm, whereas the present study showed a continuous rise after 350nm, comparable to the EPA SRFA study (chapter 4). Therefore the information presented from the SPR band patterns suggest the change is caused from NOM interference.

Figure 5.7E and 5.7F describes the average SPR band profiles for samples extracted from the bottom area of the mesocosm. Both the PVP and citrate AgNPs show a high degree of interference from the SPR banding patterns, possibly caused by other contaminants in the natural water which has blocked the UV signal. Although, signals around 400nm and stretching between 500-700nm was still observed. By days 10 (citrate AgNPs) and 11 (PVP AgNPs) the SPR profiles were indistinguishable in the lower depths due to background noise from the natural water and low AgNP concentrations from settling.

5.4.2.3 Transmission Electron Microscopy (TEM) and Energy Dispersive X-Ray (EDX) Analysis

To visualise the size and morphological transformations of the citrate and PVP particles exposed to the spring seasonal natural water, TEM imaging was conducted (where possible). The original citrate AgNPs as discussed in chapter 3, were characterised by TEM at 12 ± 2 nm (section 3.5.1.4), and 11 ± 2 nm (section 3.5.2) for the PVP AgNPs. These sizes were used to determine and compare against changes that occurred to the NPs once released in the natural water. Confirmation of the AgNPs and elemental presence was conducted using EDX (figures 5.12 and 5.13).

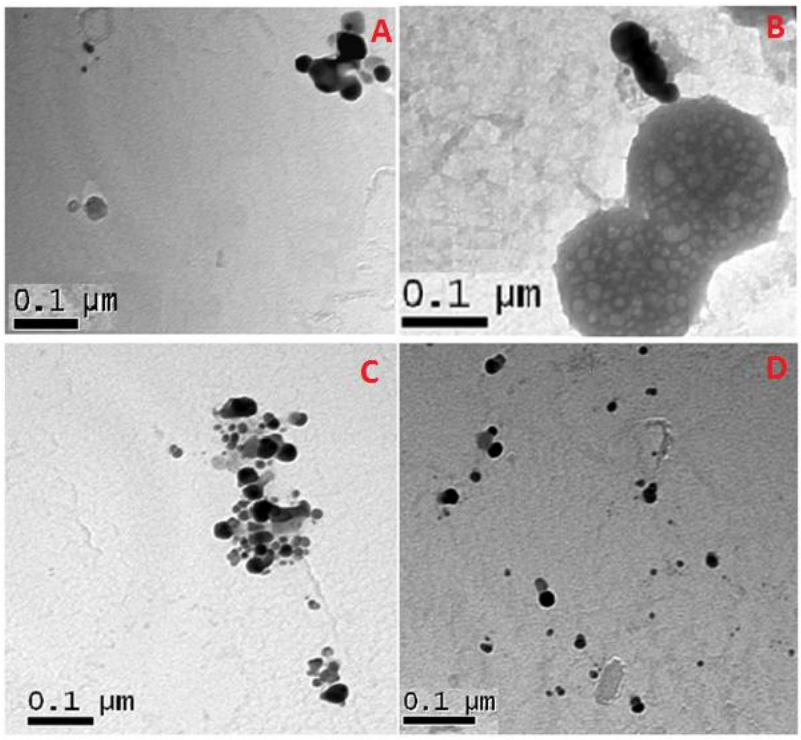

Figure 5.8: TEM images of citrate AgNPs identified at A) 24 hours in the surface, B) 24 hours at the bottom, C) 120 hours in the surface, and D) 120 hours in the bottom of the mesocosm. Corresponding histograms are presented in figure 5.9, and the EDX spectrum in figure 5.11 corresponds to image 5.7A.

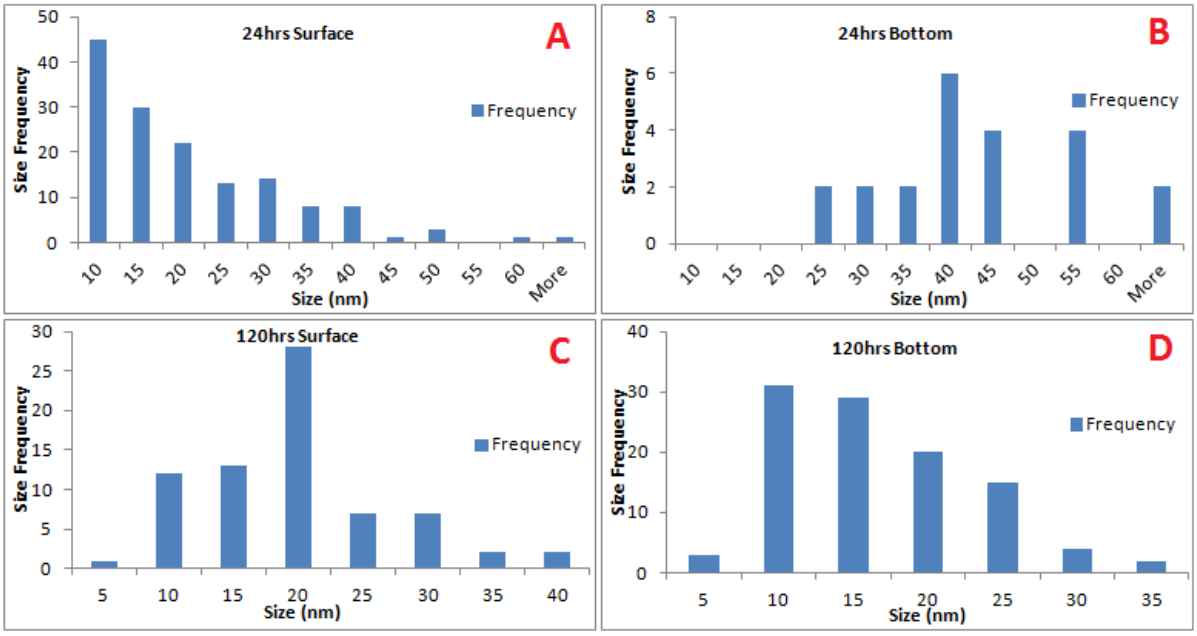

Figure 5.9: TEM size frequency histograms for citrate AgNPs at A) 24 hours in the surface, B) 24 hours at the bottom, C) 120 hours in the surface water and D) 120 hours at the bottom of the mesocosms. Histograms correspond to the images presented in figure 5.8.

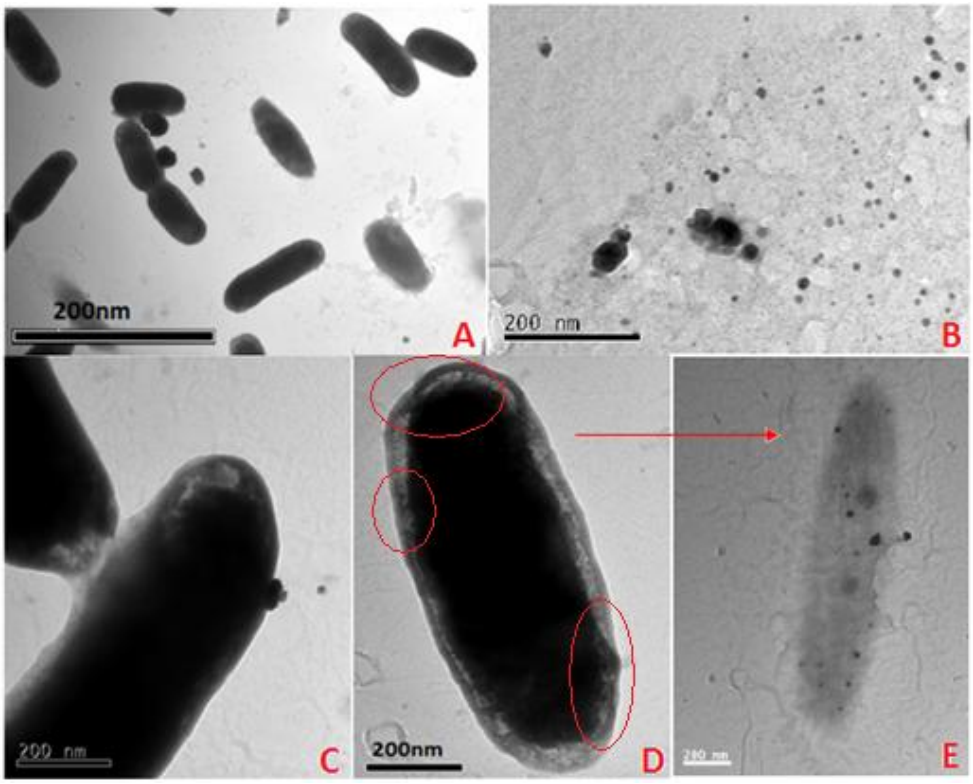

Figure 5.10: Images A-E were taken from samples derived from the surface water at 72 hours of PVP AgNPs, and unknown bacteria found naturally occurring in the water. The corresponding size histograms are presented in figure 5.11.

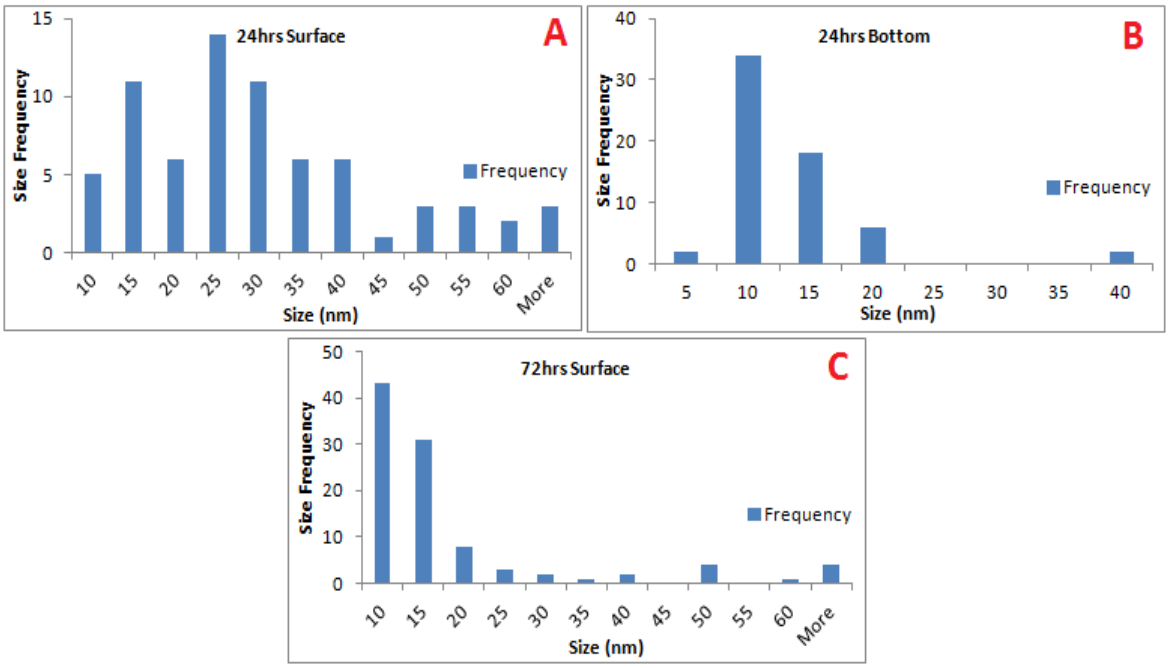

Figure 5.11: TEM size frequency histograms for PVP AgNPs at a) 24 hours in the surface, b) 24 hours at the bottom and C) 72 hours in the surface water. Histograms correspond to the images presented in figure 5.10.

Table 5.5: TEM sizes (nm) at different time points for citrate and PVP AgNPs exposed to spring natural Vale Lake water. *n= number of particles counted*ND= Not Determined. A p value <0.05 highlights that the observed particle size using the t-test is significantly different to the size of the original particle before release, at a 95% confidence level.

Table 5.5: Average Size by TEM for AgNPs Exposed to Spring Natural Water						
Time (hours)	**24**		**72**		**120**	
Area Analysed	**Surface**	**Bottom**	**Surface**	**Bottom**	**Surface**	**Bottom**
Particle type	**Citrate AgNPs**					
Size (nm)	19 ± 12	46 ± 23	18 ± 13	ND	18 ± 7	15 ± 7
N	146	25	131		74	104
***p* value**	4.20E-09	3.60E-07	4.09E-06		2.00E-07	0.00561
Particle Type	**PVP AgNPs**					
Size (nm)	28 ± 15	11 ± 6	18 ± 19	ND	ND	ND
N	72	62	101			
***p* value**	1.09E-14	0.838263	0.00116			

Due to the large proportions of impurities in the natural water, such as those identified in figure 5.8 and 5.10A, combined with low AgNPs concentrations (as low as 12 ppb for PVP AgNPs in the bottom at 24 hours), visualisations of the AgNPs were difficult. Therefore, observations were not possible for 72 hours at the bottom of the mesocosm for both citrate and PVP AgNPs, and at 120 hours for the PVP AgNPs. For each of the samples analysed the *p-values* were all below *p* 0.05 identifying that they samples were significantly different to the original AgNP sizes before they were released into natural water. As the sizes are significantly different from the original AgNPs, the data is sufficient enough to determine that the natural water has had a physicochemical impact upon the size, morphology and stability of the particles.

Analysis of the citrate AgNPs were significantly larger after (table 5.5) 24 hours exposure to the natural water with an average size of 19 ± 12 nm (*p* 4.20E-09) in the surface, when compared to the original particles before release with a starting size of 12 ± 2 nm. Figure 5.8A identified an aggregated clump of citrate AgNP of irregular sizes,

corresponding to the SPR band stretching at 500-700nm observed in figure 5.7. Results show larger AgNPs sediment to the bottom as aggregated particles were mainly represented in bottom samples. Evidence of aggregation was demonstrated by the increased sizes of 46 ± 23 nm (*p* 3.6E-07), showing significant growth compared to the original AgNPs after 24 hours.

Size determinations for citrate AgNPs from the bottom samples were based on a total count of 25 particles. Due to low concentrations of observable particles this was not a good statistical representation of the particles in this area. However, the information presented from the corresponding histogram (figure 5.9A) can be used as a good indication to the type of transformations incurred by the AgNPs exposed to the natural water. Figure 5.9A identified the most frequently counted sized citrate AgNPs were between 10-15 nm, confirming the parameters used to fit the model. However, figure 5.9A revealed AgNPs sized between 30-60 nm. The presence of larger particles, compared to the original size of 12 ± 2 nm confirmed aggregation, caused by exposure to the natural water. The settling of larger particles can be seen in figure 5.9B. AgNP settling was not accounted for in the modelled parameters, which may explain why the model does not show elevated Ag concentrations in the bottom of the mesocosm for the citrate AgNPs. Figure 5.8B identifies core fusion of the AgNPs to form a large aggregated structure, to which was in contact with an artefact from the natural water. EDX of this area did not reveal any elemental analysis, therefore the artefact is assumed to be NOM.

The citrate AgNPs were analysed from the surface water 72 hours identifying an average size of 18 ± 13 nm, close to the sizes reported at 24 hours at 19 ± 12 nm. The information shows smaller particles were retained in the surface water and larger

particles were transported to the bottom of the mesocosm, determined by the SPR profiles in figure 5.7 and the TEM size frequency histograms in figure 5.9.

On Day 5 (120 hours) based on a 74 particle number count, the surface citrate AgNPs were 18 ± 7 nm, similar to the previous observed sizes in the surface (19 ± 12 nm at 24 hours and 18 ± 13 nm at 72 hours). The corresponding histogram in figure 5.9C shows the most frequently size was 20 nm after 5 days exposure, compared to 10 nm at 24 hours, with a smaller size distribution between 5 and 40 nm. A smaller distribution shows larger particles had settled to lower depths and the presence of smaller particles at 5 nm identifies that dissolution and/or particle reformation is taking place, as seen in the $AgNO_3$ exposures. Results indicate that both aggregation and dissolution transformation processes are taking place simultaneously.

Figure 5.8C shows spherical particles of irregular sizes closely linked together by a grey matter. A similar observation was observed by Chen and Elimelech (2007), who identified aggregated particles linked together by humic acids in the presence of 1 mg L^{-1} humic acid in a high ionic solution of (40 mM) $CaCl_2$. Baalousha *et al* (2008) also observed aggregated particles linked together identified by TEM images as a grey matter surrounding the particles. Based on these observations by Chen and Elimelech (2007) and Baalousha *et al* (2008), one can suggest that the lighter grey matter surrounding the particles in figure 5.8A and 5.8C was NOM. Simultaneously, on day 5 (120 hours) the average citrate AgNP size reduced to 15 ± 7 nm in the bottom compared to 46 ± 23 nm after 24 hours exposure, further suggesting dissolution or breakage of aggregates. Li and Lenhart (2010) also observed a large degree of aggregation, followed by a decrease in particle size due to dissolution in the presence of Cl^- over time. Size distribution analysis

in figure 5.9D identifies small particles of 5 nm, suggesting dissolution or breakage of aggregates is the most likely explanation for the reduced NP size. A difference in size distribution is further evidenced in figure 5.8D, showing singular NPs of varying sizes on day 5 (120 hours) at the bottom of the mesocosm, compared to large aggregates previously observed at 24 hours. The aggregated citrate AgNPs agree with the SPR data, and the model data for the middle depth determining sedimentation as the transport mechanism.

Analysis of the PVP AgNPs (Figure 5.10) identified a multitude of features that were observed in the surface water after 72 hours exposure to the natural water. Figure 5.10A shows a bacterium in the late stage of division, which were closely located to 3 spherical nanostructures. Figure 5.10B was taken from the same TEM grid which shows a multitude of singularly spaced spherical particles of irregular sizes. Citrate particles at 24 and 120 hours show aggregated NPs, whereas the PVP particles in the surface water appeared singular and stable, further agreeing with the UV-vis data. Figure 5.10C identified a bacterium with a nanostructure in contact with its surface, and figure 5.10D shows a clear bacterium structure showing both the inner and outer cellular membrane. Closer inspection the extracellular matrix between the inner and out membrane shows tiny NPs concentrated in this area. Similar TEM images of bacteria were observed by Martin *et al* (2014) and Mellies *et al* (2012) which described the inner membrane, periplasmic space and outer membrane, as visualised in figure 5.10.

The TEM grids were left for a month to enable the degradation of the bacteria, images were re-analysed which revealed the structure shown in figure 5.10E. The image shows a degraded bacterium, the shadow represents where the cellular matrix was,

revealing AgNPs that could have been concentrated *in vivo* but were masked by the previous dark dense matrixes. The two dark circular objects are possible nuclear or mitochondrial structures.

The original PVP AgNPs for the spring batch of particles were 11 ± 2 nm (TEM) as described in chapter 3. After 24 hours exposure to the natural water the average PVP AgNP size was 28 ± 15 nm based on a 75 particle count in the surface waters, showing the particles were significantly (*p* 1.09E-14) larger than the AgNPs pre-release. The increased size results were not reflected in the SPR UV-Vis profiles demonstrating that size frequency may not be a representative of the whole area. However, parameters of the model data were changed to fit the total Ag concentration data in the middle and bottom depth using AgNPs of 300 nm (figure 5.5 and table 5.4) which confirms the presence of larger NPs in suspension.

The corresponding histogram in figure 5.11A identified a bimodal size distribution with smaller sizes between 10-40 nm and the larger at <45nm. The most frequently reported size was 25 nm, double the original PVP AgNPs. Citrate AgNPs at the same time point were recorded at a smaller average size of 19 ± 12 nm and unlike the PVP particles, a stretched tail band in the 500-700nm region was measured by UV-Vis. The information presented in the SPR profiles demonstrates further that the TEM sizing for the PVP particles was not a full representation of the total transformations in the surface water.

Figure 5.10B shows the size distribution of the PVP particles found in the bottom of the mesocosm. Particles measured include all singular NPs and aggregates. In comparison to the citrate AgNPs at 72 hours in the surface water, the PVP AgNPs show a lower size distribution, with the most frequent size of 10 nm and larger particulates

between 40-60 nm. The PVP AgNPs exhibit surface charge dependant differences. PVP AgNPs tend to remain stable in suspension in terms of persistence in the surface water as AgNPs, whereas citrate AgNPs immediately aggregate, as seen with the SPR profiles (figure 5.7) and dissolve. PVP particles were observable for 28 days in the SPR data, and were found in higher concentrations in the surface water at 321 ppb and 163 ppb in the bottom, compared to 17 ppb in the surface and 21 ppb in the bottom for the citrate AgNPs (tables A2.4 and A2.5 additional information).

Overall, the TEM data shows that the citrate AgNPs became significantly larger compared to the original sizes in each water depth, and as time increases the sizes of the AgNPs in both the surface and the bottom reduce. The reduction in size trend also seems true for the PVP particles in surface water, as at 24 hours the average size was 28 ± 15 nm (*p* 1.09E-14) compared to 18 ± 19 nm (*p* 0.001) at 72 hours. Reduced NP sizes confirm that the AgNPs dissolute, agreeing with the dissolved Ag results (figure 5.6).

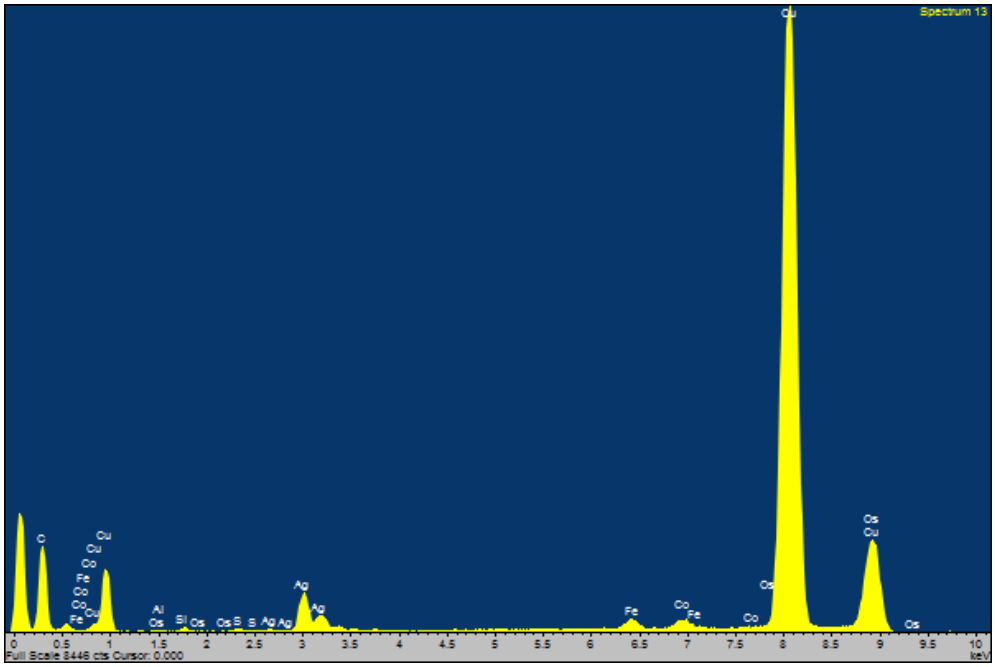

Figure 5.12: EDX spectrum of citrate AgNPs identified after 24 hours in the surface water.

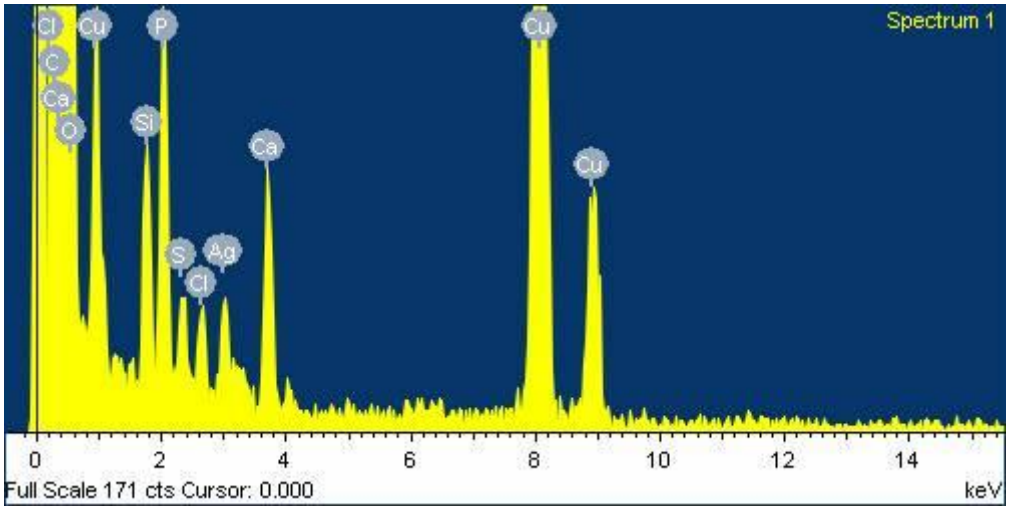

Figure 5.13: EDX spectrum of PVP AgNPs identified after 24 hours in the surface water.

The EDX spectrum (figure 5.12) for the citrate Ag NPs reveals that the water chemistry surrounding the NP surface was made up of a mixture of metalloids, transition metals and non metals. A small proportion of sulfur (S), silicon (Si), caesium (Cs), cobalt (Co), iron (Fe) and aluminium (Al) were present at low concentrations. Identifications of Cs and Co were miss-interpretations as Co should have a peak at 6.9 KeV and Cs at 4.2 keV, both of which are absent on the EDX spectrums (see energy sheet in the appendix).

Larger contributors are Ag from the NPs, with copper (Cu), and carbon (C) signals accounted from the carbon film copper mesh TEM grid used to mount the sample. Carbon may also be accounted for from NOM in the natural water as a function of TOC. Table 5.7 of the ICP-MS elemental data of the natural water confirms the presence and concentration (ppb), of some of the elements found in the EDX profile. The presence of sulfur in the natural water can lead to sulfidation of the AgNPs, transforming the AgNPs to Ag_2S structures, and lead to a decrease in dissolution rate (Levard *et al,* 2011). Simultaneously, the presence of sulfur has been demonstrated to cause aggregation of AgNPs (Levard *et al,* 2011), which is consistent with the information presented in the SPR profiles and the TEM analysis.

The EDX profile in figure 5.13 for the PVP AgNPs reveals the presence of halogenated elements, minerals, metalloids and transition metals. Contributing elements include chlorine (Cl), calcium (Ca) oxygen (O), phosphorous (P), S, and Si, all of which occur in the natural water in small concentrations (see table 5.5). Since there is a strong signal of oxygen presence, there is potential for the AgNPs to be oxidised, as this is a redox active species (Lowry *et al,* 2012). It is also possible that the oxygen contribution may be present from the air surrounding the sample, and therefore cannot be a definitive transformation to the AgNPs.

AgNPs are known to form complexes with electrolytes such as sulfide groups and chloride under environmental conditions (Blaser *et al,* 2008, Allen *et al,* 2010, Quadros and Marr, 2010, Levard *et al,* 2013). Sulfur is naturally occurring in natural waters and is known to act as an oxidant in the presence in of metals. As the EDX spectrum determined (figures 5.12 and 5.13) the presence of sulfur, this indicates the possibility of silver sulfide

(Ag_2S) structures, as previously identified by Levard *et al* (2011) who used X-ray diffraction (XRD) identification techniques. Chlorine also occurs naturally in an ionic form in the environment and has a strong affinity for metal oxides. The presence of Ag and Cl in the PVP AgNP EDX spectrum (figure 5.13) may indicate the formation AgCl particles (Ha and Payer 2011). It should also be noted that chlorine has an affinity for polyvinylpyrrolidone (PVP) to form polyvinyl chloride (used in consumer products), (Levard *et al,* 2013) which would describe why chlorine was present in the PVP AgNPs EDX spectrum and not for the citrate particles.

5.4.2.4 Inductively Coupled Plasma Mass Spectrometry (ICP-MS) and Total Organic Carbon (TOC) Analysis

As well as the elemental makeup of the natural water, it is also crucial to identify the total organic carbon that contributes to available the NOM concentrations. TOC is contributed to by dissolved organic carbon substances such as humic and fulvic substances and atmospheric carbon dioxide (CO_2). The concentration of the TOC in the natural water can affect the type of transformations that AgNPs may be subjected to once released into the environment (Cumberland and Baker, 2007). On sampling, the pH was recorded at 7.5 which agree with previously recorded seasonal data (Baker *et al,* 2007).

Table 5.6: ICP-MS Semi Quantitative (± 20%) Elemental Concentrations of Natural Spring Vale Lake Water			
Element	**Concentration (ppb)**	**Element**	**Concentration (ppb)**
Li	3.6	**Zn**	46
B	170	**Ga**	ND
Na	98000	**Ge**	ND
Mg	6400	**As**	0.8
Al	30	**Se**	0.8
Si	720	**Br**	190
P	13	**Rb**	3.8
K	3100	**Sr**	210
Ca	26000	**Zr**	ND
Ti	0.7	**Mo**	1.3
V	1.3	**Ag**	0.3
Cr	0.4	**Sn**	ND
Mn	5.3	**Sb**	ND
Fe	46	**Ba**	35
Co	0.2	**Ce**	ND
Ni	3.6	**W**	ND
Cu	4.5	**Pb**	0.3

Table 5.6 identifies the elemental concentration of the Vale lake water before the NP exposure studies. Various amounts of electrolytes such as Ca, sodium (Na), magnesium (Mg) and potassium (K) are high in concentration. Particular interest is given to the divalent cations including Ca^{2+}, Mg^{2+}, and manganese (Mn^{2+}), as in previous studies these have been demonstrated to cause aggregation (El Bradawy *et al,* 2010, Stankus *et al,* 2011, Zhang and Oyanedel-Craver, 2012), and have the ability to change the oxidation state of the AgNPs by transfer of elections (Lowry *et al,* 2012). Since the SPR profiles in figure 5.6 for the citrate AgNPs shows the presence of larger particulates, it can be assured that the water conditions favour aggregation due to the destabilizing effect on the surface charge of the citrate NPs (Stankus *et al,* 2011). The high ionic strength of the

water was sufficient enough to reduce the electrostatic double layer surrounding the particles, and reduce electrostatic repulsion, leading to aggregation (Li *et al,* 2010). However, when compared to the PVP particles the destabilization effect of the water chemistry was not presented in the surface SPR profiles, since persistence of the NPs was observed for 28 days. Only in the middle and bottom water areas observed aggregation in the SPR profiles. The information presented here contributes to surface charge dependant differences in particle behaviour. The polymer coating of the PVP AgNPs has a longer chain length, and therefore provides a thicker and complex surface stabilizer than that of citrate, which would explain why PVP AgNPs do not exhibit aggregation (Li *et al,* 2013b).

TOC in the lake water was recorded at 12.59 mg L^{-1}, which is particularly important, as the presence of NOM influences particle stability and fate and transport of NPs (Manciulea *et al,* 2009, Delay *et al,* 2011). In comparison to the EPA SRFA water exposures presented in chapter 4 which had NOM added at 1 mg L^{-1}, higher TOC concentrations in the natural lake water has further influenced particle stability of both the PVP and citrate AgNPs. When compared to the EPA SRFA study in chapter 4 the citrate particles followed aggregation and sedimentation as shown in the dissolution and modelled data. In the present study the citrate AgNPs followed the model predicted concentration based on a 12 nm AgNP transporting through the mesocosm and was present in higher AgNP concentrations (17 ppb) at the end of the study.

The PVP particles were persistent in the surface water throughout the whole study compared to 14 days in the EPA SRFA study. Therefore the increased carbon content has maintained PVP AgNP presence in the SPR and dissolution data, which

suggests that stabilization of the PVP AgNPs due to adsorption of NOM on the particle surfaces (Delay *et al,* 2011).

The multi-method analysis of the spring natural water study revealed a surface coating specific trends. The natural water conditions contributed to the destabilization, aggregation and dissolution of the citrate AgNPs compared to the PVP AgNPs. Citrate AgNPs demonstrated small amounts aggregation on immediate release into the natural water, indicated by the additional SPR band stretching in the 500-700nm region (figure 5.7). These bands were not visualised for the PVP AgNPs until after 5 days exposure which corresponds to the model data for the PVP AgNPs. The aggregated citrate particles then settled, as indicated by the modelling data presented in figure 5.4, highlighting partitioning and transportation differences between the two particle types.

The PVP AgNPs were retained (as NPs) in the surface water throughout the duration of the study, and evidence from dissolution studies (figure 5.6) demonstrate that PVP particles remain in NP form in higher concentrations and for longer periods of time when compared to the citrate AgNPs. TEM imaging and size distributions also highlighted the different size transformation that both the citrate and PVP AgNPs exhibited after exposure to the spring natural water.

5.4.3 Summer Natural Vale Lake Water

5.4.3.1 Modelled, Total and Dissolved Silver Concentrations

Using the simple diffusion-sedimentation model (Socolofsky and Jirka 2004, and Hinderliter *et al,* 2010) we were able to predict the transport processes and concentration of the AgNPs once released in to summer seasonal natural water. Results are presented in figure 5.14 and conditions in table 5.8.

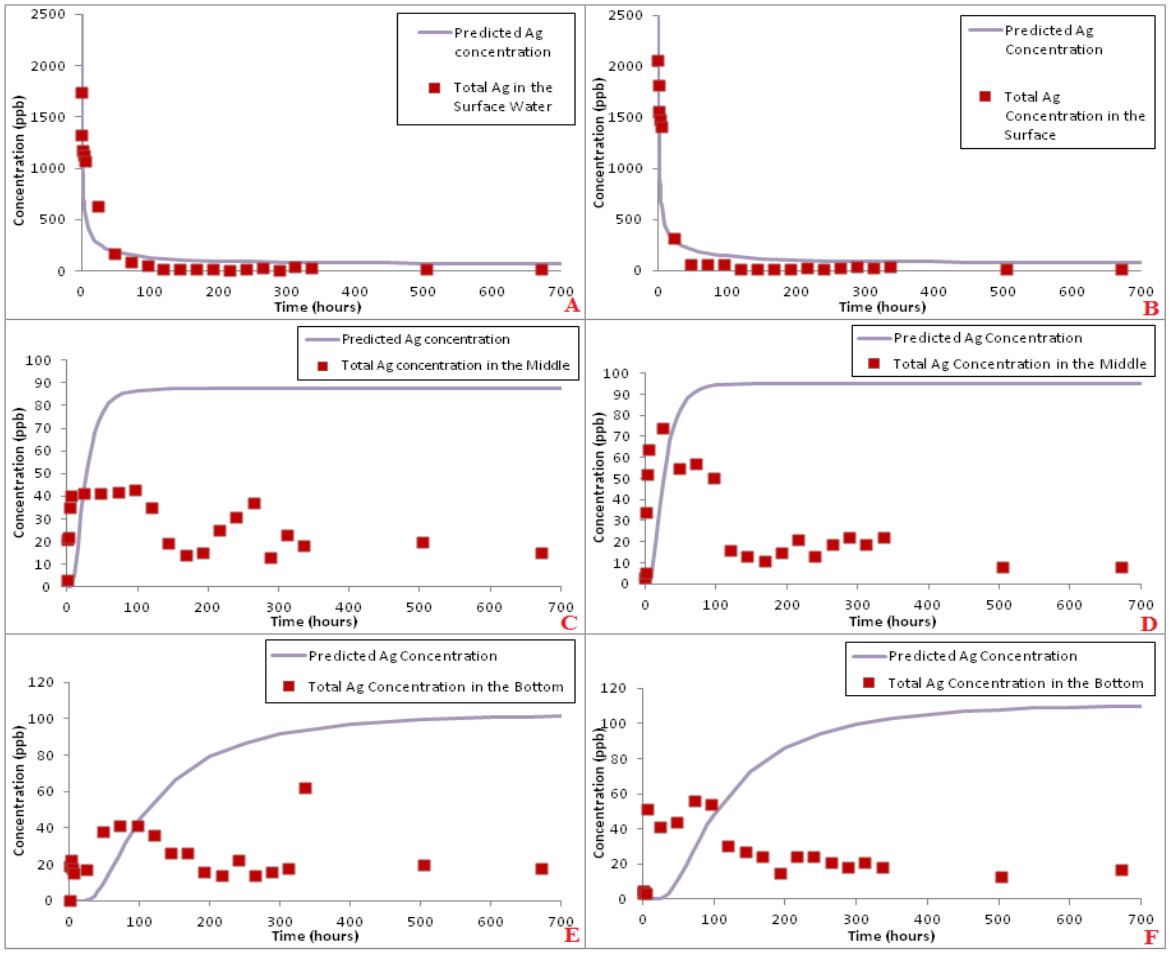

Figure 5.14: Model predicted concentrations over time plotted against the average total Ag concentration obtained from, A) citrate AgNPs in the surface, B) PVP AgNPs in the surface, C) citrate AgNPs in the middle, D) PVP AgNPs in the middle, E) citrate AgNPs in the bottom and, F) PVP AgNPs in the bottom of the summer natural lake water of the mesocosm. The model fits were based on a single 11 nm AgNP transporting through the mesocosm using parameters presented in table 5.7.

Table 5.7: Model Parameters for AgNPs in Summer Natural Lake Water				
Parameter	**Symbol**	**Unit**	**Citrate**	**PVP**
Diameter of AgNP	d	nm	11	11
Cross section area of the column	A	m^2	0.049	0.049
Column length	*L*	m	1	1
Column volume	*V*=A*L*	L	43	43
Dosing volume	*V*	L	0.391	0.215
Dosing concentration	C_0	ppm	11	20
Mass of Ag	M	mg	4.3	4.3
C column based on diffusion	M/*V*	ppb	100	100
Diffusion coefficient	*D*	$m^2 s^{-1}$	3.904.E-07	3.904.E-7
Sedimentation Velocity	*U*	ms^{-1}	6.30E-10	6.30E-10

Analysis of the citrate AgNPs shows that the R^2 value in the surface water R^2 was 0.94, showing the total Ag in the surface water followed the predicted modelled concentrations. However, the R^2 values for the middle were 0.47 and 0.26 in the bottom, showing no correlation between the observed and the modelled data with the parameters that were set in table 5.8. Further observations of the total Ag behaviour in the lower depths will help to determine the parameters that need to be set (such as TEM), to validate the behaviour and transformations of the citrate AgNPs.

As the total Ag concentrations in middle of the mesocosm show stability over the first 5 days after release are between 40 ± 0.37 ppb at 5.5 and 35 ± 0.01 ppb on day 5 (Table A2.5 additional information), we can assume the transport mechanism was diffusion. Since these concentrations were lower those predicted, losses were incurred during experimentation. After day 5 there was evidence of sedimentation, shown by the gradual decrease in concentration to 14 ± 0.03 ppb day 7 (168 hours), followed by an increase to 37 ± 0.02 ppb on day 11 (264 hours). The elevations and declines in concentrations confirm sedimentation as the AgNPs travel to the bottom of the mesocosm (Hinderliter *et al,* 2010). The trend in results may suggest either of the

following, A) immediate aggregation of the citrate AgNPs resulting in diffusion of the same sized AgNPs throughout the mesocosm, followed by increased aggregation/sedimentation, or B) citrate AgNPs are protected by NOM, but gradually become unstable and aggregate after long exposures to the natural water. Information from the SPR data (figure 5.18) and TEM size analysis (table 5.10) supports the latter statement. We tested these theories by adjusting the model parameters as seen in table 5.9 and figures 5.15A and 5.15B for the middle depth. When we reduced the concentration to account for losses due to sedimentation and settling, and used a small diameter we produce an R^2 value of 0.14, indicating no correlation between the two sets of data. Although, when we increased the AgNP size to account for aggregation and reduce concentration we produced an R^2 value of 0.55, for the best achievable fit for this depth.

Adjustments to the model parameters were used to fit the observed Ag concentrations in the bottom depth for the citrate AgNP study. The highest observed total Ag concentrations for the citrate AgNP study in the bottom depth were seen between days 2-4 (48-96 hours) at 36-41 ppb and on day 14 (336 hours) at 62 ± 0.08 ppb. If we set the model parameters (figure 5.15C and table 5.9) to account for increased particle size and Ag losses, we produce an increased R^2 value of 0.54, showing better correlations.

Overall, the citrate AgNPs were unstable and had a tendency to aggregate, settle, and dissolve over time. The combination of these AgNP transformations over time produced concentration fluctuations (outliers) and thus reduced R^2 values.

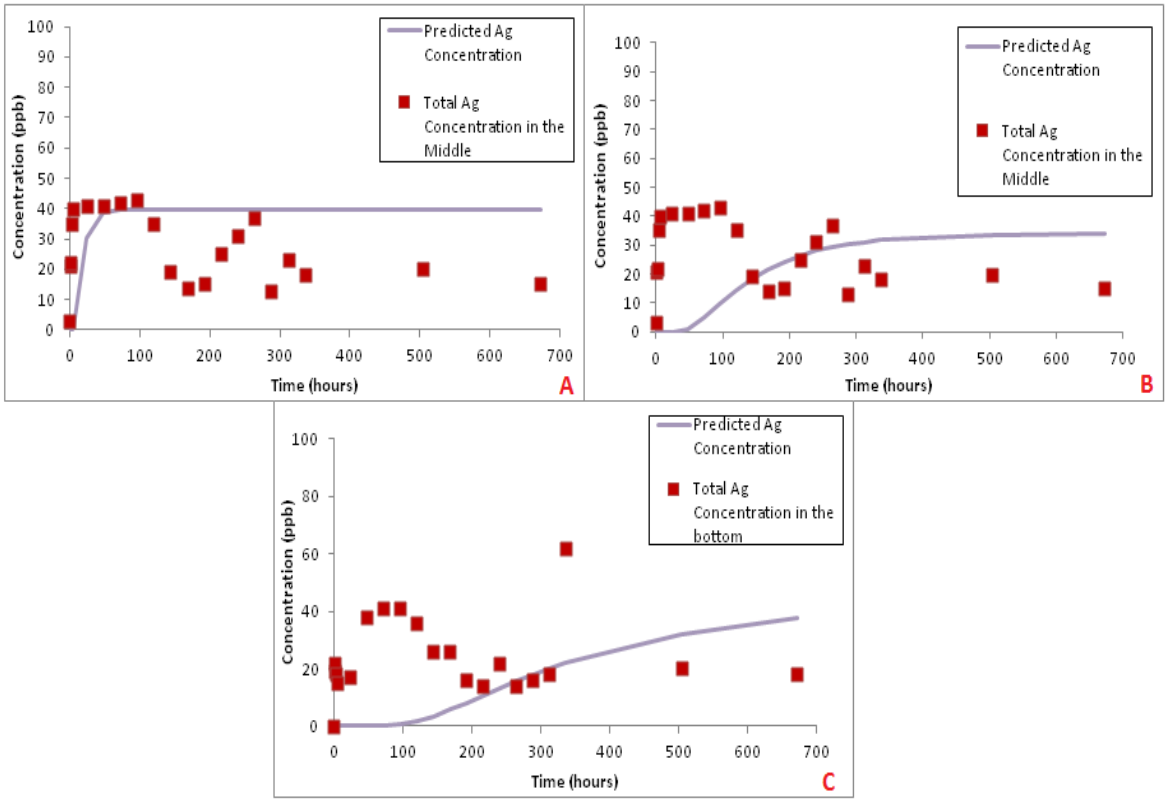

Figure 5.15: Adjusted model fits for changing model parameters for (A) the middle, (B) the middle (further adjusted) and (C) the bottom water, for citrate AgNPs exposed to summer natural lake water. New model parameters are listed in table 5.8.

Table 5.8: Adjusted Model Parameters for Citrate AgNPs in Summer Natural Lake Water

Parameter	Symbol	Unit	Middle (A)	Middle (B)	Bottom
Diameter of AgNP	d	nm	7	60	35
Cross section area of the column	A	m^2	0.049	0.049	0.049
Column length	*L*	m	1	1	1
Column volume	*V*=A*L*	L	43	43	43
Dosing volume	*V*	L	0.391	0.391	0.391
Dosing concentration	C_0	ppm	5	4	5
Mass of Ag	M	mg	2	1.6	2
C column based on diffusion	M/*V*	ppb	45.3	36.4	45.5
Diffusion coefficient	*D*	$m^2 s^{-1}$	6.14E-07	7.157E-8	8.59E-07
Sedimentation Velocity	*U*	ms^{-1}	2.5 E-10	1.9-8	6.3 E-9

Analysis of the PVP AgNP study shows immediate differences between the previous spring water study and the present study. In spring, the total Ag remained higher in concentration when compared to the citrate AgNP study, and never reached an equilibration. In the present study the concentrations of Ag were comparable to the concentrations of Ag in the citrate study. The PVP total Ag concentration followed the model predictions in the surface water based on the parameters shown in table 5.8 for an 11 nm AgNP, with an R^2 value of 0.92. Analysis of the middle depth identified a small correlation between the observed and modelled Ag concentrations, producing an R^2 value of 0.55. Adjustments to the model parameters (figure 5.16 and table 5.9) increased the R^2 value to 0.59 which was the best optimal fit between the model and observed total Ag concentrations. Nonetheless, After day 6 (144 hours) the concentration in the middle depth begins to stabilise around 19 ± 0.05 ppb, where it remained stable for the duration of the study, indicating that a diffusion gradient has been optimized, agreeing with Ficks Law (Fick, 1855). The stability of the PVP AgNPs observed is surface coating specific at this depth as the citrate study demonstrate aggregation, which was validated by the model parameters.

The total Ag concentrations for the PVP in the bottom of the mesocosm followed the process of diffusion by maintaining a concentration gradient between days 5 at 26 ± 0.03 ppb, and day 28 where the concentration dropped to 18 ± 0.09 ppb. The R^2 value was 0.66 based on the original parameters in table 5.8. Adjusting model parameters only reduced the R^2 number to 0.66 when trying to successfully improve the model fit with the observed data for bottom of the mesocosm. Nonetheless, the concentrations gradients observed in each depth infer that the transport mechanisms follow sedimentation for the

citrate AgNPs and diffusion for the PVP AgNPs. Further samples were examined from the surface and the bottom of the mesocosms to assess the difference between the dissolved and ionic form of Ag, which are presented in figure 5.17.

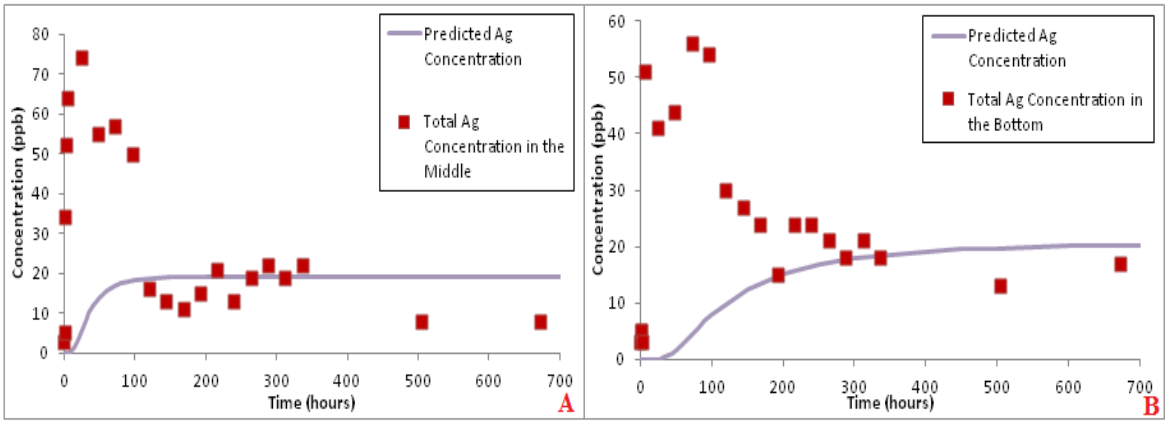

Figure 5.16: Adjusted model fits for (A) the middle, and (B) the bottom water, for citrate AgNPs exposed to summer natural lake water. New model parameters are listed in table 5.9.

Table 5.9: Adjusted Model Parameters for PVP AgNPs in Summer Natural Lake Water

Parameter	symbol	unit	middle	bottom
Diameter of AgNP	d	nm	15	12
Cross section area of the column	A	m^2	0.049	0.049
Column length	*L*	m	1	1
Column volume	*V*=A*L*	L	43	43
Dosing volume	*V*	L	0.215	0.215
Dosing concentration	C_0	ppm	4.5	4
Mass of AgNPs	M	mg	1	0.9
C column based on diffusion	M/*V*	ppb	22.5	20
Diffusion coefficient	*D*	$m^2 s^{-1}$	2.86E-7	3.58E-7
Sedimentation Velocity	*U*	ms^{-1}	1.2 E-9	7.4 E-10

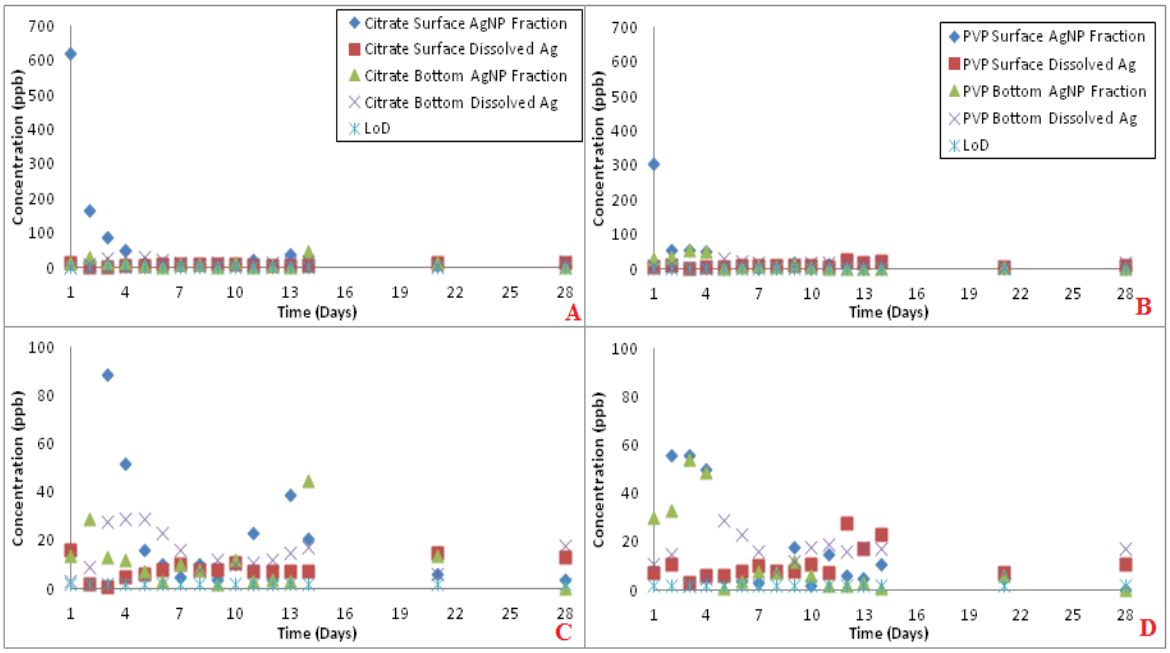

Figure 5.17: Dissolved and AgNP concentrations (ppb) using ultrafiltration in the summer lake water: A) citrate Ag^+ and AgNP concentrations in the surface and bottom depth water for each day, B) PVP Ag^+ and AgNP concentrations in the surface and bottom depth water for each day, C) shows the same graph as A for concentrations below 100 ppb, D) shows the same graph as B for concentrations below 100 ppb. Note the LoD = Instrumentation limit of detection at 2 ± 0.2ppb.

Figure 5.17 provides a good estimation of how stable the AgNPs are once released in to the summer natural water. Investigations of the citrate AgNPs revealed that the concentrations of AgNPs were lower than those recorded in the spring water releases. Although the Ag^+ concentrations were comparable to the previous water set. For example, at 24 hours in the spring the citrate study the AgNP concentration was 1410 ppb in the surface water compared to 620 ppb in the present study. Simultaneously, at the end of the study the concentration of citrate AgNPs in the surface water was 17 ppb in spring compared to 4 ppb in the present study, highlighting differences in AgNP behaviour between the seasonally variant waters.

The citrate AgNP study shows an elevation of AgNP concentration in the surface waters on days 11 at 23 ppb and day 13 at 39 ppb, although this was not observed in the total Ag concentrations presented in figure 5.14. Information may be due to instrumentation or ultrafiltration errors and can only be used as an approximation to describe AgNP behaviour. Nonetheless, explanations of the fluctuating concentrations can be due to disaggregation or dissolution, which would release smaller and lighter particles that can diffuse back into the different water compartments (Li *et al,* 2013). At 24 hours the Ag^{+} concentration was 16 ± 0.08 ppb, remaining contestant in the region of ± 8 ppb for the duration of the study.

The PVP AgNPs show a rapid decline in AgNP concentration in the surface water in the first two days after release, from 307 ppb (24 hours) to 56 ppb (48 hours), where the concentrations remain stable between 56-50 ppb until day 5. The drop in concentration was reflected in the modelled concentrations in figure 5.14. Simultaneously, as the concentration drops in the surface, the concentration of the AgNPs elevated in the bottom from 30 ppb at 24 hours to 49 ppb on day 4, confirming the model predictions. When compared to the spring water study, the present study identified both citrate and PVP AgNP fractions were lower in concentrations, with comparable ionic concentrations for each depth. In both cases AgNPs were identifiable in small concentrations at the end of the study determining their persistence.

5.4.3.2 UV Analysis

Figure 5.18 (A-F) shows the SPR profiles for citrate and PVP particles over time in the surface, middle and bottom of the mesocosm tanks.

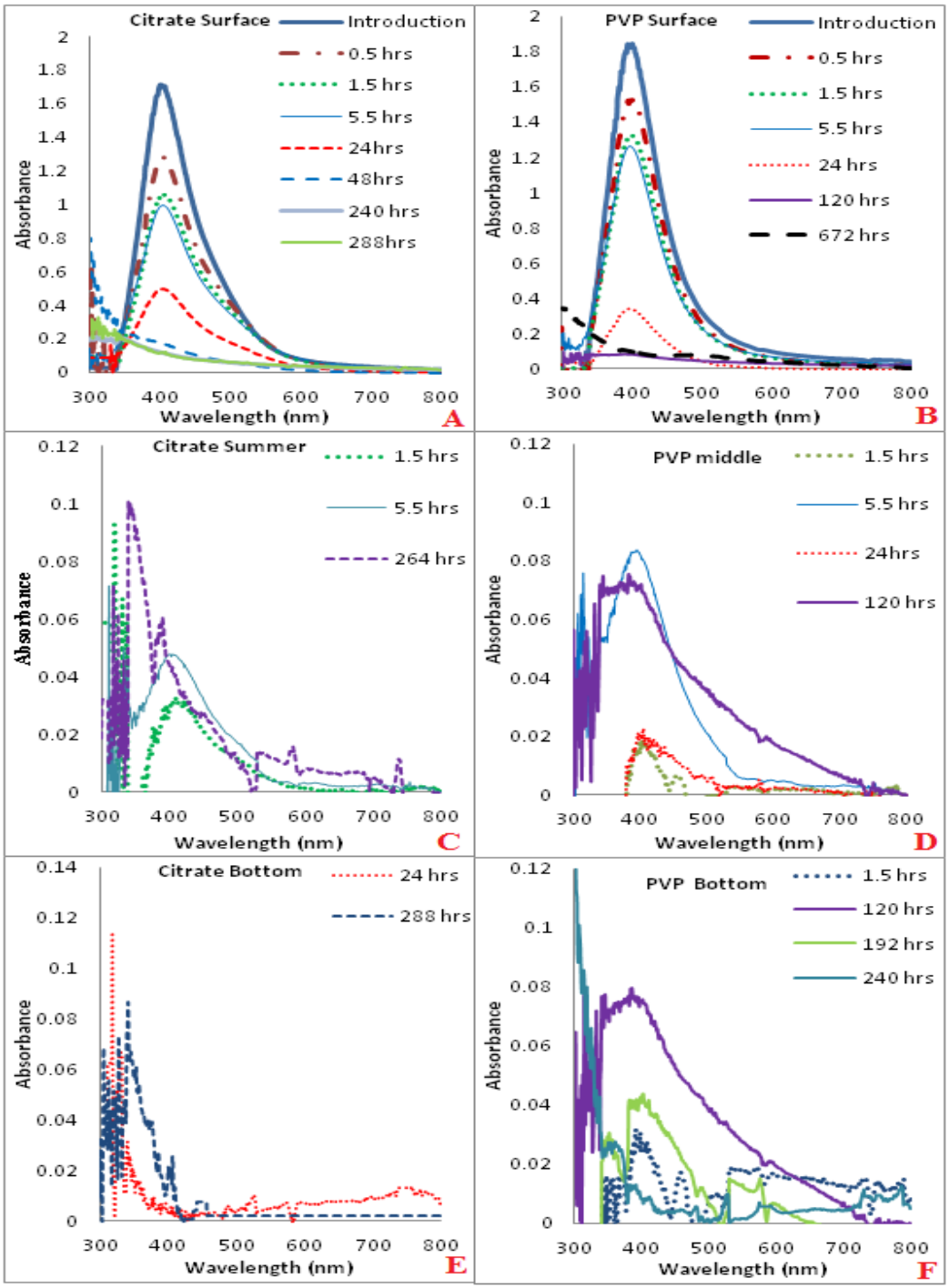

Figure 5.18: SPR profiles taken from different depths of the mesocosm column when exposed to natural Vale Lake water in summer. A) Citrate coated AgNPs at the surface, B) PVP AgNPs at the surface, C) citrate AgNPs from the middle, D) PVP AgNPs from the middle, E) citrate AgNPs from the bottom and F) PVP AgNPs from the bottom. Note that the Y axis for the graphs are not presented in the same scale for each of the depths, as detail from the lower regions would be lost.

The SPR peak (λ_{max}) for spherical pristine citrate AgNPs as characterised in chapter 3 was 392nm, and 400nm for those stabilised with PVP. In the summer water experiments, the surface water SPR profiles (figure 5.18) for the PVP and citrate coated AgNPs both show out of plane quadrupole resonance after 48 hours exposure to the natural water. Whereas in the spring season observations the SPR banding for the out of plane resonance was observed in the lower parts of the mesocosms only. Observations suggest there is a greater concentration of NOM in the summer water compared to the spring season water, which effects the SPR changes in the surface profiles. Further analysis revealed that the TOC content was 31.70 mg L^{-1} agreeing with the observed changes to the SPR peaks.

On introduction, the citrate AgNPs produced the same red shifting of the λ_{max} absorbance from 392nm before exposure (Cumberland and Lead, 2009, Tejamaya *et al,* 2012), to 403nm. The red shifting for the citrate AgNPs was higher than those previously observed in the spring water, which identified smaller shifts from 396nm to 398nm over a 24 hour period for the citrate AgNPs. The large red shift in the present study determines particle polydispersity and oxidation at the particle surface (Li and Sun, 2011) favoured by the natural water conditions. The surface SPR profiles for the citrate AgNPs also observed band stretching between 500-700nm, indicating the presence of larger particulates due to aggregation (Li *et al,* 2010). Evidence of aggregation also confirmed the total observed Ag data in figure 5.14. Therefore, despite the higher recorded TOC concentration particle aggregation is still occurring.

For the bottom depth of the mesocosm there was a strong absorbance peak for the citrate AgNPs at 11 days (264 hours) despite the interference of the NOM and natural

water at 300-400nm (Zou *et al,* 2007, and Kawaguchi *et al,* 2011). No further peaks confirming AgNP presence was observed after day 11. Data from the UV-vis does not agree with the dissolution studies presented in figure 5.17. Although AgNPs were seen in low concentrations (4 ppb) in figure 5.17 at the end of the study, it is also possible that since the sample volumes were so small from each depth for ultrafiltration (10 mL), the concentrations may not be a representation of the whole compartment. Furthermore losses could have occurred from instrumentation measurement error and adhesion of AgNPs to the mesocosm container. Despite possible losses and conflicting data, the citrate AgNPs were not observed in the previous spring seasonal water studies after 9 days (216 hours). Therefore the increased NOM concentration has increased the citrate AgNPs stability and persistence in suspension (Li and Sun, 2011).

The PVP AgNPs remained stable with the λ_{max} absorbance in the surface water staying between 400-401nm in the first 24 hours, which is comparable to the reported literature for PVP AgNPs (Tejamaya *et al,* 2012). As a whole, the PVP AgNPs show stability as reflected in the total Ag concentration data and modelled data (figure 5.14). PVP AgNPs in the surface were also detectable at day 28, confirming the results dissolution studies in figure 5.17 of AgNP persistence. The information presented in the UV-vis data confirms a surface coating specific trend in the behaviour of the PVP AgNPs compared to the unstable citrate AgNPs.

5.4.3.3 Transmission Electron Microscopy (TEM) Analysis and Energy Dispersive X-Ray (EDX) Analysis

Original citrate AgNPs as discussed in chapter 3, were characterised by TEM at 11 ± 3 nm (section 3.5.1.4), and 11 ± 3 nm (section 3.5.2) for the PVP AgNPs. These sizes were used to determine size changes that occurred to the NPs once released into the summer natural water. As with the spring water study, large proportions of impurities in the natural water and low concentrations of AgNPs introduced difficulties in visualising the AgNPs. Therefore, observations were not possible for bottom of the mesocosm for both particle coatings at 24 hours, and at 72 hours for the PVP AgNPs at the surface. EDX was used to determine and confirm the presence of PVP AgNPs, as seen in figure 5.23. Morphological characteristics are presented in figures 5.19 (citrate AgNPs) and 5.21 (PVP AgNPs).

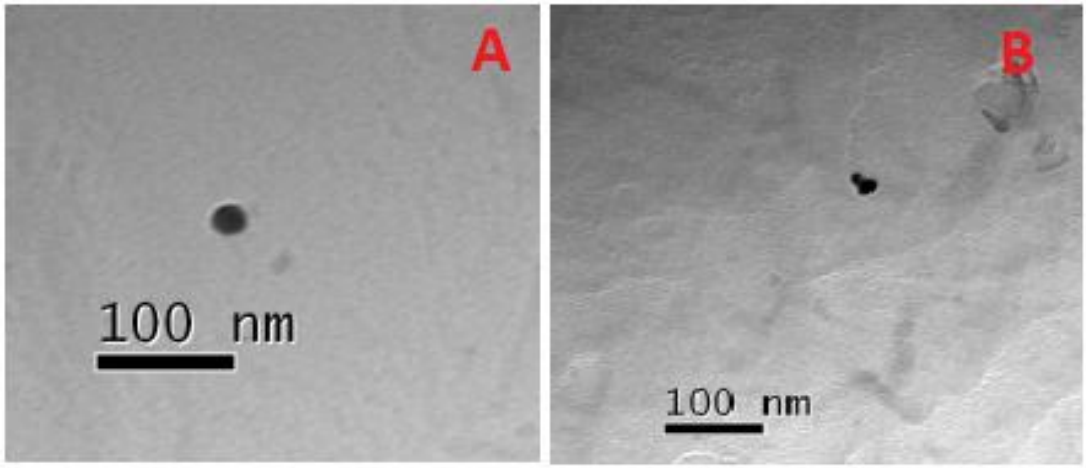

Figure 5.19: TEM images of citrate AgNPs exposed to the summer natural Vale lake water identified at A) 72 hours surface and B) 72 hours bottom of the mesocosm. Corresponding histograms are presented in figure 5.20.

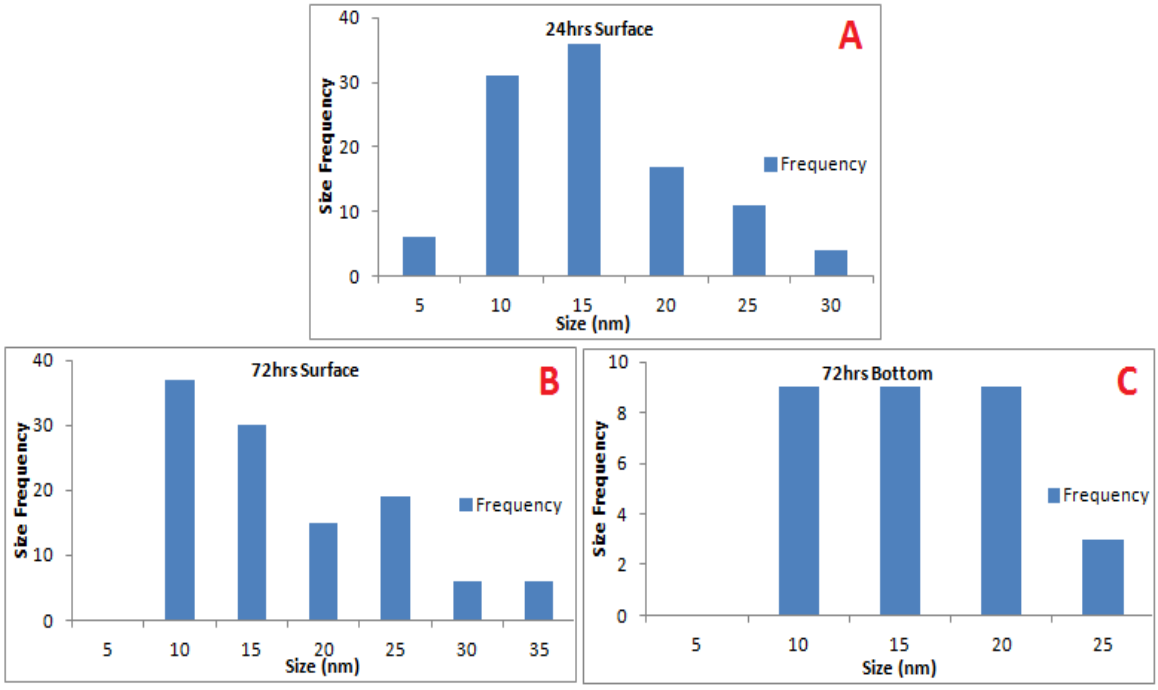

Figure 5.20: TEM size frequency histograms for citrate AgNPs exposed to summer natural Vale lake water at A) 24 hours in the surface B) 72 hours in the surface and C) 72 hours in bottom of the mesocosm. Histograms B and C correspond to the images presented in figure 5.19.

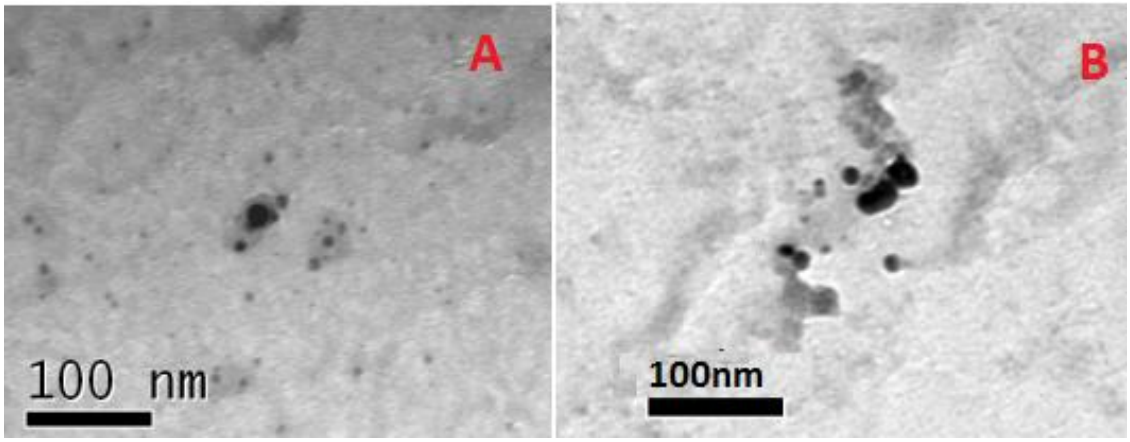

Figure 5.21: TEM images of PVP AgNPs exposed to the summer natural Vale lake water identified in the A) surface water at 24 hours and B) the bottom area at 72 hours. Corresponding histograms are presented in figure 5.22.

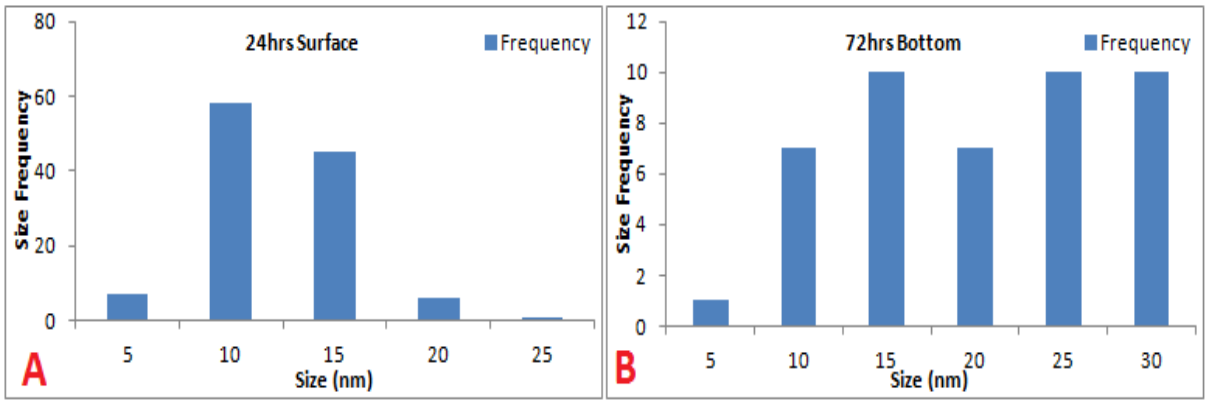

Figure 5.22: TEM size frequency histograms for PVP AgNPs exposed to summer natural Vale lake water at A) surface 24 hours, and B) the bottom at 72 hours. Histograms correspond to images presented in figure 5.21.

Table 5.14: TEM size (nm) at different time points for citrate and PVP AgNPs exposed to summer natural Vale Lake water. *n= number of particles counted*ND= Not Determined. A p value <0.05 highlights that the observed particle size using the t-test is significantly different to the size of the particle before release, at a 95% confidence level.

Table 5.10: Average Size by TEM for AgNPs Exposed to Summer Natural Water				
Time (hours)	**24**		**72**	
Area Analysed	**Surface**	**Bottom**	**Surface**	**Bottom**
Particle type	**Citrate AgNPs**			
Size (nm)	13 ± 6	ND	16 ± 8	14 ± 5
n	105		112	31
***p* value**	0.00023		5.4E-09	0.00047
Particle Type	**PVP AgNPs**			
Size (nm)	10 ± 3	ND	ND	18 ± 7
n	97			45
***p* value**	0.25104			7.3E-9

Analysis of the citrate AgNPs presented figure 5.16 show less concentrated samples than the citrate AgNPs exposed in the spring water, with only 1 particulate per image. The reduced Ag concentrations confirm the reduced AgNP concentrations identified in the dissolution studies (figure 5.17) for the summer water exposures.

The size of the citrate AgNPs in the surface water was 13 ± 6 nm (*p* 0.00023) at 24 hours, which were significantly different when compared with the original synthesised particles at 11 ± 3 nm. At 72 hours the citrate AgNPs were sized at 16 ± 8 nm (*p* 5.4E-9) in the surface water, which was also smaller than those recorded in spring at 18 ± 7 nm. The size frequencies of the NPs presented in the corresponding histograms between the spring water and the present study also show variations. The size frequencies in the present study were smaller between 5-30 nm (figure 5.20A), in comparison to those at 24

hours in the spring water study between 10-60 nm (figure 5.9A) at 24 hours in the surface water.

Continue analysis of the size frequency histograms identified at 72 hours (figure 5.20B) there were no particles smaller than 10 nm in the surface water, when compared at 24 hours. Smaller particulates have dissolved or became agglomerated, as there is a presence of larger AgNPs at 35 nm. Figure 5.19B identified two small particles fused together, found at 72 hours in the bottom of the mesocosm indicating aggregation and sedimentation.

Overall the citrate AgNPs were more stable in terms of size distribution in each of the surface and bottom area waters when compared to the spring natural water study. Increased stability is due to higher NOM concentrations. All of the size frequency data agrees with the transport method of sedimentation as followed by the citrate AgNPs presented in figure 5.14.

Analysis of the PVP AgNPs TEM images in figure 5.19A displayed small spherical NPs that were sized at 10 ± 3 nm (*p* 0.25104) in the surface water at 24 hours. These particles show no significant difference to the original sized NPs indicating particle stability over the citrate AgNPs. Information from the surface water size analysis agreed with the model data for diffusion transportation of the Ag as indicated in figure 5.14. The most frequent PVP AgNP size in the surface water at 24 hours was 10 nm, compared to 25 nm in the spring water study demonstrating the water chemistry specific stability in the summer. PVP AgNPs were 18 ± 7 nm (*p* 7.3E-09) in the bottom area after 72 hours exposure and had a size frequency of 15 nm, demonstrating settling of larger particulates. Particles were morphologically larger and aggregated in the bottom area as shown in

figure 5.21B compared to the surface at 24 hours, although there were still some singular spherical PVP AgNPs present. This was not presented in the model findings since the model was not adapted for accumulating particles settled at the bottom. For all samples, the sizes recorded were significantly different from the original particles before release into the natural water.

The TEM size distribution histograms reveal similar behaviour patterns to the citrate AgNPs. In both instances the size distribution for the summer exposures were less polydispersed than in the spring water, revealing that AgNPs released in the summer water were more stable for longer periods of time.

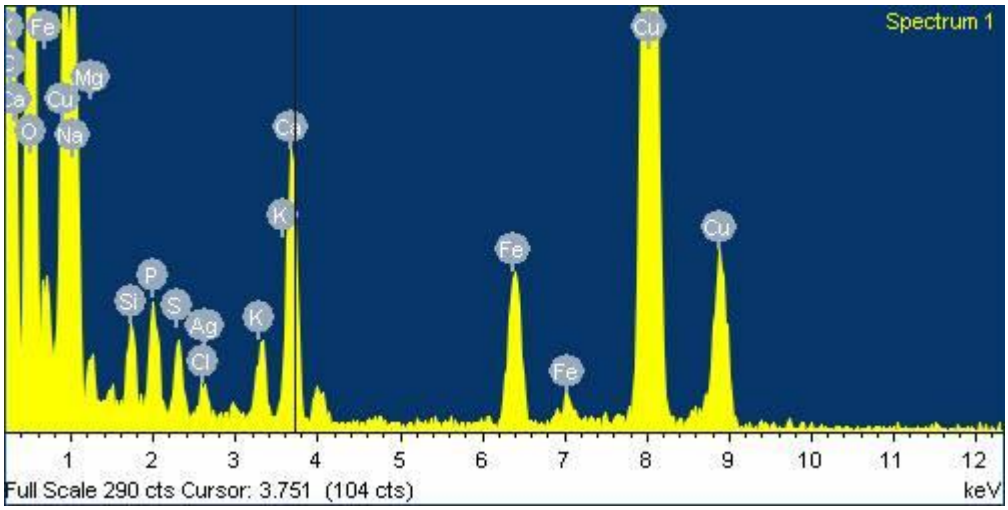

Figure 5.23: EDX spectrum of PVP AgNPs identified after 24 hours exposure in the surface of the summer natural water.

The EDX profile in figure 5.23 identified the presence of halogenated elements, minerals, metalloids and transition metals. Contributing elements included Cl, Ca, O, P, S, Si, Fe, K, Mg and Na. AgNP presence was confirmed by the Ag peak, as with the previous EDX profiles the Cu and carbon C peaks were due to background noise from the TEM grid on which the sample is mounted. Oxygen may have been a contaminant from the air surrounding the sample.

The Cl peak identifies the possible association of the AgNPs/Ag^+ with the Cl ions, which has been previously demonstrated in the literature under environmental conditions (Ha and Payer 2011, Levard *et al,* 2013). The spring water studies with the PVP AgNPs also detected the presence of Ag and Cl indicating AgCl formation. With the addition of NOM adhered to surface of the particle electrostatic repulsion can be increased in the presence monovalent electrolytes environment such as Cl (Li and Sun, 2011). These results also justify why the citrate particles have persisted in particulate form for a longer periods of time, agreeing with SPR and TEM data confirming increased stability.

Sulfur detection indicates the possibility of the AgNPs or (Ag^+ released via dissolution) forming Ag_2S structures (Levard *et al,* 2011, Lowry *et al,* 2012). Levard *et al* (2011) discovered that the PVP polymer surface coating is unable to protect the NP from aggregation in the presence of sulfur, which is consistent with the results obtained from the UV-vis. Therefore, losses of capping agent led to sulfidation of the PVP AgNPs (Levard *et al,* 2011). Sulfur has been demonstrated in natural environment to decrease the oxidation rate of the AgNPs and reduce the release of Ag^+, thus reducing the toxicity by minimizing ionic release (Levard *et al,* 2013). The amount of Ag^+ was lower in the present study (see appendix for tables and exact concentration figures) when compared to the spring study. Divalent cations Ca^{2+}, Mg^{2+}, Fe^{2+}, and Mn^{2+} were also presented in the spectrum, which are associated with aggregation and oxidation of AgNPs under environmental conditions (Zhang and Oyanedel-Craver, 2012).

5.4.3.4 Inductively Coupled Plasma Mass Spectrometry (ICP MS) and Total Organic Carbon (TOC) Analysis

The TOC content was recorded at 31.70 mg L^{-1}, twice the amount compared to spring seasonal water at 12.59 mg L^{-1}. High concentrations of organic matter have been shown to reduce aggregation (Lowry *et al,* 2012), and influence particle stability (Stankus *et al,* 2011). Information obtained from the collective data (FAAS, model, UV-vis and TEM) show increased concentrations of NOM have demonstrated behavioural changes and stability to the citrate and PVP AgNPs, when compared to the previous spring season water. Both the PVP and citrate AgNPs were shown by TEM analysis to be less polydispersed and have smaller size distributions. The elevated NOM concentrations also contributed to longer persistence and stability of the citrate AgNPs for 11 days in the lower depths of the mesocosms, compared to 9 days in spring (UV-Vis). On sampling, the pH of the natural water was recorded at 7.6 which confirm previously recorded literature (Baker *et al,* 2007) and was comparable to the spring natural water pH. Therefore changes to NP behaviour are not pH dependant.

Table 5.15: ICP-MS Semi Quantitative (± 20%) Elemental Concentrations of Natural Summer Vale Lake Water			
Element	**Concentration (ppb)**	**Element**	**Concentration (ppb)**
Li	3.7	**Zn**	27
B	140	**Ga**	ND
Na	19000	**Ge**	ND
Mg	4300	**As**	ND
Al	8.6	**Se**	0.5
Si	4300	**Br**	94
P	370	**Rb**	5.6
K	3300	**Sr**	130
Ca	19000	**Zr**	ND
Ti	2.4	**Mo**	1
V	1.1	**Ag**	0.7
Cr	0.3	**Sn**	ND
Mn	14	**Sb**	ND
Fe	260	**Ba**	22
Co	0.2	**Ce**	ND
Ni	2.3	**W**	ND
Cu	2.6	**Pb**	0.2

Table 5.11 identifies the elemental concentration of the summer seasonal Vale lake water before the AgNPs were exposed. As with the previous spring water study, various amounts of electrolytes that have vital effects on AgNP transport and behaviour were identified. Unlike the previous study Na (0.00082 mol/L), Mg (0.00017 mol/L) and Ca (0.00047 mol/L) were found in lower concentrations, which is particularly important as Ca and Mg are known to cause destabilization of the AgNP surface charge and thus cause aggregation (Li and Sun, 2011). However, the destabilizing effects caused by these divalent cations were reduced in the presence of higher NOM concentrations (Baalousha *et al,* 2013), when compared to the spring water study (UV-vis). The effects were surface coating specific as the citrate AgNPs were no longer visible by UV-Vis after 9 days in the previous study, whereas the PVP particles remained stable showing no change in the persistence throughout the duration of both studies. Other elements found in higher

concentrations such as Si, P, K, Ti, and Fe, all demonstrate that the chemical makeup of the natural water changes over the seasonal periods. Therefore, it is necessary to investigate AgNP behaviour in all seasonal conditions due to the changing water chemistry.

To summarise, the summer natural water study revealed a surface coating specific trends and differences between the seasonal water conditions. The present study contained more than double the TOC concentration when compared to the spring water study. The higher TOC concentration in this instance contributed to the persistence of the citrate AgNPs, although they aggregated and demonstrated sedimentation behaviour. Citrate AgNPs were observable for 12 days compared to 10 in the previous study. PVP AgNPs were also more stable in terms of their size and transport mechanisms when compared to the previous study. TEM size distributions revealed similar behaviour patterns to both the citrate and PVP AgNPs. In both instances the size distribution for the summer exposures was much smaller than in the spring water, further demonstrating seasonal differences in the water. Surface coating specific stability was observed by the PVP AgNPs, as they did not aggregate and followed diffusion throughout the mesocosm. ICP-MS results revealed reduced ionic strength (table 5.11) when compared to the spring water. Despite this, the water conditions were still optimal to cause destabilization, and aggregation of the citrate AgNPs, but increased NOM enabled them to be retained for longer in particulate/colloidal forms.

5.4.4 Autumn Natural Vale Lake Water

5.4.4.1 Modelled and Dissolved Silver Concentrations

The results for the observed and modelled (Socolofsky and Jirka 2004, and Hinderliter *et al,* 2010) total Ag concentrations are presented in figure 5.24 and conditions are presented in table 5.12.

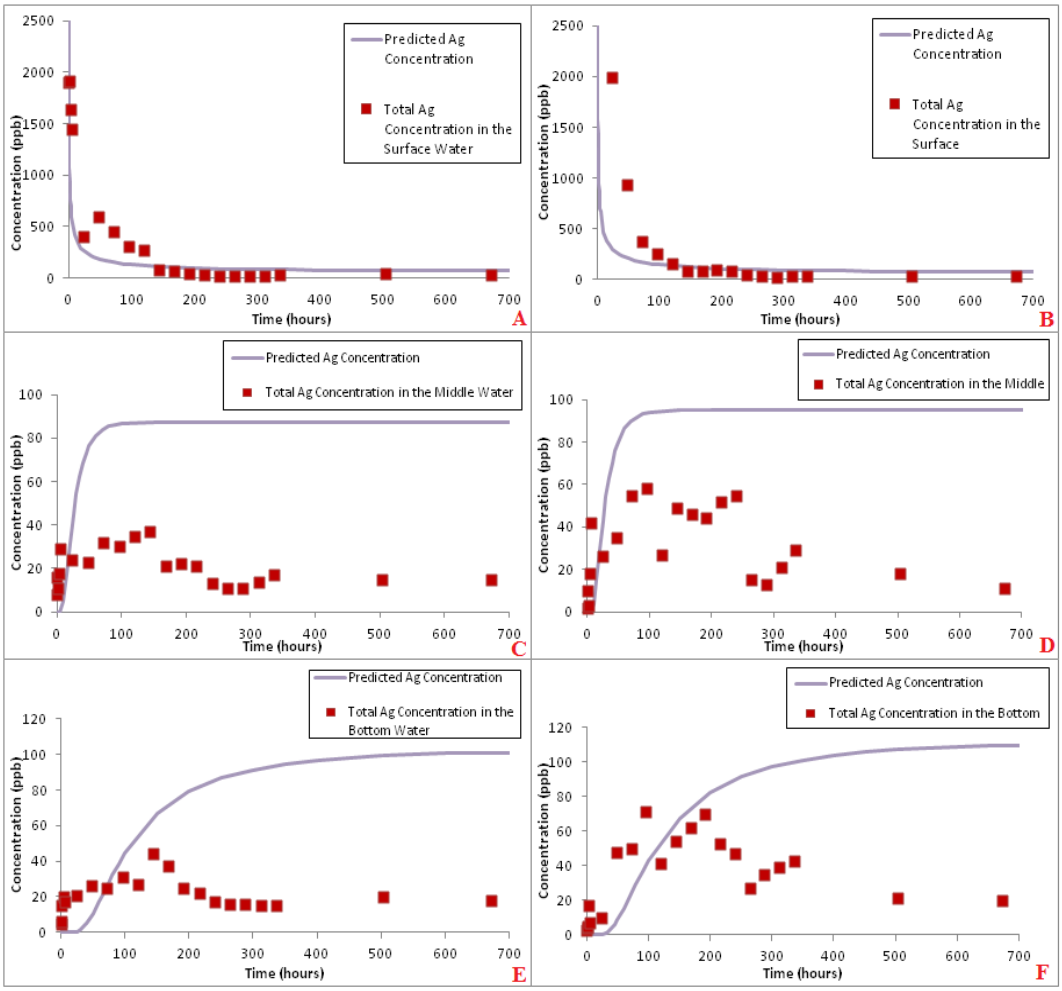

Figure 5.24: Model predicted Ag concentrations over time plotted against the average total Ag concentration obtained from the study for, A) citrate AgNPs in the surface, B) PVP AgNPs in the surface, C) citrate AgNPs in the middle, D) PVP AgNPs in the middle, E) citrate AgNPs in the bottom and F) PVP AgNPs in the bottom of the autumn natural lake water of the mesocosm. The model fits were based on a single 11 nm citrate and 12 nm PVP AgNP transporting through the mesocosm based on parameters in table 5.12.

Table 5.16: Model Parameters for AgNPs in Autumn Natural Lake Water				
Parameter	**Symbol**	**Unit**	**Citrate**	**PVP**
Diameter of AgNP	d	nm	11	12
Cross section area of the column	A	m^2	0.049	0.049
Column length	*L*	m	1	1
Column volume	*V*=A*L*	L	43	43
Dosing volume	*V*	L	0.391	0.215
Dosing concentration	C_0	ppm	11	20
Mass of Ag	M	mg	4.3	4.3
C column based on diffusion	M/*V*	ppb	100	100
Diffusion coefficient	*D*	$m^2 s^{-1}$	3.743.E-7	3.743.E-7
Sedimentation Velocity	*U*	ms^{-1}	6.40E-10	7.40E-10

Figure 5.24 shows the predicted and total Ag concentrations which were used to identify the transport behaviour of the AgNPs once released into the autumn natural water. Analysis of the citrate total Ag concentration between each depth of the mesocosm show the concentrations in the surface water fit the model predicted concentrations. A Pearsons correlation coefficient determined that the R^2 value in the surface water was 0.96, showing strong correlations between the observed and expected Ag concentrations. Over the first 5 days, high Ag concentrations between 406 ± 0.22 ppb after 24 hours and 266 ± 0.21 ppb on day 5 were retained in the surface water, which stabilise after day 8 at 41 ± 0.01 ppb (day 8) to 31 ± 0.08 ppb on day 28.

The middle and bottom depth do not follow the predicted Ag concentrations after 24 hours in the middle (R^2 0.02) and 5 days in the bottom (R^2 0.24). The parameters for an 11 nm AgNP are therefore insufficient and need to be adjusted to accommodate for size and concentration changes, due to aggregation and settling. Evidence of aggregation can be seen after 7 day, shown by sedimentation pattern of a gradual increase and decrease in concentration in the lower depths (Hinderliter *et al,* 2010). The difference in concentration over time infers a difference in the transport mechanism which changes

from diffusion in the surface water to sedimentation in the lower depths. The SPR data (figure 5.28) and TEM size analysis (table 5.16 and figure 5.29) strongly support aggregation and sedimentation of the citrate AgNPs. With this in mind, the model parameters were adjusted (table 5.13 and figure 5.25) to increase the R^2 values and show stronger correlations between the two sets of data. Due to the complexity of the transformations and behaviour changes over time, the new model parameters proved difficult to show a strong correlation between the two sets of data. The R^2 value for the middle was 0.52 and 0.47 for the bottom. Although the R^2 numbers are improved, they still do not show strong correlations between the model outputs and the observed total Ag concentration data. The best possible fits used reduced Ag concentrations with larger citrate AgNPs sizes, although these parameters only fit parts of the observed data at different times, i.e. the first 5 days for the middle and the last 14 days for the bottom, showing the citrate AgNPs were extremely unstable over time.

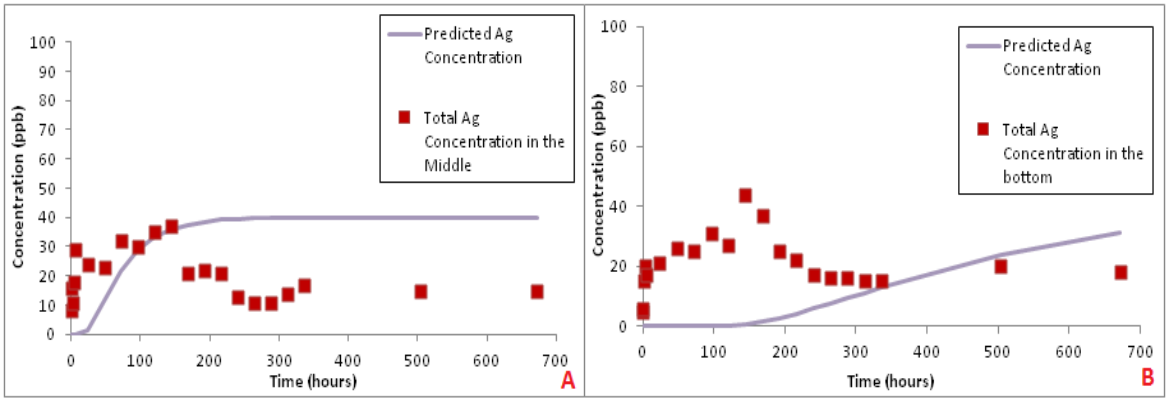

Figure 5.25: Adjusted model fits for changing model parameters for (A) the middle and (B) the bottom water, for citrate AgNPs exposed to autumn natural lake water. New model parameters are listed in table 5.13.

Table 5.17: Adjusted Model Parameters for Citrate AgNPs in Autumn Natural Lake Water			
Parameter	**Symbol**	**Unit**	**Measurement**
Diameter of AgNP	d	nm	30
Cross section area of the column	A	m^2	0.049
Column length	*L*	m	1
Column volume	*V*=A*L*	L	43
Dosing volume	*V*	L	0.391
Dosing concentration	C_0	ppm	5
Mass of AgNPs	M	mg	2
C column based on diffusion	M/*V*	ppb	45.5
Diffusion coefficient	*D*	$m^2 s^{-1}$	1.43E-7
Sedimentation Velocity	*U*	ms^{-1}	4.7 E-9

The surface concentrations for the PVP total Ag fit the model parameters based on a 12 nm particle (table 5.13) transporting through the mesocosm. The R^2 value in the surface water as 0.94, showing strong correlations between the observed and expected Ag concentrations. The total Ag concentration in the middle fits the model predictions for the first 3 days (72 hours) where the concentrations fall below the predicted and stabilises around 30 ± 0.02 ppb on day 4 (96 hours) which is continuous until day 10 (240 hours). After day 10 the concentration falls to 10 ± 13 0.01 ppb, where it remained constant for the rest of the study. Despite the drop in concentration over time, the stabilisations of total Ag concentrations in the middle follow a diffusion transport mechanism.

The total Ag for the PVP AgNP study in the bottom of the mesocosm fit the modelled parameters following diffusion with an R^2 value of 0.72, until day 9 where the concentration falls to 53 ± 0.02 ppb. From Day 9 the Ag concentration becomes unstable showing a small peak between days 10 and 14 indicating the possibility of sedimentation as larger concentrations of Ag settle. The differences in the observed concentration show a difference to the transport mechanism followed by the AgNPs. The interpretation of the

transport behaviour, and quality of the model fits between the observed and expected Ag concentrations can be achieved by adjusting the model parameters accordingly. Table 5.14 and figure 5.26 show the adjusted model parameters for the middle and bottom depth for the PVP AgNP study, accounting for concentration losses from settling. Due to changes in the behaviour over time the new model parameters proved difficult to produce a strong correlation for the middle depth, although the R^2 values were improved from 0.009 to 0.21 showing weak correlations. The R^2 value of 0.72 in the bottom was further improved to 0.97, showing stronger relationships between the model and observed concentrations.

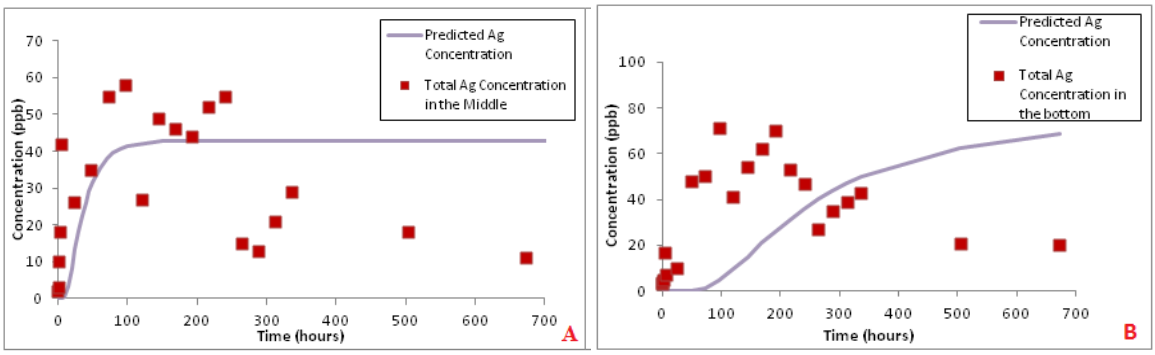

Figure 5.26: Adjusted model fits for (A) the middle and (B) the bottom water, for PVP AgNPs exposed to autumn natural lake water. New model parameters are listed in table 5.14.

Table 5.18: Adjusted Model Parameters for PVP AgNPs in Autumn Natural Lake Water

Parameter	Symbol	Unit	Middle	Bottom
Diameter of AgNP	d	nm	15	20
Cross section area of the column	A	m^2	0.049	0.049
Column length	*L*	m	1	1
Column volume	*V*=A*L*	L	43	43
Dosing volume	*V*	L	0.215	0.215
Dosing concentration	C_0	ppm	9	5
Mass of AgNPs	M	mg	1.9	1.1
C column based on diffusion	M/*V*	ppb	245	25
Diffusion coefficient	*D*	$m^2 s^{-1}$	2.86E-7	1.72E-7
Sedimentation Velocity	*U*	ms^{-1}	1.2 E-9	3.2 E-9

At the end of the study, the total Ag concentrations were comparable to the concentrations observed in both the previous natural water studies for the citrate particles only. The total Ag concentrations at the end of the PVP study were comparable with those from the summer water study, but considerably smaller than those from the spring profiles and the model predictions, indicating the possibility of losses incurred during analysis. Samples were examined to identify between the AgNP concentrations and the Ag^{+} concentrations presented figure 5.27.

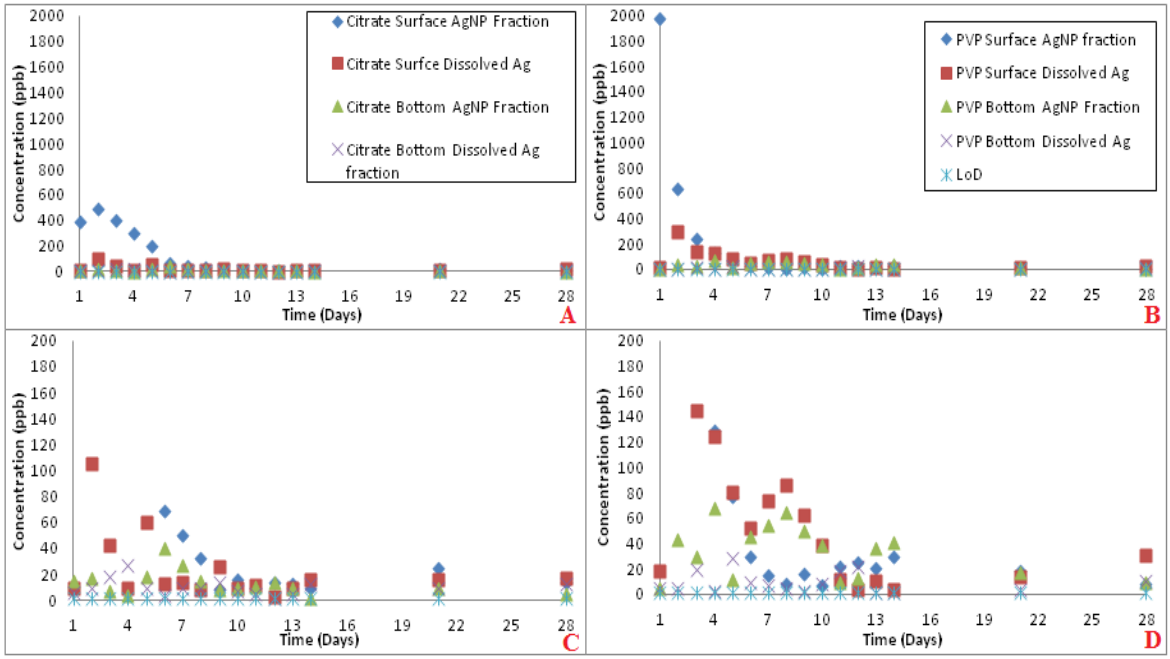

Figure 5.27: Dissolved Ag and AgNP concentrations (ppb) using ultrafiltration in the autumn lake water: A) citrate Ag^{+} and AgNP concentrations in the surface and bottom depth water for each day, B) PVP Ag^{+} and AgNP concentrations in the surface and bottom depth water for each day, C) shows the same graph as A for concentrations below 200 ppb, D) shows the same graph as B for concentrations below 200 ppb. Note the LoD = Instrumentation limit of detection at 2 ± 0.2ppb.

With reference to the summer water AgNP releases, the results presented in figure 5.27 identify that both particle coating had similar compartmental movement for the AgNP

and Ag^+ concentrations. The increased Ag^+ concentrations for both citrate and PVP AgNP studies are coherent with decreased AgNP concentrations for each depth, indicating that as the AgNPs dissolve, the Ag^+ concentrations increase in solution. Equally in reverse, when Ag^+ reduces in concentration, the AgNP concentration increase providing evidence of NP re-formations in both studies. Further explanations of rising NP concentrations within the compartments, could be due to the breakage of aggregates and the release of smaller particles that diffuse back into the different water compartments (Li *et al,* 2013).

Analysis of the citrate AgNPs in the surface water show a decline in concentration from 396 ppb on day 1 to 69 ppb on day 6. A loss of concentration indicates the movement of citrate AgNPs into the lower compartments, as the AgNP concentration in the bottom rises from 15 ppb on day 1 to 40 ppb on day 6, which is consistent with model predictions. The Ag^+ concentrations in the surface water fluctuate between 10 ± 0.23 ppb on day 1, 14 ± 0.18 ppb on day 7, 16 ± 0.01 ppb on day 14, 16 ± 0.24 ppb on day 21 and 17 ± 0.5 ppb on day 28. Therefore the concentration of Ag^+ remains stable in the surface water with only a couple of outliners on day 2 at 105 ± 1.25 ppb and day 5 at 60 ± 0.32 ppb. The outliers in concentrations may be due to increased Ag^+ from AgNP dissolution in the surface water. Although the elevations are not consistent, the information suggests Ag^+ diffuses out of the area, as concentrations in the surface water equilibrate to remain stable and consistent to the total Ag model prediction.

The citrate AgNP concentration in the bottom of the mesocosm elevates on days 2 (17 ppb) and 6 (40 ppb), indicating the sedimentation of larger particulates as visualised from the SPR and TEM data presented in figures 5.28 and 5.29. Simultaneously, as the concentration of AgNPs increase in the bottom, the Ag^+ concentrations were reduced to

9 ± 0.3 ppb on day 2, and 4 ± 0.5 ppb on day 6. Concentrations of Ag^+ in the bottom were close to the instrumentation limits of detection, nonetheless, the reduced Ag^+ concentrations indicate possible AgNP reformation and/or the diffusion of Ag^+ back into the higher compartments.

Analysis of the PVP AgNP concentration in the surface water declines from 1977 ppb (table A2.12 additional information) on day 1 to 30 ppb on day 6. After day 6 the AgNP concentration remained stable in the region of 17 ± 8 ppb for the rest of the study. The Ag^+ concentration in the surface water increases between day 2 (295 ppb ± 0.2) and day 4 (124 ± 0.03), indicating AgNP dissolution as the increased Ag^+ concentrations are consistent with reduced AgNP concentrations. Overall the total Ag concentration in the surface water fit the model profiles in the surface water. Analysis of the PVP AgNP concentrations in the bottom was consistently higher than those recorded for the citrate AgNPs (table A2.12 in the addition information), indicating surface coating specific differences and PVP AgNP stability. The total Ag concentrations for the bottom mesocosm fit the modelled parameters following diffusion until day 9 where concentrations are reduced, possibly due to AgNP losses from accumulation at the bottom of the mesocosm.

Overall, declines in PVP AgNP concentrations were consistent with rises in the Ag^+ concentrations in each depth, identifying that PVP AgNPs are subject to dissolution in natural water. Both the citrate and PVP AgNPs were still identified in small concentrations at the end of the study, despite not being seen in the UV-Vis spectra after 12 days for the citrate AgNPs and 14 days for the PVP AgNPs.

5.4.4.2 UV Analysis

Figure 5.28 (A-F) shows the SPR profiles for citrate and PVP particles over time in the surface, middle and bottom of the mesocosm tanks.

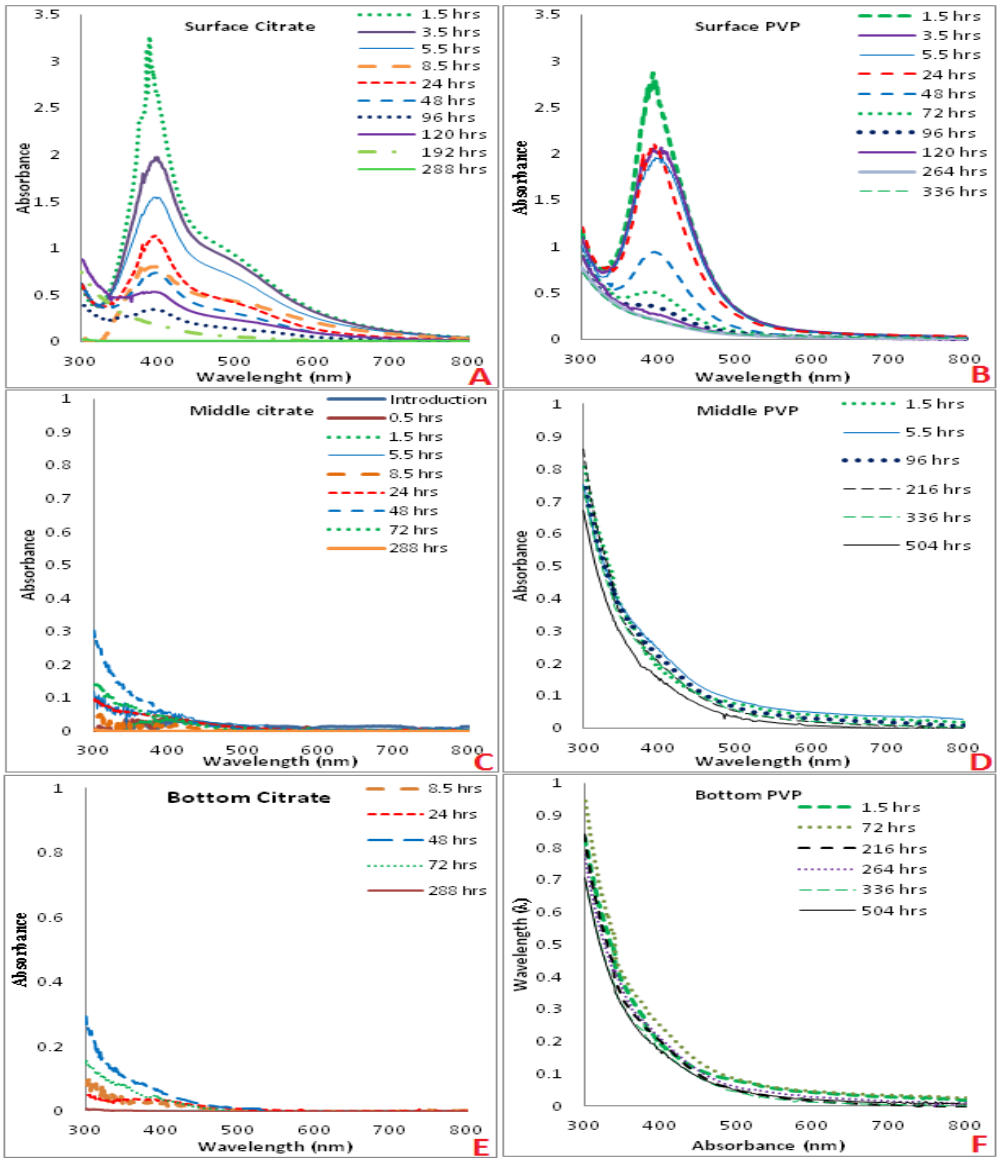

Figure 5.28: UV SPR profiles taken from different depths of the mesocosm column when exposed to natural Vale Lake water in autumn. A) Citrate coated AgNPs at the surface, B) PVP AgNPs at the surface, C) citrate AgNPs from the middle, D) PVP AgNPs from the middle, E) Citrate AgNPs from the bottom and F) PVP AgNPs from the bottom. Note that the Y axis for the graphs are not presented in the same scale for each of the depths, as detail from the lower regions would be lost.

When the citrate AgNPs were released in to the autumn seasonal natural water, they demonstrated the highest amounts of aggregation determined by the increased absorbance intensity of the tailing peak in the 500-800nm region (Chinnapongse *et al*, 2011, and Li *et al,* 2010). Aggregation of the citrate AgNPs was also evidenced in the total Ag data (figure 5.21), highlighted by the peaks in concentration in the lower depths as the larger particles settle. The additional SPR peak was also never seen in the PVP AgNP water profiles in the present study, highlighting particle coating specific behaviour and transformations. In comparison to the summer water, the autumn water exposures also show the citrate AgNPs presence in the surface water for 12 days (288 hours). The repeated persistence of the citrate AgNPs provides evidence that there was a high concentration of NOM in the autumn seasonal water. Citrate AgNPs in the lower depths were predominantly low in concentrations, as highlighted by the drop in intensity of the SPR peaks indicating the possibility of rapid dissolution when compared to the previous studies. Low concentrations of Ag were also observed in the total Ag concentration model predictions. Despite the possibility of rapid dissolution to explain the reduction in concentration, the citrate AgNPs lose UV signal after 12 days (288 hours) for each of the water depths. A small SPR quadrupole interference peak between 300-350nm for the citrate particles was due to signal from the NOM (Zou *et al,* 2007, and Kawaguchi *et al,* 2011).

PVP AgNPs in the surface water remained stable as indicated by the SPR peak, comparable to PVP AgNPs characterised in chapter 3 before release into the natural water. The stability of the PVP AgNPs confirmed the modelled data in figure 5.241 and the AgNP concentrations in figure 5.27. Visualisations of the PVP AgNPs in the lower

water were not possible in the lower depths of the mesocosms, due to large interferences of the SPR patterns. It was also not possible to visualise a UV response after 14 days (336 hours) due to the NOM signal. Therefore, more evidence was needed as later discussed to assess the transformations of the PVP AgNPs.

5.4.4.3 Transmission Electron Microscopy (TEM) Analysis and Energy Dispersive X-Ray (EDX) Analysis

As discussed in chapter 3, citrate AgNPs were characterised by TEM at 11 ± 3 nm (section 3.5.1.4), and 12 ± 2 nm (section 3.5.2) for the PVP AgNPs. These sizes were used to determine changes that occur to the NPs once released in to the natural water and were used in the modelled parameters used to predict the total Ag in each depth.

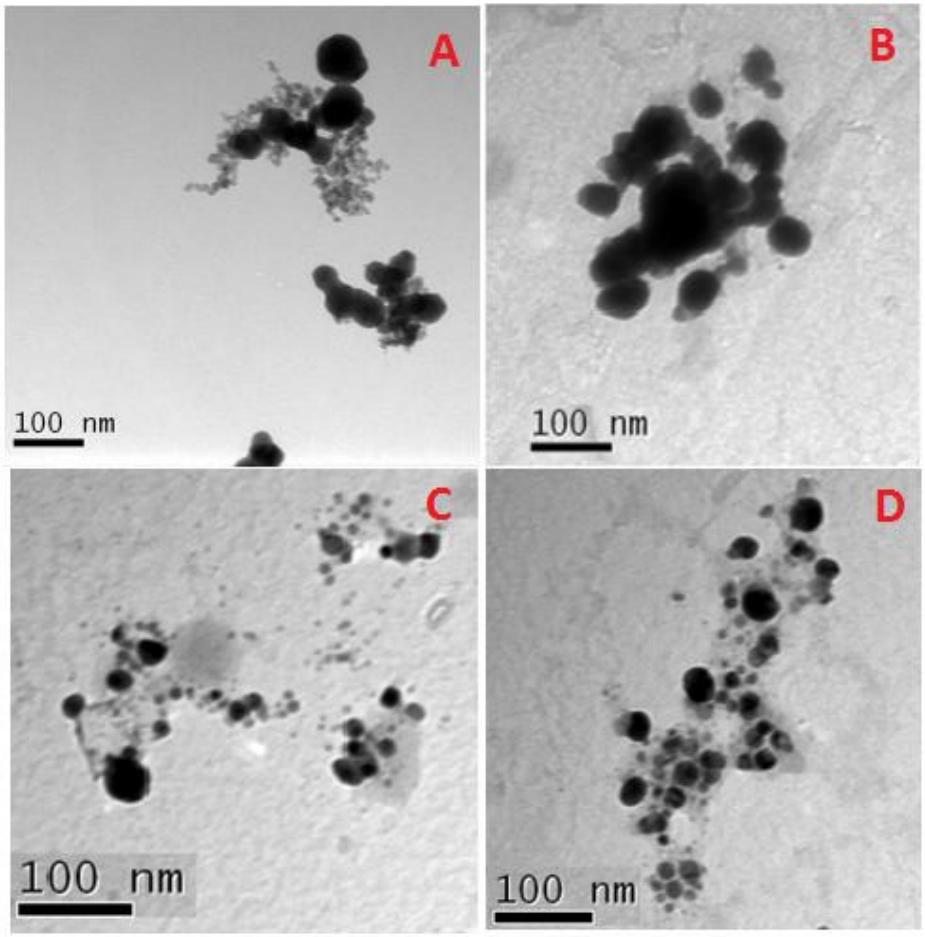

Figure 5.29: TEM images of citrate AgNPs exposed the autumn natural Vale lake water identified at A) 24 hours in the surface, B) 24 hours in the bottom, C) 120 hours in the surface surface, and D) 120 hours in the bottom of the mesocosm. Corresponding histograms are presneted in figure 5.30.

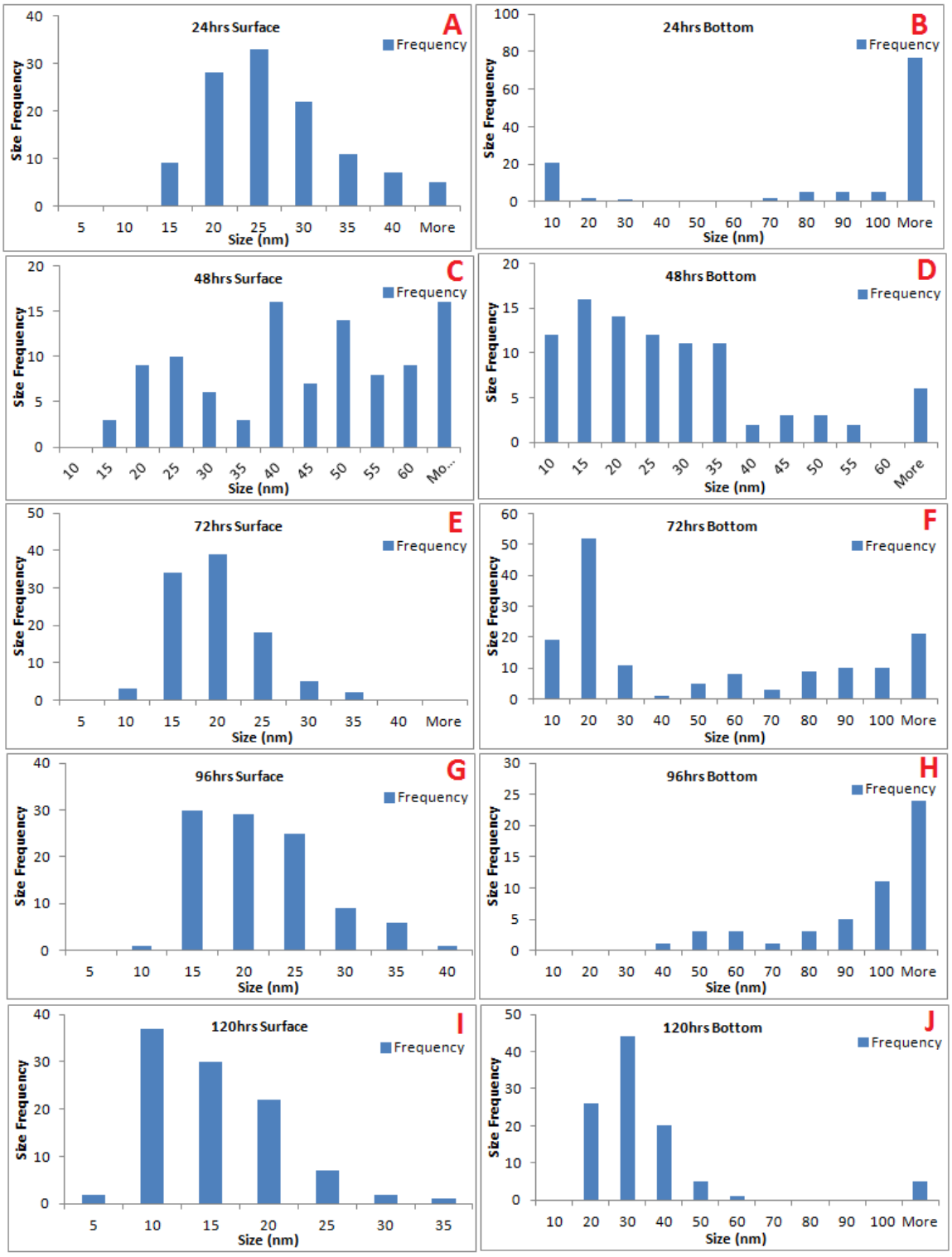

Figure 5.30: TEM size frequency histograms for citrate AgNPs exposed to autumn natural Vale lake water at A) 24 hours in the surface B) 72 hours in the surface and C) 72 hours in bottom of the mesocosm. Histograms A-J corresponds to the images presented in figure 5.29.

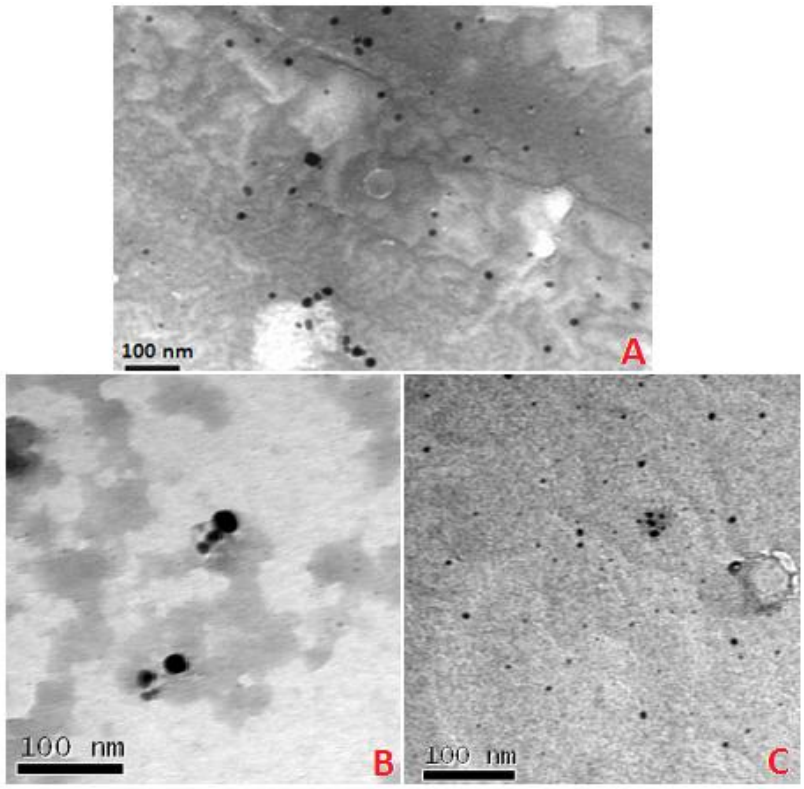

Figure 5.31: TEM image of PVP AgNPs exposed the autumn natural Vale lake water identified at A) 24 hours surface waters, B) 72 hours surface water C) 72 hours bottom water. Corresponding histograms are presented in figure 5.32.

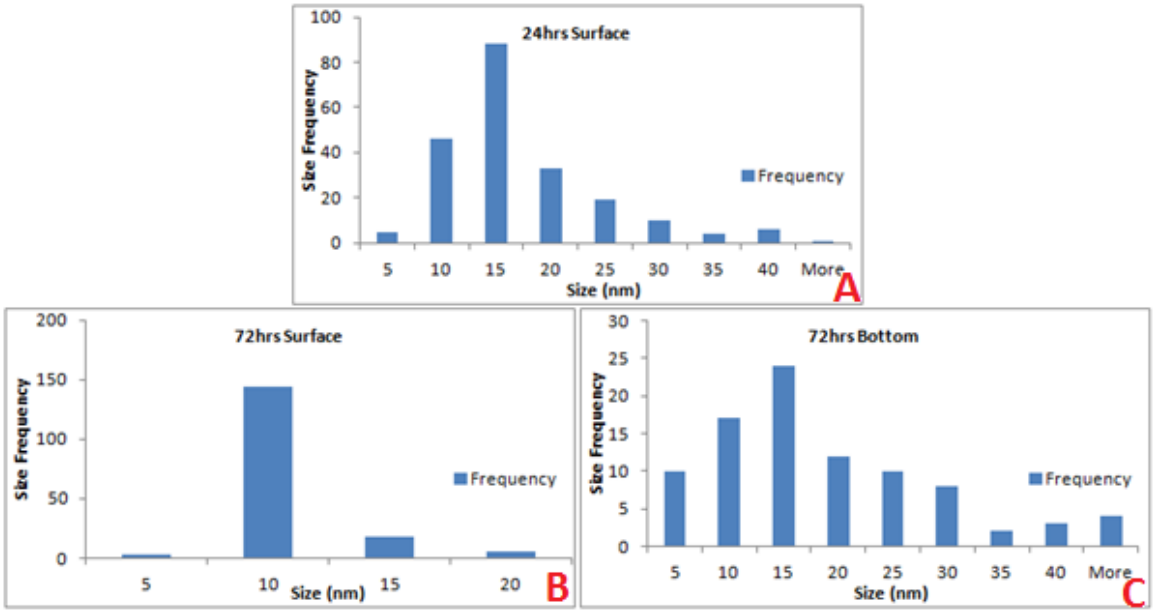

Figure 5.32: TEM size frequency histograms for PVP AgNPs exposed to autumn natural Vale lake water at A) 24 hours in the surface water, B) 72 hours in the surface water and C) 72 hours in the bottom area of the mesocosm. Histograms correspond to the images presented in figure 5.31.

Table 5.15: TEM sizes (nm) at different time points for citrate and PVP particles exposed to autumn season natural Vale Lake water. *n= number of particles counted*ND = Not Determined.

Table 5.19: Average Size by TEM for AgNPs Exposed to Autumn Natural Water										
Time (hours)	**24**		**48**		**72**		**96**		**120**	
Area Analysed	**Surface**	**Bottom**	**Surface**	**Bottom**	**Surface**	**Bottom**	**Surface**	**Bottom**	**Surface**	**Bottom**
Particle type	**Citrate AgNPs**									
Size (nm)	25 ± 8	125 ± 81	43 ± 16	33 ± 534	18 ± 5	52 ± 54	19 ± 6	101 ± 35	13 ± 6	35 ± 38
n	115	118	101	81	102	148	100	41	101	100
***p* value**	3.683E-34	1.445E-29	2.583E-35	2E-04	9E-25	6.32229E-16	2.58341E-24	7.44016E-24	0.00402	2.28E-08
Particle Type	**PVP AgNPs**									
Size (nm)	15 ± 8	ND	ND		8 ± 2	17 ± 11	ND		ND	
n	111				171	91				
***p* value**	1.521E-08				3.46E-44	5.164E-05				

Citrate AgNPs in the surface water were significantly larger at 25 ± 8 nm (*p* 3.683E-34) than the original sizes (11 ± 3 nm) after 24 hours release (TEM). Citrate AgNPs in the bottom water after 24 hours were also significantly larger at 125 ± 81 nm (*p* 1.445E-29). The most frequently sized citrate AgNP in the surface water at 24 hours was 25 nm (figure 5.25A), compared to those sized larger than 100 nm (figure 5.30B) in the bottom. Information confirms that the AgNPs have aggregated and sediment, as described by the transport patterns in the total Ag concentrations (figures 5.21C and 5.21E). Figures 5.29A and 5.29B demonstrate the significant difference in the size and morphology of the particles located in the extreme depths. Figure 5.29A shows aggregated particles surrounded by a grey matter believed to be NOM (Chen and Elimelech, 2007), or those of sulfide bridges (Levard *et al,* 2011). Although not as predominant, the grey matter surrounding the particles was also seen in figure 5.8 for the previous spring seasonal

water. NOM from the natural water can attach by adsorption on to the NP surface, which is caused by hydrophobic interactions, electrostatic interactions and hydrogen bonding depending on the surface charge (Navarro *et al,* 2008). Adsorption onto the particle surface can be seen in figure 5.29B where the NPs appear to be encapsulated by the NOM. The re-coating of the NPs could have led to increased electrostatic repulsion (Li and Sun, 2011) and thus, increased the stability of the citrate particles in the present water set compared to the spring water set.

As time increased the citrate AgNPs grow further to 43 ± 16 nm (*p* 2.583E-35) in the surface water at 48 hours, and larger particulates sediment to the bottom of the mesocosm. At 48 hours there is a completely different size distribution between the two depths, with each histogram (figures 5.30C and 5.30D) showing bimodal shape distributions. The bimodal size distribution demonstrates continuous aggregation of the previously smaller particles as the exposure time progressed. The citrate AgNPs were recorded at 33 ± 53 nm in the bottom of the mesocosm at 48 hours with a size distribution (figure 5.30D) of particulates sized between 10-35 nm not visualised 24 hours previously. The presence of smaller particulates in the lowest depths could be due to dissolution or disaggregation, resulting in reduced particle size. Disaggregation/dissolution of the larger NPs would also describe why the size distribution continuously changes in the lowest depths of the mesocosms, whereas, after 72 hours the AgNP size distributions remain stable in the surface waters.

After 5 days exposure (120 hours) the citrate AgNPs in the surface water are progressively smaller at 13 ± 6 nm. The citrate AgNPs in the bottom of the mesocosms are irregular sized over time, due to a combination of aggregation, dissolution, breakage

of aggregates and re-formed AgNPs. Despite irregular sizing of the citrate AgNPs in the bottom, they are consistently larger than those suspended in the surface water (table 5.10). Figures 5.30C and 5.30D identify citrate AgNPs after 5 days (120 hours) release in the autumn natural water, and highlight further changes in the reduced size and morphology when compared to 24 hours exposure. Particles are still surrounded by the grey matter but appear visually smaller and less aggregated. A larger proportion of very small particulates in images 5.30C and 5.30D can be observed due to dissolution, disaggregation and AgNP formation in suspension.

Observations were not possible for bottom of the mesocosm PVP AgNPs at 24 hours in the bottom area, 48 hours, 96 hours or 120 hours due to low concentrations of NPs and large amounts of impurities on the TEM grids. Despite the loss of data at these time points, the PVP AgNPs in surface water still follow the same trend as the citrate particles, with the smaller particles retained in the surface and larger particulates in the bottom of the mesocosm. When compared to the citrate AgNPs in figure 5.29A and 5.29B at 24 hours, the general size morphology of the PVP AgNPs at 24 and 72 hours (figure 5.31) are different. In the surface and bottom depth, the PVP AgNPs (figure 5.31) are small singular spheres, determining that the transformations that occur to the NPs in natural water are surface coating specific. Further surface coating differences were reported with average size of the PVP AgNPs at 15 ± 8 nm at 24 hours maintaining NP stability.

At 72 hours the PVP AgNPs were smaller than the citrate AgNPs with particulates recorded at 8 ± 2 nm in the surface and 17 ± 11 nm in the bottom. The corresponding size histograms presented in figure 5.32 also demonstrated differences in the size

distribution of the PVP AgNPs in the surface water between 24 hours and 72 hours. Overall the size and morphology of the PVP AgNPs show that they remain stable when compared to the citrate AgNPs. EDX was used to determine and confirm the presence of citrate and PVP AgNPs in figures 5.33 and 5.34.

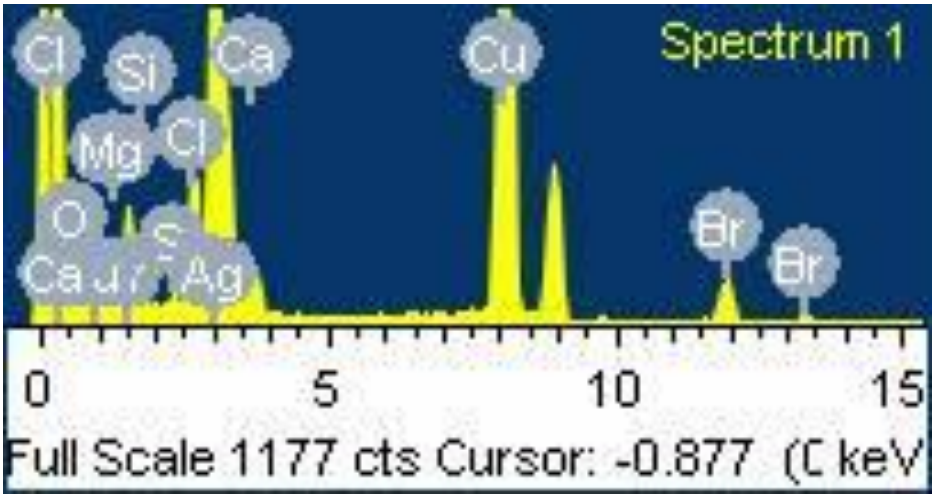

Figure 5.33: EDX spectrum of citrate AgNPs identified after 24 hours in the surface of the autumn natural water.

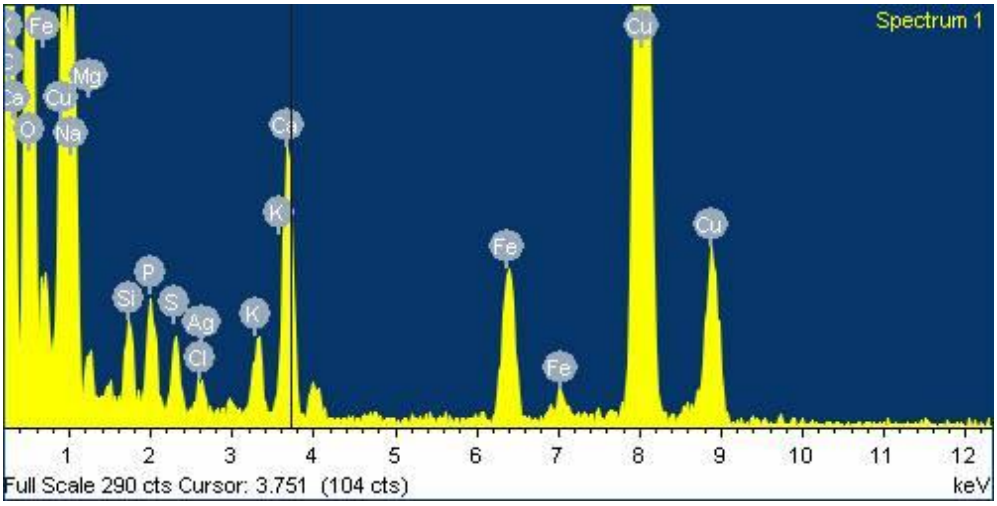

Figure 5.34: EDX spectrum of PVP AgNPs identified after 24 hours in the surface of the autumn natural water.

EDX analysis of the citrate AgNPs in autumn natural water (figure 5.33) identified bromine (Br), Cl, Ca, O, S, Mg, and Si, comparable to previous water profiles. AgNP

presence was confirmed by the Ag peak, the Cu peaks are background noise from the TEM grid used to mount the sample and the O peak is most likely from the ambient air when imaging. Although, O may indicate the presence of DO, which will contribute to the aggregation and dissolution of citrate AgNPs via oxidation at the surface of the NPs (Li and Lenhart, 2012). Zhang *et al* (2011) also observed that AgNPs aggregated 3-8 times faster in the presence of DO when compared to studies absent of DO. Depending on the redox state and the species of the elements presents, AgNPs are predicted to interact with Cl and S ions (Leavrd *et al,* 2013). The presence of S in the water profiles contributes to the possibilities of sulfide bridges linking the particles, as visualised in figure 5.29. Other transformations that may have occurred due to the water chemistry are $AgCl_2$ complexes, highlighted by the Ag and Cl presence in the EDX spectrum (figure 5.31).

In comparison to the citrate AgNPs, elemental analysis of the PVP AgNPs in the natural water (figure 5.34) revealed the presence of Cl, Mg, Si, S, O, Ca, K, C, Fe, Cu, Na, P, Ag, and Cu. The Ag peak confirms the presence of AgNPs. The Cu and C peaks are due background noise from the TEM grid. Furthermore, the C peak could also have been attained from NOM as a function of TOC, encapsulating the particle surface.

5.4.4.4 Inductively Coupled Plasma Mass Spectrometry (ICP-MS) and Total Organic Carbon (TOC) Analysis

Water chemistry is particularly important as it will determine AgNP behaviour and partitioning. The TOC was recorded at 28.31 mg L^{-1}, slightly lower than the summer season at 31.70 mg L^{-1}, but higher than spring at 12.59 mg L^{-1}. The reduction in NOM concentration is visualised in figure 5.28, by presence of the SPR peak between 300-

350nm (Zou *et al,* 2007, and Kawaguchi *et al,* 2011). The SPR peak is less predominant in the present study compared to the summer, which confirms the TOC analysis that the NOM concentration is lower in autumn. The PVP particles gave a SPR signal in the surface water until day 14, which was not comparable to the spring and summer waters. Increased Ag^{+} concentrations were also seen in the surface water (figure 5.27), confirming reduced NOM concentration reduces the stability of the PVP AgNPs. However, when compared to the summer water set, larger PVP AgNP concentrations were seen in the bottom of the mesocosm. The depth specific stability maybe due to the NOM in the water being of high molecular weight (Akaighe *et al,* 2012) and sinking to the bottom of the mesocosm, where it can absorb to particles that have settled and increase their stability. Similarly, the citrate AgNP were also more unstable in the surface water, demonstrated by a dominant SPR tailing in figure 5.28A, showing aggregation. Reduced citrate AgNP concentrations were also seen in the bottom of the mesocosm highlighting the instability of the citrate surface coating compared to PVP. The pH on sampling of the natural water was 7.4, comparable with all previous results.

Table 5.20 : ICP-MS Semi Quantitative (± 20%) Elemental Concentrations of Natural Autumn Vale Lake Water			
Element	**Concentration (ppb)**	**Element**	**Concentration (ppb)**
Li	2.6	**Zn**	67
B	120	**Ga**	ND
Na	14000	**Ge**	ND
Mg	4400	**As**	ND
Al	37	**Se**	0.8
Si	4900	**Br**	62
P	190	**Rb**	4.3
K	2200	**Sr**	120
Ca	21000	**Zr**	ND
Ti	2.3	**Mo**	1.1
V	ND	**Ag**	0.5
Cr	0.3	**Sn**	0.1
Mn	48	**Sb**	ND
Fe	450	**Ba**	35
Co	0.3	**Ce**	ND
Ni	20	**W**	ND
Cu	6.3	**Pb**	7.5

Table 5.16 describes the changes in water chemistry by identifying elevated levels of Ca, Mg, Si, Mn, Fe, Ni, Cu, and Zn when compared to summer. A decline in the concentration of Na, P, and K were also observed. Particular interest is given to the elevated levels of Ca^{2+} (0.00052 mols/L) and Mg^{2+} (0.00028 mols/L), compared to the previous water set (summer) as divalent cations have been shown to increase particle aggregation (Stankus *et al,* 2011, Zhang and Oyanedel-Craver, 2012).

To summarize, citrate AgNPs showed the highest extent of aggregation compared to the previous water sets, highlighted by the SPR profiles (figure 5.28). Larger particulates were also evidenced in the TEM analysis (Table 5.15), which identified the highest recorded sizes in the surface and bottom region compared to the previous studies. Although there was evidence of sedimentation from the movement of the total

Ag, the PVP AgNPs did not identify large aggregation as shown in the TEM imaging and the SPR peaks, showing surface coating specific behaviour differences.

ICP-MS results identified that the majority of the electrolytes present were comparable with concentrations found in the summer water. Therefore, the autumn water conditions were optimal in terms of ionic strength to cause destabilization, aggregation of the citrate AgNPs. Citrate AgNPs gave an SPR signal until 12 days after release in the surface water, comparable to the summer water results. Combined characterisation from the dissolution studies and SPR data, provides enough evidence to suggest that the effects of the reduced TOC concentration compared to the summer water saw destabilising effects to the citrate AgNPs, whereas the PVP AgNP remained stable.

5.4.5 Winter Natural Vale Lake Water

5.4.5.1 Modelled Total and Dissolved Ag Concentrations

The results for the observed and modelled (Socolofsky and Jirka 2004, and Hinderliter *et al,* 2010) total Ag concentrations are presented in figure 5.35 and conditions in table 5.17.

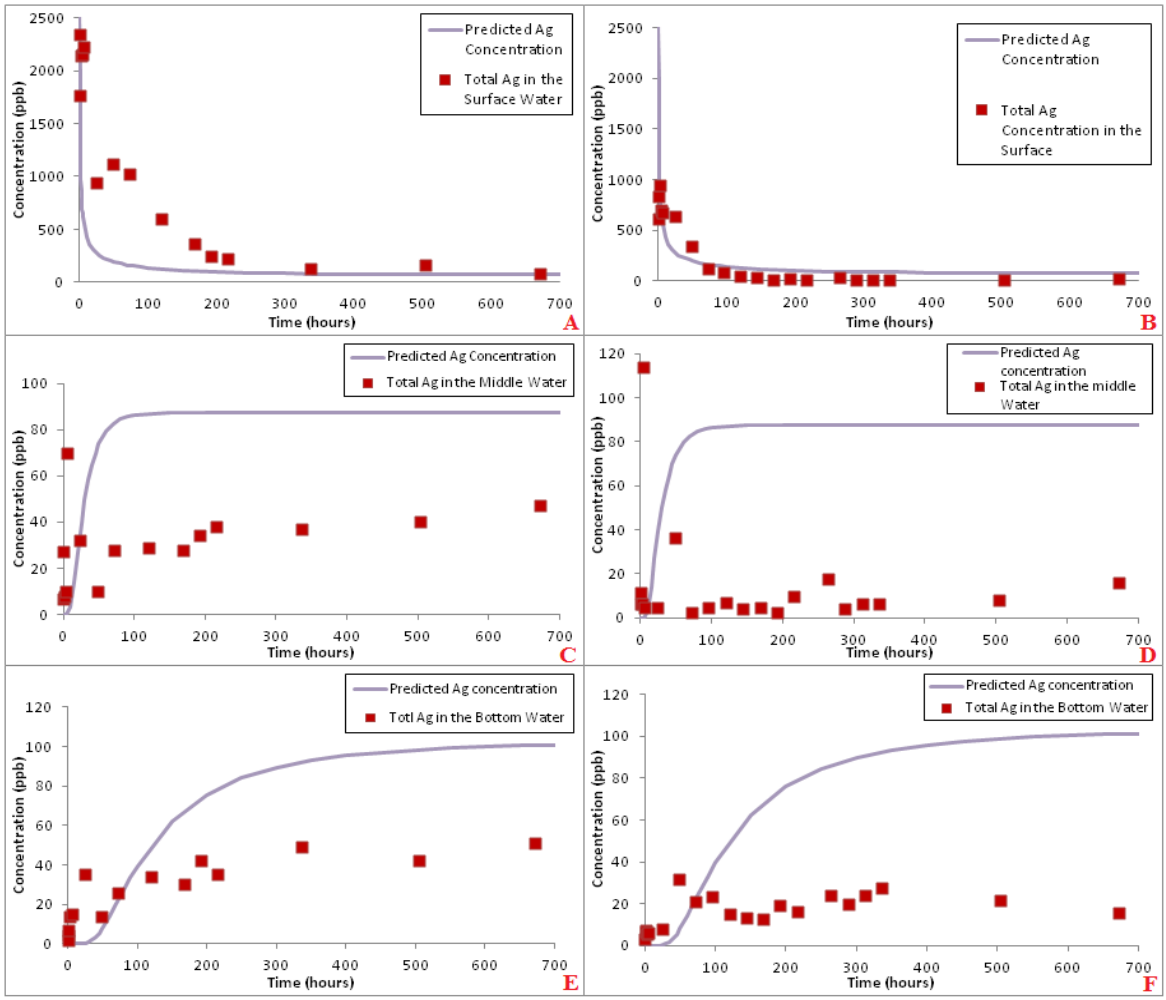

Figure 5.35: Model predicted concentrations over time plotted against the average total Ag concentration obtained from the study for, A) citrate AgNPs in the surface, B) PVP AgNPs in the surface, C) citrate AgNPs in the middle, D) PVP AgNPs in the middle E) citrate AgNPs in the bottom and F) PVP AgNPs in the bottom of the winter natural lake water of the mesocosm. The model fits were based on a single 12 nm AgNP transporting through the mesocosm based on parameters in table 5.17.

Table 5.21: Model Parameters for AgNPs in Winter Natural Lake Water				
Parameter	**Symbol**	**Unit**	**Citrate**	**PVP**
Diameter of AgNP	d	nm	12	12
Cross section area of the column	A	m^2	0.049	0.049
Column length	*L*	m	1	1
Column volume	*V*=A*L*	L	43	43
Dosing volume	*V*	L	0.391	0.215
Dosing concentration	C_0	ppm	11	20
Mass of Ag	M	mg	4.3	4.3
C column based on diffusion	M/*V*	ppb	100	100
Diffusion coefficient	*D*	$m^2 s^{-1}$	3.579.E-7	3.743.E-7
Sedimentation Velocity	*U*	ms^{-1}	7.40E-10	7.40E-10

Analysis of the citrate AgNP total Ag concentration as seen in figure 5.35, show the observed Ag concentrations follow the model predictions in the surface water based upon parameter fits listed in table 5.17. The R^2 value in the surface water was 0.77, confirming a good correlation between the modelled and observed data.

The total Ag concentrations in the middle and bottom of the mesocosm did not fit those of the predictions, suggesting potential Ag losses for both particle types. The R^2 value for the middle was 0.66 and 0.69 in the bottom, showing small correlations between the two sets of data. The lower depths are harder to model due to the changing behaviour and transformations of the AgNPs, therefore the original parameters were no longer valid after longer exposure periods. The model was adjusted to adapt to the changes in the AgNP behaviour and concentration losses due to Ag sticking to the mesocosm wall, or settling at the bottom, to which the model was not adapted for, seen in figure 5.36 and table 5.18. Original citrate AgNPs as characterised in chapter 3 for the winter batch of particles were 12 ± 2 nm (TEM). To fit the model parameters we increased the citrate AgNP size to 30 nm (middle depth) and 20 nm (bottom depth) as seen in the TEM size distributions (figure 5.41). The dosing concentration was also

reduced to account for losses of Ag. When a Pearsons correlation test was performed on the new model adjustments in comparison to the observed data, the R^2 value for the middle and bottom were both increased to 0.76, showing stronger relationships between the two sets of data and validating the transport processes. After 24 hours the total Ag in the middle of the mesocosm is 32 ± 0.01 ppb, where it remained stable for the duration of the study, with a slight increase to 47 ± 0.05 ppb on day 28. The total Ag in the bottom also showed a steady increase in concentration from 35 ± 0.05 ppb at 24 hours to 51 ± 0.05 on day 28. Information suggests the transport mechanism of the Ag follows diffusion to maintain a steady concentration gradient between the depths which is in agreement with Ficks Law (Fick, 1855).

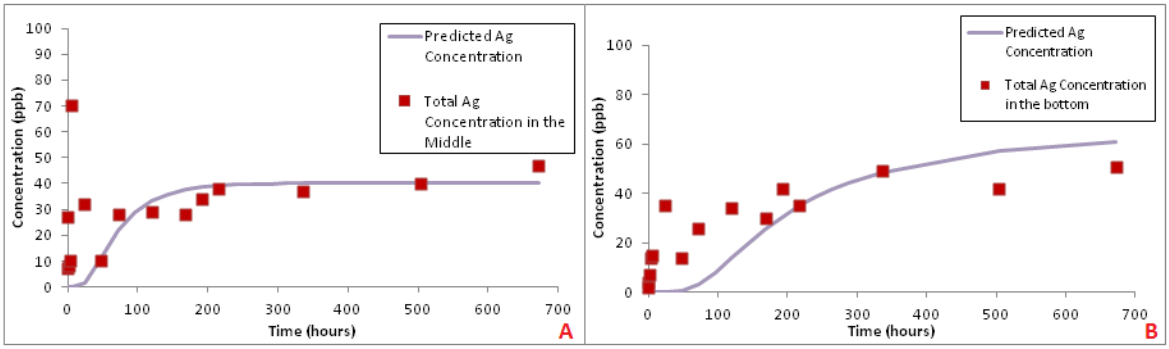

Figure 5.36: Adjusted model fits for new model parameters for (A) the middle and (B) the bottom water, for citrate AgNPs exposed to winter natural lake water. New model parameters are listed in table 5.18.

Table 5.22: Adjusted Model Parameters for Citrate AgNPs in Winter Natural Lake Water

Parameter	Symbol	Unit	Middle	Bottom
Diameter of AgNP	d	nm	30	20
Cross section area of the column	A	m^2	0.049	0.049
Column length	*L*	m	1	1
Column volume	*V*=A*L*	L	43	43
Dosing volume	*V*	L	0.391	0.391
Dosing concentration	C_0	ppm	5	7
Mass of Ag	M	mg	2	2.7
C column based on diffusion	M/*V*	ppb	45.5	63.7
Diffusion coefficient	*D*	$m^2 s^{-1}$	1.431E-7	2.147E-7
Sedimentation Velocity	*U*	ms^{-1}	4.7E-9	2.1E-9

Analysis of the PVP AgNP total Ag concentration (figure 5.35), show the observed Ag concentrations follow the model predictions in the surface water based upon parameter fits listed in table 5.17. The R^2 value in the surface water was 0.79, confirming a good correlation between the modelled and observed data. However, the R^2 values confirmed that was no correlation for the middle and bottom depths with values of 0.12 (middle) and 0.34 (bottom).

At 24 hours the concentrations of total Ag in the middle were close to the instrumentation limits of detection at 5 ± 0.02 ppb. Concentrations remained low for the duration of the study, but maintained a concentration gradient, with some deviations at 48 hours at 36 ± 0.03 ppb, 264 hours at 17 ± 0.12 ppb and day 28 at 16 ± 0.05 ppb. The deviations in concentration show Ag diffusing in and out of the middle depth as it settles to the bottom. Concentrations of Ag in the bottom of the mesocosm were higher than those recorded in the middle after 72 hours with concentrations ranging from 13-27 ppb for the duration of the study. On day 28 the surface Ag concentration was 16 ± 0.6 ppb, comparable to the middle at 16 ± 0.05 ppb and bottom at 15 ± 0.7 ppb showing equilibration. The transport behaviour does not show sedimentation and the concentration movement between the depths agree with Flicks Law (Fick, 1855). Since no sedimentation was observed in any of the characterisation methods, and the concentration gradients determined diffusion as a transport mechanism, the model parameters were adjusted (table 5.19) to account for losses of Ag only. The new parameters increased the R^2 values to 0.62 in the middle and 0.66 in the bottom. Visual fittings between the observed and expected data are seen in figure 5.37.

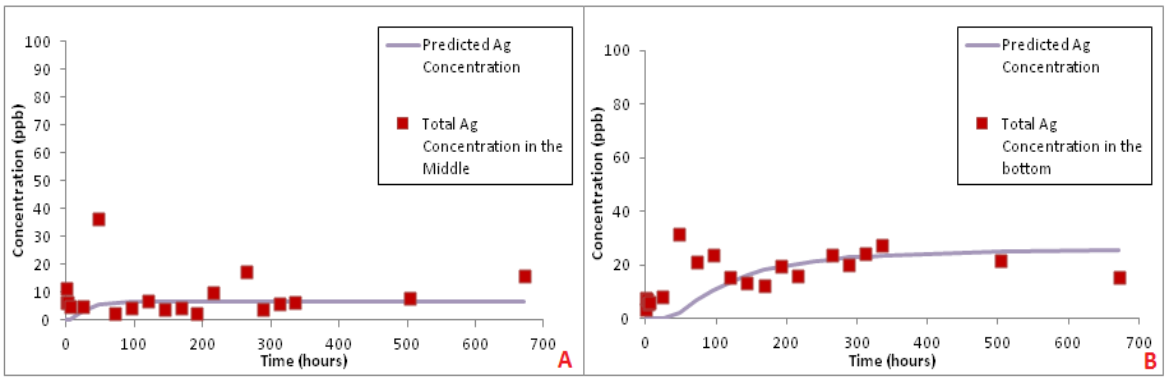

Figure 5.37: Adjusted model fits for changing model parameters for (A) the middle and (B) the bottom water, for PVP AgNPs exposed to winter natural lake water. New model parameters are listed in table 5.19.

Table 5.23: Adjusted Model Parameters for PVP AgNPs in Winter Natural Lake Water

Parameter	symbol	Unit	Middle	Bottom
Diameter of AgNP	d	nm	11	11
Cross section area of the column	A	m^2	0.049	0.049
Column Length	*L*	m	1	1
Column volume	*V*=A*L*	L	43	43
Dosing volume	*V*	L	0.215	0.215
Dosing concentration	C_0	ppm	1.5	5
Mass of Ag	M	mg	0.3	1.1
C column based on diffusion	M/*V*	ppb	7.5	25
Diffusion coefficient	*D*	$m^2 s^{-1}$	3.904E-7	3.9E-7
Sedimentation Velocity	*U*	ms^{-1}	6.3E-10	6.3E-10

Overall the total Ag concentrations in the present study were higher in the surface compared to the lower depths for the duration of the study, comparable to the results obtained from the autumn water. Results show that transportation of both particle types the total Ag concentration follow diffusion.

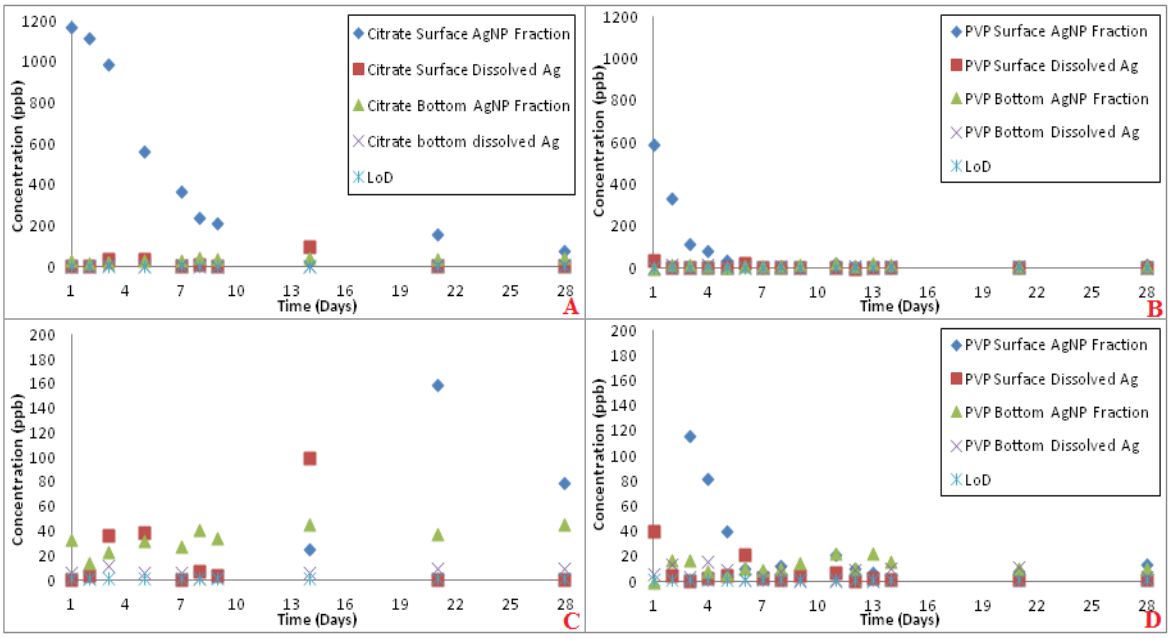

Figure 5.38: Dissolved and AgNP concentrations (ppb) using ultrafiltration in the winter lake water: A) citrate Ag^+ and AgNP concentrations in the surface and bottom depth water for each day, B) PVP Ag^+ and AgNP concentrations in the surface and bottom depth water for each day, C) shows the same graph as A for concentrations below 200 ppb, D) shows the same graph as B for concentrations below 200 ppb. Note the LoD = Instrumentation limit of detection at 2 ± 0.2ppb.

The results presented in figure 5.38 describe the stability of the citrate and PVP AgNPs when released in to the winter natural water. We must also keep in mind, due to the limitations of ultrafiltration that the results are presented as estimates of how quickly AgNPs dissolve in the different water conditions. The concentrations of the AgNPs and the Ag^+ between each depth can be used to describe the transport mechanism of total Ag which is used to validate the model predictions. Analysis of the citrate AgNP concentration in the surface water show the concentration reduces slowly from 1169 ppb after day 1, to 367 ppb after 7 days, to 159 ppb on day 21 and 79 ppb on day 28. The reduction in citrate AgNP concentration over time validates the model and total Ag data presented in figure 5.35. The citrate AgNP concentration in the bottom of the mesocosm

remains stable with concentrations beginning at 17 ppb after 2 days, to where it drops to 10 ppb on day 21 and 11 ppb on day 28. The concentrations in the bottom are comparable between each day of analysis confirming that they agree with Ficks Law (Fick, 1855) and validate the model transportation of diffusion. The Ag^{+} concentrations were too low and unreliable to be suitably assessed due to close limits of detection (table A2.15 additional information).

Analysis of the PVP AgNP stability in the surface water show the AgNP concentration after day 1 was 592 ppb, which declined to 14 ppb on day 28. The reduced concentration over time highlights that the Ag is moving out of the surface water as confirmed by the model in figure 5.35. The PVP AgNP concentration in the bottom of the water maintained a concentration gradient from 177 ppb after 2 days, to 11 ppb on day 8 and day 28. The concentration gradient observed confirms the model fits presented in figure 5.36

Overall, the concentrations presented in figure 5.38 for the citrate and PVP AgNP studies were lower than previously observed indicating Ag losses. Losses of Ag concentrations were also observed in the total Ag data presented in figure 5.35. Therefore the model was suitable adjusted (table 5.18) to compensate for Ag losses, and resulted in the total Ag concentration fitting the model to describe the transportation of the Ag via diffusion.

5.4.5.2 UV Analysis

Figure 5.39 (A-F) shows the SPR absorbance data for both citrate and PVP AgNPs released into winter seasonal water over time.

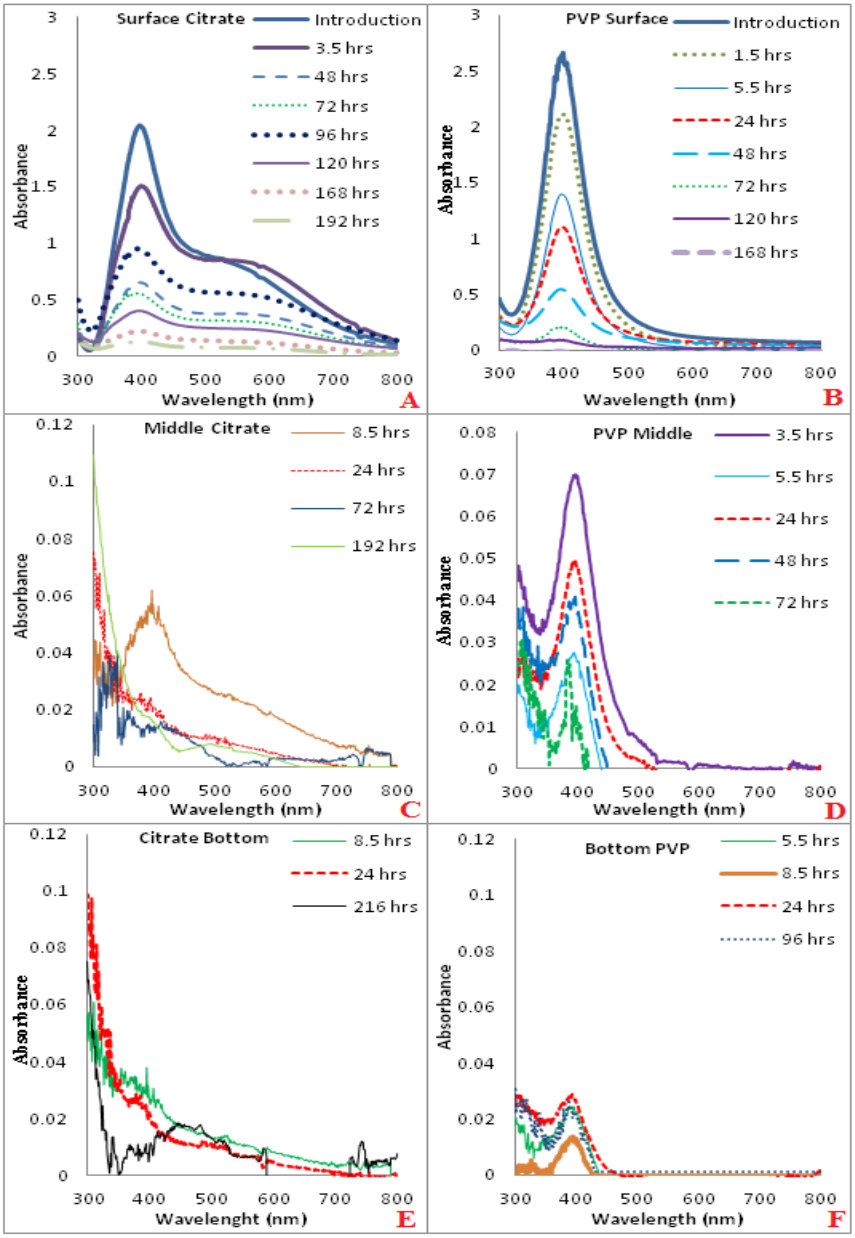

Figure 5.39: UV SPR profiles taken from different depths of the mesocosm column when exposed to winter Vale Lake water. A) Citrate coated AgNPs at the surface, B) PVP AgNPs at the surface, C) citrate AgNPs from the middle, D) PVP AgNPs from the middle, E) citrate AgNPs from the bottom and F) PVP AgNPs from the bottom. Note that the Y axis for the graphs are not presented in the same scale for each of the depths, as detail from the lower regions would be lost.

On immediate introduction to the water the citrate AgNPs aggregated, behaviour which displayed a dominant second SPR peak between 450-700nm, as seen in the previous autumn water set. No sedimentation behaviour was observed in the total Ag data, although large concentration losses were observed in the lower depths as modelled in figure 5.36. Therefore aggregated citrate AgNPs may have settled at the bottom.

Similar results of a dominant second peak were seen in the EPA SRFA synthetic water study described in chapter 4. Equally, the NOM concentration in the EPA SRFA was low at 1 mg L^{-1}, whereas the TOC concentration in present study was 4.3 mg L^{-1}. In both cases similar behavioural patterns has been observed by the citrate AgNPs, show aggregation and AgNP instability. Therefore aggregation is determined by the ionic strength of the water (table 5.21) and low NOM concentrations, despite not being observed in the total Ag concentrations due to settling (figure 5.36). Comparisons of the middle water depth show citrate AgNPs exhibit extensive band stretching in the 500-600nm (figure 5.39). The lower depths of the mesocosm identify large citrate particulates and out of plane quadrupole resonance between 300-400nm (Kawaguchi *et al,* 2011, Kelly *et al,* 2003 and Zou *et al,* 2007) as seen in figure 5.38E and 5.38F.

The PVP AgNPs show a strong sharp absorbance peak in the 400nm for the lower depths of the mesocosm, demonstrating that the majority of the AgNPs were small and spherical. A single peak confirms PVP AgNP stability compared to the citrate AgNPs. The reduced Ag concentrations identified form the model were further exhibited in the SPR data which only confirmed the PVP AgNP presence in the surface water for 7 days (168 hours), instead of the full 28 days in all the previous natural water studies.

Overall the UV-Vis data indicate that the citrate AgNPs aggregate on introduction, which is consistent with the results obtained in the other seasonal waters. PVP particles on introduction remained stable giving rise to a sharp SPR band in the 400nm region at every depth. The PVP AgNPs were inconsistent to the previous results obtained, mainly due to low observable Ag concentrations throughout the study.

5.4.5.3 Transmission Electron Microscopy (TEM) Analysis and Energy Dispersive X-Ray EDX Analysis

Original citrate AgNPs as discussed in chapter 3 for the winter batch of particles, were characterised by TEM at 12 ± 2 nm and 12 ± 3 nm for the PVP AgNPs. These sizes were used to determine transformational changes that occur to the NPs once released in the natural water. Morphological characteristics are presented in figure 5.40 (citrate AgNPs) and 5.42 (PVP AgNPs). EDX was used to determine and confirm the presence of citrate AgNPs in figure 5.44 and 5.45. PVP AgNPs were not examined using EDX in this water set.

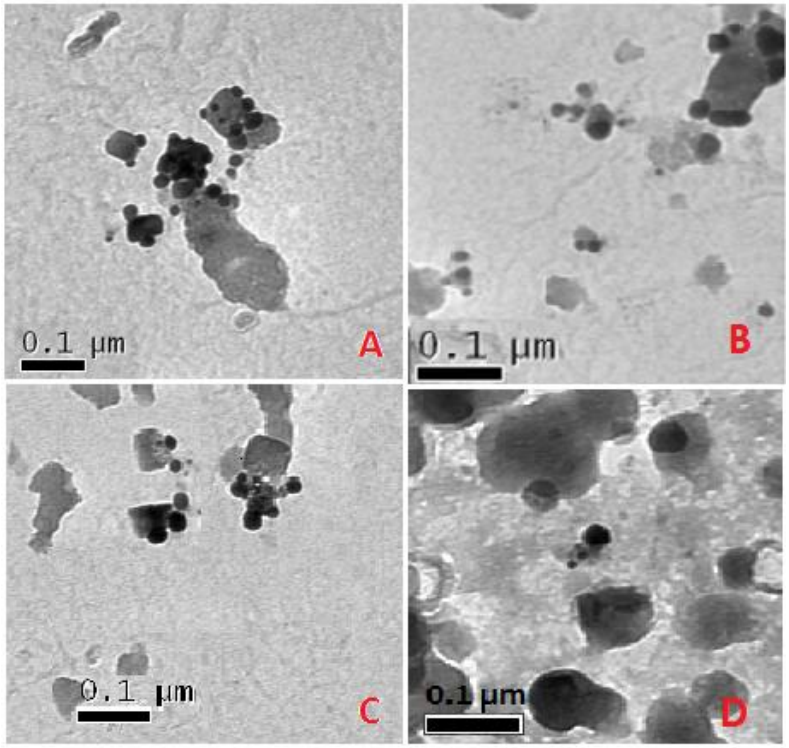

Figure 5.40: TEM images of citrate AgNPs exposed winter natural Vale Lake water identified at A) 24 hours surface waters, B) 48 hours surface water C) 72 hours surface water, and D) 168 hours surface water. Corresponding histograms are presented in figure 5.41.

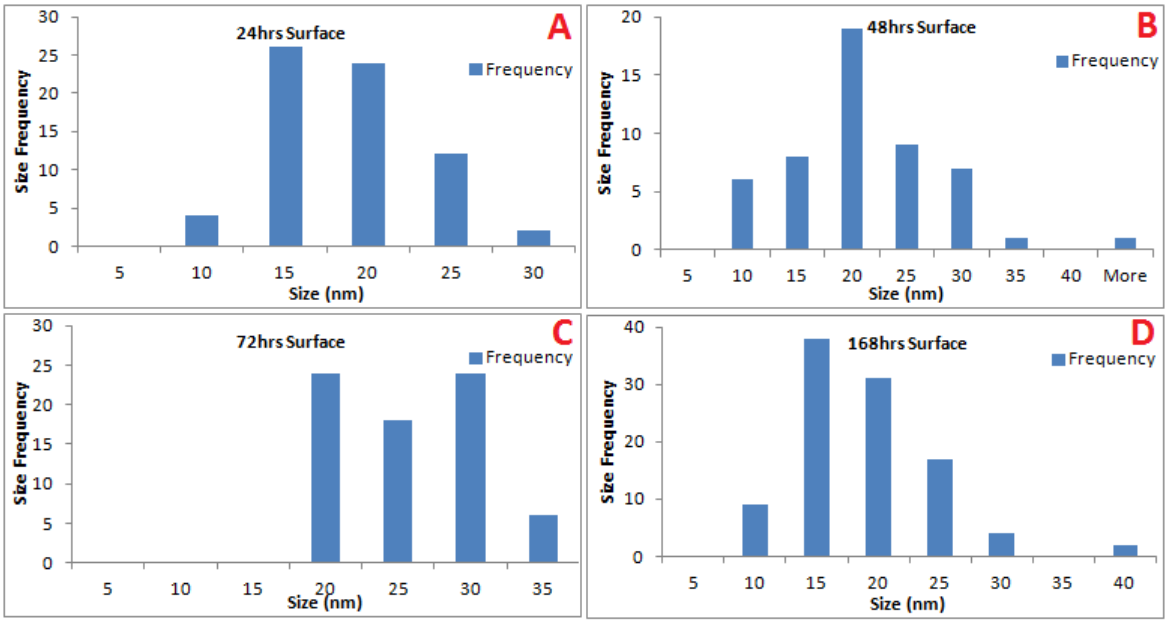

Figure 5.41: TEM size frequency distributions of citrate AgNPs exposed winter natural Vale Lake water identified at A) 24 hours surface waters, B) 48 hours surface water C) 72 hours surface water, and D) 168 hours surface water.

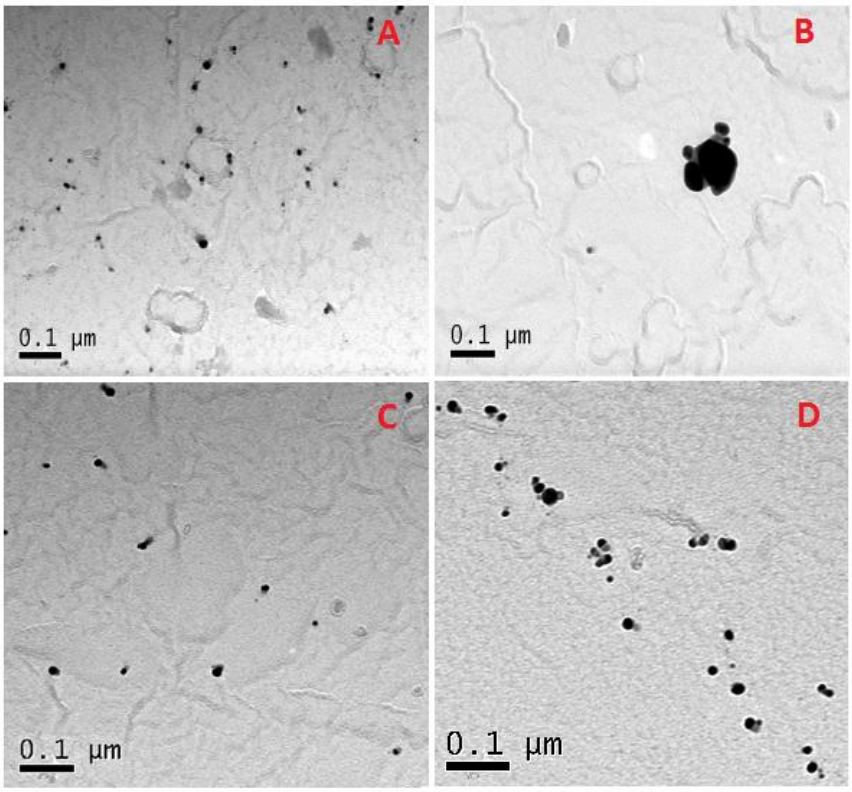

Figure 5.42: TEM images of PVP AgNPs released in winter natural Vale Lake water identified at, A) 72 hours in the surface water B) 72 hours in the bottom of the mesocosm C) 96 hours in the surface water and D) 96 hours bottom of the mesocosm. Corresponding histograms are presented in figure 5.43.

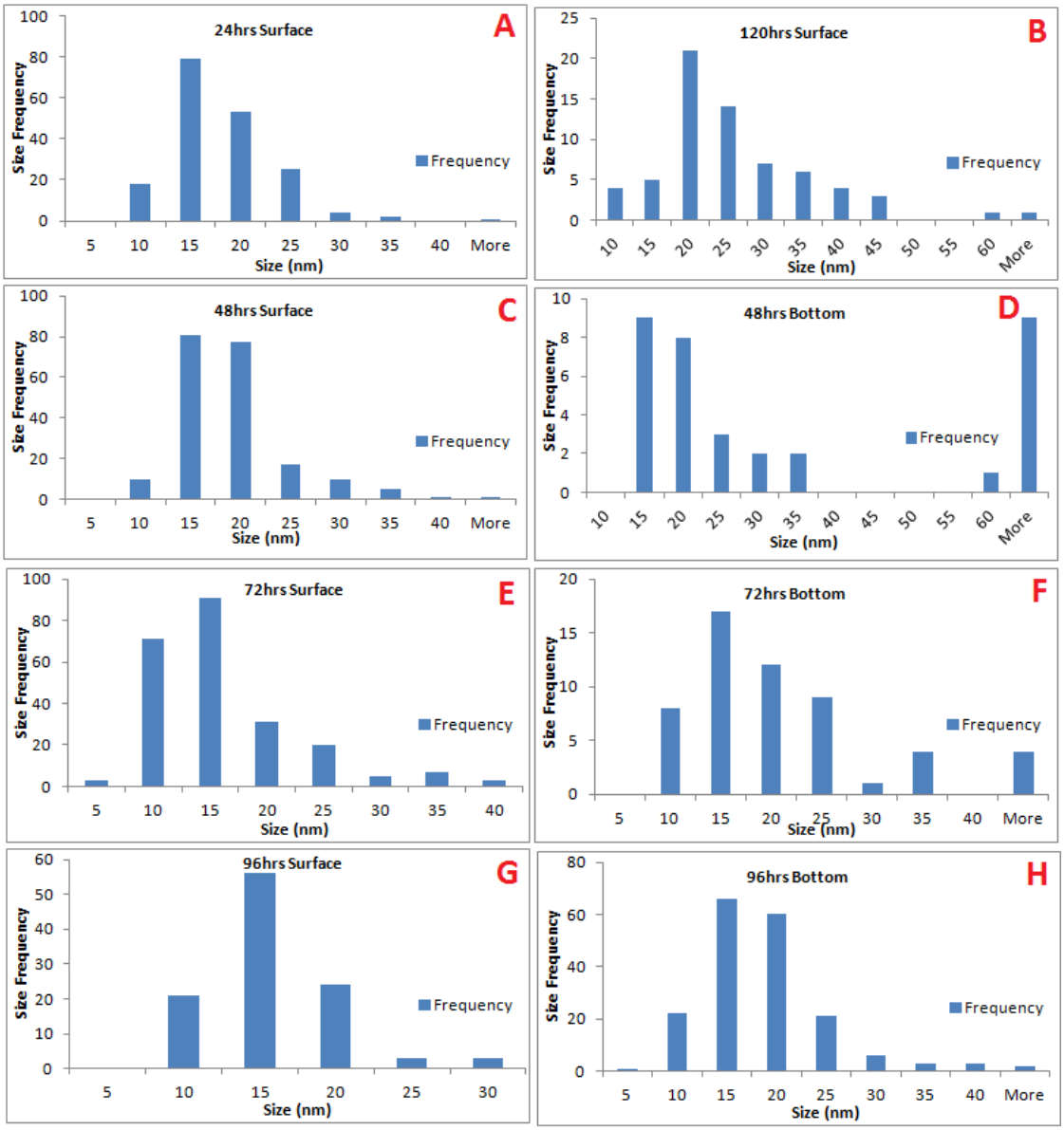

Figure 5.43: TEM size frequency distributions of PVP AgNPs exposed winter natural Vale Lake water identified at A) 24 hours surface waters, B) 120 hours surface water C) 48 hours surface water, D) 48 hours in the bottom of the mesocosm, E) 72 hours surface water, F) 72 hours in the bottom of the mesocosm, G) 96 hours in the surface water, and H) 96 hours in the bottom of the mesocosm.

Table 5.20: TEM sizes (nm) at different time points for citrate and PVP particles exposed to winter season Vale Lake water. *n= number of particles counted*ND= Not Determined. A p value <0.05 highlights that the observed particle size using the t-test is significantly different to the size of the particle before release, at a 95% confidence level.

Table 5.24: Average Size by TEM for AgNPs Exposed to Natural Winter Water										
Time (hours)	**24**	**48**		**72**		**96**		**120**		**168**
Area Analysed	**Surface**	**Surface**	**Bottom**	**Surface**	**Bottom**	**Surface**	**Bottom**	**Surface**	**Bottom**	**Surface**
Particle type	**Citrate AgNPs**									
Size (nm)	16 ± 5	19 ± 7	ND	23 ± 5	ND	ND		ND		17 ± 6
n	68	51		73						100
***p* value**	2.31E-10	9.89E-10		6.1E-32						1.212E-12
Particle Type	**PVP AgNPs**									
Size (nm)	16 ± 5	17 ± 5	41 ± 38	14 ± 7	21 ± 18	14 ± 4	17 ± 7	24 ± 11	ND	ND
n	182	203	34	233	57	109	186	68		
***p* value**	7.22E-24	2.69E-30	8.37E-05	1.9E-07	0.0001	8.98E-08	1.3E-19	2.17E-13		

Observations were not possible for bottom of the mesocosm for citrate AgNPs after 24 hours post release, due to large impurities on the TEM grids making the AgNPs indistinguishable. For both particle citrate and PVP AgNP, TEM sizing revealed that the AgNPs were all significantly (p> 0.05) larger after release when compared to the starting average sizes.

As identified from the UV-Vis data (figure 5.39), the citrate AgNPs in the surface water show aggregated AgNPs (figures 5.39A, 5.39B and 5.39C). At 24 hours the average citrate AgNP size was 16 ± 5 nm (p 2.31E-10) and the most frequent sizes in the surface water were between 15 and 20 nm, similar to size frequencies in the previous seasonal waters. Smaller particles can also arise from the breakage of aggregates and dissolution

(Li *et al,* 2013), since the NOM concentration was low reducing the stabilising effects previously seen in spring and summer.

At 72 hours the citrate AgNPs appear morphologically larger (figure 5.40C) with an increased size of 23 ± 5 nm. Although, there is an indication at 72 hours in the bottom of the mesocosm some aggregation has occurred, this was not a representative situation. The corresponding histogram at 72 hours in the bottom of the mesocosm yielded similar size distributions as the autumn study, showing the two waters are comparable in terms of PVP AgNP transport and behaviour. Evidence at 96 hours (figure 5.40C) demonstrated singular uniform particles, which provided further evidence that surface coating differences in terms of the morphological and stability differences occurred between the two types of coated AgNPs.

PVP AgNPs were analysed by TEM for 5 days (120 hours) as described in table 5.21. After 24 hours release, the PVP AgNPs are 16 ± 5 nm in the surface water comparable with the PVP AgNPs at 24 hours in the previous autumn water. Similarly the histograms representing the size frequency distributions are comparable for the PVP AgNPs from the autumn study with the present shown in figure 5.43A. At 72 hours the PVP AgNPs 14 ± 7 nm, showing a decrease in the recorded size, although the particles remain small and uniformly distributed with no evidence of aggregation, as described in the SPR data (figure 5.39).

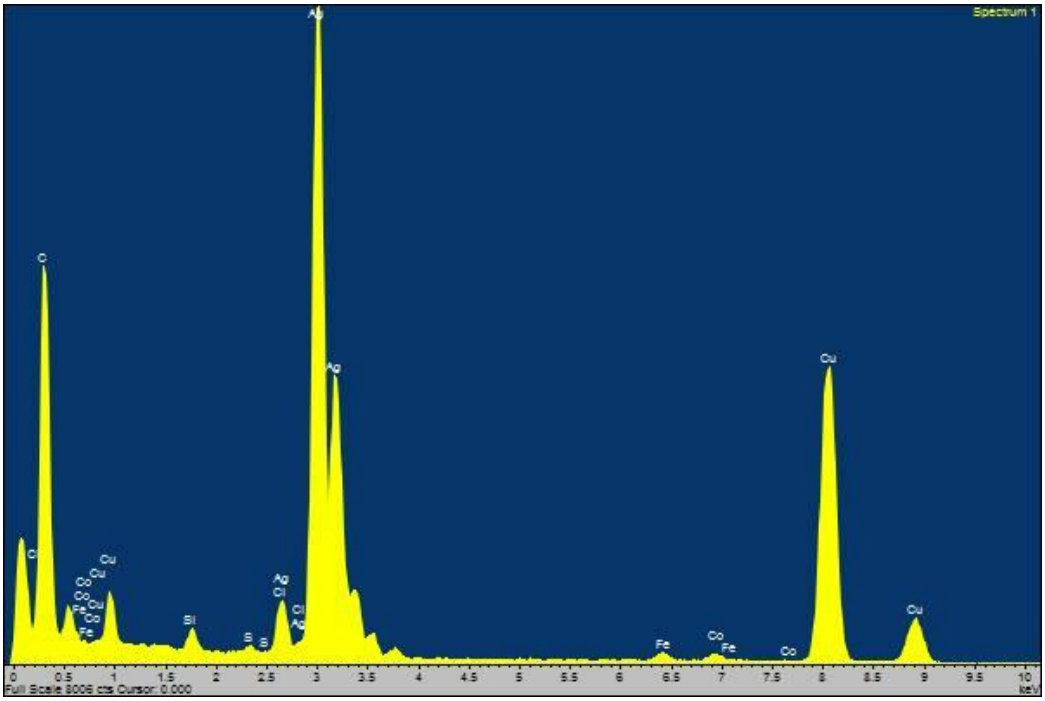

Figure 5.44: EDX spectrum of citrate AgNPs identified after 24 hours in the surface of the winter Vale Lake natural water.

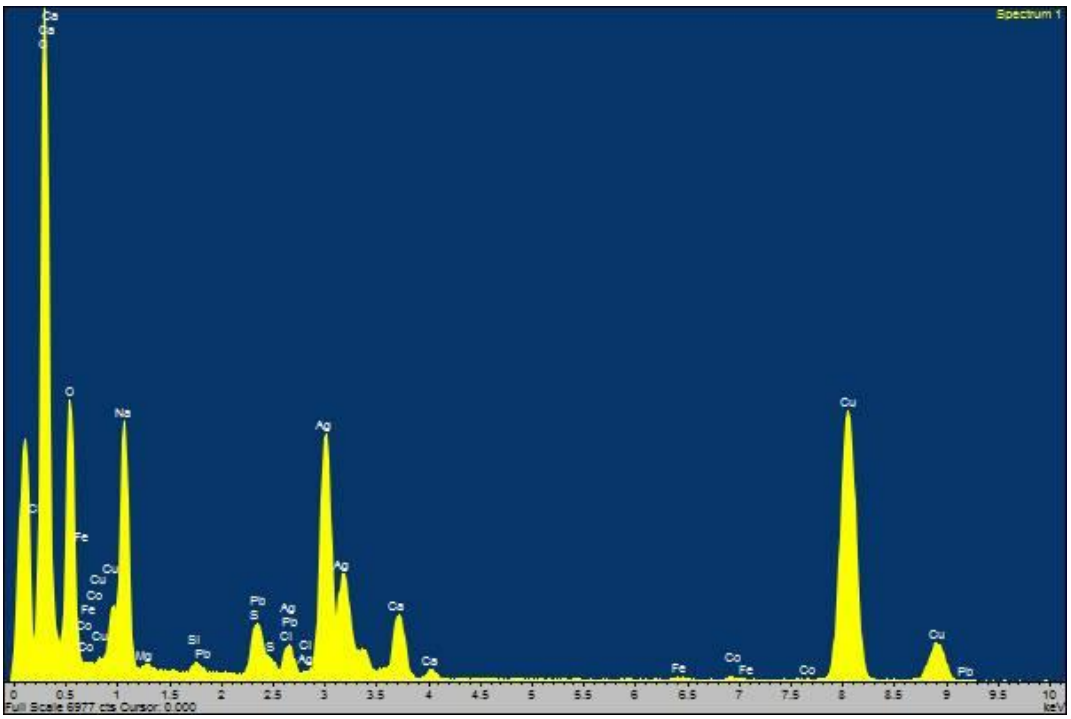

Figure 5.45: EDX spectrum of citrate AgNPs identified after 24 hours in the bottom of the mesocosm for winter natural water.

Elemental analysis of the citrate AgNPs in the surface winter natural water at 24 hours (figure 5.44) revealed C, Cu, Fe, Si, S, Ag, Cl, and O. As in the previous EDX reports the Ag peak confirms the presence of AgNPs. Signals of C can be accounted for from the background signal from the carbon grid used to prepare the sample. Although EDX cannot fully confirm the presence of O as DO as it is most likely from the ambient air.

A further sample was taken for EDX to see if there was a difference between the AgNPs from the surface and bottom of the mesocosm (figures 5.44 and 5.45). The spectrum in figure 5.44 indicated the presence of polonium (Po), although the expected energy for Po is 11.129 keV (See energy figure in appendix) which was not detected. Therefore Po is an error signal on the spectrum. Both EDX profiles contain S and Cl peaks suggesting that possible surface complex possibilities for the AgNP transformations in the natural water. Both these elements have been persistent in each of the seasonal waters. There was a further reoccurrence of Ca and Na, which were also found to be continuously high in concentration as determined by ICP-MS (table 5.21).

5.4.5.4 Inductively Coupled Plasma Mass Spectrometry (ICP-MS) and Total Organic Carbon (TOC) Analysis.

TOC was recorded at 4.3 mg L^{-1}, which was considerably lower than the previous seasons of spring at 12.59 mg L^{-1}, summer at 31.70 mg L^{-1} and 28.31 mg L^{-1} in autumn. Therefore the reduced organic carbon content showed reduced stability of both the AgNP types as described in the SPR data (figure 5.39). Citrate AgNPs did not give a UV response after 9 days and the PVP after 7 days. The pH was recorded at 7.2, comparable with the previous waters.

Table 5.25: ICP-MS Semi Quantitative (± 20%) Elemental Concentrations of Natural Winter Vale Lake Water			
Element	**Concentration (ppb)**	**Element**	**Concentration (ppb)**
Li	4	**Zn**	30
B	260	**Ga**	ND
Na	23000	**Ge**	ND
Mg	7000	**As**	ND
Al	5.6	**Se**	0.5
Si	6100	**Br**	110
P	40	**Rb**	4.2
K	3500	**Sr**	210
Ca	32000	**Zr**	ND
Ti	1.4	**Mo**	ND
V	0.6	**Ag**	0.9
Cr	0.1	**Sn**	ND
Mn	3.2	**Sb**	ND
Fe	32	**Ba**	44
Co	0.2	**Ce**	0.2
Ni	3.2	**W**	ND
Cu	3.4	**Pb**	0.1

As the TOC content was considerably lower in the present study, the ionic strength needed to be assessed for its influences on the particle behaviour. When compared to the previous seasons there were elevated concentrations of Na, Mg, K, and Ca were detected in concentrations that exceeded the previous water studies. High ionic strength reduces the electric double layer that provides electrostatic repulsion, thus leading to aggregation (Zang *et al* 2011), as evidenced in the SPR and TEM data. The elevated concentration of Ca in the presence of NOM has also been demonstrated to enhance particle aggregation (El Bradawy *et al,* 2010, Stankus *et al,* 2011 and Zhang and Oyanedel-Craver, 2012) further observed in the present study, possibly caused by bridging of the calcium to the NOM (Chen and Elimelech, 2007). Therefore, the water conditions favour a

destabilizing effect on the surface charge on both the citrate and PVP AgNPs due to high ionic strength (Jiang *et al,* 2009) and reduced NOM concentration.

ICP-MS results identified that the ionic strength of the winter water was much higher when compared to the spring and summer water, and the TOC content was at the lowest recorded at 4.3 mg L^{-1}. Therefore, the winter water conditions were optimal in terms of ionic strength to cause destabilization and aggregation of the citrate AgNPs on immediate introduction, which caused the larger particulates to sediment to the bottom, following DLVO behaviour. Aggregation was not visualised for the PVP AgNPs according the SPR profile, although the water conditions were still optimal to reduce the AgNPs persistence in both cases. Overall, reduced NOM concentrations and increased ionic strength were linked to increased aggregation of the citrate AgNPs.

5.5 Conclusion

Assessing the transport and behaviour of AgNPs in natural water will help determine exposure routes and end points for AgNPs released in to the environment. When PVP and citrate coated AgNPs were released in to seasonally changing natural water, we were successfully able to use a simple mathematical model (Socolofsky and Jirka 2004, and Hinderliter *et al,* 2010) to predict AgNP behaviour and transport. The model did prove problematic for the predictions of the lower depths, as the model can only be set for one concentration value and one size value, when realistically the concentrations and sizes of the Ag NPs changed over a daily basis. When the parameters of the model were adjusted according to the behavioural patterns we were then able to validate the transport mechanisms between the two differently coated AgNPs. Both citrate and PVP AgNPs followed same partitioning processes, where AgNPs move from the surface waters to the bottom of the mesocosm. The differences that occurred to the AgNPs were the type of transformations due to the influences of the seasonally changing water chemistry. The seasonally changing water chemistry mainly favoured aggregation, sedimentation and dissolution of the citrate AgNPs particles, which have an electrosteric surface coating. Evidence presented in this study identified surface coating specific trends that favoured PVP AgNP stability in all cases over citrate AgNPs.

Analysis of the citrate AgNPs revealed that in all experiments immediate aggregation occurred irrespective of the TOC as a function of NOM concentration, as evidenced in the SPR and TEM imaging data. However, observations of the citrate AgNP behaviour were different between the different water seasons. The winter water had the

lowest observable TOC concentrations at 4.3 mg L^{-1} and the highest electrolyte concentrations determined by elemental analysis of the natural water (ICP-MS), to which the highest effects of citrate AgNP aggregation were observed in the SPR data. The summer water had the highest recorded TOC concentration and lowest electrolyte concentrations. The SPR observed reduced aggregation effects and persistence in summer when compared to all other water exposures. TEM revealed lower polydispersity of the size frequency when compared to the other waters, demonstrating increased NOM has stabilising effects to citrate AgNPs. Analysis of the PVP AgNPs revealed that they remained stable, demonstrated by the single peaks recorded in the SPR data and smaller TEM size frequencies in both the surface and bottom depths. The model helped to validate that the PVP AgNPs transport through the mesocosms via diffusion, compared to aggregation and sedimentation observed by the citrate AgNPs.

Overall, waters with high NOM concentration enhanced the stability and persistence of the citrate AgNPs in the surface waters. Since citrate is an electrostatic stabilised coating, the NOM charge could have displaced the citrate, thereby re-coating the AgNPs with large bulky and negatively charged molecules to sustain their suspension in solution. via both electrostatic and steric stabilisation This would also explain why PVP, a polymeric coating which is tightly bound to the Ag surface, was not displaced under environmental conditions with no changes to stability, irrespective of the NOM concentrations.

TEM analysis showed a size difference between the surface and bottom depth, where larger AgNPs settled at the bottom and smaller citrate and PVP AgNPs remained suspended at the surface. Therefore at different times of the year the transformations of

the AgNPs will change, and AgNPs will persist in particulate forms for longer periods of time, particularly those with polymer coatings.

In real environmental situations AgNP releases via waste water treatment plants will come into contact with many different treatment processes before they enter surface waters. For this instance it is possible that the AgNPs will already have ligand complexes to other organic and inorganic material (Lowery *et al,* 2012). EDX of the water compositions after AgNP release also identified the availability for the AgNPs to complex with S and Cl ions. Under realistic conditions and in the presence of natural light the formation of AgNP precipitates from dissolved Ag^+ (via dissolution) is highly likely, thus increasing their environmental persistence.

The dissolution studies provided evidence that under environmental conditions AgNPs do dissolve to produce ionic species. Extensive studies have revealed that Ag^+ released from AgNPs is highly toxic (Li *et al,* 2010), therefore increased dissolved Ag levels will pose higher risks of toxicity to microorganisms. It was also demonstrated that the citrate coated AgNPs pose a greater risk of producing Ag^+ in natural waters, due to a wide range of factors in the water chemistry that favour the destabilization of the NPs, especially when compared to the PVP AgNP behaviour. Since sedimentation of the particles occurred, it is likely that the AgNPs will settle into the sediment (Stankus *et al,* 2011), making them more bioavailable to microorganisms living in this area.

Chapter 6

Conclusions and Future Work

6.1 Conclusions

The studies outlined in this thesis were conducted to produce novel methods of citrate AgNP synthesis and to determine the behaviour, fate and transport of citrate and PVP AgNPs in environmentally relevant conditions. Chapter 2 outlines the methodologies and characterisation methods used to assess newly synthesized AgNPs and to determine the transformations of AgNPs when released into synthetic and natural waters, as described in chapters 4 and 5.

Chapter 3 assessed new approaches to produce novel synthesis methods of citrate AgNPs. Using the combined effects of a fixed temperature, a 2 mM citrate concentration and 1 mM of $AgNO_3$, we were successfully able produce a new method to attain different sizes of citrate AgNPs. Heating the AgNP suspensions for 2 hours at 40^{o}C yielded stable citrate AgNPs of 35 ± 2 nm (DLS) with a PDI of 0.1, and heating the suspensions at 100^{o}C yielded smaller AgNPs of 23 ± 2 nm (DLS) with a PDI of 0.1. These particles were studied for their stability over a period of one year to which their size and polydispersity were deemed stable by suitable characterisation. Although, due to the length of time required to assess their longer term stability, the AgNPs produced were not used in any further study. However, stable citrate AgNPs (Cumberland and Lead,

2009) and PVP AgNPs (Tejamaya *et al*, 2012) have been previously documented for their long term stability and known transformations in aquatic media (Romer *et al,* 2011 and Tejamaya *et al*, 2012). Therefore we were able to reproduce these methodologies and synthesise citrate and PVP AgNPs with an average size of 11.5 ± 2.5 nm (TEM), which were further characterised using a multi-method approach (UV-vis, DLS, AFM and TEM) for use in the mesocosm studies descried in chapters 4 and 5.

Chapter 4 explored citrate and PVP AgNP release in simple synthetic waters and chapter 5 examined AgNP fate and behaviour in variations of different seasonal natural lake water. The information from each of these studies identified that the changes in the surrounding solution chemistry had a major impact upon AgNP stability and behaviour. As the water chemistry becomes more complex the physicochemical interactions and behaviours of the AgNPs change. Both citrate and PVP AgNPs that were released in UPW remained stable for the duration of the study. However, when the citrate AgNPs were released to the EPA moderately hard water present and absent of SRFA, they became unstable and demonstrated aggregation and sedimentation behaviour. In comparison, the PVP AgNPs remained stable in the EPA moderately hard water with no observable affects to NP instability. The Ag^{+} concentration was reduced in the EPA water and the PVP AgNP concentration was higher, possibly due to the formation of AgCl NPs (Baalousha *et al,* 2013). EDX was preformed to confirm the presence of Cl and S elements on the AgNPs surface to further support our claims of possible AgCl and AgS formations in solution.

Chapter 5 assessed citrate and PVP AgNP behaviours in seasonal variations of natural water. These studies revealed different behaviours between the seasonal water variations and differences between the two AgNP surface coatings. The spring seasonal

water had a TOC concentration of 12.59 mg L^{-1}, which enabled citrate AgNP persistence in the surface water for 11 days (UV-vis). On introduction the citrate AgNPs aggregated, as shown by the SPR and total Ag concentration data. Poor correlations between the modelled and observed total Ag concentrations were seen, despite several attempts to fit the model parameters to interpret AgNP behaviour. In comparison, the PVP AgNPs were detectable by the UV-vis for the duration of the study (28 days) maintaining stability and persistence. The model parameters were successfully fitted to produce strong correlations between the modelled and observed data to describe the AgNP behaviour.

The summer water contained the highest TOC concentrations of 31.70 mg L^{-1} and low ionic strength, both of which have been documented to increase AgNP stability in environmental conditions (Cumberland and Lead 2009, Bae *et al,* 2011 and Li and Chen, 2012). For the citrate AgNPs, we observed reduced aggregation, increased stability and lower size frequencies (TEM). Citrate AgNPs were also detectable in the surface water for 12 days showing increased stability when compared to the citrate AgNPs released in the spring natural water. To compare, the PVP AgNPs were detectable for 28 days in the surface water (UV-vis) maintaining their stability and low size frequency (TEM). The model data suggested the PVP AgNPs follow the process of diffusion, as the observed total Ag concentrations maintained a diffusion gradient between the depths (surface, middle and bottom) over time.

Analysis of the citrate AgNPs released in the autumn season water determined the most unstable effects when compared to the spring and summer waters. Despite a TOC concentration of 28.31 mg L^{-1}, the citrate AgNPs only persisted in the surface water for 8 days and showed increased aggregation as determined by the model Ag

concentrations, SPR and TEM data. The ionic strength was higher than the summer water which would have contributed to the reduced stability of the citrate AgNPs even in the presence of higher NOM concentrations. Similar findings by Adegboyega *et al* (2013) also observed reduced AgNP stability in the presence of high NOM concentrations and high ionic strength. The PVP AgNPs did not reveal any reduced affects to the AgNP sizes as confirmed by the modelled and TEM data, which was comparable to the results seen in the previous water studies.

Observations made in the winter water studies observed low TOC concentrations of 4.3 mg L^{-1} with high ionic strength, which has been well documented to reduce AgNP stability via aggregation and dissolution (Elzey and Grassian, 2010, Ma *et al,* 2012 and Romer *et al,* 2011). Citrate AgNPs confirmed the literature behaviour by showing increased aggregation (when compared to the other natural water releases), and increased Ag^{+} concentrations in winter. The PVP AgNPs further demonstrated their stability over the citrate AgNPs showing diffusion transport mechanisms. PVP AgNPs are well documented for their stability over citrate AgNPs (El Badawy *et al,* 2011, and Li *et al,* 2013) and the confirmed the literature reports by remaining stable in the seasonally variable natural waters when compared to the citrate AgNPs. TEM imaging revealed smaller size distributions, compared to the citrate AgNPs which were comparable between each of the natural water experiments. Evidence suggests that NOM had little impact on the fate or behaviour of the PVP AgNPs, but did have a significant impact upon the citrate AgNPs stability and persistence in the seasonally changing waters.

Complementary to assessing the surface coating impact and the roll of NOM, we were also successfully able to predict and validate the transport behaviour of the AgNPs

using a simple diffusion-sedimentation model based on the combined mathematical works of Socolofsky and Jirka (2004) and Hinderliter *et al* (2010). Using a Pearsons correlation coefficient, the model parameters provided a good fit with the observed data to validate aggregation/sedimentation and diffusion of the AgNPs. The data from the model indicated that citrate AgNPs aggregated which confirmed the data which was obtained by TEM and UV-Vis. PVP AgNPs mainly followed the process of diffusion in each of the synthetic and natural water studies, by maintaining concentration gradients in accordance to Ficks Law (Fick, 1855). The stability of the PVP AgNPs was also confirmed by the TEM and UV-Vis data presented in chapters 4 and 5. The model provided information to demonstrate that different seasonal intervals had considerably different effects to the sedimentation and diffusion behaviour of the AgNPs.

Overall, at different times of the year the transformations of the AgNPs will change with changing water chemistry (Ma *et al,* 2012). During the warmer months AgNPs will persist in particulate forms for longer periods of time, particularly those with polymer/steric coatings. Using a sedimentation-diffusion model we successfully identified the transport processes of the AgNPs in the different water conditions. As a whole, both citrate and PVP AgNPs dissolve to produce ionic species, and AgNPs concentrations are detectable in surface waters for a period of 28 days. Based on these studies, predictions of AgNPs released in a real environmental situation will see elevated concentrations of Ag^{+} and AgNPs which can be modelled for their transportation behaviours.

6.2 Future work

Particles synthesised in chapter 3, using variations of the temperature, citrate concentration and $NaBH_4$ concentration that were not used in the mesocosm studies, could be studied for their long term stability. Work could include effects of ageing, affects of storage on aging, and exposures to a range of different aquatic waters to assess their behaviour and stability. Since the AgNPs used in the mesocosms demonstrated persistence for the duration of the study (28 days) in a controlled laboratory settling, extensions of these studies for up to 6 months could be considered. Studies could assess the effects of different type of NOM such as humic substances and biopolymers up on the AgNP fate and behaviour. Other conditions could include the comparison between abiotic and biotic conditions with the addition of sediment/sediment species and living organisms in the water compartment such as *Daphnia magna* and algae. Each study could provide answers as to what happens to the NPs under these complex test conditions. AgNPs could also be tracked in the sediment compartments with the use of isotopically or chemically labelled NM variants.

Studies can also be conducted in a wetland environment using larger scale mesocosms to allow other factors to be considered such as marine life, small organisms, light, and plantation. These studies would enable the extension of knowledge from a laboratory controlled environment to a more realistic environmental release situation. Comparisons of larger AgNPs could also be used, and their behaviour mechanisms can be compared to the smaller AgNPs.

Natural lake water was used in the present study, further assessments of river water, reservoir water, estuarine water and sea waters will provide further information on the fate and behaviour of AgNPs in the aquatic environment. Changes to the mesocosm design could also be suggested via introducing a sediment matrix to assess the further partitioning of the AgNPs. Since the present studies conducted in the mesocosm were static, a mixing method could be introduced to mimic natural water movement.

References

1. Adegboyega.N.F., Sharma.V.K., Siskova.K., Zboril.R., Sohn.M., Schultz.B.J., and Banerjee.S., (2013), Interactions of Aqueous Ag^{+} with Fulvic Acids: Mechanisms of Silver Nanoparticle Formation and Investigation of Stability, *Environmental Science and Technology,* **47:** 757-764.

2. Akaighe.N., Depner.A.W., Banerjee.S., Sharma.V.K and Sohn.M., (2012), The effects of monovalent and divalent cations on the stability of silver nanoparticles formed from direct reduction of silver ions by Suwannee River humic acid/natural organic matter, *Science of The Total Environment,* **441:** 277-289.

3. Akaighe.N., MacCuspie.R.I., Navarro.D.A., Aga.D.S., Banerjee.S., Sohn.M., and Sharma.V.K., (2011), Humic Acid-Induced Silver Nanoparticle Formation Under Environmentally Relevant Conditions, *Environmental Science and Technology*, **45:** 3895-3901.

4. Allen.J.H., Imprellitteri.C.A., Macke.D.A., Heckman.J.L., Poynton.H.C., Lazorchak.J.M., Govindaswamy.S., Roose.D., and Nadagoudak.M.N., (2010), Effects from filtration, capping agents, and presence/absence of food on the toxicity of silver nanoparticles to *Daphnia Magna. Environmental Toxicology and Chemistry,* **29:** (12) 2742–2750.

5. An Huynh.K., and Chen.K.L., (2011), Aggregation kinetics of citrate and polyvinylpyrrolidone coated silver nanoparticles in monovalent and divalent electrolyte solutions. *Environ Sci Technol,* **45:** 5564.

6. Anastasova.S., Radua.A., Matzeua.G., Zuliani.C., Mattinenb.U., Bobacka.J.,and Diamonda.D., (2012), Disposable solid-contact ion-selective electrodes for environmental monitoring of lead with ppb limit-of-detection, *Electrochimica Acta,* **73:** 93–97.

7. Asharani.P.V., LianWu.Y., Gong.Z., and Valiyaveettil.S., (2008), Toxicity of silver nanoparticles in zebrafish models, *Nanotechnology,* **19:** 255102 http://iopscience.iop.org/0957-4484/19/25/255102/pdf/0957-4484_19_25_255102.pdf.

8. Auffan.M., Masion.A., Labille.J., Diot.M-A., Liu.W., Olivi.L., Proux.O., Ziarelli.F., Chaurand.P., Geantet.C., Bottero.J-Y., and Rose.J., (2014), Long-term aging of a CeO2 based nanocomposite used for wood protection, *Environmental Pollution*, **188:** 1-7.

9. Austin.L.A., Kang.B., Yen.C.W., and El-Sayed., (2011), Plasmonic Imaging of Human Oral Cancer Cell Communities during Programmed Cell Death by Nuclear-Targeting Silver Nanoparticles, *Journal Of The American Chemical Society,* **133:** (44), 17594-17597.

10. Baalousha.M., (2009), Aggregation and disaggregation of iron oxide nanoparticles: Influence of particle concentration, pH and natural organic matter, *Science of the Total Environment,* **407:** 2093-2101.

11. Baalousha.M., and Lead.J.R., (2007), Characterization of Natural Aquatic Colloids (<5 nm) by Flow-Field Flow Fractionation and Atomic Force Microscopy, *Environ. Sci. Technol,* **41:** 1111-1117.

12. Baalousha,M., and Lead.J.R., (2012), Rationalizing Nanomaterial Sizes Measured by Atomic Force Microscopy, Flow Field-Flow Fractionation, and Dynamic Light Scattering: Sample Preparation , Polydispersity and Particle Structure, *Environ. Sci. Technol,* **46:** 6134-6142.

13. Baalousha.M., and Lead.J.R., (2013), Nanoparticle Dispersity in Toxicology, *Nature Nanotechnology,* **8** (5): 308-309.

14. Baalousha.M., Manciulea.A., Cumberland.S., Kendall.K., and Lead.J.R., (2008), Aggregation and surface properties of iron oxide nanoparticles: Influence of pH and natural organic matter, *Environmental Toxicology and Chemistry* **27**(9): 1875-1882.

15. Baker.A., Elliott.S., and Lead.J.R., (2007), Effects of filtration and pH perturbation on freshwater organic matter fluorescence, *Chemosphere,* **67:** 2035-20-43.

16. Bae.S., Hwang.Y.S., Lee.Y-J., and Lee.S-K., (2013), Effects of Water Chemistry on Aggregation and Soil Adsorption of Silver Nanoparticles, *Environmental Health and Toxicology, 28*: pp.e2013006.

17. Bae.E., Park.H., Yoon.J., Kim.Y., Choi.K., and Jongheop Yi.J., (2011), Bacterial uptake of silver nanoparticles in the presence of humic acid and $AgNO_3$**,** *Korean J. Chem. Eng*., **28:** (1) 267-271.

18. Basu-Dutt.S., Minus.M.L., Jain.R., Nepal.D., and Kumar.S., (2012), Chemistry of Carbon Nanotubes for Everyone, *Journal of Chemical Education*, **89:** 221–229.

19. Benn.T.M and Westerhoff.P., (2008) Nanoparticle Silver released into Water from commercially available Sock Fabrics, *Environmental Science and Technology,* **42:** 4133-4139.

20. Binnig.G., Quate.C.F., and Gerber.C., (1986) Atomic Force Microscope, *Physical Review Letters,* 56 (9): 930-934.

21. Bhui.D.K., Bar.H., Sarkar.P., Sahoo.G.P., De.S.P and Misra.A., (2009), Synthesis and UV-vis spectroscopic study of silver nanoparticles in aqueous SDS solution, *Journal of Molecular Liquids,* **145:** 33-37.

22. Blaser.S.A., Scheringer.M., MacLeod.M., and Hungerbuhler.K., (2008) Estimation of the cumulative aquatic exposure and risk due to silver: Contribution of nano-functionalised plastics and textiles, *Science of the Total Environment,* **390:** 396-409.

23. Bogdanov.A.A., Deininger.D., and Dyuzhev.G.A., (2000) Development Prospects of the Commercial Production of Fullerenes, *Technical Physics*, **45:** (5) 521–527.

24. Boström.M., Deniz.V., Franks.G.V., and Ninham.B.W., (2006), Extended DLVO theory: Electrostatic and non-electrostatic forces in oxide suspensions*, Advances in Colloid and Interface Science*, **123–126:** 5–15.

25. Bowen.R.W., and Hilal.N., (2009), Atomic Force Microscopy in Process Engineering, An Introduction to AFM for the Improved Processes and Products, First Edition, Elsevier.

26. Boyd.R.D., Pichaimuthu.S.K., and Cuenat.A., (2011), New approach to inter-technique comparisons for nanoparticle size measurements; using atomic force microscopy, nanoparticle tracking analysis and dynamic light scattering. *Colloids and Surfaces A: Physicochem. Eng .Aspects,* **387:** 35-42.

27. Bozzola.J.J., and Russell.L.D., (1999), Electron Microscopy: Principles and Techniques for Biologists, Second Edition, Jones and Bartlett Publishers Inc.

28. Brundle.R.C., Evans Jr.C.A., and Wilson.S., (1992), Encyclopaedia of Materials Characterization: Materials Characterization Series: Surfaces, Interfaces, Thin Films. Butterworth-Heinemann, Elsevier.

29. Buffle.J., Wilkinson.K.J., Stoll.S., Filella.M., and Zhang.J.W., (1998), A generalized description of aquatic colloidal interactions: The three colloidal component approach. *Environ Sci Technol,* **32:** 2887–2899.

30. Burda.C., Chen.X., Narayanan.R., and El-Sayed.M.A., (2005), Chemistry and Properties of Nanocrystals of Different Shapes, *Chemical Reviews,* **105** (4): 1025-1102.

31. Cantle.J.E., (1982), Techniques and instrumentation in analytical chemistry: Atomic Absorption Spectroscopy, Elsevier Scientific Publishing.

32. Carmona.N., Ortega-Feliu.I., Gomez-Tubio.B., and Villegas.M.A., (2010), Advantages and disadvantages of PIXE/PIGE, XRF and EDX spectrometries applied to archaeometric characterisation of glasses, *Materials Characterization*, **61:** (2) 257-267.

33. Castellano.J.J., Shafii.S.M., Ko.F., Donate.G., Wright.T.E., Mannari.R.J., Payne.W.G., Smith.D.J, and Robson.M.C., (2007), Comparative evaluation of silver-containing antimicrobial dressings and drugs, *International Wound Journal,* **4:** (2) 114–122.

34. Chen.K.L., and Elimelech.M., (2007), Influence of humic acid on the aggregation kinetics of fullerene (C60) nanoparticles in monovalent and divalent electrolyte solutions. *J Colloid Interface Sci,* **309:**126–34.

35. Chinnapongse.S.L., MacCuspie.R.I., and Hackley.V.A., (2011),Persistance of singularly dispersed silver nanoparticles in natural freshwater, synthetic seawater and simulated estuarine waters, *Science of the Total Environment*, **409:** 2443-2450.

36. Choi.O., and Hu.O., (2008), Size Dependant and Reactive Oxygen Species Related to Nanosilver Toxicity to Nitrifying Bacterial., *Environmental Science and Technology,* **42:** 4583-4588.

37. Chopra.I., (2007), The increasing use of silver-based products as antimicrobial agents: a useful development or a cause for concern? *Journal of Antimicrobial Chemotherapy*, **59:** 587– 590.

38. Clark.B.J., and Russell.M.A., (1993), UV Spectroscopy: Techniques, Instrumentation, data handling; Techniques in Visible and Ultraviolet Spectrometry Volume 4, *Chapman and Hall.*

39. Council Directive (1976) on pollution caused by certain dangerous substances discharged into the aquatic environment of the community 76/464/EEC, *Official Journal of the European Communities.*

40. Cumberland.S.A and Baker.A, (2007), The freshwater dissolved organic matter fluorescence– total organic carbon relationship, *Hydrological Processes*, **21** (16): 2093-2099.

41. Cumberland.S.A., and Lead.J.R., (2009), Particle size distributions of silver nanoparticles at environmentally relevant conditions, *Journal of Chromatography A*, **1216:** 9099-9105.

42. Darlington.T.K., Neigh.A.M., Spencer.M.T., Nguyen.O.T., and Oldburg.S.J., (2009), Nanoparticle Characteristics Affecting Environmental Fate and Transportation Through Soil., *Environmental Toxicology and Chemistry,* **28:** (6) 1191–1199.

43. De Schamphel.K.A.C., and Jansen.C.R., (2002) A Biotic Ligand Model Predicting Acute Copper Toxicity for *Daphnia magna*: The Effects of Calcium, Magnesium, Sodium, Potassium, and pH. *Environ. Sci. Technol,* **36:** 48-54.

44. Delay. M., Dolt.T., Woellhaf.A., Sembritzki.R., and Frimmel.F.H., (2011), Interactions and stability of silver nanoparticles in the aqueous phase: Influence of natural organic matter (NOM) and ionic strength, *Journal of Chromatography A,* **1218:** 4206–4212.

45. Diegoli.S., Manciulea.A.L., Begum.S., Jones.I.P., Lead.J.R., and Preece.J.A., (2008), Interaction between manufactured gold nanoparticles and naturally occurring organic macromolecules. *Sci. Total Environ,* **402:** 51–61.

46. Doty.C,.R., Tshikhudo.R.T., Brust.M and Fernig.D.G, (2005), Extremely Stable Water-Soluble Ag Nanoparticles, *Chem. Mater.* **17:** 4630-4635.

47. Down.R.D., and Lehr.J.H, (2005), Environmental Instrumental and Analysis Handbook, Wiley Interscience, John Wiley and Sons Inc, Publication.

48. Dreyer.D., Ruoff.R.S., and Bielawshi.C.W., (2010), From Conception to Realization: An Historial Account of Graphene and Some Perspectives for Its Future, *Angewandte Chemie International Edition, **49:*** (49) 9336-9344.

49. Einstein.A., (1905), Über die von der molekularkinetischen Theorie der Wärme geforderte Bewegung von in ruhenden Flüssigkeiten suspendierten Teilchen, *Annalen der Physik,*322 (8): 549–560.

50. El Bradawy.A.M., Luxton.T.P., Silva.R.G., Scheckel.K.G., Suidan.M.T., and Tolaymat.T.M., (2010), Impact of Environmental Conditions (pH, Ionic Strength, and Electrolyte Type) on the Surface Charge and Aggregation of Silver Nanoparticles Suspensions.

51. El Badawy, A.M., Silva, R. G.; Morris, B.; Scheckel, K. G.;Suidan, M. T.; Tolaymat, T. M. (2011), Surface charge-dependent toxicity of silver nanoparticles. *Environ. Sci. Technol.* **45** (1): 283–287.

52. El Badawy.A.M., Hassan.A.A., Scheckel.K.G., Suidan.M.T., and Tolaymat.T.M., (2013), Key Factors Controlling the Transport of Silver Nanoparticles in Porous Media, *Environmental Science and Technology,* **47:** 4039-4045.

53. Elzey.S., and Grassian.V.H., (2010), Agglomeration, isolation and dissolution of commercially manufactured silver nanoparticles in aqueous environments, *J Nanopart Res,* **12:**1945–1958.

54. Esmaeili.P., Lin.F., and Yeung.A., (2012), Stability of Emulsified Heavy Oil: The Combined Effects of Deterministic DLVO Forces and Random Surface Charges, Langmuir, **28:** 4948−4954.

55. EU (2011) The European Commission Recommendation of 18 October 2011 on the definition of nanomaterial (2011/696/EU). O. J. L 275:38–40.

56. Fabrega.J., Fawcett.S.R., Renshaw.J.C., and Lead. J.R., (a) (2009), Silver Nanoparticle Impact on Bacterial Growth: Effect of pH, Concentration, and Organic Matter., *Environ. Sci. Technol*., **43**: 7285-729.

57. Fabrega.J., Renshaw.J.C., and Lead. J.R., (b) (2009), Interactions of Silver Nanoparticles with Pseudomonas putida Biofilms., *Environ. Sci. Technol*., **43**: 9004-9009.

58. Fabrega.J., Luoma.S.N., Tyler.C.R., Galloway.T.S andf Lead.J.R., (2011), Review; Silver nanoparticles: behaviour and effects in the aquatic environment, *Environment International*, **37:** 517-531.

59. Farre.M., Perez.S., Kantiani.L., and Barcelo.D., (2008), Fate and toxicity of emerging pollutants, their metabolites and transformation products in the aquatic environment, *Trends in Analytical Chemistry*, **27:** (11) 991-1007*.*

60. Feynman.R., (1959), There's plenty of room at the bottom, Lecture at the California Institute of Technology.

61. Fick,A., (1855), Ueber Diffusion, *Annalen der Physik*, **170** (1): 59-86.

62. Fiorino. D.J., (2010), VOLUNTARY INITIATIVES, REGULATION, AND NANOTECHNOLOGY OVERSIGHT: charting a path, Project on Emerging Nanotechnologies, Woodrow Wilson International Centre for Scholars, PEN 19 http://www.nanotechproject.org/process/assets/files/8347/pen-19.pdf.

63. Franchi.A., and O'Melia.C.R., (2003), Effects of Natural Organic Matter and Solution Chemistry on the Deposition and Reentertainment of Colloids in Pourous Media, *Environmental Science and Technology*, **37:** 1122-1129.

64. Freestone.I., Meeks.N., Sax.M., and Higgitt.C., (2007), The Lycurgus Cup –A Roman Nanotechnology, Gold Bulletin, **40:** (4) 270-277.

65. Gaiser.B.K., Fernandes.T.F., Jepson.M., Jamie R Lead.J.R., Tyler.C.R., and Stone.V., (2009), Assessing exposure, uptake and toxicity of silver and cerium dioxide nanoparticles from contaminated environments, *Environmental Health,* **8:** Suppl 1 pg:S2.

66. Garratt-Reed.A.J., and Bell.D.C., (2003), Energy Dispersive X-ray Analysis in the Electron Microscope, BIOS Scientific Publishers Limited.

67. Giddings.J.C., (1973), The conceptual basis of field-flow fractionation, *Journal of Chemical Education,* **50:** (10) 667-669.

68. Giddings.J.C., (1993) Field-Flow Fractionation: Analysis of Macromolecular, Colloidal, and Particulate Materials, *Science*, **260:** 1456-1465.

69. Gidings.J.C., Yang.F.J and Myers.M.N., (1977), Flow Field Fractionation: New Method for Separating, Purifying, and Characterizing the Diffusivity of Viruses, *Journal of Virology,* **21:** (1) 131-138.

70. Gimbert.L.J., Andrew.K.N., Haygarth.P.M., and Worsford.P.J., (2003), Environmental applications of flow field-flow fractionation (FIFFF), *Trends in Analytical Chemistry*, **22:** (10) 615-633.

71. Girard.J.E., (2010), Principles of Environmental Chemistry, Jones and Bartlett Publishers.

72. Goldburg.W.I., (1999), Dynamic light scattering, *American Journal of Physics*, **67** (12): 1152-1160.

73. Gorban.A.N., Sargsyan.H.P., and Wahab.H.A., (2011), Quasichemical Models of Multicomponent Nonlinear Diffusion, *Mathematical Modelling of Natural Phenomena*, **6** (5):184−262.

74. Gottschalk.F., Sonderer.T., Scholz.R.W., and Nowack.B., (2009), Modelled Environmental Concentrations of Engineered Nanomaterials (TiO_2, ZnO, Ag, CNT Fullerenes) for Different Regions. *Environmental Science and Technology,* **43**: 9216-9222.

75. Gottschalk.F., Sonderer.T., Scholz.R.W., and Nowack.B., (2010), Possibilities and limitations of modelling environmental exposure to engineered nanomaterials by probabilistic material flow analysis, *Environmental Toxicology and Chemistry*, **29:** (50) 1036-1048.

76. Gottschalk.F., Scholz.R.W., and Nowack.B., (2010b), Probabilistic material flow modelling for assessing the environmental exposure to compounds: Methodology and an application to engineered nano-TiO_2 particles. *Environmental Modelling & Software.* **25:** 320-332.

77. Grasso.D., Subramaniam.K., Butkus.M., Strevett.K., and Bergendahl.J., (2002), A review of non-DLVO interactions in environmental colloidal systems, *Re/Views in Environmental Science & Bio/Technology,* **1:** 17–38.

78. Gu.H., Ho.P.L., Tong.E., Wang.L., and Xu.B.,(2003), Presenting Vancomycin on Nanoparticles to Enhance Antimicrobial Activities, *Nano Letters*, **3:** (9) 1261-1263.

79. Ha.H., and Payer.J., (2011), The effect of silver chloride formation on the kinetics of silver dissolution in chloride solution, *Electrochima Acta*, **56:** 2781-2791.

80. Hammond.C.R., (2010), The Elements, in Handbook of Chemistry and Physics 81st edition. CRC press. ISBN 0849304814.

81. Hao.E., and Schatza.G.C., (2004), Electromagnetic fields around silver nanoparticles and dimers, *Journal of Chemical Physics,* **120:** (1)357-366.

82. Haugstad.G., (2012) Atomic Force Microscopy Understanding the Basic Modes and the Advanced Applications. Wiley.

83. Henglein.A and Giersig.M., (1999), Formation of Colloidal Silver Nanoparticles: Capping Action of Citrate*., J. Phys. Chem. B,* **103:** 9533-9539.

84. Higson.S.P., (2003), Analytical Chemistry, Oxford University Press.

85. Hinderliter.P.M., Minard.K.R., Orr.G., Chrisler.W.B., Thrall.B.D., Pounds.J.G., and Teeguarden. J.G.,(2010), ISDD: A computational model of particle sedimentation, diffusion and target cell dosimetry, for *in vitro* toxicity studies, *Particle and Fibre Toxicology*, **7:**36, http://www.particleandfibretoxicology.com/content/7/1/36.

86. Hotze.E.M., Phenrat.T., and Lowry.G.V., (2010), Nanoparticle Aggregations: Challenges to Understanding Transport and Reactivity in the Environment, *Journal of Environmental Quality,* **39:** 1909-1924.

87. International Organization for Standardization ISO (2008) Technical specification ISO/TS 27687:2008(E): Nanotechnologies—terminology and definitions for nanoprojects—nanoparticle, nanofibre and nanoplate.

88. Jiang.W., Mashayekhi.H., and Xing.B., (2009), Bacterial toxicity comparison between nano- and micro-scaled oxide particles, *Environmental Pollution,* 157: (5) 1619-1625.

89. Ju-Nam.Y. and Lead.J.R., (2008), Manufactured nanoparticles: An overview of their chemistry, interactions and potential environmental implications, *Science of the Total Environment,* **400:** 396-414.

90. Kaegi.R., Ulrich.A., Sinnet.B., Vonbank.R., Wichser.A., Zuleeg.S., Simmler.H., Brunner.S., Vonmont.H., Burkhardt.M., and Boller.M., (2008), Synthetic TiO_2 nanoparticle emission from exterior facades into the aquatic environment: *Environ.Pollut*, **156**: (2) 233-239.

91. Kaegi.R., Sinnet.B., Zuleeg.S., Hagendorfer.H., Mueller.E., Vonbank.R., Boller.M., and Burkhardt.M., (2010), Release of silver nanoparticles from outdoor facades, *Environmental Pollution*, **158:** 2900-2905.

92. Kalinin.S.V., and Gruverman.A., (2010), Scanning Probe Microscopy of Functional Materials: Nanoscale Imaging and spectroscopy, Springer.

93. Kalmykov.S.N., and Denecke.M.A., (2011), Actinide Nanoparticle Research, Springer.

94. Kannan.N., Mukunthan.K.S., Balaji.S., (2011), A comparative study of morphology, reactivity and stability of synthesized silver nanoparticles using Bacillus subtilis and Catharanthus roseus (L.) G. Don, *Colloids and Surfaces B: Biointerfaces*, **86:** 378–383.

95. Kawaguchi.K., Saito.M., Takahiro.K., Yamamoto.S., and Yoshikawa.M, (2011), Blueshift and narrowing of localised surface plasmon resonance of silver nanoparticles exposed to plasma.*Plasmonics*, **6:** 535-539.

96. Keller.A.A., Wang.H., Zhou.D., Lenihan.H.S., Cherr.G., Cardinale.B.J., Miller.R., and Ji.Z., (2010), Stability and Aggregation of Metal Oxide Nanoparticles in Natural Aqueous Matrices, *Environ. Sci. Technol*, **44:** 1962–1967.

97. Kelly. K.L., Coronado.E., Zhao.L.L., and Schatz.G.C., (2003), The Optical Properties of Metal Nanoparticles: The Influence of Size, Shape, and Dielectric Environment, *J. Phys. Chem. B,* **107:** (3) 668-677.

98. Khani.R., Shemirani.F., and Majidi.B., (2011), Combination of dispersive liquid-liquid microextraction and flame atomic absorption spectrometry for preconcentration and determination of copper in water samples, *Desalination,* **226:** 238-243.

99. Khopkar.S.M., (1998), Basic Concepts of Analytical Chemistry, Second Edition, New Age International Publishers.

100. Kim.J.Y., Lee.C., Cho.M., and Yoon.J., (2008) Enhanced inactivation of *E. coli* and MS-2 phage by silver ions combined with UV-A and visible light irradiation, *Water Research*, **42:** (1-2) 356-362.

101. Kittler.S., Greulich.C., Diendorf.J., Köller.M., and Epple.M., (2010) Toxicity of silver nanoparticles increases during storage because of slow dissolution under release of silver ions, *Chem Mater,* **22:** (16) 4548-4554.

102. Kroto.H.W., Heath.J.R., O'Brien.S.C., Curl.R.F., and Smalley.R.E., (1985), C_{60}: Buckminsterfullerene, *Nature* **318**: 162 – 163.

103. Klasen.H.J, (2000), Historical review of the use of silver in the treatment of burns. I. Early uses, *Burns*, **26:** 117-130.

104. Koelmans.A.A., Nowack.B., and Wiesner.M.R., (2009), Comparison of manufactured and black carbon nanoparticle concentrations in aquatic sediments, *Environmental Pollution*, **157:** 1110-1116.

105. Kvıtek.L., Panacek.A., Soukupova.J., Kolar.M., Vecerova.R., Prucek.R., Holecova.M., and Zboril.R., (2008), Effect of Surfactants and Polymers on Stability and Antibacterial Activity of Silver Nanoparticles (NPs), *J. Phys. Chem. C ,* **112:** 5825-5834.

106. Lakowicz.J.R., (2006), Principles of Fluorescence Spectroscopy, Third Edition, Springer.

107. Lara.H.H., Ixtepan-Turrent.L., Trevino.E.N.G., and Singh.D.K., (2011), Use of silver nanoparticles increased inhibition of cell-associated HIV-1 infection by neutralizing antibodies developed against HIV-1 envelope proteins, *J Nanobiotechnology,* **9:** (38) doi:10.1186/1477-3155-9-38.

108. Lead.J.R., K.J. Wilkinson.K.J., (2006) Environmental colloids and particles: behaviour, structure and characterisation, John Wiley and Sons.

109. Lem.K.W., Choudhury.A., Lakhani.A.A., Kuyate.P., Haw.J.R.,, Lee.D.S., Iqbal.Z., and Brumlik.C.J., (2012), Use of Nanosilver in Consumer Products, *Recent Patents on Nanotechnology* , **6:** 60-72.

110. Lee.J-H., Gomez.I., and Meredith.J.C., (2011), Non-DLVO Silica Interaction Forces in NMPWater Mixtures. I. A Symmetric System, *Langmuir,* **27:** 6897–6904.

111. Levard.C., Reinsch.B.C., Michel.F.M., Oumahi.C., Lowry.G.V., and Brown.G.E., (2011), Sulfidation Processes of PVP-Coated Silver Nanoparticles in Aqueous Solution: Impact on Dissolution Rate, *Environmental Science and Technology,* **45:** 5260–5266

112. Levard.C., Mitra.S., Yang.T., Jew.A.D., Badireddy.A.R., Lowry.G.V., and Brown.G.E., (2013), Effect of Chloride on the Dissolution Rate of Silver Nanoparticles and Toxicity to *E. coli, Environmental Science and Technology,* **47:** 5738-5745.

113. Li.C.C., Chang.S.J., Su.F.J., Lin.S.W., and Chou.Y.C., (2013), Effects of capping agents on the dispersion of silver nanoparticles, *Colloids and Surfaces A: Physicochemical and Engineering Aspects,* **419:** 209-215.

114. Li.G., and Chen.Y., (2012), Evaluation of DLVO interaction between a sphere and a cylinder, *Colloids and Surfaces A: Physicochem. Eng. Aspects,* **415:** 218– 229.

115. Li.Q., Mahendra.S., Lyon.D.Y., Brunet.L., Liga.M.V., Li.D., and Alvarez.P.J.J., (2008), Review: Antimicrobial nanomaterials for water disinfection and microbial control: Potential applications and implications, *Water Research,* **42:** 4591–4602.

116. Li.S., and Sun.W., (2011), A comparative study on aggregation/sedimentation of TiO_2nanoparticles in mono- and binary systems of fulvic acids and Fe(III), *Journal of Hazardous Materials*, 197: 70-79.

117. Li.X., Lenhart.J.J., and Walker.H.W., (2010), Dissolution-Accompanied Aggregation Kinetics of Silver Nanoparticles. *Langmuir*, **26** (22): 16690-16698.

118. Li.X., Lenhart.J.J., and Walker.H.W., (2012), Aggregation Kinetics and Dissolution of Coated Silver Nanoparticles, Langmuir, **28:** 1095−1104.

119. Li.X., and Lenhart.J.J., (2012), Aggregation and Dissolution of Silver Nanoparticles in Natural Surface Water*, Environmental Science and Technology,* **46:** 5378−5386.

120. Li.Y., Zhang.W., Niu.J., and Chen.Y., (2013b), Surface-Coating-Dependent Dissolution, Aggregation, and Reactive Oxygen Species (ROS) Generation of Silver

Nanoparticles under Different Irradiation Conditions, *Environmental Science and Technology*, **47**: 10293−10301.

121. Li.Z., Endalkachew.S., Hassan.A.A., and Sorial.G.A., (2011), Transport and deposition of CeO_2 nanoparticles in water-saturated porous media, *Water Research*, **45:** 4409-4418.

122. Liang.Y., Hilal.N., Langston.P., and Starov.V., (2007), Interaction forces between colloidal particles in liquid: Theory and experiment, *Advances in Colloid and Interface Science,* **134–135:** 151–166.

123. Linke.R. Schreiner.M., and Demortier.G., (2004), The application of photon induced X-ray analysis for the identification and characterisation of medieval silver, *Nuclear Instruments and Methods in Physics Research,* **226:** 172-178.

124. Linlin.Z., and Tanaka.K.,(2013), Dissolution of silver nanoparticles in presence of natural organic matter, *Advanced Material Letters*, **DOI:** 10.5185/amlett.2013.75.20.

125. Linskens.H.F., and Jackson.J.F., (1999), Analysis of Plant Waste Materials, Modern Methods of Plant Analysis Volume 20, Springer.

126. Liu.J., and Hurt.R.H., (2010), Ion relese kinetics and particle persistence in aqueous nano-silver colloids, *Environ. Sci. Technol,* **44:** 2169–2175.

127. Llobet.E., (2013), Gas sensors using carbon nanomaterials: A review*, Sensors and Actuators B*, **179:** 32–45.

128. Loehman.R.E., (2010), Series editors Brundle.R.C and Evans Jr.C.A., Characterization of Ceramics, Momentum Press.

129. Lovern.S.B., Strickler.J.R., and Klaper.R., (2007), Behavioral and Physiological Changes to Daphnia magna when Exposed to Nanoparticle Suspensions (Titanium Dioxide, Nano-C_{60}, and $C_{60}HxC_{70}Hx$), *Environ. Sci. Technol.* **41**, 4465-4470.

130. Lowry.G.V., Espinasse.B.P., Badireddy.A.R., Richardson.C.J., Reinsch.B.C., Lee D. Bryant.L.D., Bone.A.J., Deonarine.A., Chae.S., Therezien.M., Colman.B.P., Hsu-Kim.H., Bernhardt.E.S., Matson.C.W., and Wiesner.M.R., (2013), Long-Term Transformation and Fate of Manufactured Ag Nanoparticles in a Simulated Large Scale Freshwater Emergent Wetland, *Environmental Science and Technology,* **46:** 7027-7036.

131. Ma.R., Levard.C., Marinakos.S.M., Cheng.Y., Liu.J., Michel.F.M., Brown.G.E., and Lowry.G.V., (2012), Size-Controlled Dissolution of Organic-Coated Silver Nanoparticles, *Environmental Science and Technology*, **46:** 752-759.

132. MacCuspie.R.I., Rogers.K., Patra.M., Suo.Z., Allen.A.J., Martin.M.N., and Hackley.V.A., (2011), Challenges for physical characterization of silver nanoparticles under pristine and environmentally relevant conditions, *J. Environ. Monit,* **13:** 1212–1226.

133. Magnuson.B.A., Jonaitis.T.S, and ard.J.W., (2011) A Brief Review of the Occurrence, Use, and Safety of Food-Related Nanomaterials *Journal of Food Science*, 76: (6)126-133.

134. Malvern Instruments Ltd, (2004), Zetasizer Nano Series User Manual, MAN0317, Issue 1.1.

135. Manciulea.A., Baker.A., and Lead.J.R., (2009), A fluorescence quenching study of the interaction of Suwannee River fulvic acid with iron oxide nanoparticles, Chemosphere **76:** 1023–1027.

136. Martín.M., Carmona.F., Cuesta.R., Rondón.D., Gálvez.N., and Domínguez-Vera.J.M., (2014), Artificial Magnetic Bacteria: Living Magnets at Room Temperature, *Advanced Functional Materials*, DOI: 10.1002/adfm.201303754.

137. Mason.M.,and Weaver.W., (1924), The Settling of Small Particles in a Fluid, *Phys. Rev.* 23: 412–426.

138. Mellies.J.L., Thomas.K. Turvey.M., Evans.N.R., Crane.J., Boedeker.E., and Benison.G.C., (2012), Zinc–induced envelope stress diminishes type III secretion in enteropathogenic Escherichia coli, *BMC Microbiology*, **12:**123 DOI:10.1186/1471-2180-12-123.

139. Miao.A-J., Schwehr.K.A., Xu.C., Zhang.S-J., Luo.Z., Quigg.A., amd Santschi.P.H., (2009) The algal toxicity of silver engineered nanoparticles and detoxification by exopolymeric substances, *Environmental Pollution*, **157:** 3032-3041.

140. Misra.S.k., Dybowska.A., Berhanu.D., Luoma.S.N., and Valsami-Jones.E., (2012), The complexity of nanoparticle dissolution and its importance in nanotoxicological studies, *Science of the Total Environment,* **438:** 225-232.

141. Moriasi.D.N., Arnold.J.G., Van Liew.M.W., Bingner.R.L., Harmel.R.D., and Veith.T.L., (2007), Model Evaluation guildlines for systematic quantification of accuracy in watershed simulations, *Transactions of the ASABE*, Vol. **50** (3): 885−900.

142. Muller.N.C and Nowack.B., (2008), Exposure Modelling of Engineered Nanoparticles in the Environment, *Environmental Science and Technology*, **42:** 4447–4453.

143. Murphy.R.M., (1997), static and dynamic light scattering of biological macromolecules: what can we learn? *Current Opinion in Biotechnology*, **8:** (1) 25-30.

144. Navarro.E., Baun.A., Behra.R., Hartmann .N.B., Filser.J., Miao.A-J., Quigg.A., Santschi.P.H., and Sigg.L., (2008), Environmental behavior and ecotoxicity of engineered nanoparticles to algae, plants, and fungi, *Ecotoxicology*, **17:** 372–386.

145. Nielsen.S.S, (2010), Food Analysis, Fourth Edition, Springer.

146. Ninham.B.W.,(1999), On progress in forces since the DLVO theory, *Advances in Colloid and Interface Science,* **83:** (1-3) 1-17.

147. Nowack.B., and Bucheli.T.D., (2007), Review: Occurrence, behavior and effects of nanoparticles in the environment, *Environmental Pollution*, **150:** 5-22.

148. Nowack.B., Krug.H.F., and Height.M., (2011), 120 Years of Nanosilver History: Implications for Policy Makers, *Environmental Science and Technology*, **45:** 1177-1183.

149. Oshida.K., Murata.M., Fujiwara.K., Itaya.T., Yanagisawa.T., Kimura.K., Nakazawa.T., Kim.Y.A., Endo.M., Kim.B.H., and Yang., (2013), Structural analysis of nano structured carbon by transmission electron microscopy and image processing. *Applied Surface Science,* **275:** 409-412.

150. Park.K., Park.E-J., Chun.I.K., Choi.K., Lee.S.H., Yoon.J., and Lee.B.C., (2011),Bioavailability and Toxicokinetics of Citrate-coated Silver Nanoparticles in Rats, *Arch Pharm Res,* **34:** (1) 153-158.

151. Phenrat.T., Saleh.N., Sirk.K., Tilton.R.D., and Lowry.G.V., (2007), Aggregation and Sedimentation of Aqueous Nanoscale Zerovalent Iron Dispersions, *Environ. Sci. Technol*., **41:** 284-290.

152. Piccinno.F., Gottschalk.F., Seeger.S., and Nowac.B., (2012), Industrial production quantities and uses of ten engineered nanomaterials in Europe and the world, *J Nanopart Res,* 14:1109.

153. Pillai.Z.S., and Kamat.P.V., (2004), What Factors Control the Size and Shape of Silver Nanoparticles in the Citrate Ion Reduction Method?, *J. Phys. Chem. B,* **108:** 945-951.

154. Pinchuk.A., Hilger.A., Plessen.G., and Kreibig.U., (2004) Substrate effect on the optical response of silver nanoparticles, *Nanotechnology,* **15**: 1890–1896.

155. Project on Emerging Nanotechnologies Consumer Products Inventory (2014), Retrieved [09/02/2014] from http://www.nanotechproject.org/cpi/.

156. Quadros.M.E., and Marr.L.C., (2010), Environmental and Human Health Risks of Aerosolized Silver Nanoparticles, *J. Air & Waste Manage. Assoc*, **60:** 770 –781.

157. Radziuk.D., Skirtach.A., Sukhorukov.G., Shchukin.D., and Mohwald.H., (2007), Stabilization of Silver Nanoparticles by Polyelectrolytes and Poly(ethylene glycol), *Macromolecular Rapid Communications*, **28**(7): 848–855.

158. Raghupathi.K., Koodali.R.T., and Manna.A.C., (2011), Size-Dependent Bacterial Growth Inhibition and Mechanism of Antibacterial Activity of Zinc Oxide Nanoparticles, *Langmuir*, **27:** 4020–4028.

159. Rai.M., Yadav.A., Gade.A., (2009), Silver nanoparticles as a new generation of antimicrobials, *Biotechnology Advance,* **27:** 76–83.

160. Reidy.B.,, Haase.A., Luch.A., Dawson.K.A., and Lynch.I.,(2013), Mechanisms of Silver Nanoparticle Release, Transformation and Toxicity: A Critical Review of Current

Knowledge and Recommendations for Future Studies and Applications, *Materials*, **6:** 2295-2350.

161. Reimer.L., and Kohl.H., (2008), Transmission Electron Microscopy, Physics of Image Formation, *Springer*, Springer Series in Optical Sciences 36, Fifth Edition.

162. Reschiglian.P., Rambaldi.D.C., and Zattoni.A., (2010), Flow field-flow fractionation with multiangle light scattering detection for the analysis and characterization of functional nanoparticles, *Anal Bioanal Chem.* DOI 10.1007/s00216-010-4197-3 http://www.springerlink.com/content/w36410373x04021m/fulltext.pdf Accessed on 9/11/10.

163. Rispoli.F., Angelov.A., Badia.D., Kumar.A., Seal.S., and Shah.V., (2010), Understanding the toxicity of aggregated zero valent copper nanoparticles against *Escherichia coli, Journal of Hazardous Materials,* 180: (1-3) 212-216.

164. Romer.I., White.T.A., Baalousha.M., Chipman.K., Viant.M and Lead.J.R., (2011), Aggregation and dispersion of silver nanoparticles in exposure media for aquatic toxicity tests, *Journal of Chromatography A*, **1218:** 4226– 4233.

165. Rose.H.H., (2008), Optics of high-performance electron microscopes, *Sci. Technol. Adv. Mater.* **9** 014107 IP Address: 147.188.128.74.

166. Socolofsky.S.A., and Jirka.G.H., (2004), Environmental Fluid Mechanics 1: Mixing and Transport Processes in the Environment, Coastal and Ocean Engineering Division, 5th Edition.

167. Song.X., Gunawan.P., Jiang.R., Leong.S.S.J, Wang.K., and Xu.R., (2011), Surface activated carbon nanospheres for fast adsorption of silver ions from aqueous solutions, *Journal of Hazardous Materials*, **194:** 162–168.

168. Sotiriou.G.A and Pratsinis.S.E, (2010), Antibacterial Activity of Nanosilver Ions and Particles, *Environ. Sci. Technol,* **44:** 5649–5654.

169. Soto.K.F., Carrasco.A., , Powell.T.G., K.M. Garza.K.M., and LMurr.L.E, (2005), Comparative in vitro cytotoxicity assessment of some manufactured nanoparticulate materials characterized by transmission electron microscopy, *Journal of Nanoparticle Research,* **7:** 145–169.

170. Srivastava. R., and Khanna.K.N., (2009) Stokes-Einstein Relation in Two- and Three-Dimensional Fluids. *J.Chem.Eng.Data,* **54:** 1452-1456.

171. Stamplecoskie.K.G., and Scaiano.J.C., (2012), Silver as an example of the applications of photochemistry to the synthesis and uses of nanomaterials. *Photochemistry and photobiology,* **88:** 762-768.

172. Stankus.D.P., Lohse.S.E., Hutchison.J.E., and Nason.J.A., (2011), Interactions between natural organic matter and gold nanoparticles stabilized with different organic capping agents, *Environmental Science and Technology*, 45 (8): 3238-3244.

173. Stawikowska. J., and Livingston.A.G., (2013), Assessment of atomic force microscopy for characterisation of nanofiltration membranes, *Journal of Membrane Science,* **425–426**: 58–70.

174. Taboada-Serrano.P., Chin.C.J., Yiacoumi.S., Costas Tsouris.C., (2005), Modeling aggregation of colloidal particles, *Current Opinion in Colloid & Interface Science,* **10:** 123 – 132.

175. Tang.P., Greenwood.J., and Raper.J.A., (2002), a model to describe the settling behaviour of fractal aggregates, *Journal of Colloid and Interface Science,* **247:** 210–219.

176. Taniguchi N. (1974), On the Basic Concept of Nano-Technology. Proc. Intl. Conf. Prod. Eng. Tokyo, Part II. *Japan Society of Precision Engineering.*

177. Taylor.H.E., (2001), Inductively Coupled Plasma –Mass Spectrometry: Practices and Techniques, Academic Press.

178. Tejamaya.M., Römer.I., Merrifield.R.C., Lead.J.R., (2012), Stability of Citrate, PVP and PEG Coated Silver Nanoparticles in Ecotoxicology Media, *Environ. Sci. Technol.* **46:** 7011-7017.

179. Thomas.R., (2008) Practical Guide to ICP-MS: A Tutorial for Beginners, Practical Spectroscopy Series Volume 37, Second Edition, CRC Press.

180. Tolaymat.T.M., El Badawy.A.M., Genaidy.A., Scheckel.K.G., Luxtona.T.P., and Suidanb.M., (2010), An evidence-based environmental perspective of manufactured silver nanoparticle in syntheses and applications: A systematic review and critical appraisal of peer-reviewed scientific papers, *Science of the Total Environment,* **408:** 999-1006.

181. Tsuji.K., Injuk.J., and Grieken.R.V., (2004), X-Ray Spectrometry: Recent Technological Advances, Wiley.

182. United States Environmental Protection Agency USA EPA, (2010), Scientific, Technical, Research, Engineering and Modeling Support. Final Report State of the Science Literature Review: Everything Nanosilver and More.

183. Van Hoecke.K., De Schamphelaere.K.A.C., Van der Meeren.P., Smagghe.G., and Janssen.C.R., (2011), Aggregation and ecotoxicity of CeO_2 nanoparticles in synthetic and natural waters with variable pH, organic matter concentration and ionic strength, *Environmental Pollution,* **159:** 970-976.

184. Waychunas.G.A., Gilbert.B., Banfield.J.F., Zhang.H., Jun.Y.S., Kim.C.S., (2009), Natural Nanoparticle structure, Properties and Reactivity from X-ray Studies. 41-49 ISSN 1097-0002.

185. Wigginton.N.S., Haus.K.L., and Hochella-Jr.M.F., (2007), Aquatic environmental nanoparticles, *Journal of Environmental Monitoring*, **9:** (12) 1285-1432.

186. Wodka.D., Bielan.E.S., Socha.R.P., Elzbieciak – Wodka.M., Gurgul.J., Nowak.P., Warszyn.P. and Kumakiri.I., (2010), Photocatalytic activity of titanium dioxide modified by silver nanoparticles*, ACS Applied Materials and Interfaces,* **2:** (7) 1945-1953.

187. Xia.H., Pang.R.Y., Zhang.R., Miao.C.X., Wu.X.Y., Hou.X.S., and Zhong.C., (2012, Study of colloidal particle Brownian aggregation by low-coherence fiber optic dynamic light scattering, *Journal of Colloid and Interface Science*, **376:** 322-326.

188. Xu.P., Zeng.G.M., Huang.D.L., Feng.C.L., Shuang Hu.S., Hua Zhao.M.H., Lai.C., Wei.Z., Huang.C., Xie.G.X., and Liu.Z.F., (2012), Use of iron oxide nanomaterials in wastewater treatment: A review, *Science of The Total Environment*, **424:** 1–10.

189. Zhang.H., and Oyanedel-Craver.V.,(2012) Evaluation of the Disinfectant Performance of SilverNanoparticles in Different Water Chemistry Conditions, *Journal of Environmental Engineering*, **138:** 58-66.

190. Zhang.W., Yao.Y., Li.K., Huang.Y., and Chen.Y., (2011), Influence of dissolved oxygen on aggregation kinetics of citrate-coated silver nanoparticles, *Environmental Pollution,* **159:** (12) 3757-3762.

191. Zhang.W., Yao.Y., Sullivan.N., Chen.Y., (2011) (b) Modeling the primary size effects of citrate-coated silver nanoparticles on their ion release kinetics, *Environ Sci Technol*, **45:** 4422-4428.

192. Zhang.Y., Chen.Y., Westerhoff.P., Crittenden.J., (2009) Impact of natural organic matter and divalent cations on the stability of aqueous nanoparticles, Water Research, 43: 4249-4357.

193. Zook.J.M., Long.S.E., Cleveland.D., Geronimo.C.L.A.,and MacCuspie.R.I., (2011), Measuring silver nanoparticle dissolution in complex biological and environmental matrices using UV–visible absorbance, *Anal Bioanal Chem*, **401:** 1993–2002.

194. Zou.X., Ying.E., Chen.H., Dong.S., (2007), An approach for synthesizing nanometer- to micrometer-sized silver nanoplates, *Colloids and Surfaces A: Physicochem. Eng. Aspects*, **303:** 226–234.

Appendix 1: Chapter 4 Additional Information

$AgNO_3$ Exposure Studies

Table A1.1: Average total concentration results (ppb) for $AgNO_3$ exposed to Ultrapure water			
Time (hrs)	**Surface**	**Middle**	**Bottom**
0	5183 ± 0.17	56 ± 0.02	17 ± 0.05
0.5	4121 ± 0.14	48 ±0.17	18 ± 0.06
1.5	4025 ± 0.14	27 ±0.10	53 ± 0.19
3.5	3286 ± 0.12	217 ± 0.08	49 ± 0.17
5.5	2814 ± 0.09	566 ± 0.02	85 ± 0.03
24	744 ± 0.03	236 ± 0.08	187 ± 0.07
48	187 ± 0.07	146 ± 0.05	268 ± 0.09
72	129 ± 0.05	277 ± 0.09	190 ± 0.07
288	131 ± 0.06	136 ± 0.05	135 ± 0.08

Information presented in table A1.1 is used to describe the total Ag data in figures 4.1 and 4.2.

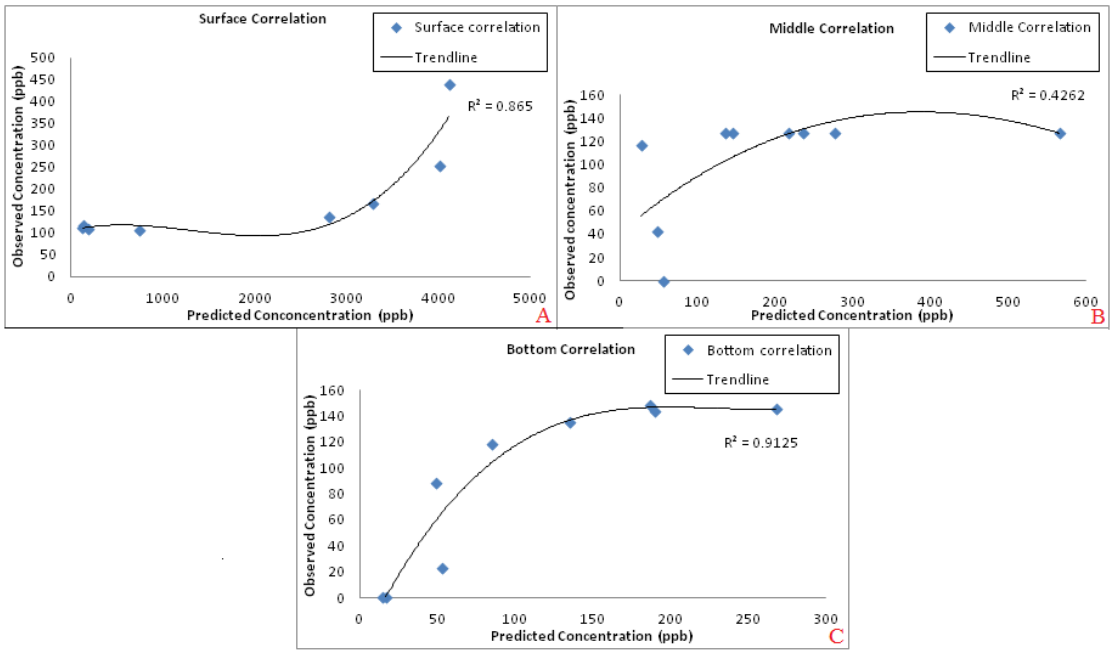

Figure A1.1: Correlation values for the observed and predicted modelled Ag concentrations for $AgNO_3$ exposed to UPW according to parameters fixed in table 4.1 in text. A) Surface correlations, B) middle depth correlations and C) bottom depth correlations.

Table A1.2: Total $AgNO_3$ concentration recovery when exposed to EPA water			
Time (hours)	**Surface**	**Middle**	**bottom**
0	1415 ± 0.05	13 ± 0.43	7 ± 0.22
0.5	906 ± 0.03	26 ± 0.91	13 ± 0.43
1.5	802 ± 0.03	39 ± 0.01	14 ± 0.05
3.5	736 ± 0.02	47 ± 0.16	39 ± 0.13
5.5	650 ± 0.23	50 ± 0.18	62 ± 0.21
24	323 ± 0.11	122 ±0.04	67 ± 0.22
48	258 ± 0.91	202 ± 0.71	89 ±0.03
72	210 ± 0.07	279 ± 0.92	78 ± 0.34
288	144 ± 0.45	147 ± 0.57	97 ±0.03

Information presented in table A1.2 is used to describe the total Ag data in figures 4.3 and 4.4

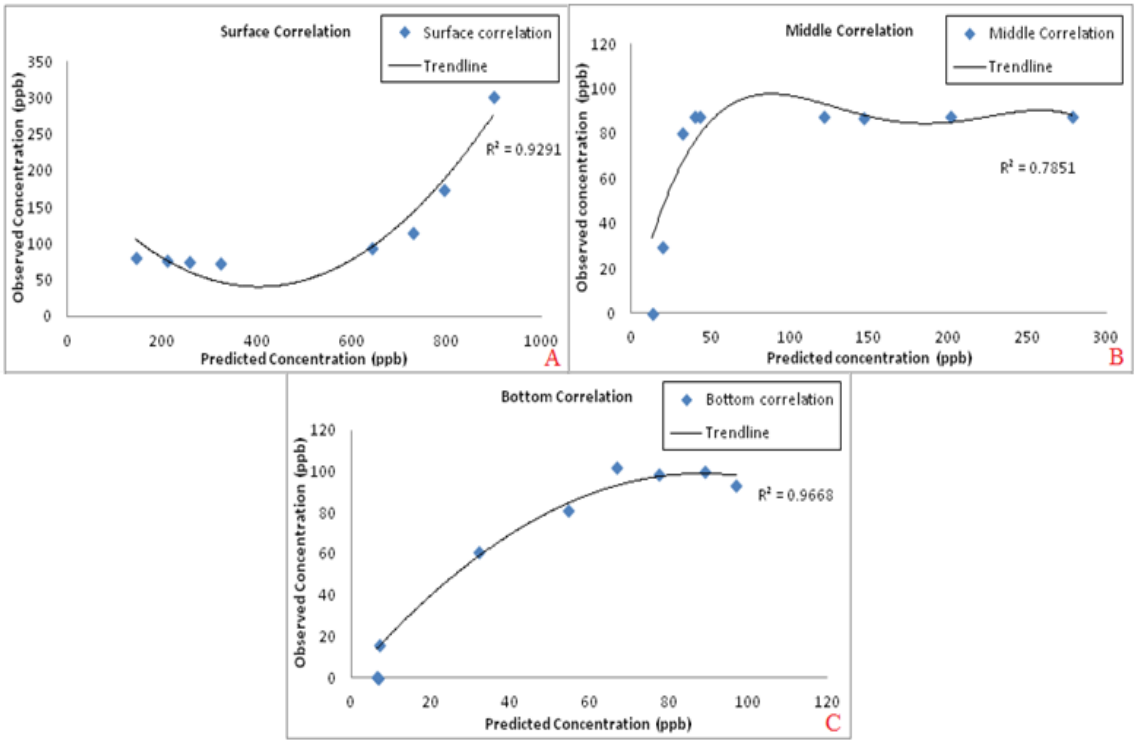

Figure A1.2: Correlation values for the observed and predicted modelled Ag concentrations for $AgNO_3$ exposed to EPA water according to parameters fixed in table 4.1 in text. A) Surface correlations, B) middle depth correlations and C) bottom depth correlations.

Ultrapure Water Exposures

Table A1.3: Average total silver concentration (ppb) recovery for citrate AgNPs in ultrapure water				
Time (Day)	Time (hours)	surface	Middle	Bottom
0	0	3040 ± 0.12	6 ± 0.11	7 ± 0.04
0	0.5	2517 ± 0.24	48 ± 0.89	7 ± 0.02
0	1.5	2395 ± 0.25	49 ± 0.19	14 ± 0.12
0	3.5	2035 ± 0.11	52 ± 0.34	27 ± 0.07
0	5.5	2564 ±0 .09	38 ± 0.01	39 ± 0.37
1	24	1599 ± 0.26	162 ± 0.50	66 ± 0.13
2	48	770 ± 0.16	110 ± 0.35	65 ± 0.34
3	72	489 ± 0.12	112 ± 0.01	62 ± 0.45
4	96	303 ± 0.12	101 ± 0.18	61 ± 0.89
5	120	214 ± 0.06	73 ± 0.08	73 ± 0.32
6	144	216 ± 0.04	103 ± 0.07	77 ± 0.23
7	168	164 ± 0.01	88 ± 0.06	74 ± 0.09
8	192	111 ± 0.21	74 ± 0.19	72 ± 0.15
9	216	87 ± 0.01	58 ± 0.09	56 ± 0.01
10	240	106 ± 0.01	77 ± 0.03	72 ± 0.39
11	264	64 ± 0.09	56 ± 0.19	63 ± 0.11
12	288	91 ±0.02	78 ± 0.09	73 ± 0.11
13	312	74 ± 0.03	60 ± 0.03	68 ± 0.01
14	336	70 ± 0.03	41 ± 0.14	63 ±0.02
21	504	61 ± 0.23	61 ± 0.12	59 ± 0.02
28	672	91 ± 0.19	69 ± 0.03	77 ± 0.03

Table A1.4 Average total Silver recovery (ppb) for PVP AgNPs in ultrapure water				
Time (Days)	time (Hours)	Surface	Middle	Bottom
0	0	5525 ± 0.28	31 ± 0.03	50 ± 0.03
0	0.5	3575 ± 0.34	36 ± 0.03	16 ± 0.08
0	1.5	2676 ± 0.57	130 ± 0.14	68 ± 0.05
0	3.5	2516 ± 0.31	52 ± 0.02	101 ± 0.09
0	5.5	1287 ± 0.37	156 ± 0.98	187 ± 0.19
1	24	1113 ± 0.28	308 ± 0.27	386 ± 0.35
2	48	381 ± 0.13	36 ± 0.23	33 ± 0.02
3	72	242 ± 0.13	27 ± 0.01	8 ± 0.05
4	96	96 ± 0.04	12 ± 0.04	47 ± 0.04
5	120	60 ± 0.05	22 ± 0.02	23 ± 0.05
6	144	71 ± 0.03	49 ± 0.12	46 ± 0.02
7	168	82 ± 0.07	75 ± 0.05	69 ± 0.05
8	192	61 ± 0.03	57 ± 0.05	45 ± 0.03
9	216	53 ± 0.04	43 ± 0.06	36 ± 0.03
10	240	28 ± 0.04	19 ± 0.04	23 ± 0.05
11	264	42 ± 0.02	35 ±0.03	37 ± 0.03
12	288	35 ± 0.01	27 ± 0.02	30 ± 0.03
13	312	39 ± 0.02	31 ± 0.25	34 ± 0.01
14	336	36 ± 0.03	61 ± 0.11	69 ± 0.02
21	504	84 ± 0.01	75 ± 0.10	68 ± 0.15
28	672	66 ± 0.02	27 ± 0.17	33 ± 0.03

Information in tables A1.3 and A1.4 were used to provide total Ag information used in figure 4.5.

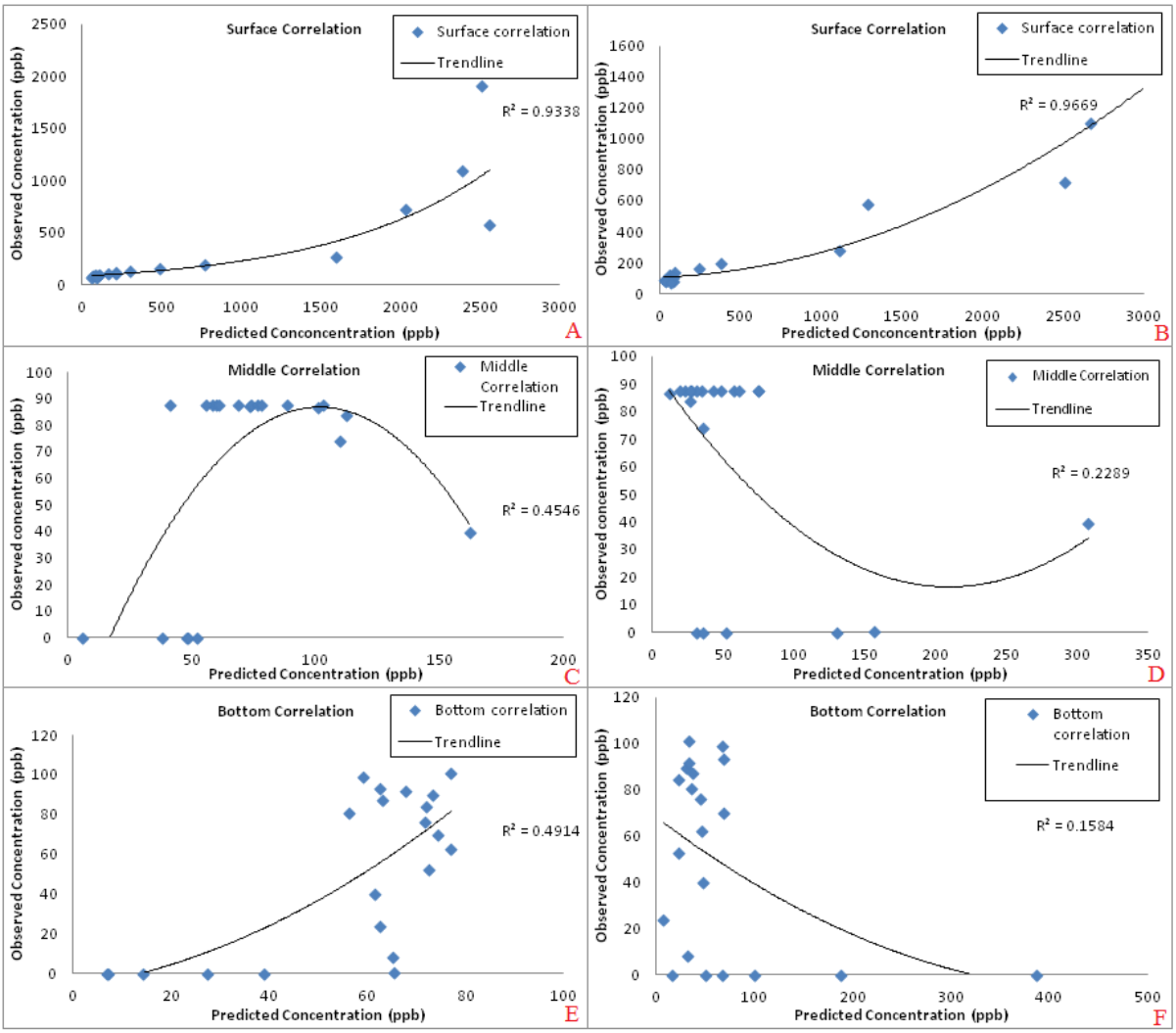

Figure A1.3: Correlation values for the observed and predicted modelled Ag concentrations for citrate and PVP AgNPs exposed to UPW according to parameters fixed in table 4.2 in text. A) citrate AgNP study in the surface, B) PVP AgNP study in the surface, C) citrate AgNP study in the middle, D) PVP AgNP study in the middle, E) citrate AgNP study in the bottom, and F) PVP AgNP study in the bottom.

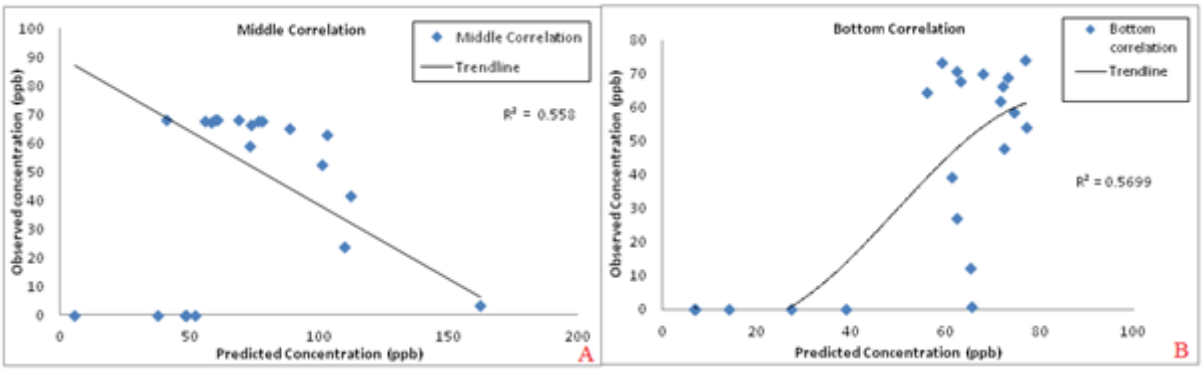

Figure A1.4: Correlation values for the observed and predicted modelled Ag concentrations for the adjusted model parameters for the citrate AgNPs according to table 4.3 in text. A) Middle correlations and B) bottom correlations.

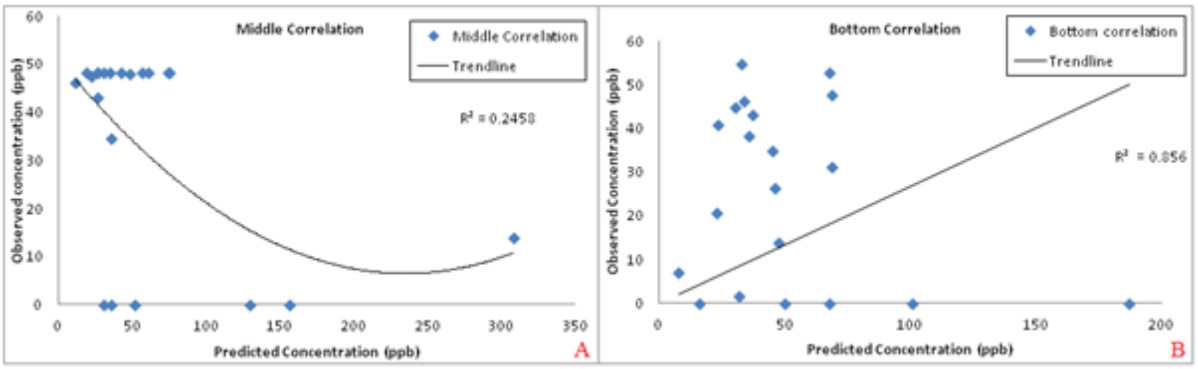

Figure A1.4: Correlation values for the observed and predicted modelled Ag concentrations for the adjusted model parameters for the PVP AgNPs according to table 4.4 in text. A) Middle correlations and B) bottom correlations.

Table A1.5: Average corrected dissolved silver (ppb) and NP fraction data for citrate AgNPs in ultrapure water using ultrafiltration								
Day	Surface				Bottom			
	Total Ag (ppb)	NP fraction	Dissolved Ag	% dissolved fraction	Total Ag (ppb)	NP fraction	Dissolved Ag	% dissolved fraction
1	1599 ± 0.26	1383	216 ± 0.23	14	66 ± 0.13	38	28 ± 0.03	42
2	770 ± 0.16	681	89 ± 0.97	12	65 ± 0.34	35	30 ± 0.83	46
3	489 ± 0.12	348	141± 0.13	29	62 ± 0.45	20	43 ± 0.01	68
4	303 ± 0.12	215	88 ± 0.09	29	61 ± 0.89	15	47 ± 0.03	76
5	214 ± 0.06	132	82 ± 0.07	38	73 ± 0.32	33	40 ± 0.04	55
6	216 ± 0.04	201	15 ±0/03	7	77 ± 0.23	52	25 ± 0.01	32
7	164 ± 0.01	128	36 ± 0.01	22	74 ± 0.09	44	31 ± 0.04	41
8	111 ± 0.21	49.2	62 ±0.04	56	72 ± 0.15	48	24 ± 0.01	33
9	87 ± 0.01	32	55 ± 0.03	63	56 ± 0.01	31	25 ±0.06	44
10	106 ± 0.01	59	47 ± 0.01	45	72 ± 0.39	46	26 ± 0.01	36
11	64 ± 0.09	30	34 ±0.01	54	63 ± 0.11	20	43 ± 0.01	68
12	91 ±0.02	37	54 ±0.01	60	73 ± 0.11	13	60 ± 0.03	82
13	74 ± 0.03	35	39 ± 0.03	53	68 ± 0.01	39	29 ± 0.01	43
14	70 ± 0.03	29	41 ± 0.07	58	63 ± 0.02	22	41 ± 0.03	65
21	61 ± 0.23	49	31 ± 0.17	39	59 ± 0.02	32	27 ± 0.03	46
28	91 ± 0.19	71	20 ± 0.16	22	77 ± 0.03	59	18 ± 0.02	23

Table A1.6: Average corrected dissolved silver (ppb) and NP fraction data for PVP AgNPs in ultrapure water using ultrafiltration								
Day	Surface				Bottom			
	Total Ag (ppb)	NP fraction	Dissolved Ag	% dissolved fraction	Total Ag (ppb)	NP fraction	Dissolved Ag	% dissolved fraction
1	1113 ± 0.28	924	189± 0.76	17	386 ± 0.35	380	6 ± 0.23	2
2	381 ± 0.13	343	38 ± 0.15	10	33 ± 0.02	1	43 ± 0.17	98
3	242 ± 0.13	219	23 ± 0.19	10	8 ± 0.05	5	40 ± 0.35	89
4	96 ± 0.04	42	54 ± 0.02	56	47 ± 0.04	7	41 ± 0.02	85
5	60 ± 0.05	15	45 ± 0.01	75	23 ± 0.05	21	23 ± 0.09	52
6	71 ± 0.03	22	49 ± 0.01	69	46 ± 0.02	14	32 ± 0.13	70
7	82 ± 0.07	53	29 ± 0.12	35	69 ± 0.05	59	10 ± 0.04	15
8	61 ± 0.03	45	16 ± 0.06	26	45 ± 0.03	33	12 ± 0.05	27
9	53 ± 0.04	34	19 ± 0.36	36	36 ± 0.03	7.8	28 ± 0.01	78
10	28 ± 0.04	3	25 ± 0.19	89	23 ± 0.05	7.3	16 ± 0.06	69
11	42 ± 0.02	4	38 ± 0.14	90	37 ± 0.03	6.2	31 ± 0.01	83
12	35 ± 0.01	4	31 ± 0.12	89	30 ± 0.03	7.1	23 ± 0.91	77
13	39 ± 0.02	4	35 ± 0.01	90	34 ± 0.01	7	27 ± 0.15	79
14	36 ± 0.03	7	29 ± 0.01	81	69 ± 0.02	51	18 ± 0.78	26
21	84 ± 0.01	68	16 ± 0.63	19	68 ± 0.15	50	18 ± 0.28	26
28	66 ± 0.02	19	47 ± 0.18	72	33 ± 0.03	8	25 ± 0.96	76

Information presented in tables A1.5 and A1.6 were used to create figure 4.6.

EPA moderately hard water

Table A1.7: Average Total Silver Recovery (ppb) for Citrate AgNPs in EPA Moderately Hard Water				
Time (days)	**Time (hours)**	**Surface**	**Middle**	**Bottom**
0	0	3247 ± 0.42	3 ± 0.16	1.2 ± 0.15
0	0.5	2947 ± 0.38	13.4 ± 0.03	5 ± 0.03
0	1.5	2312.3 ± 0.63	10 ± 0.03	3.3 ± 0.021
0	3.5	2154.4 ± 0.76	8.45 ± 0.03	2.4 ± 0.03
0	5.5	1885.1 ± 0.68	9 ± 0.15	14 ± 0.03
1	24	1231 ± 0.63	6 ± 0.06	20 ± 0.04
2	48	430 ± 0.46	20.3 ± 0.01	16 ± 0.04
3	72	190 ± 0.24	6.3 ± 0.12	12 ± 0.07
4	96	43.2 ± 0.04	8.3 ± 0.21	13 ± 0.04
5	120	29.4 ± 0.02	12 ± 0.07	13 ± 0.01
6	144	17 ± 0.01	9 ± 0.06	16 ± 0.05
7	168	28 ± 0.09	18.3 ± 0.02	19 ± 0.03
8	216	22 ± 0.01	14 ± 0.01	18 ± 0.07
9	240	29 ± 0.04	22 ± 0.13	22.4 ± 0.01
10	264	35.4 ± 0.01	30 ± 0.02	27.3 ± 0.04
11	192	20 ± 0.02	15.1 ± 0.02	18 ± 0.01
12	288	51 ± 0.02	44.2 ± 0.01	37 ± 0.06
13	312	62 ± 0.02	48.3 ± 0.01	43 ± 0.09
14	336	66.4 ± 0.04	61 ± 0.04	56.1 ± 0.01
21	504	36.2 ± 0.02	36 ± 0.021	30 ± 0.08
28	672	60 ± 0.09	10.3 ± 0.05	29 ± 0.03

Table A1.8: Average Total Silver (ppb) Recovery for PVP AgNPs in EPA Moderately Hard Water				
Time (Days)	**Time (Hours)**	**Surface**	**Middle**	**Bottom**
0	0	4463 ± 0.19	35 ± 0.04	41 ± 0.15
0	0.5	3992 ± 0.27	44 ± 0.04	52 ± 0.13
0	1.5	3650 ± 0.07	11.2 ± 0.01	49 ± 0.03
0	3.5	3429 ± 0.35	39 ± 0.04	42 ± 0.34
0	5.5	3118 ± 0.28	25 ± 0.02	49 ± 0.03
1	24	2381 ± 0.82	56 ± 0.07	48 ± 0.09
2	48	1471.3 ± 0.66	35 ± 0.04	44 ± 0.09
3	72	1147 ± 0.66	32 ± 0.03	29 ± 0.05
4	96	467.3 ± 0.32	20.4 ± 0.02	28 ± 0.07
5	120	75.2 ± 0.03	35 ± 0.04	31 ± 0.17
6	144	56.4 ± 0.02	35 ± 0.04	36 ± 0.87
7	168	38 ± 0.03	35 ± 0.04	30 ± 0.04
8	192	36 ± 0.09	43 ± 0.04	34 ± 0.11
9	216	43 ± 0.07	49 ± 0.05	43 ± 0.02
10	240	44 ± 0.04	29 ± 0.03	38 ± 0.06
11	264	51 ± 0.01	46 ± 0.05	41 ± 0.02
12	288	48 ± 0.07	37.4 ± 0.04	34 ± 0.15
13	312	55 ± 0.06	52 ± 0.05	38 ± 0.02
14	336	62 ± 0.07	66 ± 0.66	28 ± 0.02
15	360	185 ± 0.24	33 ± 0.33	48 ± 0.09
16	384	24 ± 0.04	29 ± 0.29	44 ± 0.09
17	408	13.2 ± 0.05	52 ± 0.05	29 ± 0.05
18	432	68 ± 0.06	48 ± 0.48	28 ± 0.07
21	504	52 ± 0.02	42 ± 0.04	31 ± 0.17
28	672	58 ± 0.01	14 ± 0.14	36 ± 0.87

Information presented in tables A1.7 and A1.8 was used to produce figure 4.12.

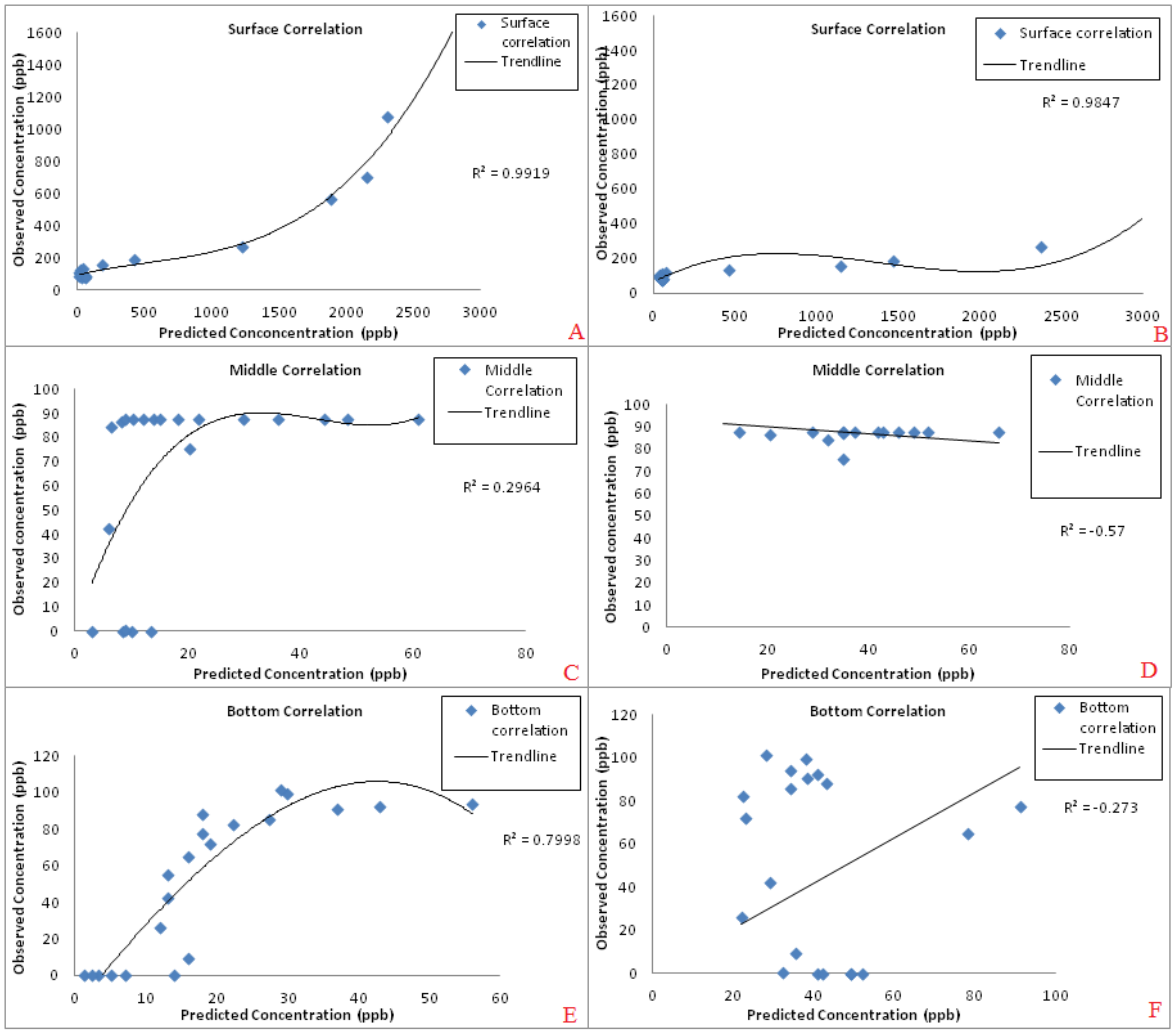

Figure A1.7: Correlation values for the observed and predicted modelled Ag concentrations for citrate and PVP AgNPs exposed to EPA moderately hard water, according to parameters fixed in table 4.6 in text. A) citrate AgNP study in the surface, B) PVP AgNP study in the surface, C) citrate AgNP study in the middle, D) PVP AgNP study in the middle, E) citrate AgNP study in the bottom, and F) PVP AgNP study in the bottom.

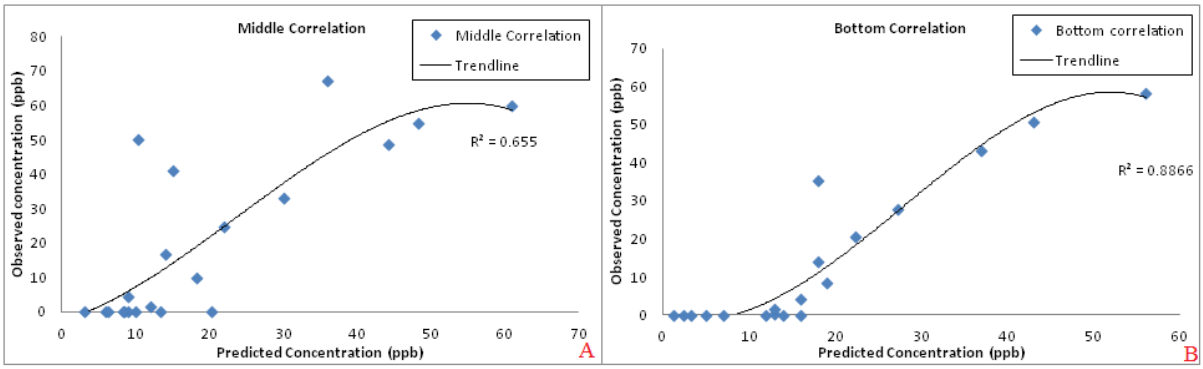

Figure A1.8: Correlation values for the observed and predicted modelled Ag concentrations for the adjusted model parameters for the citrate AgNPs in EPA moderately hard water, according to table 4.7 in text. A) Middle correlations and B) bottom correlations.

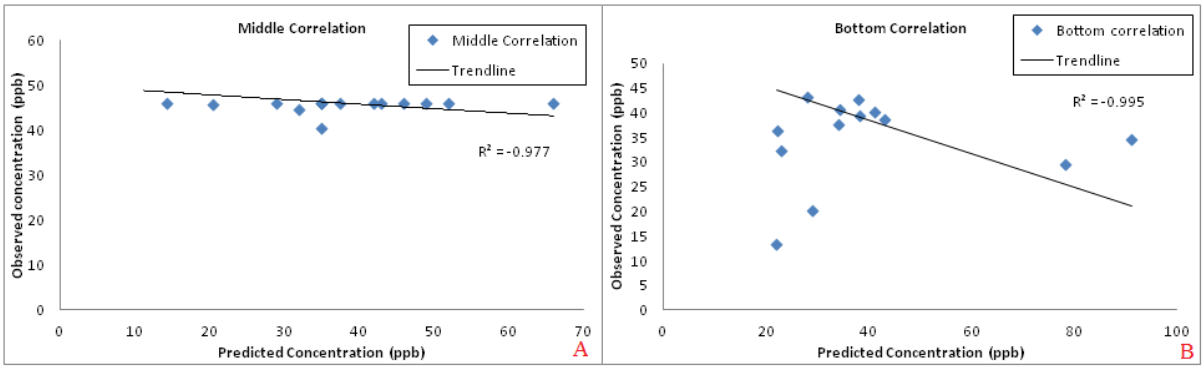

Figure A1.9: Correlation values for the observed and predicted modelled Ag concentrations for the adjusted model parameters for the PVP AgNPs in EPA moderately hard water, according to table 4.8 in text. A) Middle correlations and B) bottom correlations.

Table A1.9: Average Corrected Dissolved Silver (ppb) and NP Concentration Data for Citrate AgNPs in EPA Moderately Hard Water								
	Surface				Bottom			
Day	Total Ag (ppb)	NP fraction	Dissolved Ag	% dissolved fraction	Total Ag (ppb)	NP fraction	Dissolved Ag	% dissolved fraction
1	1231 ± 0.63	1226	5 ± 0.11	0.4	20 ± 0.04	2	18 ± 0.31	92
2	430 ± 0.46	318	112 ± 0.03	26	16 ± 0.04	6	10 ± 0.43	63
3	190 ± 0.24	24	166 ± 0.18	87	12 ± 0.07	3.8	8 ± 0.28	68
4	43.2 ± 0.04	19.2	24 ± 0.02	56	13 ± 0.04	11	3 ± 0.01	19
5	29.4 ± 0.02	20.4	9 ± 0.94	31	13 ± 0.01	8	5 ± 0.88	41
6	17 ± 0.01	1	19 ± 0.48	95	16 ± 0.05	8	8 ± 0.28	50
7	28 ± 0.09	14	14 ± 0.63	50	19 ± 0.03	16	3 ± 0.15	17
8	22 ± 0.01	13	9 ± 0.73	41	18 ± 0.07	5	13 ± 0.92	72
9	29 ± 0.04	17	12 ± 0.12	41	22.4 ± 0.01	7	15 ± 0.29	67
10	35.4 ± 0.01	18.4	17 ± 0.34	48	27.3 ± 0.04	7	20 ± 0.34	73
11	20 ± 0.02	2	18 ± 0.02	90	18 ± 0.01	6	12 ± 0.16	67
12	51 ± 0.02	28	23 ± 0.01	45	37 ± 0.06	16	21 ± 0.27	57
13	62 ± 0.02	33	29 ± 0.01	47	43 ± 0.09	24	19 ± 0.54	44
14	66.4 ± 0.04	36.1	30 ± 0.92	46	56.1 ± 0.01	26	30 ± 0.03	53
21	36.2 ± 0.02	22	40 ± 0.98	65	30 ± 0.08	27	3 ± 0.03	9
28	60 ± 0.09	30	30 ± 0.04	50	29 ± 0.03	26	3 ± 0.03	11

Table A1.10: Average corrected dissolved silver (ppb) and NP fraction data for PVP AgNPs in EPA water								
	Surface				Bottom			
Day	Total Ag (ppb)	NP fraction	Dissolved Ag	% dissolved fraction	Total Ag (ppb)	NP fraction	Dissolved Ag	% dissolved fraction
1	2381 ± 0.82	2380	1 ± 0.4	0.05	48 ± 0.09	6	42 ±0.73	88
2	1471.3 ± 0.66	1459	12 ±0.11	0.8	44 ± 0.09	6	38 ±0.04	86
3	1147 ± 0.66	1129	18 ±0.73	2	29 ± 0.05	6	20 ±0.02	77
4	467 ± 0.32	460	7 ±0.2	2	28 ± 0.07	19	10 ±0.04	36
5	75 ± 0.03	64	11 ±0.43	15	31 ± 0.17	22	11 ±0.43	33
6	56 ± 0.02	49	7 ±0.22	12	36 ± 0.87	8	20 ±0.27	71
7	38 ± 0.03	35	3 ±0.12	8	30 ± 0.04	3	28 ±0.01	90
8	36 ± 0.09	30	6 ±0.02	17	34 ± 0.11	4	32 ±0.28	89
9	43 ± 0.07	37	6 ±0.02	14	43 ± 0.02	4	26 ±0.06	87
10	44 ± 0.04	32	12 ±0.47	27	38 ± 0.06	13	21 ±0.83	62
11	51 ± 0.01	46	5 ±0.17	10	41 ± 0.02	25	18 ±0.66	42
12	48 ± 0.07	39	9 ±0.15	19	34 ± 0.15	19	19 ±0.37	50
13	13 ± 0.05	48	7 ±0.18	13	38 ± 0.02	22	19 ±0.52	46
14	68 ± 0.06	60	2 ±0.76	3	28 ± 0.02	15	19 ±0.72	56
21	52 ± 0.02	51	1 ±0.04	2	38	24	14 ±0.05	37
28	58 ± 0.01	57	1 ±0.02	1	28	11	17 ±0.33	61

Information presented in tables A1.9 and A1.10 was used to produce figure 4.14.

EPA moderately hard water with added SRFA

Table A1.11: Average total silver recovery (ppb) for Citrate AgNPs in EPA SRFA				
Time (days)	**Time (hours)**	**Surface**	**Middle**	**Bottom**
0	0	2614 ± 0.21	17 ± 0.01	6 ± 0.04
0	0.5	2365 ± 0.26	22 ± 0.01	19 ± 0.04
0	1.5	1937 ± 0.57	15 ± 0.02	18 ± 0.02
0	3.5	1451 ± 0.03	34 ± 0.03	20 ± 0.01
0	5.5	1230 ± 0.11	51 ± 0.15	33 ± 0.04
1	24	784 ± 0.13	36 ± 0.08	25 ± 0.42
2	48	395 ± 0.17	54 ± 0.01	39 ± 0.02
3	72	195 ± 0.14	82 ± 0.02	76 ± 0.02
4	96	164 ± 0.05	130 ± 0.07	171 ± 0.01
5	120	173 ± 0.03	92 ± 0.09	126 ± 0.13
6	144	156 ± 0.04	83 ± 0.08	102 ± 0.24
7	168	43 ± 0.02	26 ± 0.02	45 ± 0.01
8	192	33 ± 0.02	24 ± 0.02	32 ± 0.05
9	216	38 ± 0.02	25 ± 0.02	38 ± 0.03
10	240	35 ± 0.02	25 ± 0.02	35 ± 0.04
11	264	64 ± 0.01	48 ± 0.02	44 ± 0.09
12	288	55 ± 0.01	46 ± 0.01	39 ± 0.21
13	312	157 ± 0.03	50 ± 0.02	49 ± 0.01
14	336	70 ± 0.54	90 ± 0.08	83 ± 0.01
21	504	39 ± 0.3	49 ± 0.04	43 ± 0.24
28	672	21 ± 0.03	6 ± 0.01	4 ± 0.48

Table A1.12: Average total silver recovery (ppb) for PVP AgNPs in EPA SRFA Water				
Time (Days)	**Time (Hours)**	**Surface**	**Middle**	**Bottom**
0	0	2287 ± 0.22	3 ± 0.24	6 ± 0.07
0	0.5	2750 ± 0.64	1 ± 0.07	10 ± 0.04
0	1.5	2248 ± 0.61	11 ± 0.01	9 ± 0.05
0	3.5	2045 ± 0.46	27.4 ± 0.01	6 ± 0.05
0	5.5	1845 ± 0.47	37.2 ± 0.47	15 ± 0.03
1	24	1146 ± 0.02	18 ± 0.56	6 ± 0.16
2	48	718 ± 0.69	17 ± 0.24	9 ± 0.21
3	72	325 ± 0.36	27 ± 0.02	23 ± 0.15
4	96	96 ± 0.09	28 ± 0.01	24 ± 0.14
5	120	72 ± 0.06	27 ± 0.01	24 ± 0.21
6	144	55 ± 0.05	28 ± 0.02	25 ± 0.15
7	168	48 ± 0.03	26 ± 0.09	27 ± 0.15
8	192	32 ± 0.02	27 ± 0.02	26 ± 0.16
9	216	40 ± 0.02	26 ± 0.07	27 ± 0.02
10	240	36 ± 0.09	27 ± 0.05	26 ± 0.16
11	264	52 ± 0.02	51 ± 0.07	36 ± 0.29
12	288	47 ± 0.02	49 ± 0.05	49 ± 0.13
13	312	56 ± 0.03	54 ± 0.08	48 ± 0.93
14	336	58 ± 0.06	60 ± 0.01	53 ± 0.06
21	504	39 ± 0.01	31 ± 0.07	31 ± 0.01
28	672	19 ± 0.02	25 ± 0.01	10 ± 0.14

Information presented in tables A1.11 and A1.12 was used to produce figure 4.20.

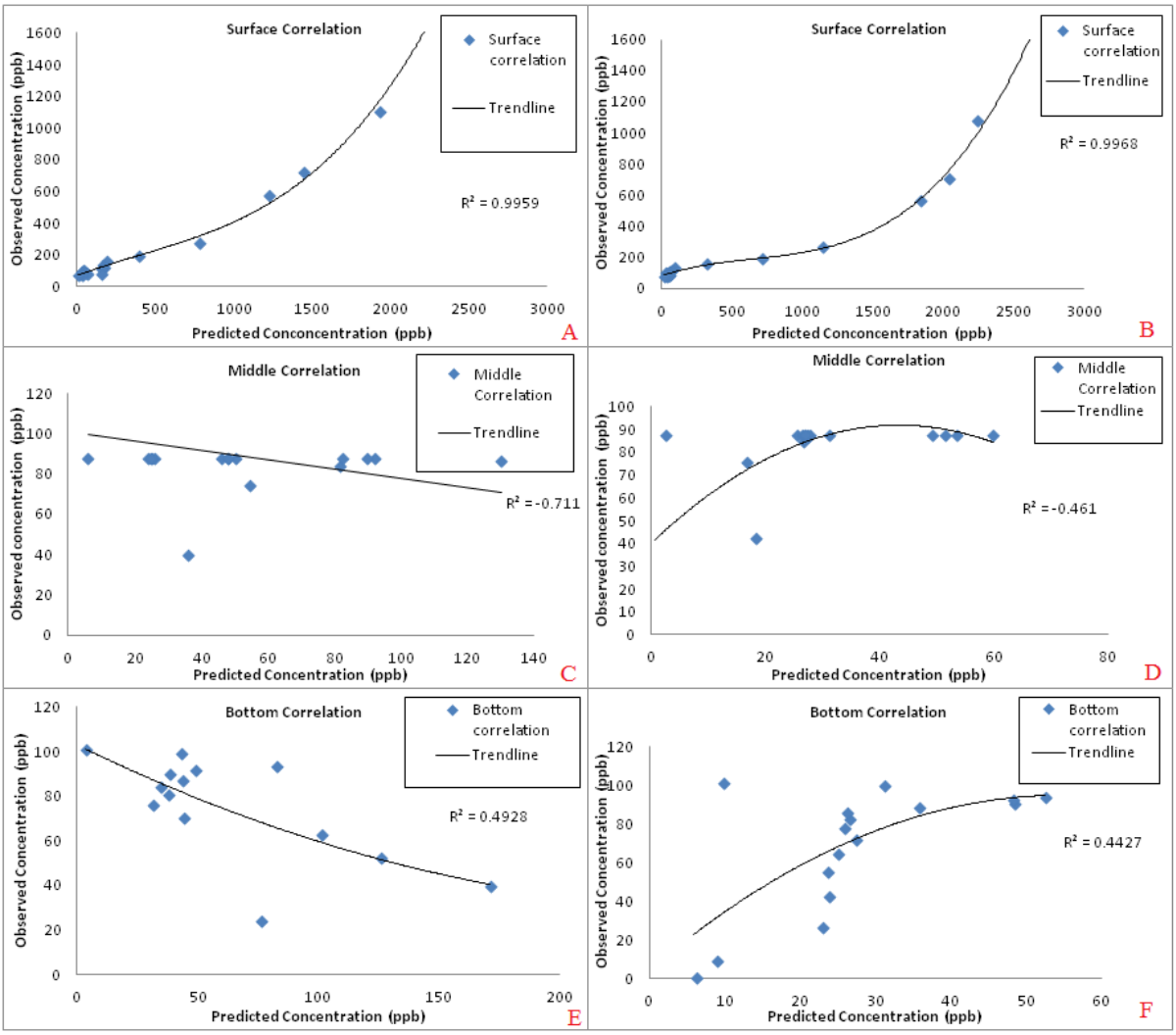

Figure A1.10: Correlation values for the observed and predicted modelled Ag concentrations for citrate and PVP AgNPs exposed to EPA moderately hard water with added SRFA, according to parameters fixed in table 4.6 in text. A) citrate AgNP study in the surface, B) PVP AgNP study in the surface, C) citrate AgNP study in the middle, D) PVP AgNP study in the middle, E) citrate AgNP study in the bottom, and F) PVP AgNP study in the bottom.

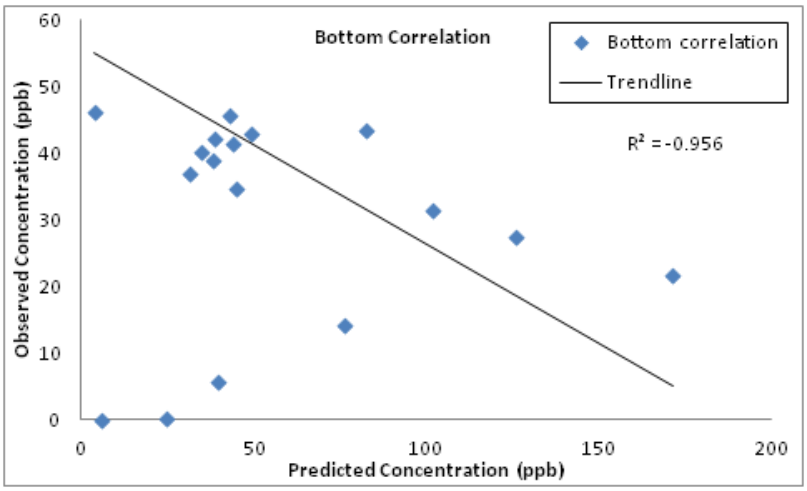

Figure A1.11: Correlation values for the observed and predicted modelled Ag concentrations for the adjusted model parameters for the citrate AgNPs in EPA moderately hard water with added SRFA, according to table 4.10 for the bottom depth correlations.

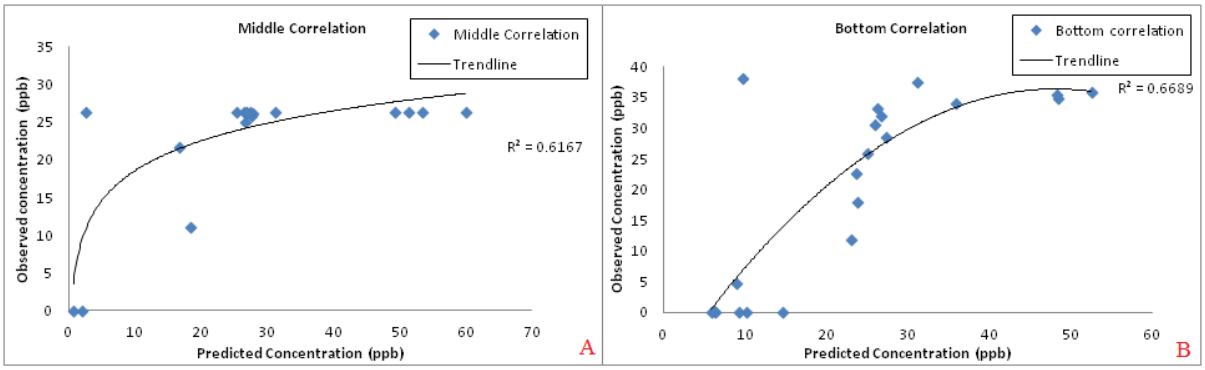

Figure A1.12: Correlation values for the observed and predicted modelled Ag concentrations for the adjusted model parameters for the PVP AgNPs in EPA moderately hard water with added SRFA, according to table 4.11 in text. A) Middle correlations and B) bottom correlations.

Table A1.13: Average corrected dissolved silver (ppb) and NP fraction data for citrate AgNPs in EPA SRFA water using ultrafiltration								
Day	Surface				Bottom			
	Total Ag (ppb)	NP fraction	Dissolved Ag	% dissolved fraction	Total Ag (ppb)	NP fraction	Dissolved Ag	% dissolved fraction
1	784 ± 0.13	538	246 ± 0.69	31	25 ± 0.42	17	8 ± 0.19	32
2	395 ± 0.17	351	44 ± 0.29	11	39 ± 0.02	18	21 ± 0.03	53
3	195 ± 0.14	181	14 ± 0.7	7	76 ± 0.02	73	4 ± 0.17	5
4	164 ± 0.05	114	50 ± 0.02	30	171 ± 0.01	152	19 ± 0.95	11
5	173 ± 0.03	146	27 ± 0.09	16	126 ± 0.13	95	31 ± 0.75	25
6	156 ± 0.04	119	37 ± 0.03	24	102 ± 0.24	60	42 ± 0.02	41
7	43 ± 0.02	24	19 ± 0.01	45	45 ± 0.01	30	15 ± 0.03	33
8	33 ± 0.02	19	14 ± 0.03	44	32 ± 0.05	10	22 ± 0.03	69
9	38 ± 0.02	26	12 ± 0.02	32	38 ± 0.03	20	18 ± 0.03	47
10	35 ± 0.02	22	13 ± 0.02	37	35 ± 0.04	15	20 ± 0.03	57
11	64 ± 0.01	51	13 ± 0.02	20	44 ± 0.09	25	19 ± 0.22	43
12	55 ± 0.01	30	25 ± 0.04	46	39 ± 0.21	0.8	38 ± 0.24	98
13	157 ± 0.03	144	13 ± 0.01	8	49 ± 0.01	35.3	14 ± 0.18	28
14	70 ± 0.54	58	12 ± 0.03	18	83 ± 0.01	70	13 ± 0.02	16
21	39 ± 0.3	22	17 ± 0.02	44	43 ± 0.24	24	19 ± 0.33	44
28	21 ± 0.03	1	20 ± 0.02	95	4 ± 0.48	17	23 ± 0.54	58

Table A1.14: Average corrected dissolved silver (ppb) and NP fraction data for PVP AgNPs in ultrapure water using ultrafiltration								
Day	Surface				Bottom			
	Total	NP fraction	Dissolved Ag	% dissolved fraction	Total	NP fraction	Dissolved Ag	% dissolved fraction
1	1146 ± 0.02	657	489 ± 0.15	43	6 ± 0.16	-6.9	13 ± 0.34	211
2	718 ± 0.69	181	537 ± 0.15	75	9 ± 0.21	-2	11 ± 0.22	122
3	325 ± 0.36	321	4 ± 0.86	1	23 ± 0.15	13.1	10 ± 0.01	43
4	96 ± 0.09	41	55 ± 0.02	57	24 ± 0.14	21	3 ±0.93	13
5	72 ± 0.06	41	31 ± 0.02	43	24 ± 0.21	17.7	6 ± 0.01	26
6	55 ± 0.05	38	17 ± 0.06	31	25 ± 0.15	23.1	2 ± 0.03	8
7	48 ± 0.03	34	14 ± 0.07	29	27 ± 0.15	11.2	16.± 0.02	59
8	32 ± 0.02	20	12 ± 0.04	38	26 ± 0.16	16	10 ± 0.02	38
9	40 ± 0.02	27	13 ± 0.16	33	27 ± 0.02	14	13 ± 0.02	48
10	36 ± 0.09	24	12 ± 0.01	34	26 ± 0.16	15	11 ± 0.02	43
11	52 ± 0.02	40	12 ± 0.2	24	36 ± 0.29	23.9	12 ± 0.19	34
12	47 ± 0.02	35	12 ± 0.03	26	49 ± 0.13	40	9 ± 0.14	18
13	56 ± 0.03	44	12 ± 0.03	21	48 ± 0.93	35.3	13 ± 0.11	27
14	58 ± 0.06	45	13 ± 0.08	22	53 ± 0.06	33.7	19 ± 0.27	36
21	39 ± 0.01	25	14 ± 0.04	36	31 ± 0.01	27.9	3± 0.22	11
28	19 ± 0.02	4	15 ± 0.05	78	10 ± 0.14	4	6 ± 0.11	60

Information presented in tables A1.13 and A1.14 was used to produce figure 4.21

Appendix 2: Chapter 5 Additional Information

$AgNO_3$ natural water exposure studies

Table A2.1: Average total silver recovery (ppb) for $AgNO_3$ exposed to vale lake water			
Time (hours)	**Surface**	**Middle**	**Bottom**
0	4728 ± 2.45	22 ± 0.11	41± 0.51
0.5	2533 ± 2.31	19 ± 0.66	12± 0.03
1.5	2401± 1.84	15 ± 0.02	30± 0.34
3.5	1548 ± 1.5	19 ± 0.61	49± 0.13
24	309 ± 0.34	140 ± 0.71	30± 0.91
48	30 ± 0.17	126 ± 0.85	36± 0.04
72	72 ± 0.61	66 ± 0.03	59± 0.03
96	72 ± 0.08	71 ± 0.02	63± 0.02
120	72 ± 0.03	76 ± 0.01	67± 0.02

Information presented in table A2.1 is used to describe the total Ag data in figures 5.1 and 5.2.

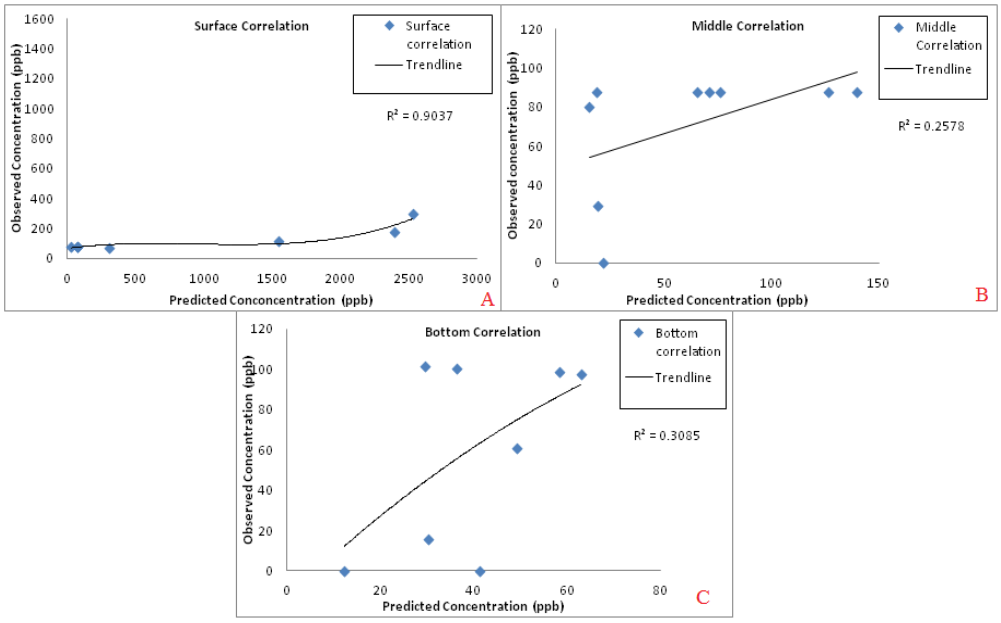

Figure A2.1: Correlation values for the observed and predicted modelled Ag concentrations for $AgNO_3$ in natural water. A) Surface correlations, B) middle depth correlations and C) bottom depth correlations.

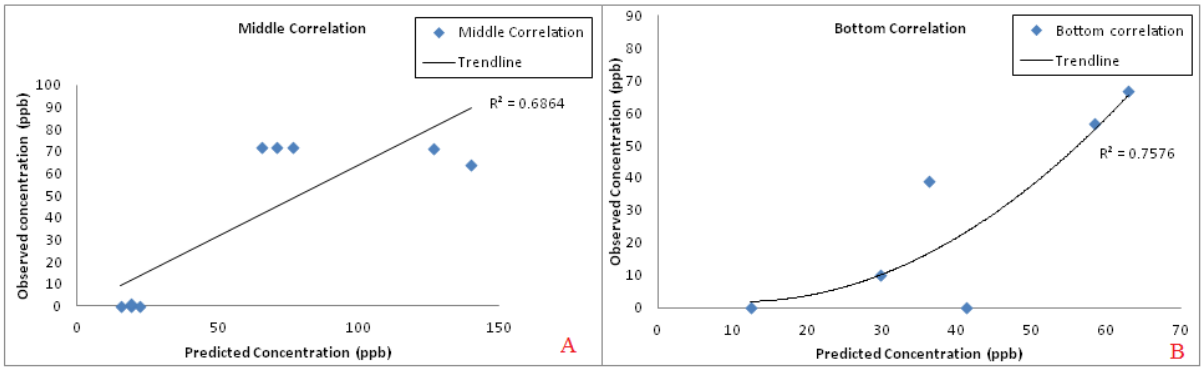

Figure A2.2: Adjusted model parameters for $AgNO_3$ in natural water.

AgNP Exposures

Spring natural water exposures

Table A2.2: Total silver recover concentration (ppb) for citrate AgNPs in spring water				
Time (day)	**Time (hours)**	**Surface**	**Middle**	**Bottom**
0	**0**	2573 ± 0.34	28 ± 0.06	28 ± 0.83
0.020833	**0.5**	1901 ± 0.41	19 ± 0.06	44 ± 0.27
0.0625	**1.5**	1500 ± 0.03	15 ± 0.01	35 ± 0.02
0.145833	**3.5**	1458 ± 0.04	35 ± 0.24	34± 0.05
0.229167	**5.5**	1403 ± 0.04	12 ± 0.01	34 ± 0.03
1	**24**	1442 ± 0.26	96 ± 0.03	84 ± 0.03
2	**48**	1244 ± 0.09	35 ± 0.15	89 ± 0.03
3	**72**	800 ± 0.01	48 ± 0.17	91 ± 0.06
4	**96**	775 ± 0.16	61 ± 0.16	108 ± 0.03
5	**120**	576 ± 0.08	23 ± 0.03	91 ± 0.07
6	**144**	319 ± 0.12	41 ± 0.01	76 ± 0.69
7	**168**	239 ± 0.06	71 ± 0.03	72 ± 0.02
8	**192**	160 ± 0.01	125 ± 0.48	80 ± 0.75
9	**216**	108 ± 0.12	38 ± 0.03	69 ± 0.02
10	**240**	187 ± 0.07	89 ± 0.36	76 ± 0.02
11	**264**	147 ± 0.07	118 ± 0.07	80 ± 0.02
12	**288**	107 ± 0.05	113 ± 0.28	83 ± 0.061
13	**312**	191 ± 0.01	94 ± 0.29	80 ± 0027
14	**336**	275 ± 0.42	75 ± 0.63	77 ± 0.06
21	**504**	110 ± 0.09	20 ± 0.77	31 ± 0.08
28	**672**	24 ± 0.02	32 ± 0.22	32 ± 0.18

Table A2.3: Average total silver recovery (ppb) for PVP AgNPs in spring water				
Time (Days)	**Time (hours)**	**Surface**	**Middle**	**Bottom**
0	**0**	2687 ± 0.41	77 ± 0.08	12 ± 0.02
0.020833	**0.5**	2825 ± 0.79	39 ± 0.02	53 ± 0.04
0.0625	**1.5**	2572 ± 0.63	27 ± 0.16	61 ± 0.04
0.145833	**3.5**	2346 ± 0.54	61 ± 0.02	31 ± 0.01
0.229167	**5.5**	1780 ± 0.29	47 ± 0.03	18 ± 0.01
1	**24**	1397 ± 0.38	59 ± 0.34	28 ± 0.07
2	**48**	1084 ± 0.77	72 ± 0.02	39 ± 0.04
3	**72**	690 ± 0.79	81 ± 0.03	77 ± 0.07
4	**96**	613 ± 0.55	112 ± 0.11	109 ± 0.06
5	**120**	549 ± 0.41	161 ± 0.15	192 ± 0.21
6	**144**	501 ± 0.29	170 ± 0.16	190 ± 0.19
7	**168**	452 ± 0.17	178 ± 0.16	187 ± 0.16
8	**192**	354 ± 0.05	192 ± 0.15	247 ± 0.20
9	**216**	404 ± 0.02	290 ± 0.13	352 ± 0.06
10	**240**	388 ± 0.04	391 ± 0.08	400 ± 0.01
11	**264**	455 ± 0.04	476 ± 0.10	475 ± 0.12
12	**288**	496 ± 0.06	477 ± 0.13	493 ± 0.14
13	**312**	538 ± 0.08	477 ± 0.16	511 ± 0.16
14	**336**	604 ± 0.19	612 ± 0.30	521 ± 0.23
15	**360**	526 ± 0.20	550 ± 0.27	550 ± 0.27
16	**384**	621 ± 0.41	482 ± 0.27	470 ± 0.27
21	**504**	412 ± 0.04	475 ± 0.04	435 ± 0.03
28	**672**	343 ± 0.01	413 ± 0.48	188 ± 0.01

The information presented in tables A2.2 and A2.3 shows the total Ag concentrations which were used in figure 5.3 and plotted alongside the predicated modelled concentrations. The information from table A2.3 was also used in figure 5.4.

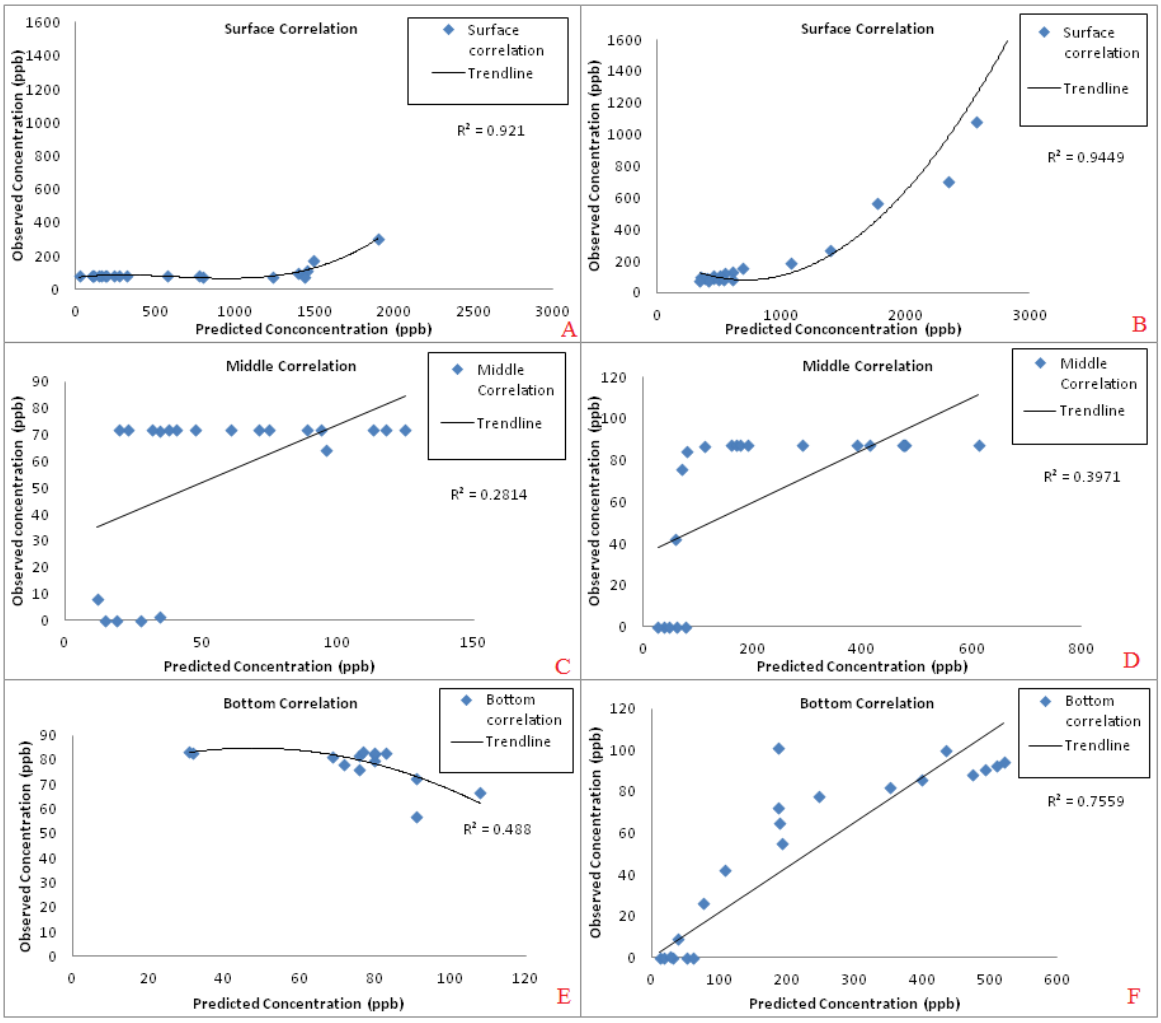

Figure A2.3: Correlation values for the observed and predicted modelled Ag concentrations for citrate and PVP AgNPs exposed to spring natural water. A) citrate AgNP study in the surface, B) PVP AgNP study in the surface, C) citrate AgNP study in the middle, D) PVP AgNP study in the middle, E) citrate AgNP study in the bottom, and F) PVP AgNP study in the bottom.

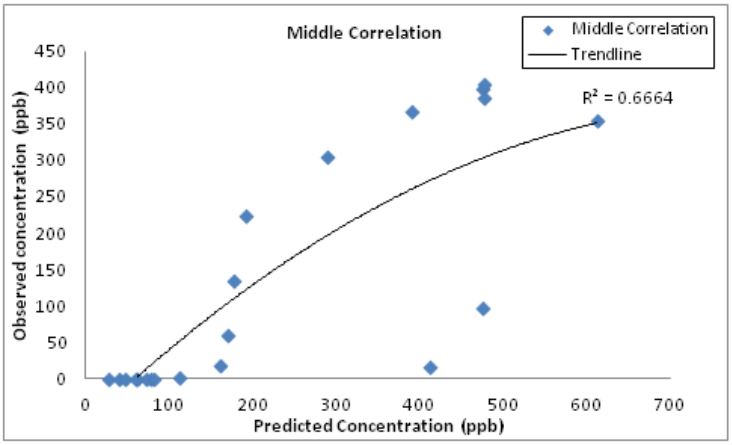

Figure A2.4: Middle adjusted correlation for the PVP total Ag concentrations in the spring natural water.

Table A2.4: Average corrected dissolved silver (ppb) and NP fraction data for citrate AgNPs in spring water using ultrafiltration								
Day	Surface				Bottom			
	Total Ag (ppb)	NP Fraction	Dissolved Ag	% Dissolved Fraction	Total Ag (ppb)	NP Fraction	Dissolved Ag	% Dissolved Fraction
1	1442 ± 0.26	1410	32 ± 0.04	2	84 ± 0.03	35	49 ± 0.06	58
2	1244 ± 0.09	1213	31 ± 0.01	2	89 ± 0.03	59	30 ± 0.02	34
3	800 ± 0.01	765	35 ± 0.06	4	91 ± 0.06	25	66 ± 0.88	73
4	775 ± 0.16	733	42 ± 0.02	5	108 ± 0.03	44	64 ± 0.32	59
5	576 ± 0.08	524	52 ± 0.08	9	91 ± 0.07	28	63 ± 0.06	69
6	319 ± 0.12	269	50 ± 0.35	16	76 ± 0.69	43	33 ± 0.98	43
7	239 ± 0.06	222	17 ± 0.01	7	72 ± 0.02	40	32 ± 0.03	44
8	160 ± 0.01	130	30 ± 0.54	19	80 ± 0.75	48	32 ± 0.45	40
9	108 ± 0.12	72	36 ± 0.63	33	69 ± 0.02	54	15 ± 0.87	22
10	187 ± 0.07	171	16 ± 0.02	9	76 ± 0.02	65	11 ± 0.23	14
11	147 ± 0.07	129	18 ± 0.05	12	80 ± 0.02	61	19 ± 0.87	24
12	107 ± 0.05	88	19 ± 0.13	18	83 ± 0.061	56	27 ± 0.02	33
13	191 ± 0.01	162	29 ± 0.02	15	80 ± 0027	43	37 ± 0.16	46
14	275 ± 0.42	235	40 ± 0.22	15	77 ± 0.06	30	47 ± 0.32	61
21	110 ± 0.09	107	3 ± 0.14	3	31 ± 0.08	20	11 ± 0.12	35
28	24 ± 0.02	17	7 ± 0.55	29	32 ± 0.18	21	11 ± 0.87	34

Table A2.5: Average corrected dissolved silver (ppb) and NP fraction data for PVP AgNPs in spring water using ultrafiltration								
Day	Surface				Bottom			
	Total Ag (ppb)	NP fraction	Dissolved Ag	% dissolved fraction	Total Ag (ppb)	NP fraction	Dissolved Ag	% dissolved fraction
1	1397 ± 0.38	1383	14 ± 0.17	1	28 ± 0.07	12	16 ± 0.42	57.
2	1084 ± 0.77	1069	15 ± 0.19	1	39 ± 0.04	14	25 ± 0.28	64
3	690 ± 0.79	635	55 ± 0.01	8	77 ± 0.07	52	25 ± 0.31	32
4	613 ± 0.55	587	26 ± 0.02	4.	109 ± 0.06	80	29 ± 0.13	27
5	549 ± 0.41	475	74 ± 0.53	13	192 ± 0.21	164	28 ± 0.30	15
6	501 ± 0.29	442	59 ± 0.07	12	190 ± 0.19	161	29 ± 0.05	15
7	452 ± 0.17	409	43 ± 0.8	10	187 ± 0.16	137	50 ± 0.08	27
8	354 ± 0.05	315	39 ± 0.31	11	247 ± 0.20	151	96 ± 0.34	39
9	404 ± 0.02	345	59 ± 0.86	1	352 ± 0.06	331	21 ± 0.09	6
10	388 ± 0.04	309	79 ± 0.12	20	400 ± 0.01	390	10 ± 0.11	3
11	455 ± 0.04	425	30 ± 0.82	7	475 ± 0.12	416	59 ± 0.32	12
12	496 ± 0.06	467	29 ± 0.78	6	493 ± 0.14	423	70 ± 0.03	14
13	538 ± 0.08	509	29 ± 0.74	5	511 ± 0.16	430	81 ± 0.35	16
14	604 ± 0.19	579	25 ± 0.56	4	521 ± 0.23	445	76 ± 0.03	15
21	412 ± 0.04	388	24 ± 0.03	6	435 ± 0.03	407	28 ± 0.35	6
28	343 ± 0.01	321	22 ± 0.13	6	188 ± 0.01	163	25 ± 0.24	13

The dissolved and AgNP concentrations presented in tables A2.4 and A2.5 were used to produce figure 5.5.

Summer natural water exposures

Table A2.5: Average total silver recovery (ppb) for citrate AgNPs in summer natural water				
Time (days)	**Time (hours)**	**Surface**	**Middle**	**Bottom**
0	**0**	1738 ± 0.16	3 ± 0.17	0 ± 0.32
0.020833	**0.5**	1321 ± 0.28	21 ± 0.25	19 ± 0.16
0.0625	**1.5**	1177 ± 0.22	22 ± 0.34	22 ± 0.01
0.145833	**3.5**	1130 ± 0.15	35 ± 0.01	18 ± 0.92
0.229167	**5.5**	1070 ± 0.16	40 ± 0.37	15 ± 0.66
1	**24**	636 ± 0.18	41 ± 0.01	17 ± 0.17
2	**48**	167 ± 0.08	41 ± 0.03	38 ± 0.08
3	**72**	90 ± 0.032	42 ± 0.26	41 ± 0.03
4	**96**	57 ± 0.43	43 ± 0.07	41 ± 0.03
5	**120**	22 ± 0.29	35 ± 0.01	36 ± 0.69
6	**144**	18 ± 0.56	19 ± 0.05	26 ± 0.03
7	**168**	15 ± 0.84	14 ± 0.07	26 ± 0.33
8	**192**	18 ± 0.89	15 ± 0.25	16 ± 0.08
9	**216**	12 ± 0.08	25 ± 0.68	14 ± 0.37
10	**240**	21 ± 0.45	31 ± 0.02	22 ± 0.01
11	**264**	30 ± 0.83	37 ± 0.023	14 ± 0.09
12	**288**	11 ± 0.07	13 ± 0.09	16 ± 0.09
13	**312**	46 ± 0.73	23 ± 0.07	18 ± 0.88
14	**336**	28 ± 0.54	18 ± 0.11	62 ± 0.85
21	**504**	21 ± 0.22	20 ± 0.33	20 ± 0.11
28	**672**	17 ± 0.03	15 ± 0.25	18 ± 0.89

Table A2.6: Average Total Silver Recovery (ppb) for PVP AgNPs in summer natural water				
Time (Day)	**Time (Hours)**	**Surface**	**Middle**	**Bottom**
0	**0**	2065 ± 0.04	3 ± 0.28	3 ± 0.29
0.020833	**0.5**	1811 ± 0.15	5 ± 0.37	5 ± 0.43
0.0625	**1.5**	156 ± 0.08	34 ± 0.29	5 ± 0.07
0.145833	**3.5**	1485 ± 0.14	52 ± 0.01	3 ± 0.01
0.229167	**5.5**	1415 ± 0.03	64 ± 0.03	51 ± 0.03
1	**24**	314 ± 0.31	74 ± 0.06	41 ± 0.02
2	**48**	67 ± 0.12	55 ± 0.09	48 ± 0.01
3	**72**	59 ± 0.06	57 ± 0.01	56 ± 0.06
4	**96**	56 ± 0.25	50 ± 0.02	54 ± 0.76
5	**120**	11 ± 0.03	16 ± 0.04	30 ± 0.18
6	**144**	12 ± 0.03	13 ± 0.05	27 ± 0.17
7	**168**	13 ± 0.03	11 ± 0.06	24 ± 0.18
8	**192**	15 ± 0.07	15 ± 0.01	15 ± 0.01
9	**216**	26 ± 0.08	21 ± 0.01	24 ± 0.02
10	**240**	13 ± 0.07	13 ± 0.09	24 ± 0.17
11	**264**	22 ± 0.06	19 ± 0.39	21 ± 0.04
12	**288**	34 ± 0.05	22 ± 0.45	18 ± 0.04
13	**312**	22 ± 0.06	19 ± 0.38	21 ± 0.04
14	**336**	34 ± 0.05	22 ± 0.45	18 ± 0.03
21	**504**	12 ± 0.49	8 ± 0.24	13 ± 0.02
28	**672**	11 ± 0.28	8 ± 0.02	17 ± 0.04

Information presented in tables A2.5 and A2.6 correspond to the total Ag data presented in figure 5.13.

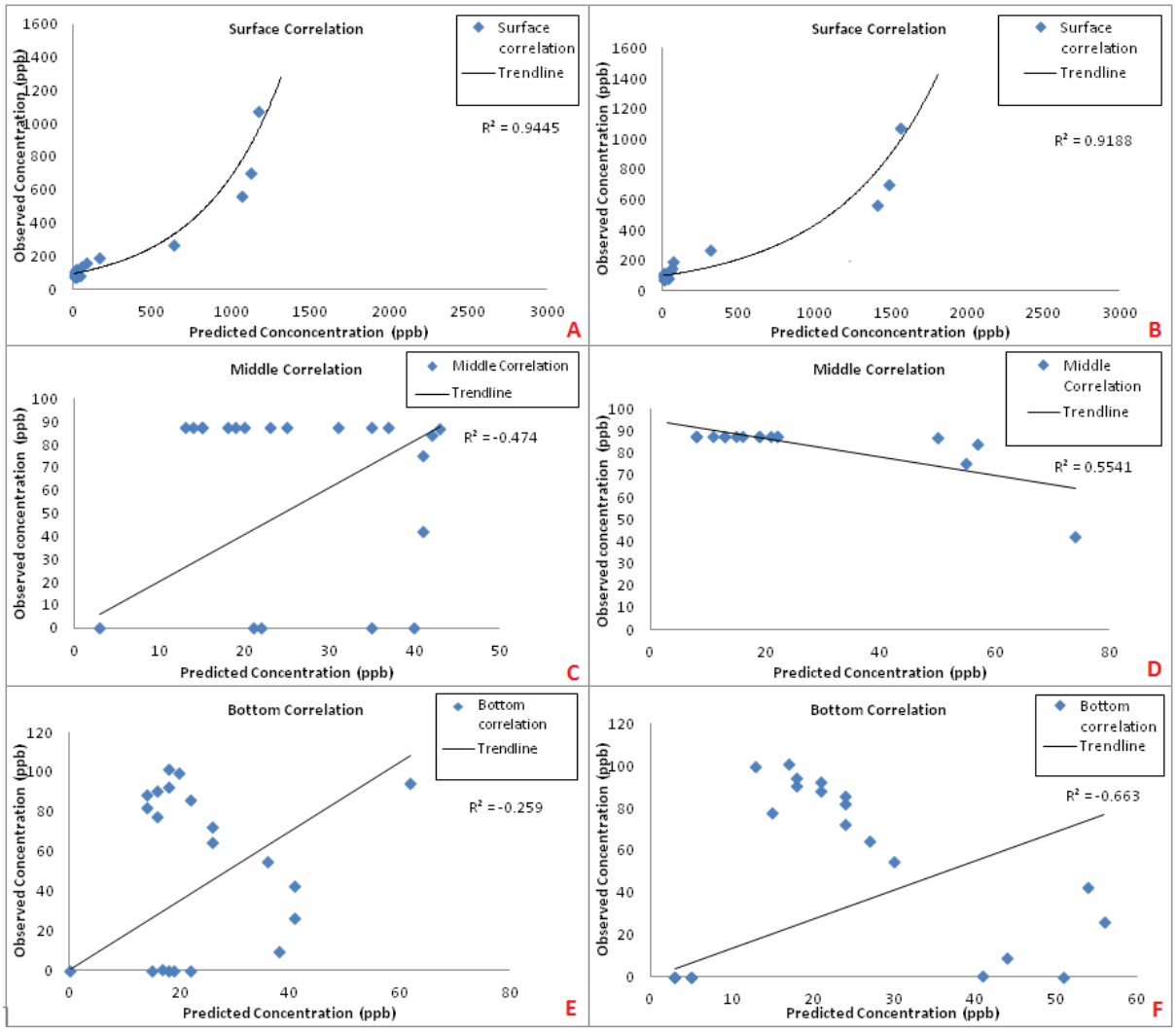

Figure A2.5: Correlation values for the observed and predicted modelled Ag concentrations for citrate and PVP AgNPs exposed to summer natural water. A) citrate AgNP study in the surface, B) PVP AgNP study in the surface, C) citrate AgNP study in the middle, D) PVP AgNP study in the middle, E) citrate AgNP study in the bottom, and F) PVP AgNP study in the bottom.

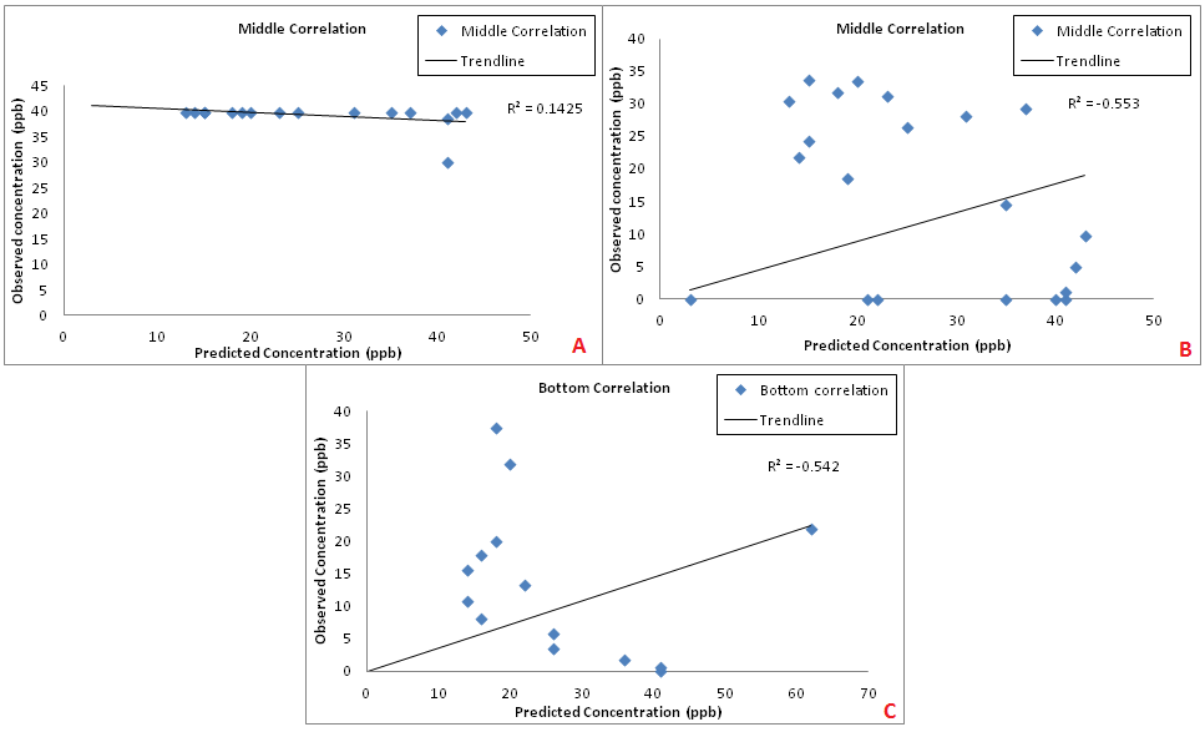

Figure A2.6: Correlation values for the observed and predicted modelled Ag concentrations for the adjusted model parameters for the citrate AgNPs A and B) Middle correlations and C) bottom correlations for summer water.

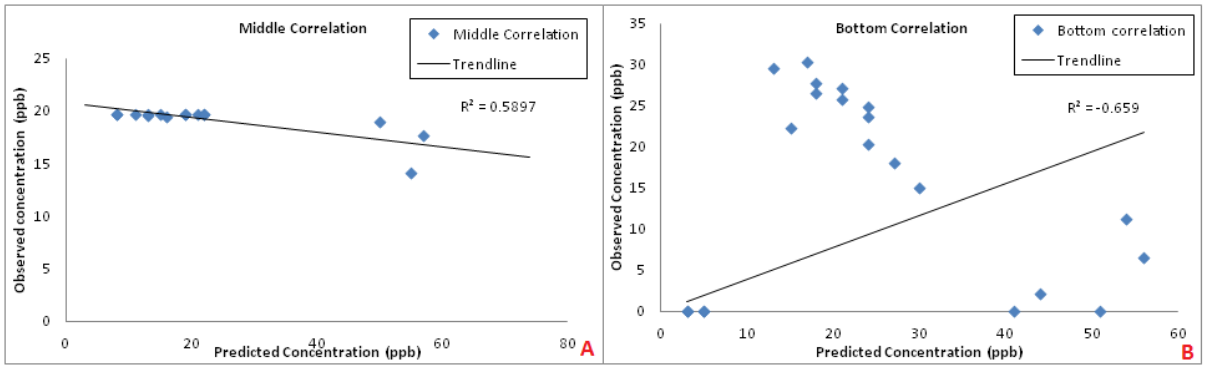

Figure A2.7: Correlation values for the observed and predicted modelled Ag concentrations for the adjusted model parameters for the PVP AgNPs A) Middle correlations and B) bottom correlations for summer water.

Table A2.7: Average corrected dissolved silver (ppb) and NP fraction data for citrate AgNPs in summer water								
Day	Surface				Bottom			
	Total Ag (ppb)	NP fraction	Dissolved Ag	% dissolved fraction	Total Ag (ppb)	NP fraction	Dissolved Ag	% dissolved fraction
1	636 ± 0.18	620	16 ± 0.08	3	17 ± 0.17	14	3 ± 0.02	18
2	167 ± 0.08	165	2 ± 0.13	1	38 ± 0.08	29	9 ± 0.03	24
3	90 ± 0.032	89	1 ± 0.01	1	41 ± 0.03	13	28 ± 0.25	68
4	57 ± 0.43	52	5 ± 0.49	9	41 ± 0.03	12	29 ± 0.06	71
5	22 ± 0.29	16	6 ± 0.82	27	36 ± 0.69	7	29 ± 0.20	81
6	18 ± 0.56	10	8 ± 0.04	44	26 ± 0.03	3	23 ± 0.62	88
7	15 ± 0.84	5	10 ± 0.06	67	26 ± 0.33	10	16 ± 0.77	62
8	18 ± 0.89	10	8 ± 0.62	44	16 ± 0.08	8	8 ± 0.05	50
9	12 ± 0.08	4	8 ± 0.29	67	14 ± 0.37	2	12 ± 0.07	86
10	21 ± 0.45	10	11 ± 0.45	52	22 ± 0.01	12	10 ± 0..13	45
11	30 ± 0.83	23	7 ± 0.38	23	14 ± 0.09	3	11 ± 0.39	79
12	11 ± 0.07	4	7 ± 0.46	64	16 ± 0.09	4	12 ± 0.20	75
13	46 ± 0.73	39	7 ± 0.22	15	18 ± 0.88	3	15 ± 0.33	83
14	28 ± 0.54	21	7 ± 0.35	25	62 ± 0.85	45	17 ± 0.25	27
21	21 ± 0.22	6	15 ± 0.55	71	20 ± 0.11	14	6 ± 0.04	30
28	17 ± 0.03	4	13 ± 0.69	76	18 ± 0.89	0	18 ± 0.99	100

Table A2.8: Average corrected dissolved silver (ppb) and NP fraction data for PVP AgNPs in summer water								
Day	Surface				Bottom			
	Total Ag (ppb)	NP fraction	Dissolved Ag	% dissolved fraction	Total Ag (ppb)	NP fraction	Dissolved Ag	% dissolved fraction
1	314 ± 0.31	307	7 ± 0.43	2	41 ± 0.02	30	11 ± 0.32	27
2	67 ± 0.12	56	11 ± 0.26	16	48 ± 0.01	33	15 ± 0.21	31
3	59 ± 0.06	56	3 ± 0.21	5	56 ± 0.06	54	2 ± 0.86	4
4	56 ± 0.25	50	6 ± 0.77	11	54 ± 0.76	49	5 ± 0.15	9
5	11 ± 0.03	5	6 ± 0.15	55	30 ± 0.18	1	29 ± 0.02	97
6	12 ± 0.03	4	8 ± 0.49	67	27 ± 0.17	4	23 ± 0.06	85
7	13 ± 0.03	3	10 ± 0.82	77	24 ± 0.18	8	16 ± 0.77	67
8	15 ± 0.07	7	8 ± 0.39	53	15 ± 0.01	7	8 ± 0.63	53
9	26 ± 0.08	18	8 ± 0.06	31	24 ± 0.02	12	12 ± 0.72	50
10	13 ± 0.07	2	11 ± 0.63	85	24 ± 0.17	6	18 ± 0.01	75
11	22 ± 0.06	15	7 ± 0.06	32	21 ± 0.04	2	19 ± 0.08	90
12	34 ± 0.05	6	28 ± 0.05	82	18 ± 0.04	2	16 ± 0.76	89
13	22 ± 0.06	5	17 ± 0.53	77	21 ± 0.04	3	18 ± 0.38	86
14	34 ± 0.05	11	23 ± 0.32	68	18 ± 0.03	1	17 ± 0.15	94
21	12 ± 0.49	5	7 ± 0.12	58	13 ± 0.02	6	7 ± 0.99	54
28	11 ± 0.28	0	11 ± 0.33	100	17 ± 0.04	0	17 ± 0.18	100

Information presented in tables A2.7 and A2.8 correspond to the total Ag data presented in figure 5.14.

Autumn natural water exposures

Table A2.9: Average Total silver concentration (ppb) data for citrate AgNPs in Autumn water				
Time (day)	**Time (hours)**	**Surface**	**Middle**	**Bottom**
0	**0**	2636 ± 0.14	8 ± 0.56	5 ± 0.55
0.020833	**0.5**	1907 ± 0.41	16 ± 0.02	6 ± 0.19
0.0625	**1.5**	1910 ± 0.28	11 ± 0.13	15 ± 0.02
0.145833	**3.5**	1635 ± 0.46	18 ± 0.24	20 ± 0.05
0.229167	**5.5**	1452 ± 0.38	29 ± 0.27	17 ± 0.02
1	**24**	406 ± 0.29	24 ± 0.06	21 ± 0.06
2	**48**	598 ± 0.47	23 ± 0.07	26 ± 0.05
3	**72**	446 ± 0.42	32 ± 0.03	25 ± 0.08
4	**96**	313 ± 0.36	30 ± 0.04	31 ± 0.05
5	**120**	266 ± 0.24	35 ± 0.05	27 ± 0.16
6	**144**	82 ± 0.05	37 ± 0.03	44 ± 0.03
7	**168**	64 ± 0.03	21 ± 0.01	37 ± 0.21
8	**192**	41 ± 0.13	22 ± 0.2	25 ± 0.23
9	**216**	34 ± 0.05	21 ± 0.08	22 ± 0.08
10	**240**	25 ± 0.75	13 ± 0.01	17 ± 0.02
11	**264**	21 ± 0.08	11 ± 0.06	16 ± 0.09
12	**288**	17 ± 0.09	11 ± 0.06	16 ± 0.49
13	**312**	22 ± 0.67	14 ± 0.09	15 ± 0.58
14	**336**	26 ± 0.93	17 ± 0.09	15 ± 0.48
21	**504**	41 ± 0.06	15 ± 0.07	20 ± 0.87
28	**672**	31 ± 0.82	15 ± 0.65	18 ± 0.01

Table A2.10: Total silver recover concentration (ppb) for PVP AgNPs in Autumn water				
Time (day)	**Time (hours)**	**Surface**	**Middle**	**Bottom**
0	**0**	3187 ± 0.36	2 ± 0.18	3 ± 0.37
0.020833	**0.5**	2940 ± 0.02	10 ± 0.01	4 ± 0.06
0.0625	**1.5**	2736 ± 0.04	3 ± 0.03	5 ± 0.02
0.145833	**3.5**	2720 ± 0.18	18 ± 0.01	17 ± 0.56
0.229167	**5.5**	2639 ± 0.26	42 ± 0.03	7 ± 0.051
1	**24**	1995 ± 0.02	26 ± 0.01	10 ± 0.68
2	**48**	934 ± 0.06	35 ± 0.07	48 ± 0.86
3	**72**	382 ± 0.12	55 ± 0.49	50 ± 0.92
4	**96**	253 ± 0.05	58 ± 0.01	71 ± 0.29
5	**120**	157 ± 0.16	27 ± 0.01	41 ± 0.99
6	**144**	82 ± 0.89	49 ± 0.03	54 ± 0.07
7	**168**	89 ± 0.18	46 ± 0.03	62 ± 0.74
8	**192**	94 ± 0.46	44 ± 0.06	70 ± 0.02
9	**216**	79 ± 0.18	52 ± 0.05	53 ± 0.23
10	**240**	46 ± 0.13	55 ± 0.02	47 ± 0.17
11	**264**	34 ± 0.12	15 ± 0.04	27 ± 0.04
12	**288**	29 ± 0.05	13 ± 0.88	35 ± 0.09
13	**312**	32 ± 0.14	21 ± 0.01	39 ± 0.12
14	**336**	34 ± 0.14	29 ± 0.02	43 ± 0.35
21	**504**	32 ± 0.22	18 ± 0.09	21 ± 0.96
28	**672**	39 ± 0.35	11 ± 0.06	20 ± 0.17

Information presented in tables A2.9 and A2.10 correspond to the total Ag data presented in figure 5.21.

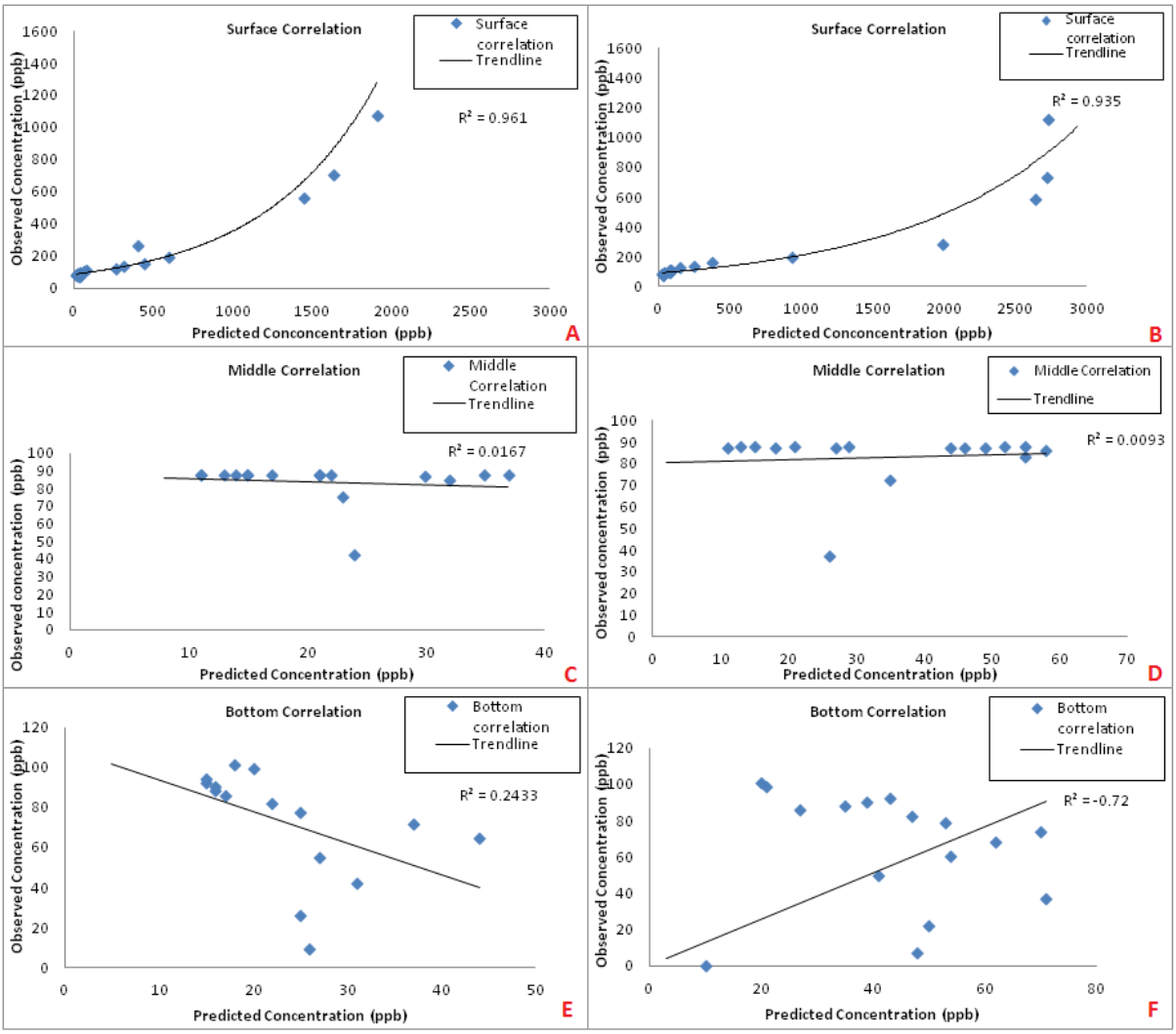

Figure A2.8: Correlation values for the observed and predicted modelled Ag concentrations for citrate and PVP AgNPs exposed to autumn natural water. A) citrate AgNP study in the surface, B) PVP AgNP study in the surface, C) citrate AgNP study in the middle, D) PVP AgNP study in the middle, E) citrate AgNP study in the bottom, and F) PVP AgNP study in the bottom.

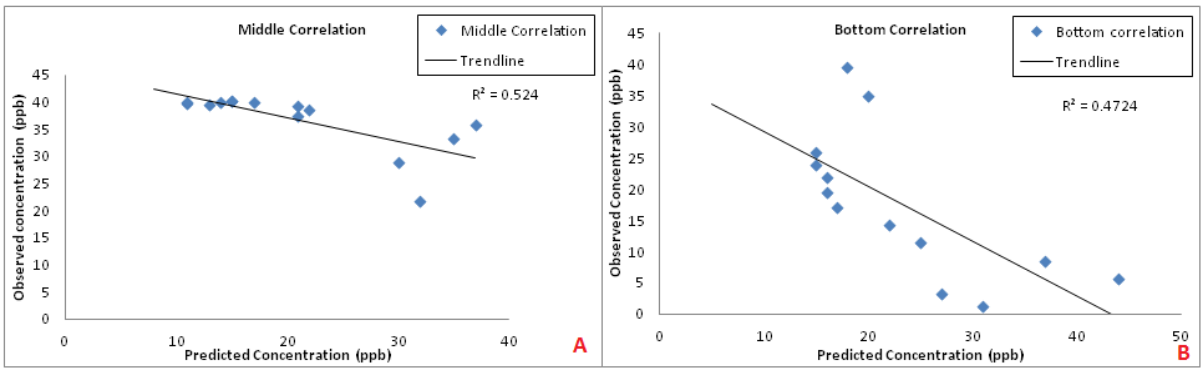

Figure A2.9: Correlation values for the observed and predicted modelled Ag concentrations for the adjusted model parameters for the citrate AgNPs in autumn natural water. A) Middle correlations and B) bottom correlations.

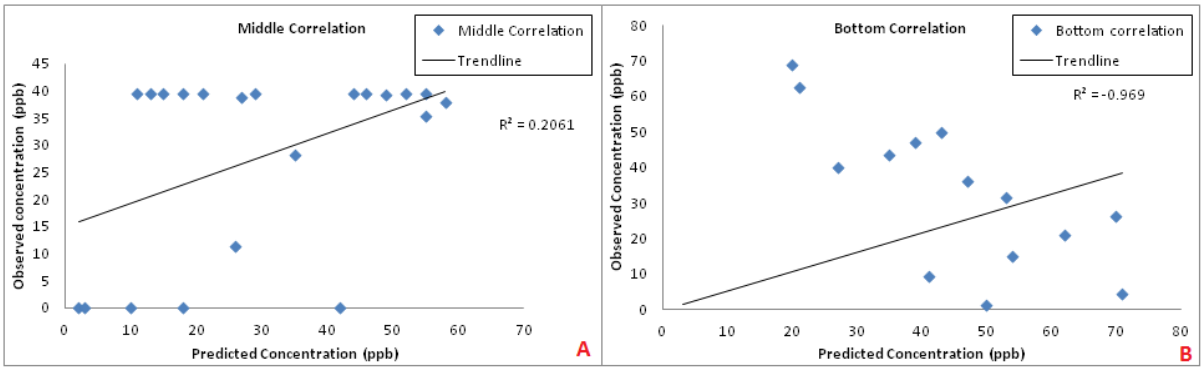

Figure A2.10:Correlation values for the observed and predicted modelled Ag concentrations for the adjusted model parameters for the PVP AgNPs in autumn natural water. A) Middle correlations and B) bottom correlations.

Table A2.11: Average corrected dissolved silver (ppb) and NP fraction data for citrate AgNPs in Autumn water								
Day	Surface				Bottom			
	Total Ag (ppb)	NP fraction	Dissolved Ag	% dissolved fraction	Total Ag (ppb)	NP fraction	Dissolved Ag	% dissolved fraction
1	406 ± 0.29	396	10 ± 0.23	2	21 ± 0.06	15	6 ± 0.44	29
2	598 ± 0.47	493	105 ± 1.25	18	26 ± 0.05	17	9 ± 0.28	35
3	446 ± 0.42	403	43 ± 0.48	10	25 ± 0.08	7	18 ± 0.01	72
4	313 ± 0.36	303	10 ± 0.11	3	31 ± 0.05	4	27 ± 0.08	87
5	266 ± 0.24	206	60 ± 0.32	23	27 ± 0.16	18	9 ± 0.1	33
6	82 ± 0.05	69	13 ± 0.17	16	44 ± 0.03	40	4 ± 0.47	9.
7	64 ± 0.03	50	14 ± 0.17	22	37 ± 0.21	27	10 ± 0.55	27.
8	41 ± 0.13	33	8 ± 0.09	20	25 ± 0.23	15	10 ± 0.96	40
9	34 ± 0.05	8	26 ± 0.08	76	22 ± 0.08	8	14 ± 0.53	64
10	25 ± 0.75	16	9 ± 0.12	36	17 ± 0.02	10	7 ± 0.14	41
11	21 ± 0.08	9	12 ± 0.15	57	16 ± 0.09	11	5 ± 0.17	31
12	17 ± 0.09	14	3 ± 0.23	18	16 ± 0.49	14	2 ± 0.26	12.5
13	22 ± 0.67	13	9 ± 0.19	41	15 ± 0.58	10	5 ± 0.28	33
14	26 ± 0.93	10	16 ± 0.14	62	15 ± 0.48	2	13 ± 0.31	87
21	41 ± 0.06	25	16 ± 0.24	39	20 ± 0.87	10	10 ± 0.69	50
28	31± 0.72	14	17 ± 0.50	55	18 ± 0.01	5	13 ± 0.16	72

Table: A2.12: Average corrected dissolved silver (ppb) and NP fraction data for PVP AgNPs in Autumn water								
Day	Surface				Bottom			
	Total Ag (ppb)	NP fraction	Dissolved Ag	% dissolved fraction	Total Ag (ppb)	NP fraction	Dissolved Ag	% dissolved fraction
1	1995 ± 0.02	1977	18 ±0.02	1	10 ± 0.68	5	5 ± 0.49	50
2	934 ± 0.06	639	295±0.22	32	48 ± 0.86	43	5 ±0.77	10
3	382 ± 0.12	237	145±0.01	38	50 ± 0.92	30	20 ±0.01	40
4	253 ± 0.05	129	124±0.02	49	71 ± 0.29	68	3 ±0.12	4
5	157 ± 0.16	77	80 ±0.02	51	41 ± 0.99	12	29 ±0.14	71
6	82 ± 0.89	30	52 ±0.08	63	54 ± 0.07	45	9 ±0.26	17
7	89 ± 0.18	15	74 ±0.11	83	62 ± 0.74	55	7 ±0.18	11
8	94 ± 0.46	8	86 ±0.15	91	70 ± 0.02	65	5 ±0.33	7
9	79 ± 0.18	16	63 ±0.05	80	53 ± 0.23	50	3 ±0.09	6
10	46 ± 0.13	7	39 ±0.13	85	47 ± 0.17	39	8 ±0.65	17
11	34 ± 0.12	22	12 ±0.01	35	27 ± 0.04	9	18 ± 0.16	67
12	29 ± 0.05	25	4 ±0.01	14	35 ± 0.09	13	22 ±0.06	63
13	32 ± 0.14	21	11 ±0.02	34	39 ± 0.12	37	2 ±0.79	5.
14	34 ± 0.14	30	4 ±0.08	12	43 ± 0.35	41	2 ±0.89	5
21	32 ± 0.22	18	14 ±0.39	44	21 ± 0.96	17	4 ±0.65	19
28	39 ± 0.35	8	31 ±0.55	79.	20 ± 0.17	9	11 ±	55

Information presented in tables A2.11 and A2.12 correspond to the total Ag data presented in figure 5.22.

Winter natural water exposures

Table A2.13: Average total silver recovery (ppb) for citrate AgNPs in winter natural water				
Time (hours)	**Time (days)**	**Surface**	**Middle**	**Sediment**
0	**0**	1769 ± 0.868	27 ± 0.023	4 ± 0.028
0.5	**0.020833**	2337 ± 0.196	7 ± 0.088	2 ± 0.133
1.5	**0.0625**	2139 ± 0.257	8 ± 0.061	7 ± 0.098
3.5	**0.145833**	2157 ± 0.049	10 ± 0.098	14 ± 0.010
5.5	**0.229167**	2221 ± 0.079	70 ± 0.034	15 ± 0.011
8.5	**0.354167**	1949 ± 0.181	36 ± 0.044	22 ± 0.028
24	**1**	939 ± 0.526	32 ± 0.011	35 ± 0.046
30	**1**	1170 ± 0.409	52 ± 0.08	35 ± 0.058
48	**2**	1122 ± 0.567	10 ± 0.083	14 ± 0.016
72	**3**	1024 ± 0.598	28 ± 0.025	26 ± 0.017
120	**5**	603 ± 0.383	29 ± 0.011	34 ± 0.018
168	**7**	368 ± 0.338	28 ± 0.031	30 ± 0.077
192	**8**	248 ± 0.268	34 ± 0.063	42 ± 0.017
216	**9**	218 ± 0.248	38 ± 0.083	35 ± 0.011
336	**14**	124 ± 0.076	37 ± 0.028	49 ± 0.019
360	**21**	160 ± 0.088	40 ± 0.017	42 ± 0.036
672	**28**	80 ± 0.056	47 ± 0.046	51 ± 0.045

Table A2.14: Average total silver recovery (ppb) for PVP AgNPs in winter natural water				
Time (day)	**Time (hours)**	**Surface**	**Middle**	**Sediment**
0	**0**	608 ± 0.353	12 ± 0.011	3 ± 0.463
0.020833	**0.5**	838 ± 0.198	6 ± 0.057	7± 0.685
0.0625	**1.5**	938 ± 0.207	7 ± 0.043	7 ± 0.648
0.145833	**3.5**	703 ± 0.137	114 ± 0.188	5 ± 0.238
0.229167	**5.5**	673 ± 0.293	5 ± 0.044	6 ± 0.653
0.354167	**8.5**	418 ± 0.352	13 ± 0.03	13 ± 0.736
1	**24**	632 ± 0.286	5 ± 0.015	6 ± 0.52
2	**48**	337 ± 0.232	36 ± 0.033	31 ± 0.021
3	**72**	117 ± 0.187	3 ± 0.022	21 ± 0.827
4	**96**	85 ± 0.131	5 ± 0.043	24 ± 0.025
5	**120**	45 ± 0.575	7 ± 0.054	15 ± 0.494
6	**144**	32 ± 0.19	4 ± 0.042	13 ± 0.327
7	**168**	10 ± 0.092	5 ± 0.015	13 ± 0.219
8	**192**	15 ± 0.08	3 ± 0.035	19 ± 0.561
9	**216**	11 ± 0.09	10± 0.06	16 ± 0.696
11	**264**	28 ± 0.061	17 ± 0.12	24 ± 0.065
12	**288**	11 ± 0.086	4 ± 0.384	20 ± 0.017
13	**360**	10 ± 0.046	6 ± 0.14	24 ± 0.028
14	**384**	4 ± 0.015	6 ± 0.063	27 ± 0.011
21	**504**	10 ± 0.02	8 ± 0.031	22 ± 0.033
28	**672**	16 ± 0.58	16 ± 0.053	15 ± 0.7

Information presented in tables A2.13 and A2.14 were used in figure 5.30.

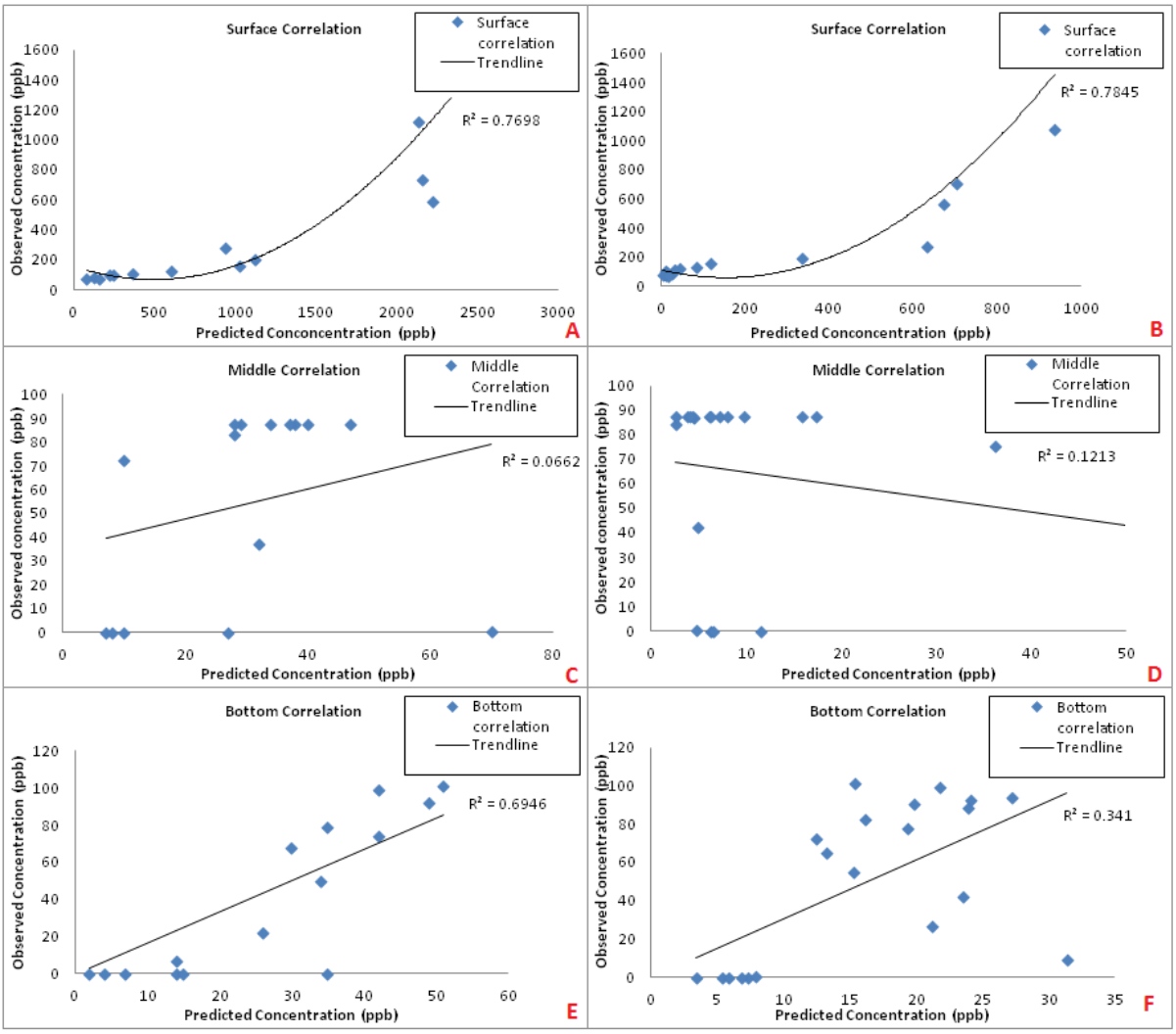

A2.11: Correlation values for the observed and predicted modelled Ag concentrations for citrate and PVP AgNPs exposed to winter natural water. A) citrate AgNP study in the surface, B) PVP AgNP study in the surface, C) citrate AgNP study in the middle, D) PVP AgNP study in the middle, E) citrate AgNP study in the bottom, and F) PVP AgNP study in the bottom.

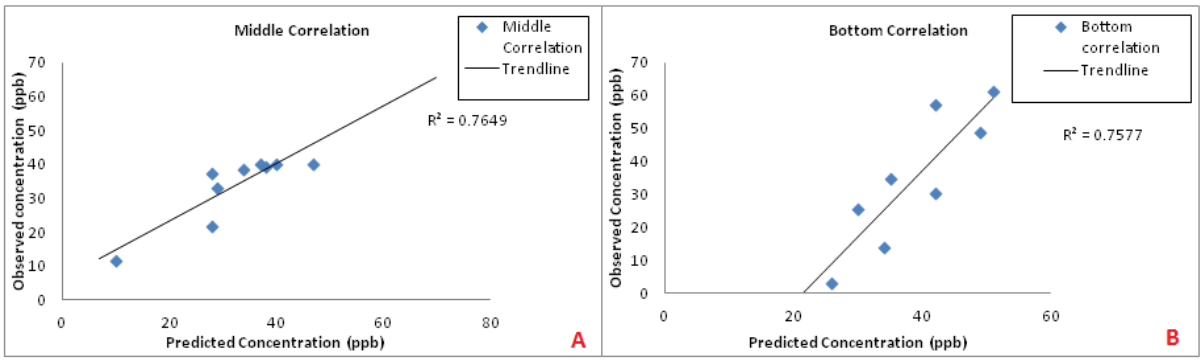

A2.12: Correlation values for the observed and predicted modelled Ag concentrations for the adjusted model parameters for the citrate AgNPs in winter natural water. A) Middle correlations and B) bottom correlations.

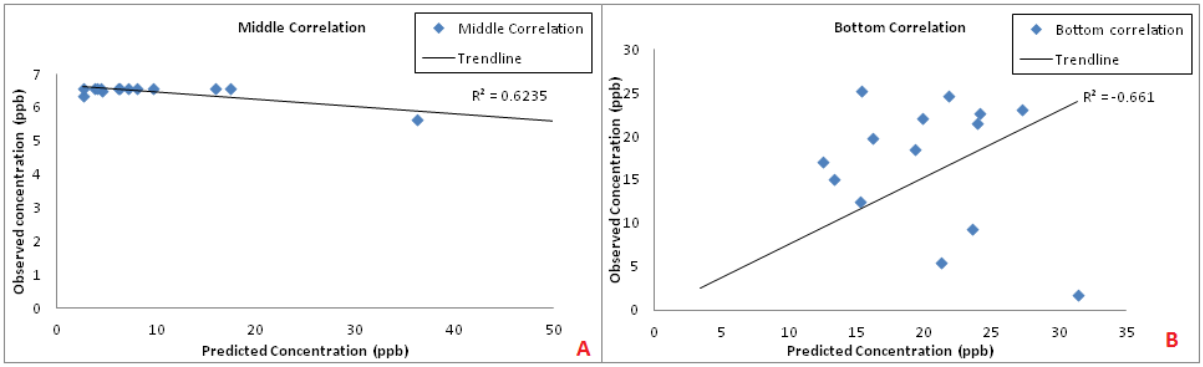

A2.13: Correlation values for the observed and predicted modelled Ag concentrations for the adjusted model parameters for the PVP AgNPs in winter natural water. A) Middle correlations and B) bottom correlations.

Table A2.15: Average corrected dissolved silver (ppb) and NP fraction data for citrate AgNPs in winter water								
Day	Surface				Bottom			
	Total	NP fraction	Dissolved Ag	% dissolved fraction	Total	NP fraction	Dissolved Ag	% dissolved fraction
1	1170 ± 0.409	1169	0.8 ± 0.13	0.06	35 ± 0.58	33	2 ± 0.05	6
2	1122 ± 0.567	1118	4 ± 0.39	0.4	14 ± 0.06	13.8	0.2 ± 0.13	1
3	1024 ± 0.598	987	37 ± 0.28	4	26 ± 0.07	23	3 ± 0.03	12
5	603 ± 0.383	564	39 ± 0.15	6	34 ± 0.018	32	2 ± 0.02	6
7	368 ± 0.338	367	1 ± 0.59	0.3	30 ± 0.077	28	2 ± 0.09	7
8	248 ± 0.268	241	7 ± 0.15	3	42 ± 0.17	41.5	0.5 ± 0.22	1
9	218 ± 0.248	214	4 ± 0.08	2	35 ± 0.011	34	1 ± 0.44	3
14	124 ± 0.076	25	99 ± 0.97	80	49 ± 0.19	46	3 ± 0.78	6
21	160 ± 0.088	159	1 ± 0.99	0.6	42 ± 0.36	38	4 ± 0.79	10
28	80 ± 0.056	79	1 ± 1.24	1	51 ± 0.45	46	5 ± 0.89	10

Table A2.16: Average corrected dissolved silver (ppb) and NP fraction data for PVP AgNPs in Winter water								
Day	Surface				Bottom			
	Total Ag (ppb)	NP fraction	Dissolved Ag	% dissolved fraction	Total Ag (ppb)	NP fraction	Dissolved Ag	% dissolved fraction
1	632 ± 0.286	592	40±0.15	6.	6 ± 0.52	0	6 ± 0.16	100
2	337 ± 0.232	332	5±0.16	1	31 ± 0.021	17	14 ± 0.04	45
3	117 ± 0.187	116.3	0.7±0.95	0.6	21 ± 0.827	17	4 ± 0.12	19.
4	85 ± 0.131	82	3±0.01	4	24 ± 0.025	8	16 ± 0.16	67
5	45 ± 0.575	40	5±0.11	11	15 ± 0.494	6	9 ± 0.86	60
6	32 ± 0.19	11	21±0.01	66	13 ± 0.327	11	2 ± 0.01	15.
7	10 ± 0.092	7	3±0.99	30	13 ± 0.219	9	4 ± 0.12	31
8	15 ± 0.08	13	2±0.04	13	19 ± 0.561	11	8 ± 0.87	42
9	11 ± 0.09	6	5±0.65	45	16 ± 0.696	15	1 ± 0.05	6
11	28 ± 0.061	21	7±0.25	25	24 ± 0.065	23	1 ± 0.03	4.
12	11 ± 0.086	10.9	0.1±0.59	0.9	20 ± 0.017	11	9 ± 0.04	45
13	10 ± 0.046	7	3±0.55	30	24 ± 0.028	23	1 ± 0.42	4
14	4 ± 0.015	2	2±0.05	50	27 ± 0.011	16	11 ± 0.04	41
21	10 ± 0.02	8	2±0.19	20	22 ± 0.033	10	12 ± 0.09	55
28	16 ± 0.58	14	2±0.38	13	15 ± 0.7	11	4 ± 0.17	27

Information presented in tables A2.15 and A2.16 were used in figure 5.31.

Appendix 3: EDX Energy Table